VNiVERSiDAD
D SALAMANCA

Facultad de Ciencias
Departamento de Geología-Área de Paleontología

VARIABILIDAD CLIMÁTICA ORBITAL Y SUBORBITAL EN EL ATLÁNTICO NORTE DURANTE EL PLEISTOCENO (1.070.000-780.000 AÑOS)

Iván Hernández Almeida

TESIS DOCTORAL

Salamanca, 2011

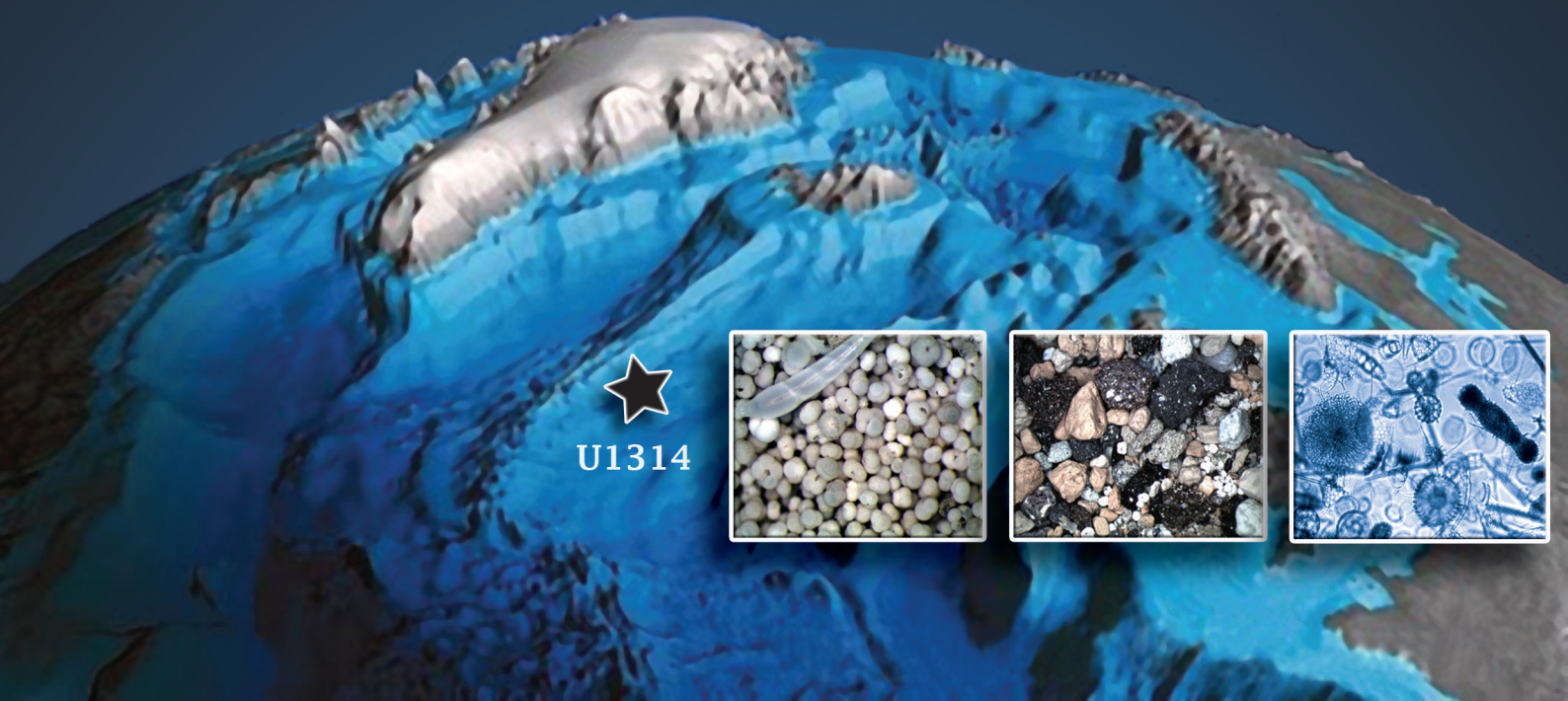

VNiVERSiDAD
D SALAMANCA

Facultad de Ciencias
Departamento de Geología-Área de Paleontología

VARIABILIDAD CLIMÁTICA ORBITAL Y SUBORBITAL EN EL ATLÁNTICO NORTE DURANTE EL PLEISTOCENO (1.070.000-780.000 AÑOS)

Iván Hernández Almeida

TESIS DOCTORAL

Salamanca, mayo de 2011

VNiVERSiDAD
D SALAMANCA

Facultad de Ciencias
Departamento de Geología-Área de Paleontología

VARIABILIDAD CLIMÁTICA ORBITAL Y SUBORBITAL EN EL ATLÁNTICO NORTE DURANTE EL PLEISTOCENO (1.070.000-780.000 AÑOS)

Memoria presentada por Iván Hernández Almeida para optar al Grado de Doctor en Geología por la Universidad de Salamanca con Mención *"Doctor Europeus"*

Esta Tesis Doctoral se ha realizado bajo la dirección de los profesores:

Dr. D. Francisco Javier Sierro Sánchez

Dr. D. José Abel Flores Villarejo

D. Francisco Javier Sierro Sánchez y **D. José Abel Flores Villarejo** profesores del Área de Paleontología del Departamento de Geología de la Facultad de Ciencias (Universidad de Salamanca)

CERTIFICAN que,

D. Iván Hernández Almeida ha realizado en el Departamento de Geología y bajo nuestra supervisión el trabajo:

Variabilidad climática orbital y suborbital en el Atlántico Norte durante el Pleistoceno (1.070.000-780.000 años)

Y para que conste, firman el presente certificado en Salamanca en mayo de 2011

Los directores

Francisco J. Sierro Sánchez

José Abel Flores Villarejo

El doctorando

Iván Hernández Almeida

"By endurance, we conquer"

Ernest Shackleton

RESUMEN. La presente Tesis es un estudio geoquímico, micropaleontológico y sedimentológico de la secuencia sedimentaria de testigos del *Site* U1314, recuperada durante la expedición 306 del IODP, en la formación *Gardar Drift* (sur de Islandia), en el Atlántico Norte subpolar. El objeto principal de esta Tesis es el estudio de las variaciones climáticas a diferentes escalas temporales (orbital y suborbital), la evolución de los patrones de circulación superficial y profunda, la dinámica de las masas de hielo en el Atlántico Norte, y los cambios en diferentes parámetros de la columna de agua (nutrientes, salinidad, temperatura, etc.), que tuvieron lugar durante el período comprendido entre 1.070.000 a 780.000 años (MIS 31-19), conocido como Transición del Pleistoceno Medio. Se ha realizado un registro a alta resolución de isótopos estables de oxígeno y carbono en foraminíferos bentónicos y planctónicos, un análisis faunístico de las asociaciones de radiolarios y foraminíferos planctónicos, un registro de la acumulación de material terrígeno y diversas técnicas geoquímicas en sedimento (composición elemental, ópalo biogénico, y en conchas de foraminíferos planctónicos.

Los resultados obtenidos indican una variabilidad climática centrada en periodos de alta frecuencia, representada principalmente por incrementos abruptos en material terrígeno en la secuencia sedimentaria, que son interpretados como periodos de expansión de las masas de hielo hacia el océano. Acompañando a las descargas de material terrígeno se han registrado dramáticos cambios en las asociaciones de radiolarios y foraminíferos planctónicos que se relacionan directamente con rápidas oscilaciones en las propiedades físico-químicas (salinidad, temperatura, nutrientes, etc.) de las aguas superficiales, como resultado de la transferencia de grandes cantidades de agua dulce desde el continente al océano. Estos eventos catastróficos tuvieron un gran impacto en los patrones de circulación superficial y profunda, registrados como rápidos avances hacia el sur de aguas frías polares y una reducción en la producción de aguas profundas en los mares nórdicos (Groenlandia, Islandia y Noruega) así como un aumento de la presencia de aguas profundas originadas en el Hemisferio Sur en el Atlántico Norte.

Los resultados de los análisis espectrales de los registros de IRD, reconstrucción de temperaturas superficiales del oceáno y de $\delta^{18}O$ en foraminíferos planctónicos revelan frecuencias centradas en periodos de 21.000 y 11.000, años, aproximadamente. Estas ciclicidades están relacionadas con la señal de precesión y sus harmónicos, y han sido observadas en registros climáticos marinos en latitudes bajas. Esto sugiere que la variabilidad climática señalada por los indicadores superficiales de nuestro testigo viene controlada por el transporte de la señal cálida de bajas latitudes a través de procesos convectivos tropicales, atmosféricos y/o oceánicos, a la región del Atlántico Norte subpolar. El registro de paleotemperaturas a partir de la relación Mg/Ca de *Neogloboquadrina pachyderma* sin. muestra evidencias de un ascenso de temperaturas durante el depósito o inmediatamente después de los IRD que acelerarían el retroceso de las masas de hielo. Además, superimpuesta a esta ciclicidad suborbital, observamos una evolución del sistema climático hacia un incremento progresivo de la ciclicidad de 100.000 años en la dinámica de los ciclos glaciales desde ~ 950.000 años. Esta reconfiguración se observa en nuestros datos como un aumento gradual del volumen de hielo global y una mayor amplitud de la variabilidad climática glacial-interglacial.

ABSTRACT. This thesis is a geochemical, micropaleontological and sedimentological study of a sedimentary sequence from Site U1314, recovered during IODP Expedition 306, located in the *Gardar Drift* (south Iceland), in the subpolar North Atlantic. The main subject of this Thesis is the study of the climatic variations at different time-scales (orbital and suborbital) that took place during the period between 1.070.000 a 780.000 years (MIS 31-19), known as the Mid-Pleistocene Transition, the evolution of surface and deep circulation patterns, ice-sheet dynamics in the North Atlantic, and changes in different patterns of the water column (nutrients, salinity, temperature, etc.). We have elaborated a high-resolution record of stable oxygen and carbon isotopes from benthic and planktonic foraminifera, a faunistic analysis of radiolarian and planktonic foraminifera assemblages, a record of terrigenous material accumulation and several geochemical analyses on bulk sediment (elemental composition, biogenic opal, carbon components and P sequential extraction) and on planktonic foraminifera shells (Mg/Ca paleothermometry).

Results obtained indicate a climatic variability centered mainly at high-frequency periods, shown by abrupt increases in the amount of terrigenous material in the sedimentary sequence, that are interpreted as ice-sheet advances toward the ocean. Linked to these terrigenous discharges, there are dramatic changes in the radiolarian and planktonic foraminifera assemblages, related to rapid oscillations in the physico-chemical properties of the surface waters that resulted from the transference of large amounts of freshwater from the continent to the ocean. These catastrophic events had a large impact on the surface and deep circulation patterns, recorded as rapid southward advances of polar water masses and reduced deep-water production in the Nordic Seas (Greenland, Iceland and Norway) and increased flow of southern Hemisphere source deep-waters in the North Atlantic.

Results from the spectral analyses on the IRD, sea surface temperature reconstructions and planktonic $\delta^{18}O$ records reveal frequencies centered at periods, of around 21000 and 11000 years. These cyclicities are related with a precession signal and its harmonics, and they have been observed in many marine climatic records at low-latitudes. This suggests that the climatic variability indicated by the surface proxies from our Site is driven by a low-latitude forcing transported by tropical convective processes, either atmospheric or oceanic, toward the subpolar North Atlantic. Paleotemperature estimates based on Mg/Ca values from *Neogloboquadrina pachyderma* sin. show evidences of rising temperatures during or following the IRD discharge which would accelerate ice-sheet retreat. Moreover, superimposed to this suborbital climate variability, we observe an evolution of the climatic system toward an increasing influence of the 100-kyr cycle on glacial-interglacial variability since ~ 950 ka. This reconfiguration is observed in our data set as a global increase in ice-volume and higher amplitude of glacial-interglacial climate variability.

El estudio de los eventos climáticos abruptos y los mecanismos causa/efecto implicados en estos eventos es uno de los mayores retos a los que se enfrenta la investigación climática hoy en día. La identificación de los mecanismos de retroalimentación entre los sistemas océano-atmósfera-criosfera son de vital importancia para el entendimiento de la variabilidad climática presente en registros sedimentarios del fondo oceánico.

El Atlántico Norte es una de las áreas de mayor sensibilidad climática en la Tierra, debido que está expuesta a los efectos dinámicos de la interacción entre océano, atmósfera y las masas de hielo continentales circundantes, que han ocurrido a lo largo de la historia geológica en diferentes escalas de tiempo. Entre esta diferente temporalidad, destacan los cambios climáticos abruptos que sucedieron en intervalos de miles de años, que produjeron rápidas reducciones en la producción de aguas profundas que ventilan los océanos mundiales. Entender el mecanismo que causa estos dramáticos episodios es uno de los mayores retos hoy en la investigación climática. Sin embargo, muchos de los registros paleoclimáticos existentes que cuentan con suficiente resolución para revelar episodios de rápidos cambios climáticos sólo se extienden hasta unos pocos cientos de miles de años atrás en el tiempo (e.g. Bond *et al.*, 1992; Bond *et al.*, 1997; Sarnthein *et al.*, 2000; van Kreveld *et al.*, 2000). Para arrojar un poco más de luz sobre los mecanismos implicados en esta variabilidad climática, la investigación paleoceanográfica ha desarrollado durante los últimos años un extenso y detallado registro de indicadores paleoclimáticos (e.g., componentes del sedimento que aportan información acerca de condiciones oceanográficas, atmosféricas y del hielo en el pasado) que se extiende hasta mucho más atrás en el tiempo (Jouzel *et al.*, 2007).

Partiendo de estas premisas, y con la voluntad de proporcionar un nuevo enfoque a las investigaciones paleoceanográficas existentes, la presente Tesis Doctoral se enmarca en el estudio de los cambios climáticos y oceanográficos ocurridos en la región del Atlántico Norte durante el intervalo de tiempo conocido como Transición Climática del Pleistoceno Medio, entre 1,1 y 0,6 Ma. Numerosos estudios paleoclimáticos y paleoceanográficos han puesto de manifiesto los profundos cambios que sufrió el sistema terrestre durante la MPT, los cuales consistieron en un aumento en la acumulación de volumen de hielo en las masas continentales del Hemisferio Norte. Dada la estrecha relación entre hidrosfera y criosfera, esta reconfiguración del volumen de hielo global tuvo gran repercusión en los patrones de circulación oceánica superficial y profunda a nivel global y muy especialmente en la región del Atlántico Norte. Establecer cuales son los mecanismos de retroalimentación implicados en esta reconfiguración del sistema climático a escala orbital y suborbital es uno de los grandes retos de la paleoclimatología moderna.

El trabajo aquí presentado se basa en el análisis de una secuencia sedimentaria del sondeo marino profundo U1314, perforado en la formación *Gardar Drift* (sur de Islandia), durante la

expedición 306 del *Integrated Ocean Drilling Program* (IODP) en el Atlántico Norte subpolar. El material recuperado proporciona un registro de alta resolución del intervalo comprendido entre 1.070.000 y 780.000 años. En este estudio se han utilizado de manera conjunta técnicas basadas en el análisis faunístico de asociaciones planctónicas (foraminíferos y radiolarios), caracterización petrográfica, granulométrica y geoquímica del sedimento ($CaCO_3$, ópalo, Al, Ti, Fe, Mn, Mg, Ba, etc.) e isótopos estables (carbono y oxígeno) y elementos traza (relación Mg/Ca) en foraminíferos. Esta *suite* de indicadores paleoceanográficos permite una reconstrucción de los cambios en las masas de agua superficiales en el Atlántico Norte subpolar, de procesos verticales en la columna de agua, y de la interacción de las masas de hielo continental circundantes con él océano (procesos de hielo/deshielo). Así mismo, la profundidad a la que se sitúa el testigo U1314 (2.820 m) también permite realizar una monitorización de las variaciones temporales de las aguas profundas del Atlántico Norte, lo cual es una novedad respecto a otros estudios con testigos marinos profundos en la zona, recuperados a profundidades más someras (< 2.000 m) (Kleiven *et al.*, 2003; Raymo *et al.*, 1997; Venz *et al.*, 1999; Wright and Flower, 2002).

Entro los requisitos exigidos para la obtención de la mención *"Doctor Europeus"*, al que opta esta Tesis Doctoral, se incluye que si la tesis se presentara en castellano, una parte de la misma deberá redactarse y presentarse en alguna de las lenguas oficiales de la Unión Europea distinta a cualquiera de las lenguas oficiales en España. Para cumplir esta disposición, los Capítulos 3, 4 y 5 han sido redactados en inglés. Estos capítulos aparecen estructurados en forma de artículos científicos, algunos en revisión y otros en espera de ser enviados para su publicación. Se ha considerado pertinente incluir al principio de cada uno de estos capítulos un resumen en castellano, al igual que un resumen en inglés para los Capítulos 6 y 7, redactados en castellano. Debido a que muchos de los términos usados en la presente Tesis se encuentran exclusivamente escritos en inglés en la literatura científica que hemos utilizado, se ha optado por incluir estos términos (en cursiva junto al término en castellano) y utilizar sus respectivos acrónimos en el presente manuscrito. Las referencias bibliográficas aparecen como un apartado independiente al final de la Tesis, a fin de facilitar su lectura.

La presente Tesis Doctoral se divide en ocho capítulos y siete anexos:

En el Capítulo 1 se hace una introducción al período de estudio, el Pleistoceno Inferior y Medio, su definición y la identificación de los principales cambios ambientales asociados a la reorganización climática que tuvo lugar en ese período observado en el registro geológico global. En este capítulo también se hace referencia a los cambios climáticos a diferentes escalas de tiempo, orbital y suborbital, y en especial al registro de oscilaciones climáticas abruptos en el Atlántico Norte, y una descripción del contexto geológico y oceanográfico de la zona de estudio. El Capítulo 2 es una breve recopilación explicativa de los paleoindicadores que componen nuestros registros climáticos, describiendo su fundamento, aplicación paleoceanográfica y técnicas analíticas empleadas para su obtención. En esta sección también se incluye una amplia descripción de los materiales empleados durante la Tesis.

Los siguientes capítulos (3, 4, 5 y 6) presentan los resultados de tres publicaciones científicas enviadas a diferentes revistas de ámbito internacional y nacional en las que el doctorando ha sido el autor principal:

- Hernández-Almeida, I., Sierro, F.J., Cacho, I. and Flores, J.A. Impact of suborbital climate changes in the North Atlantic on ice-sheets dynamics at the Mid-Pleistocene Transition. *Paleoceanography* (en preparación).

En este trabajo, que corresponde al Capítulo 3, se aplican metodologías basadas en la composición isotópica de oxígeno y carbono en conchas de foraminíferos planctónicos y bentónicos, junto con estudio de la fracción detrítica > 150 μm, para abordar la caracterización y distribución de masas de agua profundas en el Atlántico Norte, así como estudiar las diferentes periodicidades que dominan los cambios climáticos en la región.

- Hernández-Almeida, I., Sierro, F.J., Filippelli, G.M., Cacho, I. and Flores, J.A. Millennial scale variability of planktonic foraminifer assemblages and changes in North Atlantic circulation during the Mid-Pleistocene Transition (1069-779 ka). *Marine Micropaleontology* (en preparación).

Este estudio correspondiente al Capítulo 4 supone un complemento al capítulo anterior, ya que presenta una reconstrucción de las condiciones oceanográficas superficiales del Atlántico Norte, centrándose en la dinámica regional del Frente Ártico.

- Hernández-Almeida, I., Bjørklund, K.R., Sierro, F.J., Filippelli, G.M., Cacho, I. and Flores, J.A., 2011a. A high resolution opal and radiolarian record from the subpolar North Atlantic during the Mid-Pleistocene Transition (1069-779 ka): palaeoceanographic implications. *Palaeogeography, Palaeoclimatology, Palaeoecology* (en revisión).

El trabajo presentado en el Capítulo 5 supone la primera contribución de registro de alta resolución de radiolarios y de ópalo para el Atlántico Norte subpolar durante el Pleistoceno Inferior y Medio. Los resutaldos obtenidos confirman muchas hipótesis planteadas en el trabajo anterior, y supone una demostración del potencial de estos indicadores en las reconstrucciones paleoambientales en esta región.

- Hernández-Almeida, I., Sierro, F.J., Suarez, M., Filippelli, G.M. and Flores, A., 2011b. Caracterización e interpretación de las capas ricas en detríticos en sedimentos del Site U1314 (Atlántico Norte) durante los estadios isotópicos marinos 21-19 (~ 830-779 ka) . *Geogaceta* (en revisión).

El Capítulo 6 se presentan resultados y conclusiones de un trabajo centrado en el uso de diferentes indicadores (geoquímicos, mineralógicos, etc.) para identificar capas ricas en material detrítico del testigo U1314 durante y determinar su posible origen.

En el Capítulo 7 se presenta un nuevo registro a alta resolución de la composición

geoquímica del testigo U1314, utilizando técnicas de composición elemental del sedimento y de análisis de la relación Mg/Ca en conchas de foraminíferos planctónicos para la reconstrucción de paleotemperaturas. Se prevé que el material presentado en este capítulo de lugar a una publicación científica.

El Capítulo 8 resume las principales conclusiones presentadas en los capítulos anteriores. Este capítulo ha sido redactado tanto en inglés como en castellano.

Finalmente, se han adjuntado siete anexos. El primero ellos incluye un artículo en el cual se presentan los resultados de un estudio de trampas de sedimento en el Mar de Alborán, que sirvió al doctorando como introducción a la investigación con microfósiles.

- Hernández-Almeida, I., Bárcena, M.A., Flores, J.A., Sierro, F.J., Sanchez-Vidal, A., Calafat, A., 2011. Microplankton response to environmental conditions in the Alboran Sea (Western Mediterranean): One year sediment trap record. *Marine Micropaleontology*, 78(1-2): 14-24.

Los siguientes anexos incluyen de forma detallada los listados de figuras y tablas, abreviaturas, y especies de radiolarios y foraminíferos planctónicos identificados en este estudio, así como los protocolos de limpieza para elementos traza, digestión total de sedimento y digestión secuencial de fósforo, utilizados en el desarrollo de esta Tesis.

OBJETIVOS

El objeto fundamental de la realización de esta Tesis Doctoral es aumentar el conocimiento acerca de las variaciones climáticas y oceanográficas que tuvieron lugar en el Atlántico Norte a escala orbital y suborbital durante el Pleistoceno Inferior y Medio, de su dinámica y de sus posibles causas. Para desarrollar este objetivo principal se han planteando una serie de objetivos particulares, los cuales son:

- Determinar con exactitud el marco cronoestratigráfico que permita situar los resultados obtenidos en un contexto paleoceanográfico y paleoclimático global y que permita la correlación con testigos oceánicos próximos.
- Estudiar los cambios ocurridos en las asociaciones de foraminíferos planctónicos y radiolarios en la zona de estudio en relación con las variaciones en la circulación del agua superficial, y determinar que factores controlan los cambios en la productividad primaria en el Atlántico Norte.
- Entender el comportamiento de las grandes masas de hielo continental mediante el estudio de aportes de IRD a los sedimentos de la zona de *Gardar Drift* y de indicadores de volumen de hielo (isótopos de oxígeno en foraminíferos bentónicos).
- Conocer el comportamiento de la circulación profunda en el Atlántico Norte mediante el análisis de isótopos de carbono y oxígeno en foraminíferos bentónicos, principalmente, con el objetivo de monitorizar la intensidad de la circulación termohalina y la mayor o menor influencia de aguas antárticas en la región.
- Realizar un estudio de la composición geoquímica y mineralógica del sedimento que permita reconstruir los procesos implicados en el transporte y acumulación de partículas en el *Gardar Drift*, e identificar posibles áreas fuente.
- Elaborar un registro de paleotemperatura del agua superficial para el periodo estudiado basándonos en las asociaciones de foraminíferos planctónicos y en el análisis de la relación Mg/Ca medida en la concha de estos organismos.
- Identificar la existencia de patrones de variabilidad climática orbital y suborbital y de los mecanismos subyacentes que originan esas ciclicidades, así como las posibles inferencias de procesos de retroalimentación a escala regional y global.
- Evaluar los principales cambios climáticos que acontecieron en la región del Atlántico Norte subpolar durante la Transición del Pleistoceno Medio, y su relación con otras evidencias presentes en el registro geológico global para ese mismo período.

TABLA DE CONTENIDOS

Capítulo 1

INTRODUCCIÓN

INTRODUCCIÓN

1. OCÉANOS Y CLIMA

Los océanos son una parte integral del sistema climático de la Tierra. Actualmente, está ampliamente aceptado por la comunidad científica que los océanos son uno de los sistemas más vulnerables a los efectos del cambio climático global inducido por las actividades antrópicas. Esto se debe al importante papel que juega la circulación oceánica, superficial y profunda, regulando el clima. Los océanos almacenan gran cantidad de calor, dióxido de carbono y vapor de agua, por lo que tienen un efecto regulador en el calentamiento invernadero inducido por la actividad antrópica. Quizás por esta creciente sensibilidad hacia los cambios medioambientales y su repercusión en nuestra sociedad (IPCC, 2001), o por el puro interés de avanzar en un campo científico tan inexplorado como el de la paleoclimatología, la comunidad científica ha reconstruido una serie de registros climáticos básicos para entender como el clima de la Tierra ha variado de forma natural en el pasado. Por esto, con el fin de profundizar en la naturaleza de la relación entre circulación oceánica y cambio climático, la paleoclimatología emerge como la ciencia dedicada al estudio de procesos climáticos en el pasado. Iniciativas científicas llevadas a cabo durante las últimas décadas, como el *Climate: Long Range Interpreation Mapping and Prediction* (CLIMAP), *Greenland Ice-Core* Project (GRIP) o el *Integrated Ocean Drilling Program* (IODP), han producido un gran número de registros fiables de la variabilidad climática en el pasado, y han revelado las fuertes conexiones existentes entre los componentes del clima (Fig. 1.1). Una mejor comprensión de las fuerzas que originan los cambios climáticos, como responden los componentes del sistema climático a estas fuerzas e interacciones y mecanismos de retroalimentación entre los mismos, puede ayudarnos a anticipar, solventar y/o mitigar futuras consecuencias derivadas de la situación climática actual.

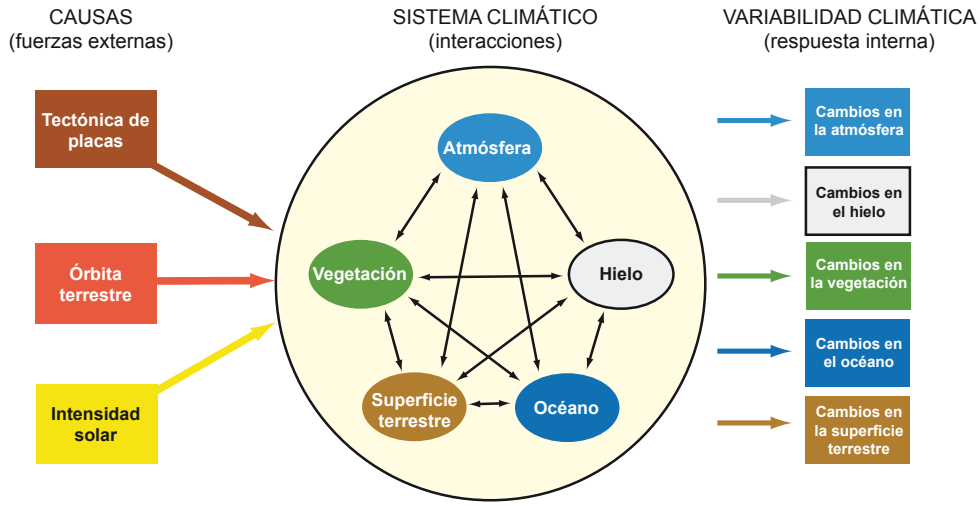

Figura 1.1. Representación de los componentes del sistema climático e interacciones entre sus componentes, factores que los modifican y posibles variaciones climáticas. Basado en Ruddiman (2001).

2. PALEOCLIMA Y ASTRONOMÍA

2.1. Variaciones climáticas orbitales: los ciclos de Milankovitch

El registro geológico mundial ofrece claras evidencias de la existencia de movimientos episódicos de avance y retroceso de las masas de hielo continentales durante el Período Cuaternario, las cuales se corresponden con saltos del sistema climático global entre glaciales (con aumento de las masas de hielo) e interglaciales (con un clima similar o incluso más cálido al actual). A lo largo del último millón de años, el registro de estas variaciones climáticas ha demostrado que los sucesivos ciclos glaciales-interglaciales han ocurrido siguiendo una cuasi-periodicidad de 400.000 y 100.000 años, superimpuesta a ciclos de menor amplitud pero mayor frecuencia de 41.000 y 21.000 años, aproximadamente. Estas ciclicidades presentan una alta correspondencia con las diferentes frecuencias de los ciclos astronómicos de radiación solar predichos por el astrónomo serbio Milutin Milankovitch (1941). Los tres tipos de oscilaciones de la órbita terrestre como moduladores del clima planteados en el trabajo de Milankovitch son los mostrados en la figura 1.2.

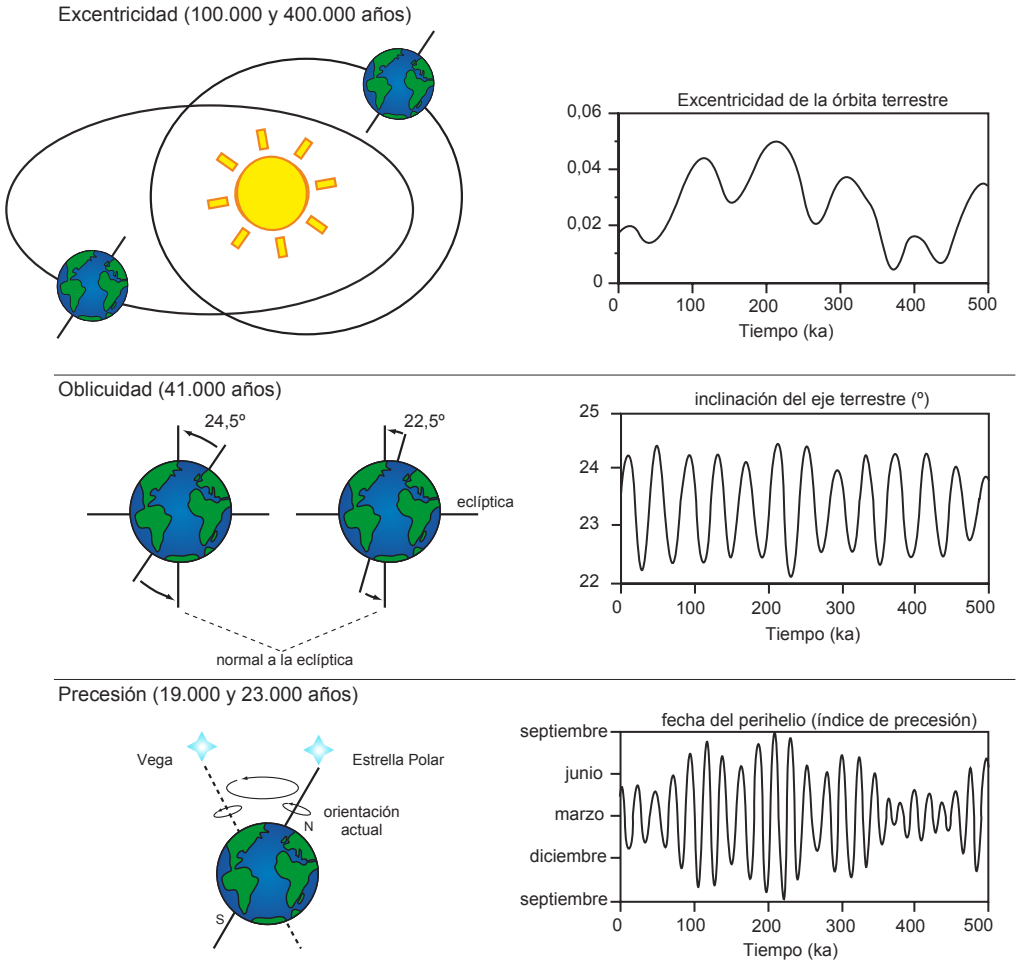

Figura 1.2. Componentes orbitales terrestres que influyen en la cantidad de radiación solar que recibe nuestro planeta. A la izquierda, los diferentes parámetros orbitales predichos por Milankovitch. A la derecha, registro de los mismos parámetros durante los últimos 500.000 años, de acuerdo al método de Laskar (2004), obtenidos con el programa *Analyseries 2.0*. (Paillard , 1996).

De una forma amplia, esta teoría afirma que los cambios de los parámetros orbitales y rotaciones de la Tierra son suficientes para inducir significantes cambios en la distribución estacional y latitudinal de radiación solar recibida, y por lo tanto, de forzar la variabilidad climática glacial-interglacial tal y como se observa en el registro geológico. El análisis espectral de la curva LR04 corrobora lo expuesto anteriormente (Fig. 1.3). El análisis revela que los ciclos que se repiten corresponden a las frecuencias de 100.000, 41.000 y 21.000 años predichas por Milankovitch, y demuestra que las variaciones en la insolación solar son la causa principal de los cambios climáticos del Cuaternario (Imbrie *et al.*, 1992). Sin embargo, la relación exacta entre variaciones en insolación y cambios climáticos durante momentos puntuales de la historia del Cuaternario no parece poder ser explicada solamente a través de las teorías de Milankovitch. Estas discrepancias de los registros climáticos respecto de las ecuaciones astronómicas pueden ser explicadas por la intervención de otras variables en el sistema climático, como la concentración de gases invernadero en la atmósfera, tales como CO_2, CH_4, y/o por la influencia del albedo en cada momento, etc. (e.g. Denton *et al.*, 2010; Kennett *et al.*, 2000; Ruddiman, 2003; Shackleton and Pisias, 1985; Toggweiler *et al.*, 2006). Asimismo, algunos cambios climáticos no se producen hasta que no se superan unas condiciones umbral de insolación y volumen de hielo, como ocurre por ejemplo en los procesos que conducen a una deglaciación (Parrenin and Paillard, 2003).

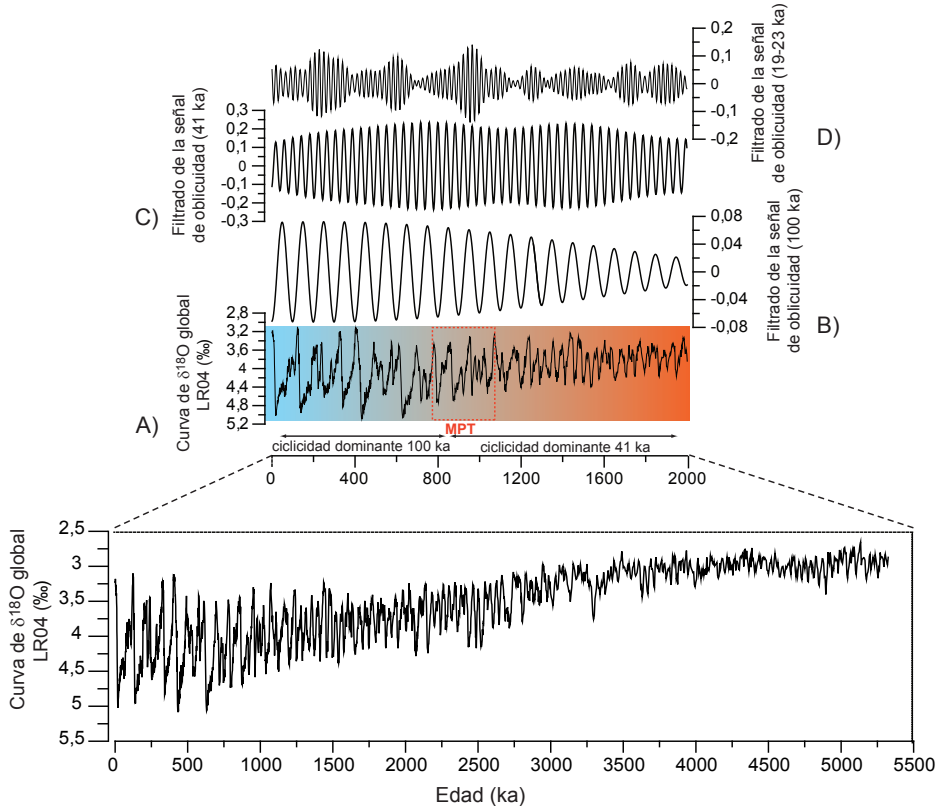

Figura 1.3. A) Curva de $\delta^{18}O$ bentónico global LR04 (Lisiecki y Raymo, 2005), como indicador de volumen de hielo y paleoclima. El intervalo encuadrado en rojo corresponde con la MPT, B) filtrado de las frecuencia de 100 ka en el registro LR04,C) 41 ka; y D) 23 ka. Se destaca el aumento de los valores de $\delta^{18}O$ durante la MPT y después, junto con el aumento de los ciclos de 100 ka.

2.2. Variaciones climáticas suborbitales: eventos Heinrich y oscilaciones Dansgaard/ Oeschger

Numerosas evidencias procedentes de archivos paleoclimáticos marinos y terrestres ponen de manifiesto la existencia de cambios climáticos con una frecuencia mayor que la que puede ser explicada a través de la respuesta lineal a los cambios cíclicos de la geometría orbital de la Tierra predichos por Milankovitch. En lo que a la investigación paleoceanográfica se refiere, son los testigos marinos profundos y de hielo los que mejor captan esta variabilidad climática de alta frecuencia. Por ejemplo, durante el último ciclo glacial se han registrado variaciones en el $\delta^{18}O$ de testigos de hielo en Groenlandia, equivalentes a variaciones en la temperatura del aire entre 5 y 12 ºC, en escalas de tiempo de 2-3 ka (Dansgaard *et al.*, 1971; Oeschger *et al.*, 1984), mientras que en el Océano se produjeron oscilaciones de la temperatura del agua superficial en ritmos de 1-2 ka que han quedado registradas en diferentes testigos del Atlántico Norte y del Mediterráneo (Bond *et al.*, 1997; Cacho *et al.*, 1999; van Kreveld *et al.*, 2000), así como descargas masivas de agua de fusión de los hielos al océano junto con bruscos descensos de las temperaturas del océano superficial, cada 5-10 ka (Bond *et al.*, 1993; Bond and Lotti, 1995; Heinrich, 1988) (Fig. 1.4) Estos eventos se han pasado a denominar ciclos Dansgaard-Oeschger (D-O) y eventos Heinrich (H), respectivamente (Bond *et al.*, 1992; Broecker *et al.*, 1992; Grootes *et al.*, 1993). El origen de estas oscilaciones climáticas suborbitales no está claro del todo. Se han barajado varias hipótesis, desde los procesos ligados a la dinámica interna de las masas de hielo continental (Clarke *et al.*, 1999; MacAyeal, 1993a; MacAyeal, 1993b), a la acción de fuerzas externas relacionadas a cambios seculares en los parámetros orbitales de la Tierra (Broecker *et al.*, 1990). Registros paleoclimáticos a alta resolución han demostrado que esta variabilidad milenaria no está circunscrita a períodos glaciales, sino que también son un rasgo común de periodos caracterizados por registrar temperaturas altas y estables, como el Holoceno o el último período interglaciar (Bond *et al.*, 2001; Bond *et al.*, 1997; deMenocal *et al.*, 2000; Mayewski *et al.*, 2004; Oppo *et al.*, 2001).

La amplitud de estas variaciones climáticas cambió a lo largo del registro geológico (Weirauch *et al.*, 2008), y como se ha demostrado recientemente con estudios que abarcan registros temporales anteriores al millón de años, han venido ocurriendo con la misma frecuencia que en escalas de tiempo más recientes, a pesar de que las condiciones de volumen de hielo global han variado considerablemente durante el Período Cuaternario (Bartoli *et al.*, 2006; Bolton *et al.*, 2010; Grützner and Higgins, 2010; Hayashi *et al.*, 2010; McIntyre *et al.*, 2001; Raymo *et al.*, 1998).

Por último, aunque estos eventos se describieron inicialmente en el Atlántico Norte y parecían estar limitados a esta región, se ha demostrado con posterioridad que los efectos de esta variabilidad milenaria son claramente identificables en otras regiones del planeta (e.g. Burns *et al.*, 2003; Hemming, 2004; Leuschner and Sirocko, 2000; Overpeck and Cole, 2006; Schulz *et al.*, 1998; Zhao *et al.*, 1995), demostrando que las teleconexiones existentes entre zonas remotas de lplaneta

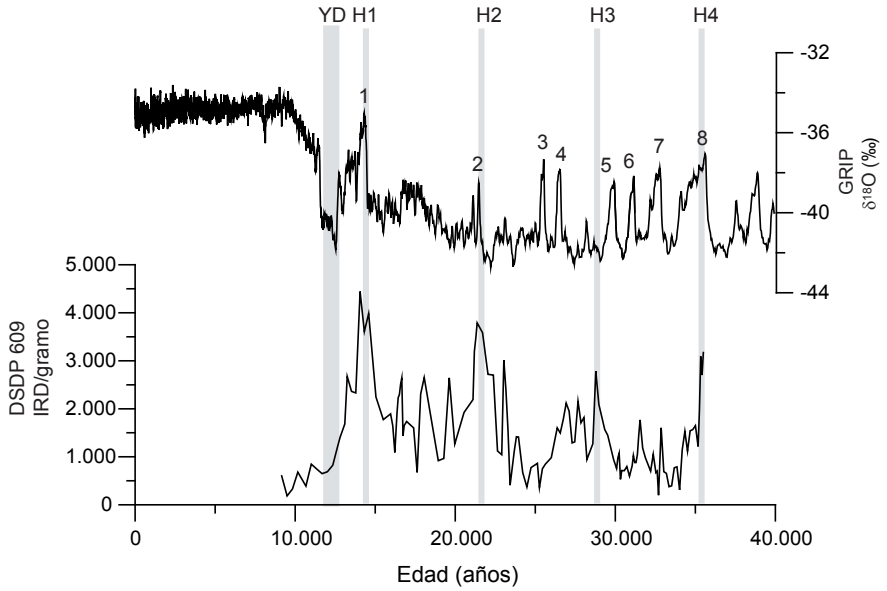

Figura 1.4. A) Registro de $\delta^{18}O$ del testigo de hielo de Groenlandia GRIP, mostrando 8 de los 25 eventos Dansgaard-Oeschger (D-O) observados durante el último periodo glacial (Grootes et al., 1993), B) registro de IRD/g durante los eventos Heinrich en el mismo periodo de tiempo, observados en un testigo profundo del Atlántico Norte (Bond y Lotti, 1995).

3. EVOLUCIÓN CLIMÁTICA DURANTE EL PLEISTOCENO

Para comprender los mecanismos que han controlado la variabilidad climática a lo largo de la historia de la Tierra, es necesario hacer especial hincapié en el Pleistoceno Inferior y Medio, ya que representa un intervalo temporal crucial para entender el clima. El clima durante el Pleistoceno ha variado en tiempo y espacio dejando gran cantidad de evidencias tanto en continentes como en océanos. Éstas reflejan la evolución del sistema climático durante los últimos 2,5 Ma, más o menos el mismo límite que el correspondiente a la actual configuración de océanos y continentes, localización y altura de grandes cadenas montañosas (e.g. Tibet) y pasajes inter-oceánicos (e.g. Estrecho Panamá). Un intervalo crucial del Pleistoceno, de intensa reorganización climática, es el comprendido entre 1,2 Ma (Pleistoceno Inferior y Medio) y 0,5 Ma (Pleistoceno Superior), el cual se conoce como Transición del Pleistoceno Medio (*Mid-Pleistocene Transition*, MPT) (Berger and Jansen, 1994b). Mientras que la ciclicidad climática del Pleistoceno Inferior y Medio estuvo en gran parte dominada por los ciclos de oblicuidad de 41 ka, estos fueron progresivamente reemplazados por una ciclicidad de excentricidad de 100 ka, caracterizada por oscilaciones climáticas de mayor amplitud, que permitió una mayor acumulación de hielo en las masas continentales del Hemisferio Norte (Fig 1.3). Esta reconfiguración del sistema climático produjo ciclos glaciales asimétricos, caracterizados por un periodo de lento incremento de volumen de hielo hacia condiciones de máximo glacial, interrumpidas por un rápido período de desglaciación y giro del sistema hacia condiciones más cálidas. La variabilidad glacial-interglacial de los últimos ciclos climáticos es el resultado último de la evolución climática experimentada durante la MPT.

Dada la interconexión entre los diferentes componentes del sistema terrestre (atmósfera, biosfera, geosfera, criosfera y biosfera), un cambio climático de la magnitud del experimentado durante la MPT dejó una profunda huella a nivel global claramente identificable en el registro sedimentario: rápidos avances de glaciales continentales sobre Europa Central (Haeuselmann *et al.*, 2007; Muttoni *et al.*, 2003), crecimiento de la capa de hielo de Norte América (Barendregt and Irving, 1998), cambios en ecosistemas/biotas marinos y terrestres (Kawagata *et al.*, 2005; Marino *et al.*, 2008; O'Regan *et al.*, 2005; Potts and Deino, 1995; Schefuß *et al.*, 2003; Shimada *et al.*, 2008; Wang *et al.*, 2000), variaciones en los patrones de circulación oceánica superficial y profunda, así como en la dinámica atmosférica (Ferretti *et al.*, 2005; Kleiven *et al.*, 2003; McClymont *et al.*, 2008; Raymo *et al.*, 1997; Schmieder *et al.*, 2000; Wright and Flower, 2002) y aumento en la aridez global (deMenocal, 1995; Heslop *et al.*, 2002; Larrasoaña *et al.*, 2003; Trauth *et al.*, 2009), la cual tuvo un especial impacto en los cambios evolutivos y dispersión geográfica de los homínidos hacia latitudes altas de Asia y Europa (Dennell, 2004; McNabb, 2005; Muttoni *et al.*, 2010; Palombo, 2009).

Aunque las consecuencias de la MPT están bien identificadas, la causa y/o origen que desencadenó este cambio climático no está tan clara. Se han propuesto diferentes hipótesis que apuntan a distintos mecanismos de retroalimentación interna del sistema climático terrestre como causantes del cambio, especialmente la reorganización del sistema climático se habría producido al sobrepasarse un cierto umbral crítico durante la MPT. Entre las hipótesis que se han propuesto están las siguientes: variación de niveles de CO_2 y/o gases invernadero en la atmósfera (Medina-Elizalde and Lea, 2005; Ruddiman, 2003; Tziperman and Gildor, 2003), transformación del lecho rocoso en el que se asienta el hielo continental en Norte América (Clark and Pollard, 1998), elevación de la topografía del fondo marino en el Mar de Groenlandia con efecto en la formación de aguas profundas y transporte de humedad a altas latitudes (Denton, 2000), o un descenso gradual en las temperaturas globales (Zachos *et al.*, 2001).

4. CIRCULACIÓN ATMOSFÉRICA, OCEÁNICA Y PALEOCEANOGRAFÍA DE LA ZONA DE ESTUDIO

El Atlántico Norte es una de las regiones de la Tierra más sensibles a los cambios climáticos debido a que cualquier cambio ocurrido en sus aguas tiene un impacto en la Corriente de Retorno Atlántica (*Atlantic Meridional Overturning Circulation*, AMOC), por lo que cualquier fluctuación en los parámetros que la componen (balance agua dulce/salinidad) conllevaría drásticos cambios en el clima global (Broecker *et al.*, 1990) (Fig. 1.5).

El rasgo más característico de la circulación atmosférica del Atlántico Norte es el sistema de altas presiones en las Islas Azores, que genera vientos de levante y una circulación oceánica superficial anticiclónica, y el de bajas presiones de Islandia, que produce vientos de poniente y es el responsable del giro oceánico subpolar en el Atlántico Norte (Barry and

Chorley, 2003). Este último sistema de bajas presiones funciona de forma permanente durante todo el año, aunque su localización e intensidad pueden variar estacionalmente, principalmente de invierno, cuando los vientos de poniente alcanzan su máxima intensidad, a verano, cuando registran menos actividad. Además, el clima del Atlántico Norte está fuertemente influenciado, especialmente en invierno, por la Oscilación del Atlántico Norte (*North Atlantic Oscillation*, NAO), que es un índice que se define como la diferencia en la presión atmosférica a nivel del mar entre los sistemas de presiones de Islandia y Azores. Las variaciones de la NAO (positivas o negativas) tienen una marcada influencia en el clima desde Florida a Groenlandia y hasta en regiones más remotas como el norte de Asia o África (Visbeck *et al.*, 2001).

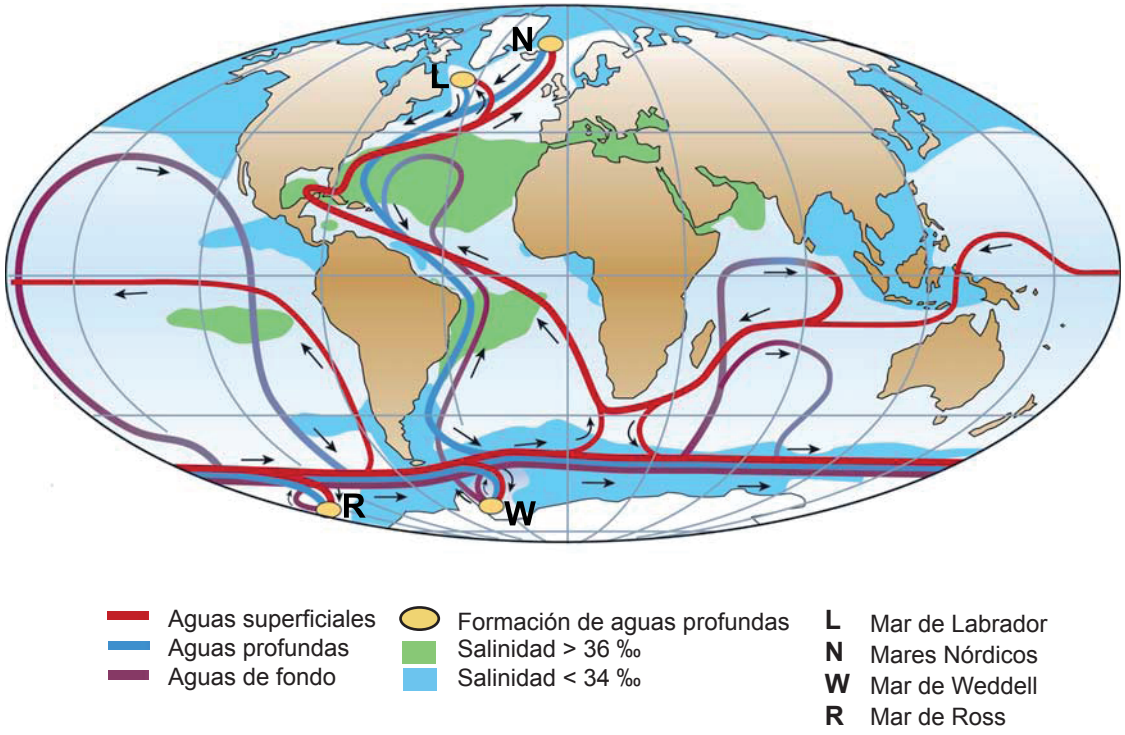

Figura 1.5. Esquema simplificado de la circulación termohalina del océano. Aguas cálidas (rojo) son transportadas superficialmente desde los trópicos a latitudes altas del Atlántico Norte, donde en contacto con masas de aire frías, se enfrían y ganan densidad suficiente para hundirse hacia el fondo del océano. Las aguas profundas (azul) recién formadas fluyen hacia el sur, rodean la Antártida y circulan por el fondo de todos los océanos, donde van mezclando hasta retornar de nuevo como una masa de agua cálida superficial a las zonas de hundimiento en el Atlántico Norte. Modificado de Rahmstorf (2002).

La hidrografía superficial actual del Atlántico Norte está fuertemente influenciada por el flujo hacia el norte de aguas cálidas Noratlánticas (*North Atlantic Current*, NAC), la cual cumple una acción de regulador climático suavizando las temperaturas de toda Europa noroccidental, en contraste con los inviernos más rigurosos del noreste americano. Estas aguas que tienen su origen en el calentamiento estacional de aguas en el Golfo de Méjico, viajan hacia el norte cruzando la dorsal meso-atlántica entre 53º N y 60º N, donde se bifurca y extiende longitudinalmente. Una de las ramificaciones, la denominada Corriente de Irminger (*Irminger Current*, IC), gira hacia el noroeste, constituyendo el giro subpolar, donde se mezcla

con aguas polares más frías de la corriente del este de Groenlandia (*East Greenland Current*, EGC) y del Labrador (*Labrador Current*, LC). La rama principal del flujo de la NAC sobrepasa la cordillera de Islandia-Faeroe para penetrar en los mares Nórdicos (Mar de Groenlandia, Noruega e Islandia), donde se convierte en la corriente de Noruega (*Norwegian Current*, NC) (Krauss, 1986) (Fig. 1.6). Otro rasgo característico del Atlántico Norte es que está sometido a las oscilaciones estacionales del Frente Ártico (*Arctic Front*, AF), que es el límite que separa las masas de aguas árticas, de las atlánticas que corresponden a la NC, y que delimita la máxima extensión invernal hacia el sur del hielo marino (Swift and Aagaard, 1981). A su vez, el Frente Polar (*Polar Front*, PF), separa las aguas árticas de de las aguas polares de la EGC, frías y de menor salinidad, y que delimitaría la mínima extensión de la banquisa de hielo en verano (Swift and Aagaard, 1981).

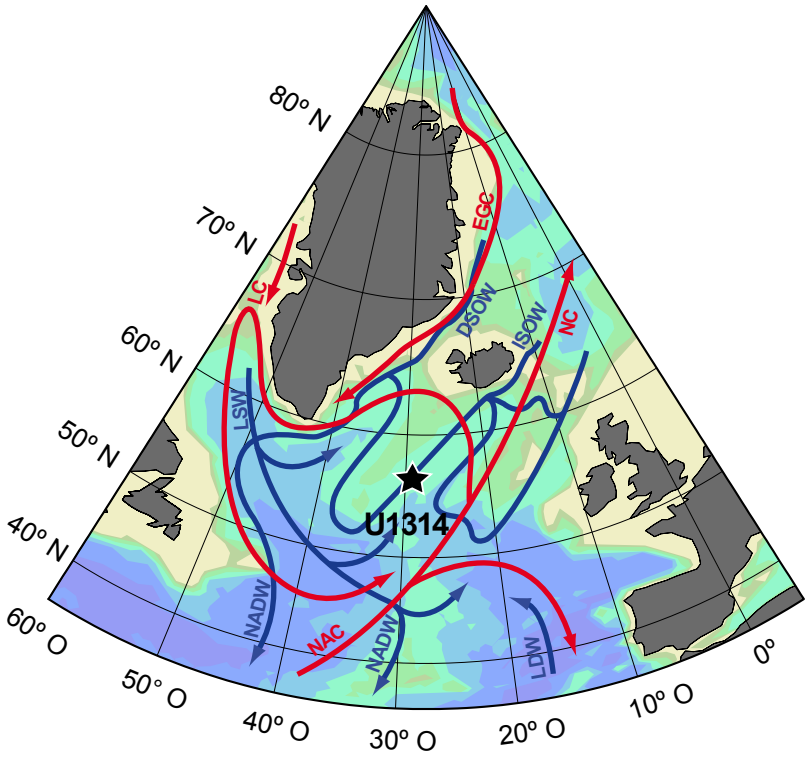

Figura 1.6. Localización de la perforación U1314 (estrella: 56º21'N, 27ºW; 2.820 m de profundidad), circulación superficial (rojo) y profunda (azul) en el Atlántico Norte (Krauss, 1986; Schmitz y McCartney, 1993). Mapa generado con el programa *Ocean Data View v.3.4.4.* (Schlitzer, 2008). *East Greenland Current* (EGC), *Norwegian Current* (NC), *Labrador Current* (LC), *North Atlantic Current* (NAC), *Denmark Strait Overflow Water* (DSOW), *Iceland Scotland Overflow Water* (ISOW), *Labrador Sea Water* (LSW), *North Atlantic Deep Wate*r (NADW), y *Lower Deep Water* (SSW).

El flujo hacia altas latitudes del Hemisferio Norte de las aguas salinas y cálidas de latitudes más bajas, es parcialmente compensado con el flujo de aguas densas que retornan hacia el sur en profundidad. Estas aguas profundas se forman en el invierno boreal por la pérdida de calor y hundimiento por convección de aguas superficiales atlánticas en zonas de hundimiento en la zona del Labrador y en los mares Nórdicos (Krauss, 1986; Schmitz and

McCartney, 1993) (Fig. 1.7). Las masas de agua más importantes son las que salen a través del estrecho de Dinamarca (*Denmark Strait Overflow Water*, DSOW) y por el de Islandia-Escocia (*Iceland-Scotland Overflow Water*, ISOW). Estos flujos se unen para formar una masa de agua profunda resultante que se denomina Agua Noratlántica Profunda (*North Atlantic Deep Water*, NADW), en la cual se diferencian dos componentes: uno superior, que ocupa los primeros 2.500 metros de la columna de agua, caracterizada por un mínimo contenido en silicatos y máximo en salinidad; y uno inferior, fluyendo a más de 2.500 metros de profundidad, caracterizado por su alto contenido en oxígeno disuelto (Kawase and Sarmiento, 1986). Mientras que la rama superior del NADW está compuesta por una mezcla de las aguas profundas formadas en la región del Mar de Labrador (*Labrador Sea Water*, LSW) y otras aguas intermedias que fluyen hacia altas latitudes, como las procedentes del Mediterráneo o de la Antártida, la rama inferior es una combinación de las aguas profundas originadas en los mares de Noruega y del Labrador, y del flujo hacia el norte de aguas antárticas profundas (*Lower Deep Water*, LDW) (McCartney, 1992; Schmitz and McCartney, 1993).

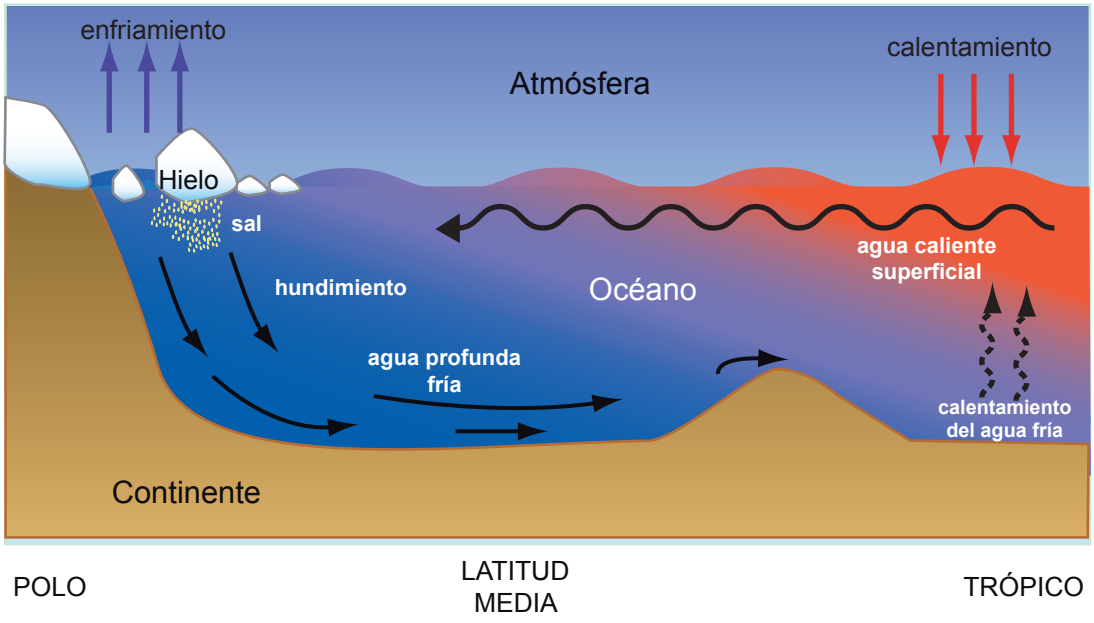

Figura 1.7. Representación esquemática de los procesos de hundimiento y movimiento de las masas de agua en la circulación termohalina.

Sin embargo, el registro geológico marino profundo ofrece numerosas evidencias de que esta geometría de las masas de agua profundas en el Atlántico Norte ha sufrido constantes variaciones. Durante la última glaciación, se produjo una interrupción en la producción de la rama inferior de la NADW debido a las condiciones de estratificación superficial por aporte al océano de aguas menos salinas como consecuencia de la fusión de hielo continental, descenso de temperaturas superficiales y formación de hielo marino que impedía la convección de aguas profundas en las zonas de hundimiento del Atlántico Norte (Broecker and Denton, 1990). Esta reducción en la ventilación del océano profundo desde latitudes altas del Hemisferio Norte es compensada con un aumento de aguas profundas ricas en nutrientes originadas en el océano

Antártico (*Antarctic Bottom Water*, AABW) (Curry and Oppo, 2005; Duplessy *et al.*, 1988; Oppo and Fairbanks, 1987; Oppo *et al.*, 1997; Oppo and Lehman, 1993; Oppo *et al.*, 1998) (Fig. 1.8). La densidad de la masa de agua formada en el Atlántico Norte era insuficiente para hundirse a gran profundidad, por ello, la masa de agua resultante, llamada Agua Glacial Intermedia Noratlántica (*Glacial North Atlantic Intermediate Water*, GNAIW), pasó a ocupar profundidades entre 1.000 y 2.000 m.

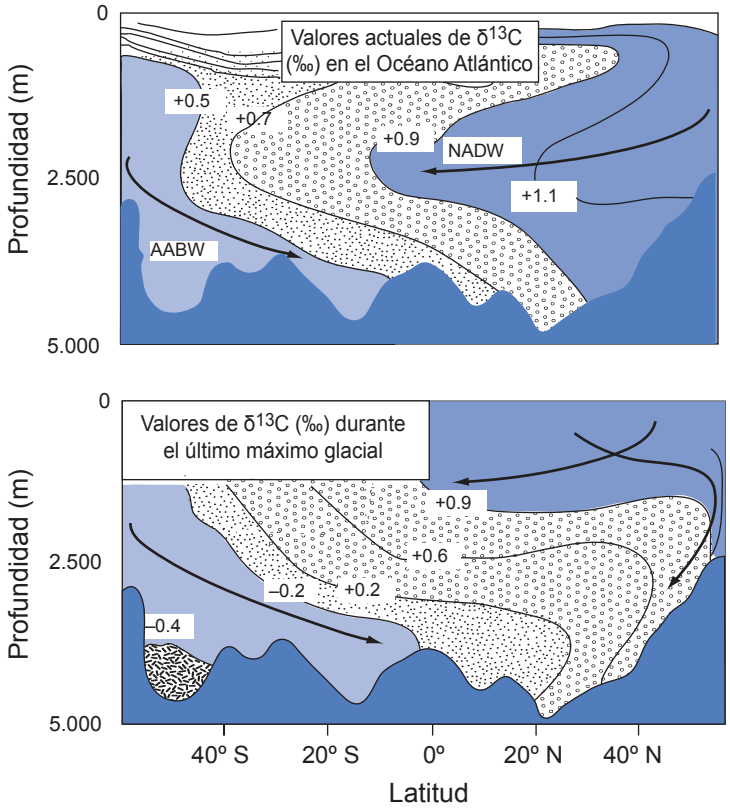

Figura 1.8. (arriba) Sección mostrando el valor de $\delta^{13}C$ (‰) a diferentes profundidades y latitudes en el Océano Atlántico en la actualidad, y durante el último máximo glacial (*Last Glacial Maximum*, LGM) (abajo). El valor de $\delta^{13}C$ está basado en el análisis de conchas de foraminíferos bentónicos. Las flechan muestran la las masas de agua NADW y AABW en la actualidad, y durante el LGM. Modificado de Duplessy *et al.* (1988).

5. LA FORMACIÓN *GARDAR DRIFT*

La formación *Gardar Drift* es un depósito contornítico de 1.100 km de longitud, situado en el flanco suroriental de la dorsal Reykjanes, en el margen occidental de la cuenca de Islandia. Esta zona de alta acumulación de sedimentos está ligada a los cambios en los patrones de circulación de aguas profundas en el Atlántico Norte (e.g. Dickson and Brown, 1994) y su forma y localización está controlado por la topografía del fondo oceánico y por los cambios en los aportes de sedimento (Johnson and Schneider, 1969; McCave and Tucholke, 1986). La principal fuente de material al *Gardar Drift* es el sedimento pelágico depositado por la ISOW originada en los mares Nórdicos (Bianchi and McCave, 2000).

Capítulo 2

MATERIALES Y MÉTODOS

MATERIALES Y MÉTODOS

1. IODP *Site* U1314

Para la realización de esta Tesis se han estudiado muestras de varios testigos extraidos en el IODP *Site* U1314, recuperado por el barco D/V *JOIDES Resolution* (Fig. 2.1) en la parte sur de la formación *Gardar Drift*, en el Atlántico Norte (56.36° N, 27.88° W, 2.820 m), durante la expedición oceanográfica 306 del IODP, en Abril de 2005. El *Site* U1314 se localiza en la cuenca de Islandia, la cual limita al oeste con la dorsal de Reykjanes, al este con el banco de Rockall, al norte con la dorsal de Islandia-Faeroes y al sur con la zona de fractura Charlie-Gibbs. Esta cuenca central separa la cuenca oriental de Rockall con la occidental de Irminger (Fig. 2.2).

Figura 2.1. Imagen del barco de exploración oceanográfica D/V *JOIDES Resolution*. Imagen tomada de la página web del IODP (http://www.iodp.org).

Con anterioridad a la expedición 306 del IODP, dos campañas del *Ocean Drilling Program* (ODP) ya recuperaron testigos en zonas de alta acumulación de sedimentos en la región sur de Islandia (Fig. 2.2). Durante las campañas 162 y 172 se recuperaron los testigos 980, 982, 983 y 984, que ya proveían evidencias de la variabilidad climática milenaria en el Atlántico Norte subpolar (Flower *et al.*, 2000; Kleiven *et al.*, 2003; McManus *et al.*, 1999; Raymo *et al.*, 1998; Raymo *et al.*, 2004). La diferencia y justificación de un nuevo testigo en esta región del Atlántico Norte es la necesidad de obtener un registro de la respuesta de las aguas superficiales a los eventos milenarios de descarga de IRD, y la de monitorizar los cambios en las masas de agua a profundidades entre 2.500 y 3.000 metros, condiciones ambas satisfechas con la recuperación del sondeo U1314.

En el *Site* U1314 se perforaron tres sondeos paralelos denominados A, B y C, alcanzando una longitud máxima de 279.91 metros bajo el nivel del mar (*meters below sea floor*, mbsf) en el sondeo B. Los testigos continuos se extrajeron mediante un sacatestigos de pistón múltiple. Los tres sondeos fueron correlacionadas a bordo usando diferentes propiedades físicas del sedimento con la finalidad de construir una sección compuesta sin hiatos ni interrupciones

para el testigo, la cual alcanza los 281 metros de profundidad compuesta (*meters composite depth*, mcd) (Channell *et al.*, 2006). La sección utilizada en el presente estudio es el tramo comprendido entre 60 y 84,16 mcd. La secuencia sedimentaria recuperada por el testigo U1314 se caracteriza por tener un alto contenido en material biogénico carbonatado, principalmente nanofósiles y foraminíferos, con una porción minoritaria de sílice biogénica, representada por diatomeas, radiolarios, y en menor medida, silicoflagelados, y terrígena, mayoritariamente minerales arcillosos detríticos con proporciones variables de material de grano más grueso cuarcítico y volcánico. Los sedimentos son predominantemente gris verdoso, con variaciones de matiz en bandeados de unas pocas decenas de centímetros (Fig. 2.3). Estos cambios de color se deben a cambios en la proporción relativa de material biogénico carbonatado y minerales detríticos arcillosos en el sedimento (Channell *et al.*, 2006).

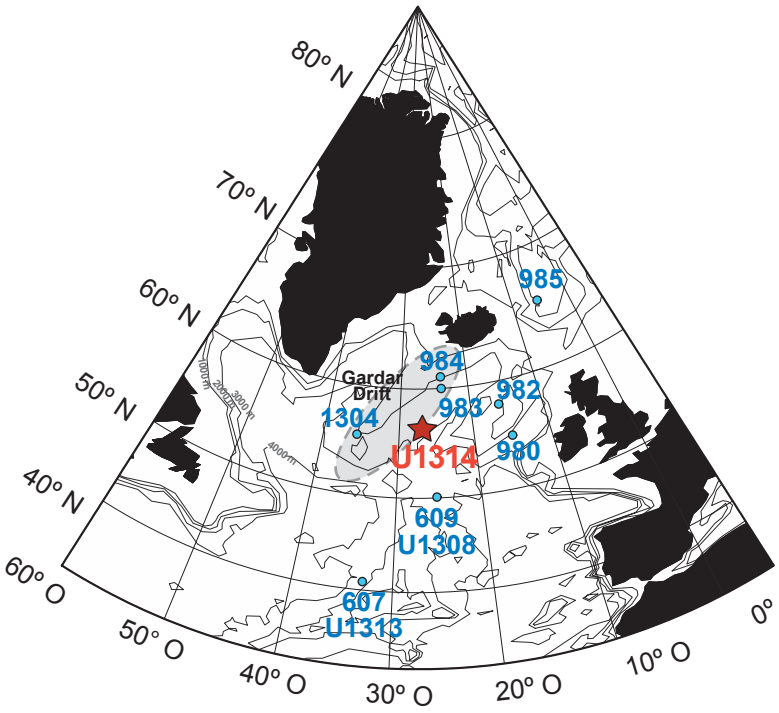

Figura 2.2. Localización de la perforación U1314 (estrella: 56º21'N, 27ºW; 2820 m de profundidad) y de otras perforaciones próximas del ODP. Mapa generado con el programa *Ocean Data View v.3.4.4.* (Schlitzer, 2008).

De acuerdo con los modelos cronoestratigráficos hechos de forma preliminar en el barco, la secuencia sedimentaria entre el Plioceno Superior y el Holoceno del testigo U1314 está caracterizada por tasas de sedimentación de 7 a > 11 cm/ka. La sección comprendida entre 60-84,16 m registra importantes eventos paleomagnéticos y bioestratigráficos, entre los que se incluyen el techo de Jaramillo (0,99 Ma), la inversión magnética Brunhes/Matuyama (0,78 ± 1) (Shackleton *et al.*, 1990), última aparición de *Neodenticula seminae* (0,84 Ma) (Koç *et al.*, 1999b), última aparición de *Reticulofenestra asanoi* (0,85 Ma) y primera aparición de *Gephyrocapsa parallela* (0,95 Ma) (Sato *et al.*, 1999), algunos de los cuales han sido de gran utilidad a la hora de elaborar el modelo de edad en el barco (Channell *et al.*, 2006) y en la presente Tesis Doctoral (ver Capítulo 2).

Adicionalmente, se realizaron en el barco una serie de medidas de diferentes propiedades físicas del sedimento como la radiación gamma natural, susceptibilidad magnética, densidad atenuada por rayos gamma, velocidad de ondas *P*, densidad y porosidad. Estos registros ofrecen interesante información acerca de procesos relacionados con cambios litológicos en el sedimento, y como ya hemos mencionado en el párrafo anterior, en la correlación estratigráfica de los tres sondeos perforados en el *Site* U1314. Para más detalles ver Channell *et al.* (2006).

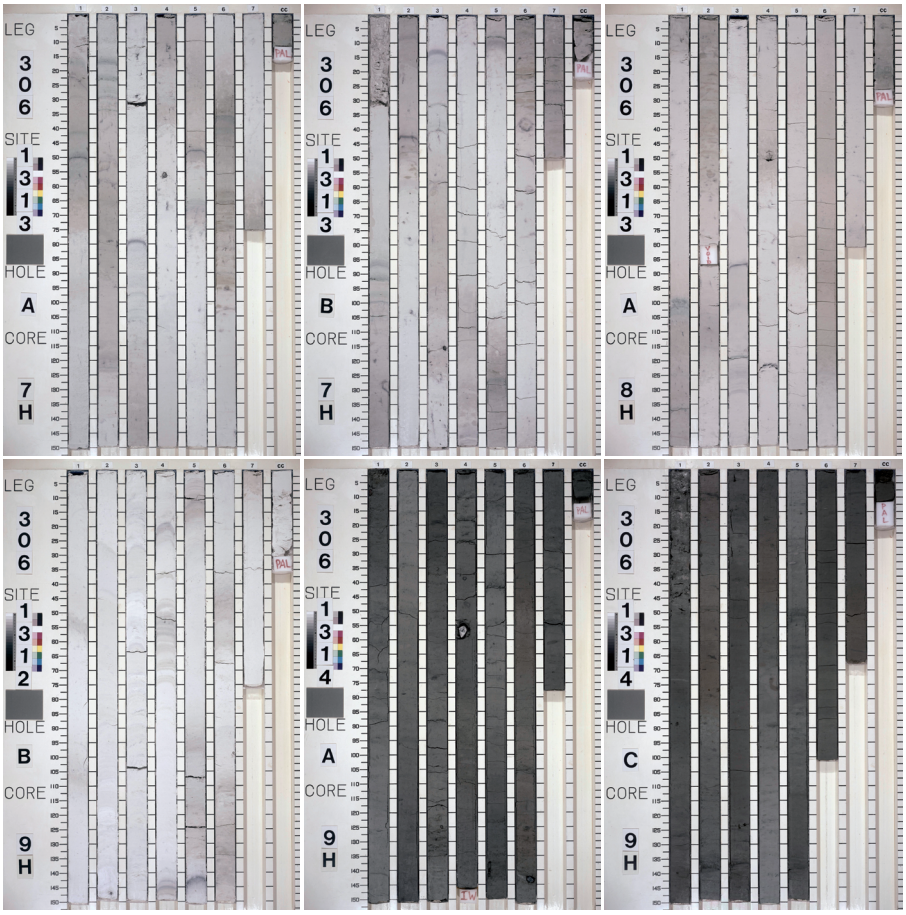

Figura 2.3. Imágenes de las secciones estudiadas del testigo U1314 en esta Tesis doctoral (Channel *et al.*, 2006).

2. INDICADORES PALEOCLIMÁTICOS

El presente trabajo es el resultado de la combinación de diferentes técnicas analíticas con el fin de elaborar un registro robusto de los parámetros y procesos oceanográficos y climáticos ocurridos en el Atlántico Norte durante el Pleistoceno Inferior y Medio. Para ello se han utilizado los siguientes paleoindicadores:

2.1. Asociaciones fósiles

Las asociaciones de organismos fósiles presentes en el registro sedimentario son excelentes indicadores de condiciones paleoambientales, incluyendo atributos tales como

cambios en nutrientes, salinidad, luz incidentes, oxígeno disuelto… En estudios con registros sedimentológicos oceánicos, son los organismos planctónicos marinos los seleccionados para realizar estas reconstrucciones paleoambientales. En nuestro caso, nos hemos centrado en las asociaciones fósiles de foraminíferos planctónicos y radiolarios, aunque otros organismos o restos de organismos (espículas de esponja, ostrácodos, diatomeas, foraminíferos bentónicos) también han sido tenidos en cuenta debido a que pueden proporcionar información complementaria de los medios en los que viven.

2.1.1. Foraminíferos planctónicos

Los foraminíferos planctónicos son protozoos que viven en la zona fótica de ambientes marinos. Los tamaños de individuos adultos oscilan entre 63 μm-1 mm de longitud. Estos individuos secretan una concha de carbonato cálcico multicamerada con una morfología y reconocible dependiendo de la especie (Fig. 2.4). La distribución geográfica de los foraminíferos planctónicos actuales está fuertemente controlada por las variables ambientales temperatura y salinidad, aunque la concentración de nutrientes en la columna de agua, densidad, CO_2 y O_2 disuelto, distribución de organismos simbiontes y disponibilidad de presas son también factores significantes. Información acerca de la distribución de foraminíferos planctónicos actuales se obtiene principalmente a través del uso de redes de plancton y trampas de sedimento. Estos estudios demuestran que las diferentes especies se distribuyen vertical y latitudinalmente. En la actualidad se pueden encontrar foraminíferos planctónicos en cualquier océano, ocupando generalmente los primeros 200 m de la columna de agua, y a temperaturas que van desde cerca del punto de congelación del agua del mar (~ -1.8 ºC) a las temperaturas más altas registradas en el océano superficial (~ 31 ºC) (Bé and Tolderlund, 1971).

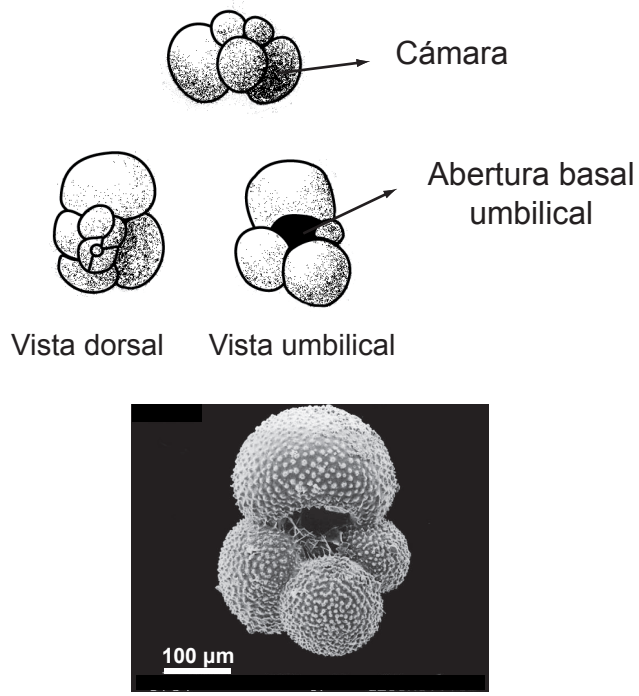

Figura 2.4. (Arriba) Representación desde diferentes vistas del foraminífero planctónico *G. bulloides*. (Abajo) Imagen de microscopio electrónico de barrido del foraminífero planctónico *G. bulloides*. Modificada del *Electronic Microfossil Image Database System* (EMIDAS): (http://www.emidas.org/).

Desde el punto de vista de distribución latitudinal, se distribuyen en asociaciones biogeográficas; tropical, subtropical, transicional, subpolar, y polar, que están distribuidas de una forma bipolar a ambos lados del ecuador (Fig. 2.5). Las asociaciones de foraminíferos planctónicos en regiones polares están dominadas por la especie *Neogloboquadrina pachyderma* con dirección de enrollamiento sinistrorso (sin.) (Bé and Tolderlund, 1971; Kucera *et al.*, 2005b; Pflaumann *et al.*, 1996). Esta especie vive a temperaturas por debajo de 10 ºC, aunque a 2 ºC se encuentra en concentraciones máximas (Bé and Tolderlund, 1971; Tolderlund and Be, 1971), y tolera un amplio rango de salinidades, proliferando incluso en zonas bajo proceso de formación de banquisa de hielo (Hemleben *et al.*, 1989). *N. pachyderma* sin. es más abundante entre los 50-100 m en la columna de agua, aunque numerosos estudios han observado que el proceso de calcificación de sus conchas tiene lugar a profundidades entre 100 y 200 m (Bauch *et al.*, 1997; Simstich *et al.*, 2003; Stangeew, 2001). Algunos trabajos han destacado la existencia de una forma de *N. pachyderma* sin. con morfología "encrustada", más pequeña y robusta, la cual ha sido considerada como ejemplares con una calcificación secundaria (Kohfeld *et al.*, 1996), o como un morfotipo diferente al normal.

Las regiones subpolares se caracterizan por altos contenidos en *Turborotalita quinqueloba*, *N. pachyderma* dextrorsa (dex.), *Globigerina bulloides*, *Globorotalia inflata*, *Globorotalia scitula* y *Globigerinita glutinada*.

T. quinqueloba es una especie típica subpolar, aunque también se puede encontrar en pequeños porcentajes en ambientes polares, que vive en aguas frías pero en un rango de temperaturas más cálidas que *N. pachyderma* sin., entre 4.6 y 12 ºC (Bauch, 1994; Bé and Tolderlund, 1971; Stangeew, 2001). Está asociado a condiciones de alta productividad, y al estar acompañado de algas simbióticas, su distribución está limitada a la zona fótica (Hemleben *et al.*, 1989; Simstich *et al.*, 2003). En altas latitudes del Atlántico Norte, esta especie ha sido frecuentemente usada como un paleoindicador de la proximidad del AF, debido a la alta productividad que caracteriza este ambiente (Johannessen *et al.*, 1994).

N. pachyderma dex. es una especie típica de masas subpolares y transicionales, con altas abundancias en torno a temperaturas entre 10 y 18 ºC, ocupando los primeros 100 m de la columna de agua en su estadio juvenil, y por debajo cuando es adulto (Bé and Tolderlund, 1971; Hemleben *et al.*, 1989; Tolderlund and Be, 1971). Se alimenta y desarrolla en la zona de mayor concentración de clorofila en la base de la zona eufótica. Aunque está asociado a sistemas de *upwelling*, estudios recientes en el Atlántico Norte han destacado su afinidad con aguas estratificadas durante los meses de verano (Fraile *et al.*, 2008).

G. bulloides es una especie superficial (vive en los primeros cien metros de la columna de agua), abundante tanto en zonas subpolares como de transición (Bé, 1977). La temperatura no parece un factor limitante en la distribución de esta especie, que aparece más dependiente de la concentración de productores primaros que son el alimento principal de esta especie. Por lo tanto, aparece en altas concentraciones en zonas de alta productividad (Hemleben *et al.*, 1989).

G. inflata es una especie transicional, aunque también puede aparecer en la asociación subpolar, siendo su rango de temperaturas entre 10.4 y 19.9 ºC (Bé, 1977; Bé and Tolderlund, 1971). Vive a cierta profundidad, por debajo del máximo profundo de clorofila, y es un componente importante de la asociación en los meses otoño e invierno (Hemleben *et al.*, 1989; Tolderlund and Be, 1971).

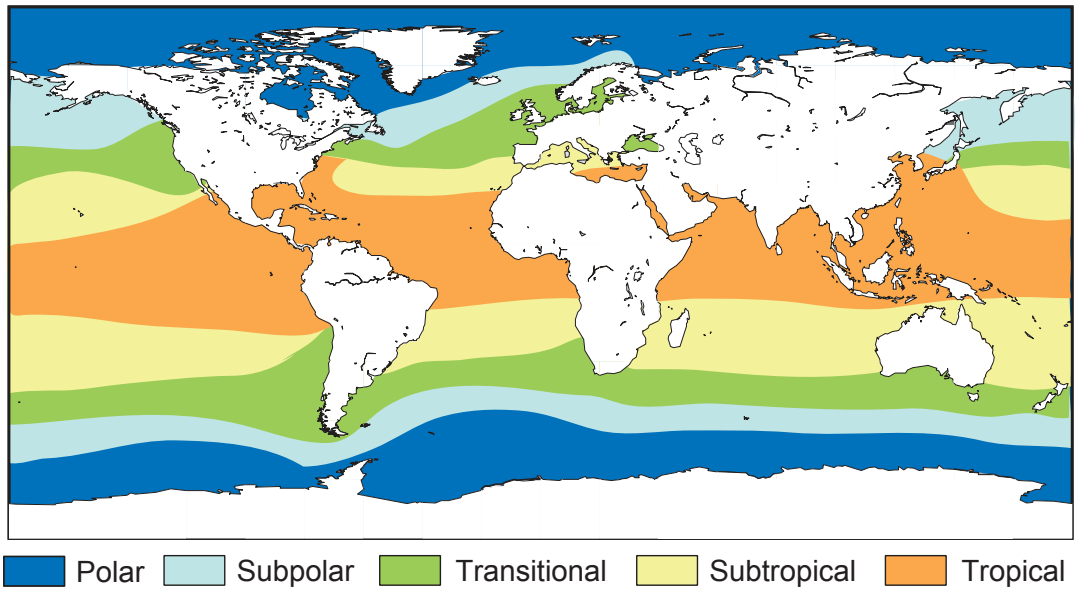

Figura 2.5. Distribución geográfica de foraminíferos planctónicos actuales agrupados por asociaciones biogeográficas. Modificado de Bé (1977).

Otras especies que aparecen en ambientes subpolares son *G. glutinada*, asociada a aguas con alta producitividad primaria, siendo las diatomeas su principal fuente de alimento (Hemleben *et al.*, 1989), y con *G. scitula*, especie que puede vivir por debajo de los 100 m en aguas frías (Bé, 1977). La diversidad aumenta en general hacia los trópicos, llegando a alcanzar entre 25-30 diferentes especies en asociaciones de océano abierto. En latitudes tropicales y subtropicales, las especies más abundantes son *Globigerinoides ruber*, *Orbulina universa, Globorotalia truncatulinoides, Globigerinlla siphonifera, Globorotalia hirsuta* y *Glogorotalia crassaformis*. Aunque presentes en las muestras del testigo U1314, estas especies aparecen en cantidades no significativas para ser tenidas en cuenta en el estudio de la asociación de foraminíferos planctónicos.

Al estar localizado a una profundidad por encima del nivel de compensación de calcita en el Atlántico Norte (> 4.000 m, e.g. Berger, 1970a), los sedimentos del testigo U1314 son ricos en foraminíferos planctónicos. Esto, unido a que las asociaciones de foraminíferos planctónicos son especialmente sensibles a las variaciones de distintos parámetros del agua superficial (temperatura, salinidad, nutrientes) (Bé, 1977; Hemleben *et al.*, 1989), los convierte en herramientas especialmente interesantes en estudios cuantitativos paleoceanográficos (e.g. Kellogg, 1977; Kucera *et al.*, 2005b; Pflaumann *et al.*, 1996).

2.1.2. Radiolarios

Los radiolarios son también protozoos exclusivamente marinos de esqueleto compuesto por sílice biogénica (ópalo), que se encuentran en todos los océanos del mundo ocupando un amplio rango de hábitats en cuanto a profundidad, temperatura, nutrientes, etc. La taxonomía de los radiolarios es muy variada y se agrupan en torno a dos grandes órdenes dependiendo de la simetría del esqueleto silíceo: orden *Nasellaria* radiolarios (simetría lateral) y orden *Spumellaria* (simetría bilateral) (Fig. 2.6).

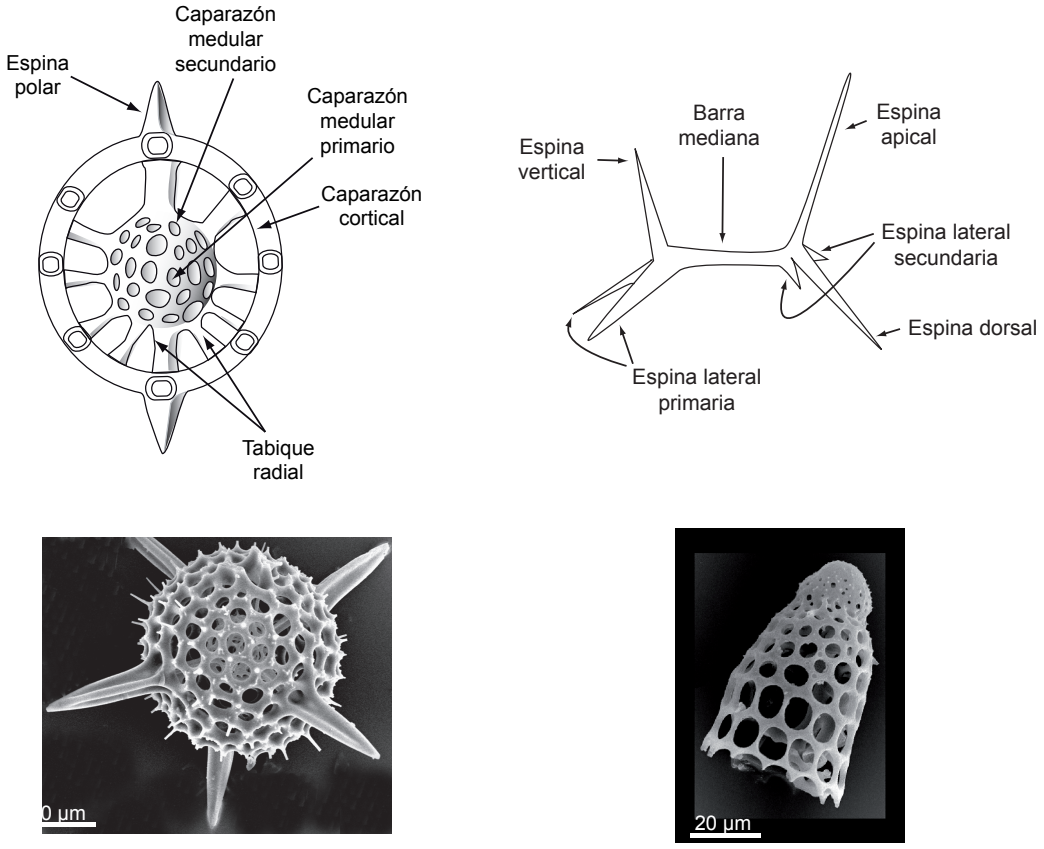

Figura 2.6. (arriba) Elementos fundamentales del esqueleto que caracterizan un radiolario de los órdenes *Nasellaria* (derecha) y *Spumellaria* (izquierda) Basado en Kling (1978). (abajo). Imagen de microscopio electrónico de barrido; *Hexacontium pachydermum* (izquierda) y *Artostrobus joergenseni* (derecha). Fotos cedidas por Jane K. Dolven (http://tolweb.org/tree/phylogeny.html).

Los radiolarios son importantes herramientas en la bioestratigrafía de sedimentos oceánicos (Morley and Hays, 1979), así como precisos indicadores de paleotemperaturas (Cortese *et al.*, 2003; Cortese *et al.*, 2005), paleoproductividad (Molina-Cruz, 1984) y de masas de agua (Bjørklund *et al.*, 1998; Itaki *et al.*, 2008), lo que los convierte en una excelente herramienta paleoclimática. Abundan en zonas de divergencia ecuatorial en todos los océanos, y aunque presentes en zonas de altas latitudes (Norte y Sur) reducen su abundancia en detrimento de las diatomeas (Boltovskoy *et al.*, 2010; de Wever *et al.*, 1994a; Lisitzin, 1972). Aunque la zona del Atlántico Norte donde está localizado el testigo U1314 no es de las más ricas en cuanto a contenido de radiolarios y sílice biogénica, cuenta con suficiente abundancia de estos

organismos como para realizar un estudio paleoceanográfico centrado en este grupo, como ya han constatado varios trabajos en la zona (Goll and Bjørklund, 1971; Matul, 1989a; Matul, 1989b; Matul, 1994a; Matul, 1994b; Matul and Yushina, 1999; Petrushevskaya and Bjørklund, 1974) (Fig. 2.7).

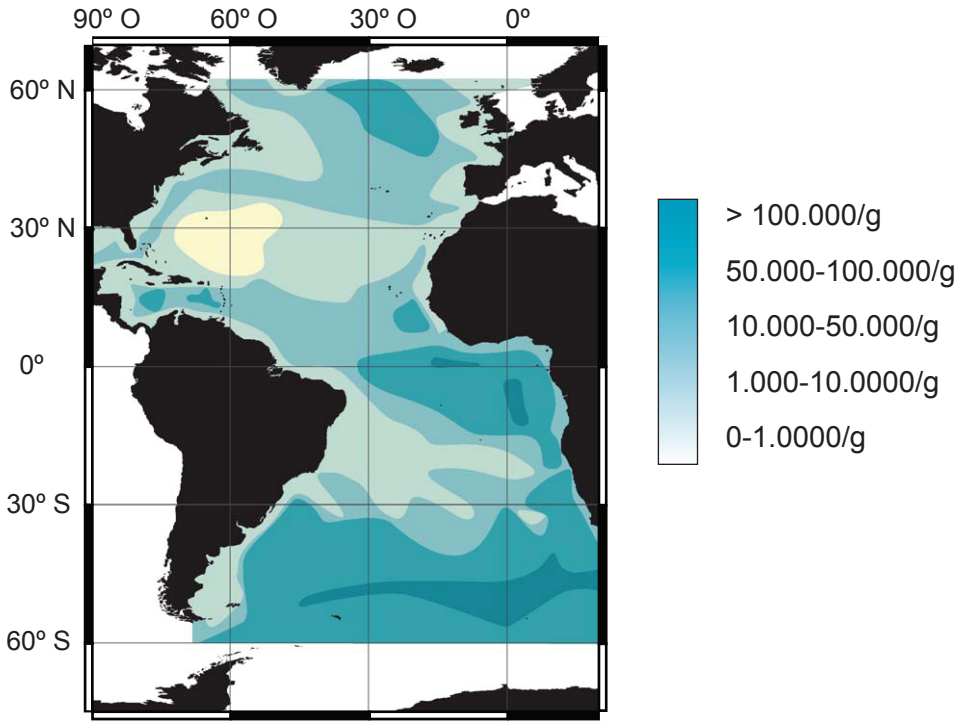

Figura 2.7. Abundancia de radiolarios en los sedimentos superficiales del Atlántico Norte. La acumulación de radiolarios (barra vertical) está expresada en esqueletos/gramo de sedimento. Modificado de Goll y Bjorklund (1971; 1974).

Actualmente, las especies más abundantes en altas latitudes del Atlántico Norte son: (Spumellaria) *Actinomma boreale, A. leptodermum/boreale, A. medianum, Larcospira minor, Phorticium clevei,* (Nassellaria) *Amphimelissa setosa, Artobotrys boreale, Lithomelissa setosa, Lithocampe platycephala, Pseudodictyophimus gracilipes, Cycladophora davisiana* y *Lithomitra lineata* (Bjørklund *et al.*, 1998; Cortese *et al.*, 2003). Su distribución espacial responde a la afinidad con las masas de agua superficiales e intermedias de la región, siendo agrupadas de este modo en:

Asociación de aguas noratlánticas: son especies distribuidas a lo largo de la trayectoria principal del NAC hacia el norte y transportadas desde latitudes subtropicales. Son muy abundantes en la zona de la dorsal de Reykjanes, al sur de Islandia, y aparecen con temperaturas > 8 ºC (Matul and Yushina, 1999). Pertenecen a este grupo *A. medianum* y *P. clevei*.

Asociación de aguas árticas y atlánticas: representan la mezcla y transformación de aguas noratlánticas con aguas más frías de latitudes altas, en su viaje hacia zonas de formación de aguas profundas en el Mares Nórdicos. Son más abundantes hacia el margen continental de Noruega. Dentro de este grupo, mientras que *P. gracilipes, L. setosa* tienen más afinidad

por la aguas calientes dentro del frente de mezcla de aguas superficiales, especies como *A. leptodermum/boreale, L. platycephala, L. lineata* aparecen asociados a zonas próximas a la banquisa de hielo (Molina-Cruz and Bernal-Ramirez, 1996).

Asociación de aguas árticas y polares: dominado por *A. setosa* y *C. davisiana*, esta asociación caracteriza el avance del AF hacia el sur, y la expansión de aguas salinas frías y poco salinas, con posible formación de hielo estacional (Matul, 1989b; Matul and Yushina, 1999).

2.2. Isótopos estables y relación Mg/Ca

La señal química obtenida de conchas o esqueletos de organismos presentes en el registro sedimentario puede proporcionar importante información acerca de diversos parámetros ambientales como temperatura o salinidad. En nuestro caso particular hemos aplicado estudios de isótopos estables y de paleotermometría basados en la relación Mg/Ca en la concha de foraminíferos. Estos organismos segregan una concha calcárea que es construida en equilibrio con el ambiente en el que viven, esto es, el análisis geoquímico de su concha proporciona una instantánea de la composición química de la masa de agua en la que vivían (suponiendo que esta concha permanezca inalterada y no haya sufrido procesos de alteración de recristalización post-diagenéticos).

Los isótopos estables más usados en estudios paleoclimáticos marinos con los de oxígeno (^{16}O y ^{18}O) y de carbono (^{12}C y ^{13}C) en conchas de foraminíferos planctónicos y bentónicos. Al realizar análisis de isótopos estables en foraminíferos planctónicos y bentónicos obtendremos un registro comparativo de las masas de agua superficial y profunda, con lo que podremos inferir ciertos procesos verticales que tienen lugar en la columna de agua, como la eficiencia del bombeo biológico (Broecker, 1971), estratificación de aguas (Bauch *et al.*, 2000).

La relación de un isótopo respecto al otro, la cual se puede medir de forma precisa mediante espectrometría de masas, se representa como ratio (δ) que se determina por comparación de la relación isotópica de la muestra con un estándar, y el resultado es un valor expresado en partes por mil (‰):

$$\delta^{18}O = \frac{(^{18}O/^{16}O)_{muestra} - (^{18}O/^{16}O)_{estándar}}{(^{18}O/^{16}O)_{estándar}} \times 1000$$

$$\delta^{13}C = \frac{(^{13}C/^{12}C)_{muestra} - (^{13}C/^{12}C)_{estándar}}{(^{13}C/^{12}C)_{estándar}} \times 1000$$

Actualmente, el estándar está referenciado al valor isotópica del agua marina, *Vienna Estándar Mean Ocean Water* (VSMOW).

2.2.1. Isótopos de oxígeno

El ratio $^{18}O/^{16}O$ de los foraminíferos también está afectado por las oscilaciones en el volumen de hielo continental. Cuando hay evaporación del agua del océano se condensa en forma de nubes en zonas altas de la atmósfera para luego precipitar en forma de lluvia o nieve (Fig. 2.8). Durante la primer parte del ciclo son las moléculas de agua con mayor contenido en el isótopo ligero ($H_2{}^{16}O$) las que se evaporan con más facilidad, enriqueciendo relativamente el vapor de agua atmosférico en el isótopo ligero. Durante la parte en la que esta agua retorna al océano (precipitación), es el isótopo pesado ($H_2{}^{18}O$) el que condensa preferentemente. Ambos procesos (evaporación y precipitación) reducen la cantidad de isótopo pesado respecto al ligero en la atmósfera. Cuando el vapor de agua con alto contenido en ^{16}O precipita como nieve en latitudes altas, ésta tendrá un bajo contenido en ^{18}O en relación al océano. En consecuencia, cuanto mayor sea el volumen de hielo continental, mayor será la proporción relativa de ^{18}O en el agua del océano y menor en el hielo continental. Los foraminíferos incorporan diferentes proporciones de ^{16}O y ^{18}O dependiendo de la temperatura del agua del mar en el que crecen; a menos temperatura, mayor es el ratio $^{18}O/^{16}O$ en el carbonato cálcico secretado. Aunque esta condición se cumple para todos los foraminíferos, el ratio $^{18}O/^{16}O$ varía dependiendo de la especie y del estadio ontogénico, por lo que es necesario seleccionar individuos lo más homogéneos posibles a fin de obtener una señal robusta.

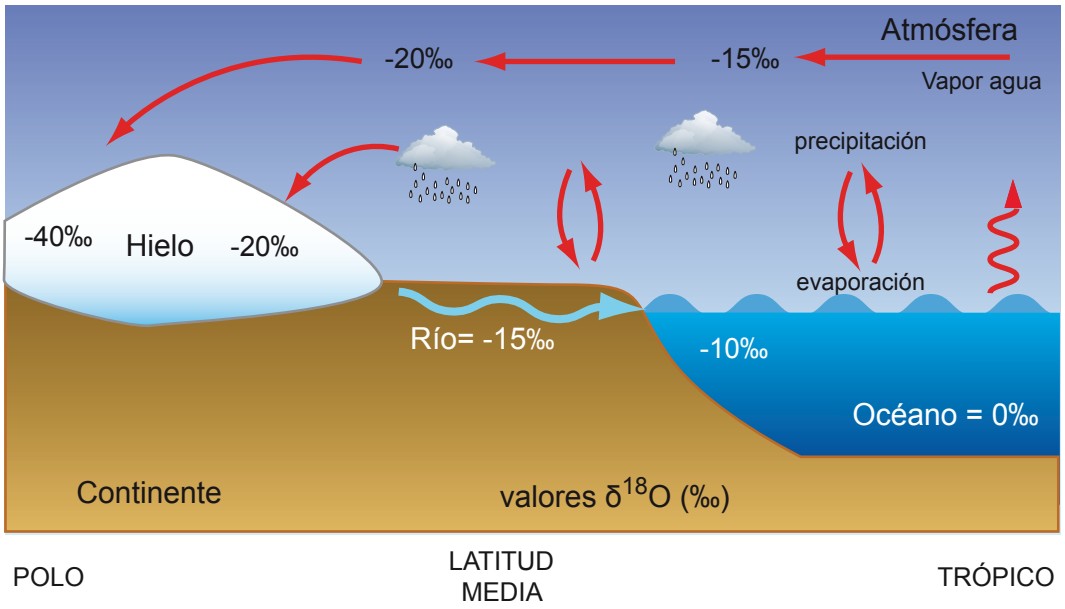

Figura 2.8. Fraccionamiento isotópico del oxígeno. Los sucesivos procesos de evaporación/precipitación hacen que el vapor de agua que va desde los trópicos hacia latitudes altas hace que se vaya enriqueciendo progresivamente en isótopo ligero (^{16}O). Este proceso hace que la nieve que precipita en los polos tenga valores de $\delta^{18}O$ muy negativos. Basado en Ruddiman (2001).

2.2.2. Isótopos de carbono

El carbono está presente en la naturaleza como una mezcla de dos isótopos, al igual que el oxígeno, uno muy abundante, ^{12}C, y otro mucho más raro, ^{13}C. En el océano, la actividad fotosintética discrimina el ^{13}C a favor del ^{12}C, por lo que la materia orgánica producida por organismos fotosintéticos marinos tiene valores altos de $\delta^{13}C$ relativo a la atmósfera e hidrosfera (Fig. 2.9).

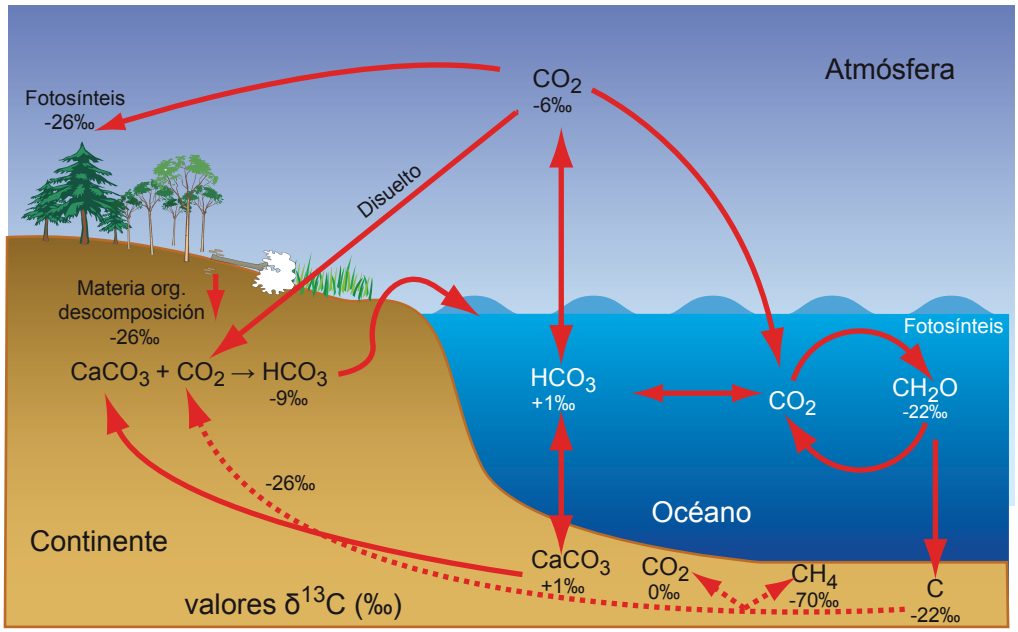

Figura 2.9. Representación esquemática y simplificada del ciclo del carbono orgánico e inorgánico en los sistemas terrestre y oceánico, con valores medios de $\delta^{13}C$ para las principales fases. Las flechas dobles indican equilibrio isotópico. Basado en Rohling y Cooke (2003).

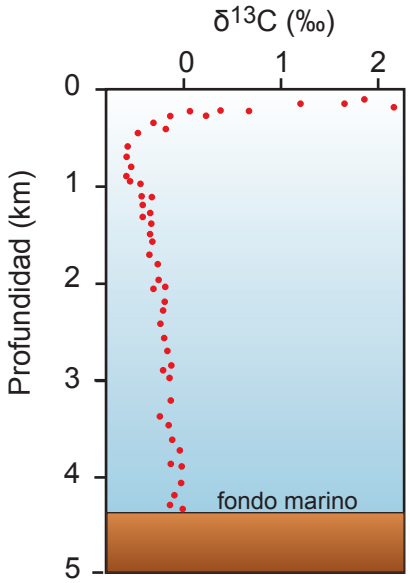

Figura 2.10. Perfil del $\delta^{13}C$ del carbono inorgánico disuelto en el océano. Basado en James (2005).

Un rasgo muy importante en el $\delta^{13}C$ de los océanos es la diferencia existente entre aguas superficiales y profundas. Mientras que las aguas superficiales están generalmente

empobrecidas en ^{12}C debido a que los productores primarios incorporan $^{12}CO_2$ durante los procesos fotosintéticos. Una vez mueren estos organismos y caen al fondo marino, la materia orgánica que contiene se oxida liberando ^{12}C que se acumula en aguas profundas (Rohling and Cooke, 2003) (Fig 2.10). Como consecuencia de estos procesos, el perfil batimétrico del $\delta^{13}C$ es inverso al contenido en nutrientes en el océano (fosfato); aguas superficiales con alto $\delta^{13}C$ (bajo ^{12}C) y bajo en fosfato, y bajo $\delta^{13}C$ y alto fosfato en aguas profundas (Broecker and Peng, 1982; Kroopnick, 1985).

Finalmente, al igual que ocurre con los isótopos de oxígeno, existen diferentes factores a tener en cuenta cuando se realizan estudios con isótopos de carbono en foraminíferos. El ratio $^{13}C/^{12}C$ es muy sensible a variaciones de hábitat (especialmente en los bentónicos) (McCorkle *et al.*, 1990), presencia de simbiontes fotosintéticos en algunas especies de foraminíferos (Rohling and Cooke, 2003) o a la advección de masas de agua con temperaturas diferentes (Johannessen *et al.*, 1994).

2.2.3. Relación Mg/Ca

El uso de técnicas basadas en el contenido en elementos traza en el esqueleto de organismos marinos ofrece un gran potencial a la hora de inferir las condiciones fisicoquímicas de los océanos en tiempos pasados. En este estudio, se ha utilizado la relación de Mg/Ca en la concha de foraminíferos planctónicos de la especie *Neogloboquadrina pachyderma* sin. para realizar una reconstrucción de paleotemperaturas. Este indicador se basa en la incorporación de Mg en la calcita biogénica. Esta reacción es sensible a la temperatura, por lo que la relación Mg/Ca de la calcita aumenta en proporción al incremento de la temperatura (Lea *et al.*, 1999; Rosenthal *et al.*, 1997b). Esta relación de Mg/Ca en la concha de los foraminíferos permite deducir las temperaturas superficiales a través de diferentes calibraciones, que varían según la especie utilizada y la región donde se vaya aplicar (Elderfield and Ganssen, 2000; Kozdon *et al.*, 2009; Lea *et al.*, 2002; Meland *et al.*, 2005; Nürnberg *et al.*, 1996a).

2.3. Evidencias sedimentológicas

La identificación y separación de los componentes del sedimento es una valiosa herramienta para caracterizar procesos oceánicos, como el transporte de sedimento al océano y redistribución del mismo por corrientes en el caso del material terrígeno. De acuerdo con las variaciones en la composición, tamaño de grano o flujo de material terrígeno al mar, se pueden inferir variables paleoambientales como velocidad y dirección del viento, aridez continental, actividad glacial y corrientes de fondo (Hemming, 2007). En regiones polares y subpolares, como en la que está localizado el testigo U1314, la fusión de grandes masas de hielo continental asociada con cambios climáticos abruptos libera una gran cantidad de material terrígeno al océano, llamado *ice-rafted-detritus* (IRD) (Bond *et al.*, 1992). La identificación de este material

es de gran importancia para los estudios paleoceanográficos en los que la dinámica de las masas de hielo juega un papel importante, ya que nos ayuda a reconstruir la distribución, extensión y flujo de masas de hielo y corrientes superficiales que transportaron ese material terrígeno (Fig. 2.11). El material que compone los IRD comprende un amplio espectro de tamaños de grano, desde arcilla a grava, aunque normalmente su presencia se relaciona con un aumento en el material tamaño arena (> 63 μm). Este material arenoso se encuentra en gran concentración en numerosas capas del registro sedimentario oceánico en el Atlántico Norte, en la región conocida como cinturón de IRD (Ruddiman, 1977). En el presente estudio, el uso de técnicas petrográficas (diagnosis de los tipos de minerales y/o rocas en el sedimento) y granulométricas (estudio de los tamaños de grano), han servido como indicadores de la procedencia del material terrígeno presente en las capas de IRD (ver revisión en Hemming, 2004), y han proporcionado información acerca del agente de transporte sedimentario (e.g. Bianchi and McCave, 1999; Prins *et al.*, 2002).

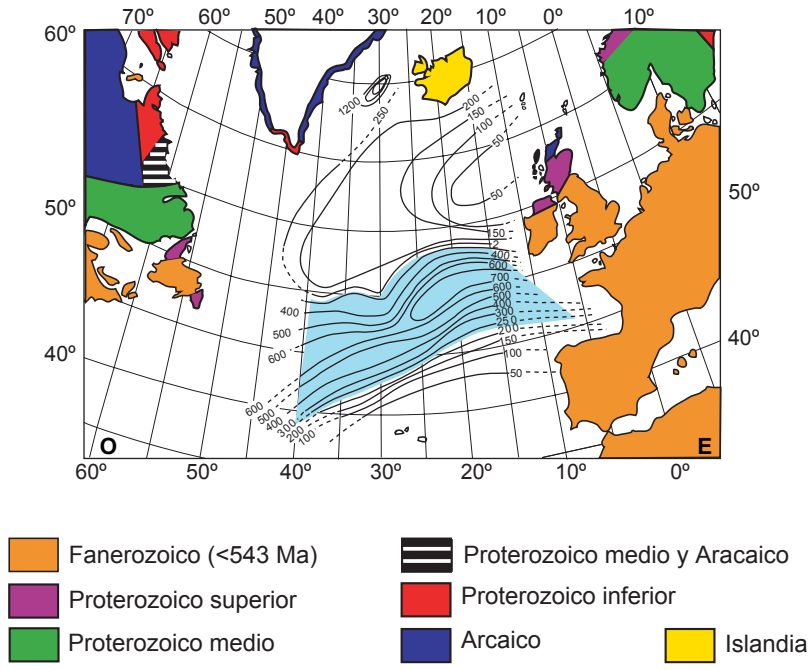

Figura 2.11. Mapa de flujo de IRD al Atlántico Norte entre 25-13 ka (LGM). Unidades están en mg/cm^2/ka de silicatos terrígenos en la fracción >63μm. La zona de mayor acumulación, denominada cinturón de IRD (Ruddiman, 1977), está coloreada de azul. Modificado de Ruddiman (1977).

2.4. Indicadores geoquímicos

El análisis geoquímico del registro sedimentario oceánico, en combinación con los otros indicadores descritos anteriormente, ofrece un enorme potencial a la hora de desarrollar una hipótesis más precisa sobre los procesos que tienen lugar a nivel oceánico (superficial y profundo), atmosférico y glaciológico. El contenido elemental de los sedimentos oceánicos es usado como indicador del modo de transporte y dirección del sedimento, circulación oceánica profunda, paleoproductividad y de procesos post-deposicionales en el fondo oceánico (e.g.

Dymond *et al.*, 1992; Grützner and Higgins, 2010; Hyun and Kim, 1999; Latimer and Filippelli, 2001). En esta Tesis, se ha procedido a realizar un amplio estudio de diferentes componentes geoquímicos del sedimento, que implica el uso de múltiples técnicas de laboratorio para su determinación. De forma resumida, los indicadores geoquímicos usados en esta Tesis son: determinación de carbono orgánico e inorgánico, sílice biogénica (ópalo), extracción secuencial de fósforo y análisis de concentración total para elementos mayores (Fe, Ca y Al) y menores (Mg, Mn, Zn, P, Ba, Ti, S y Sr).

3. TÉCNICAS Y PREPARACIÓN DE MUESTRAS

La selección de las muestras a estudiar se realizó utilizando la profundidad compuesta que combina los tres sondeos A, B y C. Los 24,16 m de testigo se muestrearon regularmente cada 4 cm, excepto donde se cambiaba de testigo y/o sección, que el muestreo era duplicado. El número total de muestras es de 624, representando cada muestra 2 cm de testigo. Las muestras, una vez secadas y pesadas para obtener el peso seco, fueron lavadas en húmedo a través de un tamiz de 63 μm para eliminar la fracción arcilla. Después, fueron nuevamente secadas en el horno, y luego tamizadas en seco con un tamiz de 150 μm, para luego pesar las fracciones resultantes (63-150 μm y > 150 μm).

3.1. Técnicas de estudio micropaleontológico y sedimentológico

Los análisis faunísticos en foraminíferos planctónicos y radiolarios, y de recuento de minerales terrígenos y otro tipo de partículas se realizaron en 326 muestras alternas. Dado que el uso de foraminíferos planctónicos de pequeño tamaño en general dificulta su identificación y es una labor tediosa, para minimizar errores debido a incertidumbres taxonómicas por el tamaño utilizado, y siguiendo consideraciones preestablecidas por CLIMAP *Project Members* (1976), se decidió utilizar la fracción > 150 μm en el presente estudio. La muestra se cuarteó utilizando un microcuarteador hasta obtener una alícuota con 400 individuos aproximadamente. Después, utilizando un microscopio estereoscópico se contaron foraminíferos planctónicos a nivel de especie, siguiendo los criterios taxonómicos de Hemleben *et al.* (1989) y Bé (1977), fragmentos, minerales autigénicos y fragmentos líticos separados según su naturaleza, radiolarios de gran tamaño, foraminíferos bentónicos, ostrácodos y espículas de esponja (Fig. 2.12).

En el estudio de radiolarios se utilizaron 299 muestras, diferentes de las usadas en el estudio de foraminíferos planctónicos y componentes líticos. Para separar y concentrar los esqueletos de radiolarios del sedimento se ha seguido la técnica de Goll y Bjorklund (1974), la cual explicamos a continuación brevemente. Las muestras de sedimento son secadas y entre 1-5 gramos de sedimento son tratados con una solución con 15% de H_2O_2 y HCl para eliminar materia orgánica y carbonato cálcico, respectivamente. Las muestras ya tratadas se lavaron en húmedo con un tamiz de 45 μm para eliminar la fracción arcilla y la materia orgánica, después

de lo cual se montaron dos tipos de láminas delgadas con "bálsamo de Canadá", una para cuantificar la concentración absoluta de radiolarios (lámina Q) y la otra para los recuentos relativos de especies (lámina F). En la lámina Q, además se determinaron dos índices de abundancia cualitativa de diatomeas y de IRD, que varían entre 0 (ausente) y 5 (muy abundante). En la lámina F, el censo de radiolarios se realizó a partir de 300 individuos identificados al nivel taxonómico más bajo cuando fue posible. Los criterios taxonómicos seguidos son los de Nigrini y Moore (1979), Bjørklund *et al.* (1998) y Hatakeda y Bjørklund (2009). La preparación de las láminas y el recuento se llevo a cabo en los laboratorios del Museo de Historia Natural de Oslo (Noruega).

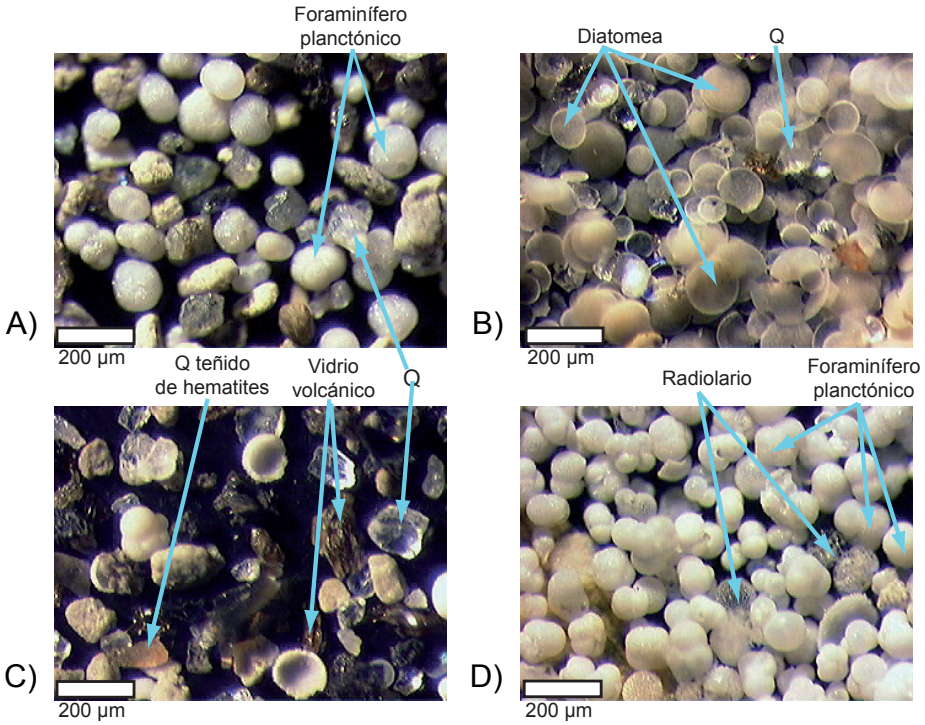

Figura 2.12. Imágenes de diferentes muestras del testigo U1314 tomadas a través de lupa binocular en las que se pueden observar los diferentes componentes líticos y biogénicos presentes en la fracción >150 µm. Profundidades de las muestras en mcd: A) 61,74 cm; B) 68,65 cm; C) 77,12 cm; D) 81,1 cm.

Por último, una parte del testigo (59 muestras entre 60-64,76 mcd) fue seleccionada para determinar la distribución mineralógica tipo que se puede encontrar en el sedimento del testigo U1314. Estos análisis fueron realizados por la profesora Mercedes Barrios Suárez, en el Área de Mineralogía del Departamento de Geología de la Universidad de Salamanca. Las muestras seleccionadas se molieron en mortero manual de ágata y se analizaron por difracción de rayos X utilizando un difractómetro Siemens D8 Advance, utilizando radiación de cobre K_{α}. Las condiciones de trabajo fueron: velocidad de barrido de 1º/min, 30 mA y 40 kv y zona explorada de 2 a 65º de 2Θ.

3.2. Técnicas isotópicas y de análisis de elementos traza en foraminíferos

Los análisis de isótopos de oxígeno y carbono se realizaron sobre individuos de la especie *N. pachyderma* sin. para análisis planctónicos y *Cibicidoides* spp. (*Cibicidoides wuellerstorfi* preferentemente), y *Melonis barleeanum* cuando la primera no se encontraba, para bentónicos. Los análisis de elementos traza estaban principalmente enfocados a obtener la relación Mg/Ca en la concha de los foraminíferos planctónicos, y la relación de otros elementos traza (Sr/Ca, Mn/Ca, Al/Ca y Cd/Ca) de forma complementaria, para lo que se usaron individuos de la especie de foraminífero planctónico *N. pachyderma* sin.

Los individuos seleccionados para los análisis fueron 15 para el análisis isotópico y entre 60-65 para el de elementos traza de la fracción entre 150-250 μm en planctónicos y entre 1-8 individuos de la fracción 300-600 μm en bentónicos. El protocolo de limpieza de ambos tipos de análisis se inicia rompiendo ligeramente los individuos. Para el análisis de isótopos estables la limpieza continúa con un tratamiento con metanol y ultrasonidos para eliminar partículas, mayoritariamente arcillosas, adheridas en el interior de la concha. El proceso de limpieza en el análisis de elementos traza continúa con un tratamiento oxidativo-reductivo, y dada la complejidad del proceso y la exposición a posibles contaminaciones, se realiza en un laboratorio blanco (Fig. 2.13). La contaminación por material terrígeno fue monitorizado a través de la concentración de Al; de la que no se encontró cantidades significativas a lo largo del muestreo. Una descripción detallada de las fases de las que consta el protocolo de limpieza para los análisis de Mg/Ca y demás relaciones con elementos traza aplicado a nuestras muestras, establecido por Pena *et al.* (2005), se encuentra en el Anexo 5.

Figura 2.13. Fotografía del laboratorio en el que se realizaron la limpieza para análisis de elementos traza, en la Facultad de Geología de la Universidad de Barcelona (izquierda), espectrómetro de masas Finnigan MAT 252 (centro) utilizado en el análisis de isótopos estables, y el espectrómetro con ICP en el se analizaron los elementos traza (derecha). Imágenes de la página web de los servicios científico-técnicos de la Universidad de Barcelona (http://www.sct.ub.es).

Los análisis isotópicos y de Mg/Ca se realizaron en la Universidad de Barcelona, utilizando un espectrómetro de masas Finnigan MAT 251 y un espectrómetro de masas acoplado a una antorcha de plasma de acoplamiento inductivo (*Inducted Coupled Plasma*, ICP) Perkin-Elmer Elan 6000, respectivamente (Fig. 2.13). La calibración de los resultados de los isótopos estables se realizó con el estándar NBS-19. El resultado está referido al estándar *Vienna Pee Dee Belemnite* (VPDB) (Coplen, 1996), siendo la precisión analítica superior a 0,07 para el $\delta^{18}O$ y 0,05 para el $\delta^{13}C$.

3.3. Técnicas geoquímicas con sedimento

Muestras del testigo U1314 fueron analizadas usando técnicas de digestión total del sedimento para obtener concentraciones de P, Fe, Al, Ti, Mn, Zn, Mg, Ba, Sr y Ca , y extracción secuencial de fósforo, la cual incluye las cuatro fases diferentes de P que se encuentran en el océano; autogénico, orgánico, ligado a fases de Fe-Mn y el detrítico (Filippelli and Delaney, 1996; Ruttenberg, 1992; Ruttenberg and Berner, 1993) . Para la digestión total, se seleccionaron 300 muestras alternas, separadas cada 8 cm. Se procedió a disolver el sedimento usando un sistema de digestión por microondas MDS 2000 y los ácidos HNO_3, HF y HCl, siguiendo el método SW-846 3051 de la agencia de protección ambiental de los EEUU (*Enviromental Protection Agency*, EPA), de acuerdo a lo establecido por Link *et al*. (1998). Una vez la digestión fue completa, se añadió ácido bórico para estabilizar la solución. Las muestras fueron después transferidas a un nuevo vial y diluidas con 50 ml de agua purificada. Para la determinación final de la concentración elemental se usó un espectrómetro Leeman Labs P950 con ICP y con un nebulizador ultrasónico CETAC Corp. AT500$^+$ acoplado. Para más detalles acerca de los procedimientos usados en esta técnica, ver Anexo 6.

Debido a lo laborioso del procedimiento para separar y analizar los cuatro componentes de fósforo, sólo se realizó en 64 muestras, separadas cada 40 cm aproximadamente. La metodología a seguir en este caso fue la de Filippelli y Delaney (1996), modificado de Ruttenberg (1992). Dado lo extenso de esta técnica analítica, hemos preferido incluir este protocolo de forma más detallada en el Anexo 7.

Los análisis de contenido total de carbono en el sedimento (*Total Carbon*, TC) se realizaron en un total de 586 muestras, usando un analizador de carbono UIC Coulometrics CM150. El carbono orgánico total (*Total Organic Carbon*, TOC) se determinó eliminando primero el carbono inorgánico de la muestra con una solución HCl 2M, y después medido usando un analizador CHNS/O por combustión Flash 2000. El carbonato cálcico ($CaCO_3$) fue calculado usando los porcentajes relativos de TC y TOC mediante la siguiente ecuación:

$$CaCO_3\% = (TC\ \% - TOC\ \%) \times 8.33$$

Para el análisis del ópalo biogénico (SiO_2) se seleccionaron 572 muestras y se trataron de acuerdo al procedimiento de Mortlock y Froelich (1989), añadiendo 10 ml de Na_2CO_3 2M a las muestras, que permanecieron en un baño en agua a 85º C durante ~5 horas, para la disolución de la sílice. La determinación final del ópalo se realizó con el mismo espectrómetro que con el que se analizó la composición elemental. Todos los análisis geoquímicos aquí presentados fueron realizados en los laboratorios de biogeoquímica del Departamento de Ciencias de la Tierra de la Universidad de Indianápolis-Universidad de Purdue, en Indianápolis (EEUU) (Fig. 2.14).

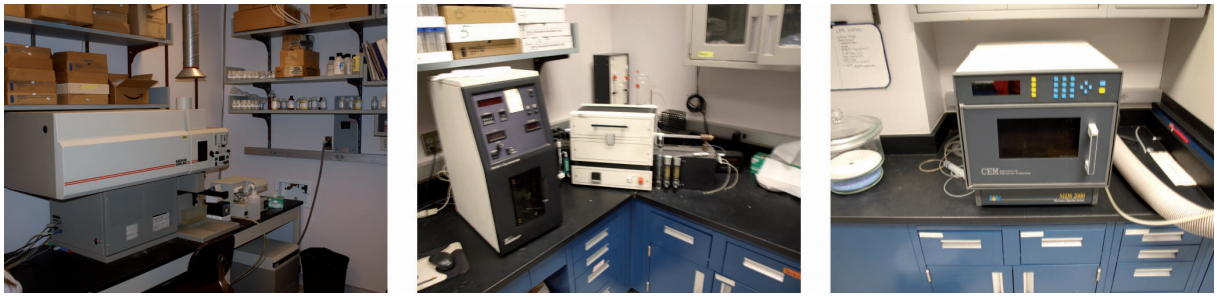

Figura 2.14. Fotografías de parte del equipamiento de los laboratorios del Departamento de Ciencias de la Tierra de la Universidad de Indianápolis-Universidad de Purdue en el que se realizaron los análisis geoquímicos con sedimento. Espectrómetro Leeman Labs P950 con ICP y nebulizador (izquierda), analizador de carbón UIC Coulometrics CM150 (centro), y microondas para digestión total MDS 2000 (derecha).

3.4. Construcción del modelo de edad

El modelo de edad para la sección estudiada del testigo U1314 se ha realizado comparando los isótopos de oxígeno realizados en foraminíferos bentónicos con la curva de $\delta^{18}O$ bentónico global de Lisiecki y Raymo (2005) (de aquí en adelante nos referiremos a ella como LR04), usando el programa *Analyseries 2.0* (Paillard, 1996). Esta curva de referencia contiene datos de $\delta^{18}O$ bentónico de 57 diferentes localizaciones distribuidas a lo largo de la Tierra, siendo utilizada de forma generalizada para construir modelos de edad en multitud de estudios para el Plio-Pleistoceno (e.g. Hodell *et al.*, 2008; Hönisch *et al.*, 2009; Toucanne *et al.*, 2009). Una explicación más detallada de la elaboración del modelo de edad para esta Tesis Doctoral, incluyendo los puntos de correlación (*tie points*) entre nuestro registro de oxígeno bentónico y la curva LR04, se encuentra en el Capítulo 3.

3.5. Herramientas para análisis estadístico y de series temporales

En la elaboración de esta Tesis Doctoral se han empleado dos programas de uso común en paleoclimatología, estos son *PAST* (Hammer *et al.*, 2001) y *Analyseries 2.0* (Paillard, 1996). El programa *Analyseries 2.0* ha sido usado para el estudio de las frecuencias dominantes en el registro de isótopos e IRD (ver Capítulo 3). Para ello se realizaron análisis espectrales utilizando el método de Blackman-Tukey (Jenkins and Watts, 1968). En líneas básicas, este método genera la autocovarianza de la serie (remuestreada a intervalos equidistantes), aplica una ventana espectral y realiza una transformada de Fourier para obtener el espectro de frecuencias.

El programa *PAST* ha sido aplicado principalmente a los datos de recuento de especies de radiolarios (ver Capítulo 5), con el cálculo del índice de diversidad Shannon-Weaver (*H*) (Shannon and Weaver, 1963) y el estudio de la distribución de las diferentes especies usando el análisis de correspondencia sin tendencia (*Detrended Correspondance Análisis*, DCA), para evaluar el posible control de algún factor ambiental sobre la sucesión ecológica de las especies de radiolarios. Dada la capacidad de este programa para determinar las frecuencias dominantes en

series temporales de asociaciones fósiles con un gran número de especies, aplicamos la técnica del periodograma de Mantel (Hammer, 2007) a la asociación de radiolarios para identificar las periodicidades orbitales dominantes en la composición específica de la asociación de radiolarios del testigo U1314. Finalmente, el programa *SPSS* fue empleado en el análisis estadístico de la composición geoquímica elemental (ver Capítulo 7) con el objeto de identificar variables subyacentes que expliquen la correlación entre los elementos geoquímicos que componen el sedimento del testigo U1314.

Capítulo 3

*IMPACT OF SUBORBITAL CLIMATE CHANGES IN THE NORTH ATLANTIC ON ICE-SHEETS DYNAMICS AT THE MID-PLEISTOCENE TRANSITION**

*Este capítulo está basado en: Hernández-Almeida, I., Sierro, F.J., Cacho, I. and Flores, J.A. *Paleoceanography* (en preparación).

RESUMEN. Se ha reconstruido el clima y la hidrografía del océano profundo durante el Pleistoceno Medio e Inferior usando un registro de datos a alta resolución (isótopos de oxígeno y carbono en foraminíferos planctónicos y bentónicos, reconstrucción de temperaturas oceánicas superficiales basadas en asociaciones faunísticas y detritus transportados por el hielo -IRD-) procedentes de una secuencia sedimentaria con altas tasas de depósito en la formación *Gardar Drift* en el Atlántico Norte subpolar (*Integrated Ocean Drilling Program Leg* 306, *Site* U1314). La profundidad y ubicación a la que se encuentra este testigo hace que sea sensible a la interacción entre aguas Noratlántica profundas y aguas procedentes del sur a escalas temporales orbital y suborbital. Nuestro registro sedimentario abarca desde el estadio isotópico marino 31 al 19 (1069-779 ka). La diferente tendencia del registro de isótopos estables en foraminíferos bentónicos antes y después del estadio isotópico marino 25 indica una gran aumento en el volumen de hielo oen el Hemisferio Norte y un deterioro gradual de la ventilación del océano profundo, ambos procesos asociados al cambio de ciclicidad dominante de 41 ka a 100 ka que tuvo lugar durante la Transición del Pleistoceno Medio. Además la variabilidad glacial-interglacial, numerosas fluctuaciones a escala milenaria relacionadas a secuencias de avance/retroceso de los casquetes de hielo tuvieron lugar durante el periodo de tiempo estudiado. El análisis de series temporales en indicadores de aguas superficiales muestra que la duración media de estos cambios climáticos a escala milenaria están relacionados al componente hemi-precesional (10 ka) de la insolación, lo cual se interpreta como un transporte de calor a través del ecuador hacia latitudes altas durante máximos de insolación en los equinoccios en el ecuador.

Palabras clave: Atlántico Norte; Transición del Pleistoceno Medio; isótopos estables; detritus transportado por el hielo; agua profunda; milenaria; insolación; *Site* U1314.

ABSTRACT. Early and Mid-Pleistocene climate and deep-ocean hydrography have been reconstructed using a high-resolution data set (planktonic and benthic $\delta^{18}O$ and $\delta^{13}C$ time series, faunal-based SST reconstruction and ice-rafted debris) record from a high-deposition-rate sedimentary succession recovered at the Gardar Drift formation in the subpolar North Atlantic (Integrated Ocean Drilling Program Leg 306, Site U1314). The location and water depth of this Site makes it sensitive to the interaction between North Atlantic Deep Water (NADW) and southern source waters at orbital and sub-orbital time-scales. Our sedimentary record spans from late in Marine Isotope Stage (MIS) 31 to MIS 19 (1069-779 ka). Different trend of the benthic stable isotopes record before and after MIS 25 evidence the large increase in Northern Hemisphere ice-volume and gradual deterioration of ventilation of the deep-ocean, both linked to the cyclicity change from the 41-kyr to the 100-kyr that occurred during the Mid-Pleistocene Transition (MPT). Beside longer glacial-interglacial (G-IG) variability, millennial-scale fluctuations related to ice-sheet advance/retreat sequences occurred along the time-period studied. Time series analysis on surface water proxies shows that the timing of these millennial-scale climate changes are related to half-precessional (10 kyr) components of the insolation forcing, which are interpreted as cross-equatorial heat transport toward high latitudes during both equinox insolation maxima at the equator.

Key words: North Atlantic; Mid-Pleistocene Transition; stable isotopes; ice-rafted debris; deep-water; millennial; insolation; Site U1314.

IMPACT OF SUBORBITAL CLIMATE CHANGES IN THE NORTH ATLANTIC ON ICE-SHEETS DYNAMICS AT THE MID-PLEISTOCENE TRANSITION

1. INTRODUCTION

The North Atlantic Ocean is a key area for global ocean conveyor belt system, which is the main moderating force of the climate over Europe. Modern North Atlantic conditions are based on the steady northward transport of warm, saline surface waters. This energy transport to high latitudes is balanced by a southerly return flow of North Atlantic Deep Water (NADW), formed by deep convection in the Nordic Seas, which ventilates more than a half of the volume of the deep oceans. However, this robust feature today has experienced abrupt and dramatic alterations over both glacial-interglacial and shorter time scales during the past. Vertical water mass structure in the North Atlantic has changed during glacial periods and millennial-scale climate events that caused significant global eustatic changes and modified the relative proportion of northern versus southern source waters in the North Atlantic. Although these events have been well studied for the last glacial cycle (e.g. Bond *et al.*, 1992; Boyle and Keigwin, 1987; Oppo and Lehman, 1993), less is know about their occurrence in older glacial periods of the Pleistocene.

Specially intriguing is the so-called "Mid-Pleistocene Transition" (MPT), which is defined as the period in which the climatic cyclicity shifted from the ~ 41 kyr cycles, related to obliquity, to the ~ 100 kyr cycles, related to eccentricity (Berger and Jansen, 1994a). During the "41-kyr world", continental ice-sheets were reduced in size and glacial periods milder compared to those during the "100-kyr world" (Clark *et al.*, 2006), that led to dramatic global reorganizations in climatic system. Records from North Hemisphere and time-series modelling document the global glacial expansion since MIS 24, which represents a first step toward an increased global ice-volume (Maslin and Ridgwell, 2005; Mudelsee and Stattegger, 1997; Prell, 1982). However, multiple evidences indicate that MIS 22 (c. 870-880 ka) was the first of the major cold events that characterizes the Later Pleistocene. Glacial erosion in central Europe (Haeuselmann *et al.*, 2007; Muttoni *et al.*, 2003), large growth of North America ice-sheets (Barendregt and Irving, 1998), increased aridity in northern Eurasia (Heslop *et al.*, 2002) document the severity of these first major glaciations in continents. In an oceanographic context, the response to the increased intensity of climatic deterioration and duration of climatic events was a strong reduction in North Atlantic thermohaline circulation (Ferretti *et al.*, 2005; Raymo *et al.*, 1997; 2004; Schmieder *et al.*, 2000) and cooling of surface temperatures by expansion of subarctic waters (McClymont *et al.*, 2008; Shimada *et al.*, 2008; Wright and Flower, 2002).

Despite the wide evidence for climatic and oceanographic changes at glacial-interglacial time scale during the Early and Mid-Pleistocene, several studies have found evidences for millennial-scale variations with pacing indistinguishable from that of the last glacial cycle

(Ferretti *et al.*, 2010; Grützner and Higgins, 2010; Hayashi *et al.*, 2010; Raymo *et al.*, 1998). These observations suggest that some boundary conditions associated with millennial-climate scale variability were already surpassed within the time window of the MPT, and before the establishment of the 100-kyr cycles from the Late Pleistocene. The mechanism triggering these millennial-scale instabilities is still controversial, but several studies point toward a low-latitude insolation origin, independent of ice-volume, that would explain the presence of these fluctuations before the establishment of high-amplitude 100-kyr glacial cycles (McIntyre and Molfino, 1996; Short *et al.*, 1991).

In this paper, we present a series of high-resolution isotopical, sedimentological and sea surface temperature (SST) records that extends the time-slice between 1069 to 779 ka from Site U1314, in the subpolar North Atlantic. Changes in iceberg delivery to the ocean and thermohaline circulation were examined by looking at the evolution of temporal and spatial IRD, $\delta^{13}C$ and $\delta^{18}O$ records in the North Atlantic in response to the large growth of ice-volume associated with the 41-to-100 kyr transition. Moreover we investigate the millennial scale variability of upper ocean temperature, iceberg activity in the North Atlantic site, and hypothesize about how low-latitude changes in insolation can be transported to high-latitudes through ocean-atmosphere-cryosphere interactions.

2. SITE LOCATIONS AND OCEANOGRAPHIC SETTINGS

IODP Site U1314 (2820 m) was cored by the D/V JOIDES Resolution in the southern Gardar Drift, in the subpolar North Atlantic (56.36°N, 27.88°W) during IODP Expedition 306 (Fig. 3.1). Today, this site shoaled by Iceland-Scotland Overflow Water (ISOW), which occurs deeper than 2000 m and is characterised by high salinity and oxygen content (Bianchi and McCave, 2000) and is main precursor of Lower North Atlantic Deep Water (LNADW), originated in the Greenland, Iceland, and Norwegian (GIN) Seas by deep convection (Krauss, 1986; Schmitz and McCartney, 1993). Varying proportions of Labrador Sea Water (LSW) and Sub-Polar Mode Water (SPMW) mixes with the main ISOW flow generated in the GIN Seas (Van Aken and De Boer, 1995). The southward flow of cold deep waters from the GIN seas is partly balanced by a northward flow of a Antarctic bottom derived waters, Lower Deep Waters (LDW) into the Iceland Basin (McCartney, 1992). Hence, Site U1314 position close to the ice-rafted debris (IRD) belt (Ruddiman, 1977) is ideal to study variations in ISOW flow and ice instability during the Pleistocene (Bianchi and McCave, 1999; Grützner and Higgins, 2010; Hodell *et al.*, 2009; Wang and McCave, 1990).

At surface, Site U1314 is located in the path of an extension of the North Atlantic Current (NAC), the Irminger Current (IC), and is seasonally affected by the southward extension of the Artic Front (AF), that is the boundary between Artic and Atlantic waters that delimitate the maximum extent of winter sea-ice (Swift and Aagaard, 1981).

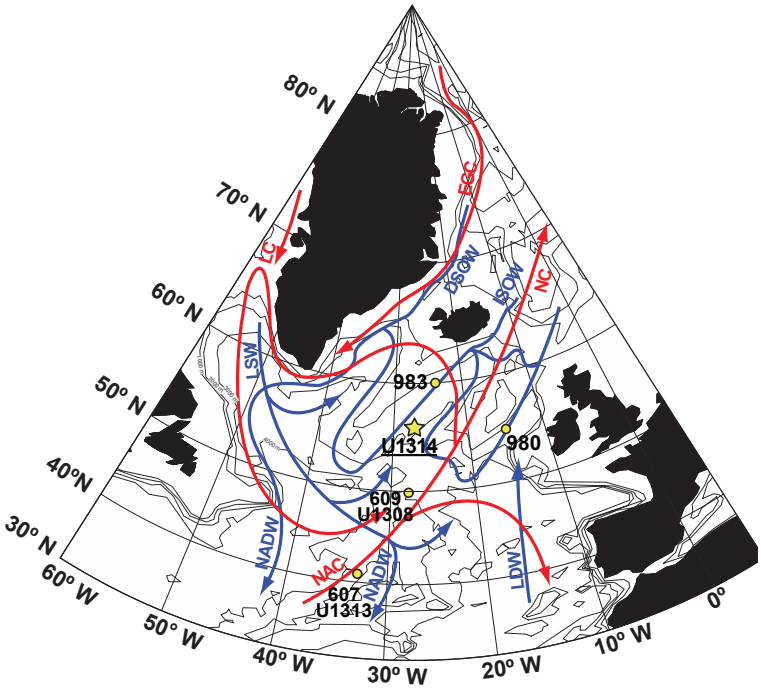

Figure 3.1. Location of IODP Site U1314 (black star: 56º21'N, 27ºW; 2820 m water depth), and other North Atlantic sites (see Table 3.2). Modern surface (red), and deep circulation (blue) in the North Atlantic (Krauss, 1986; Schmitz and McCartney, 1993). Map generated with *Ocean Data View v.3.4.3.* software (Schlitzer, 2008). East Greenland Current (EGC), Norwegian Current (NC), Labrador Current (LC), North Atlantic Current (NAC), Irminger Current (IC), Denmark Strait Overflow Water (DSOW), Iceland Scotland Overflow Water (ISOW), Labrador Sea Water (LSW), North Atlantic Deep Water (NADW), and Lower Deep Water (LDW).

Early and Mid-Pleistocene Sediments at Site U1314 consist predominantly of biogenic oozes with varying proportion of calcareous (e.g., nannofossils and foraminifers) and siliceous organisms (e.g., diatoms and radiolarians) and lower content of terrigenous components, such as quartz, volcanic material and clay. More detailed core description is given in Expedition 306 Scientists (Channell *et al.*, 2006).

3. MATERIAL AND METHODS

Samples from Site U1314 were taken every 4 cm between the 60 to 84.16 meters composite depth (mcd). Each sample was washed through a 63 μm sieve to eliminate clay and fossil ooze and dried. Later, the sample was dry sieved into two fractions, 63-150 μm and > 150 μm. Census counts and picking for the stable isotope analyses were carried out in the > 150 μm fraction. The deep-water record was obtained from *Cibicidoides* spp. (mainly *C. wuellerstorfi* and occasionally *C. pachyderma*), an epifaunal benthic foraminifer species which is a reliable indicator of the $\delta^{13}C$ of dissolved CO_2 in the bottom water (Belanger *et al.*, 1981). One to eight tests of *Cibicidoides* were picked from the > 250 μm size fraction and one to eight individuals were used for isotopic analysis. When this species was absent, we picked specimens of *Melonis pompilioides* from

the same size fraction to produce a continuous signal. In order to elaborate a homogenous isotope record from both species, we calculated the mean difference between both. The average difference is -0.11 ‰ for the oxygen and +1‰ for the carbon isotopes. This "correction factor" was then applied to the *M. pompilioides* isotope values to produce a uniform isotope data set.

For the surface water record, we chose to analyse *Neogloboquadrina pachyderma* sinistrorsa (sin.), because this species is present throughout the studied section. A minimum of 15 specimens from the size range between 150-250 μm were picked. Benthic and planktonic specimens of each sample were crushed, ultrasonicated and cleaned with methanol before the isotopic analyses. Benthic and planktonic foraminifera stable isotope analyses were carried out in a Finnigan MAT 252 mass spectrometer at the University of Barcelona. Calibration to the Vienna Pee Dee Belemnite (VPDB) standard scale (Coplen, 1996) was made through the NBS-19 standard, and the analytical precision was better than 0.06 ‰ for $\delta^{18}O$ and 0.02‰ for $\delta^{13}C$.

The accumulation of coarse-grained ice-rafted debris (IRD) was determined by examination of the > 150μm size fraction. Full census counts were completed every other sample. Each samples was split to about 400 planktonic foraminifers, then species of planktonic and benthic foraminifers, as well as mineral grains, ash, lithic fragments, radiolarians, ostracodes and planktonic foraminifer fragments were counted under a binocular microscope and relative percentages were calculated.

The relative abundance of planktonic foraminifer is based on census counts of splits of the > 150 μm fraction containing approximately 300 planktonic foraminifers. The planktonic foraminifer a fauna is characterized by polar, subpolar and transitional species. The dominant species are *Neogloboquadrina pachyderma* sinistrorsa, *Neogloboquadrina pachyderma* dextrorsa, *Globigerina bulloides*, *Globorotalia inflata* and *Globigerina quinqueloba.* Based on these counts we performed a sea surface temperature estimation using the artificial neural network (ANN) technique (Malmgren *et al.*, 2001) trained on the MARGO project database (Kucera *et al.*, 2005a). Modern temperatures from the calibration data set were extracted from the World Ocean Atlas vesion 2 (Conkright *et al.*, 1998) at 10 m water depth. SST was calculated for summer, winter and the annual mean. The ANN SST estimates are based on the average values of 10 temperatures provided by the neural network.

Finally, the existence of possible periodic behaviour of the Early and Mid-Pleistocene climate has been investigated by performing time series analyses on the benthic oxygen record and on the record relative to surface water proxies of IRD and planktonic $\delta^{18}O$. Time series results were obtained by the Blackman-Tuckey Method of spectral estimation from the *AnalySeries* software (Paillard, 1996). The records were initially prepared by removing linear trends and resampling at constant 1 kyr intervals for the benthic and planktonic $\delta^{18}O$ and IRD record. The confidence interval was set at 80 %. To recognize possible dominant frequency variations trough time, we split the MIS 31 to 19 interval into two slices (MIS 31 to 26, and 35 to 19).

4. RESULTS

4.1. Age model

We converted depth to age matching the distinct glacial and interglacial periods in Site U1314 according to the benthic $\delta^{18}O$ with their temporal equivalent in the orbitally tuned benthic isotope stack of Lisiecki and Raymo (2005) (hereinafter referred to as LR04) by using *AnalySeries* 2.0 software (Paillard, 1996). using the program *Analyseries* (Paillard, 1996). Two magnetostratigraphic events corroborate the age model: the Brunhes-Matuyama boundary (780 kyr) was identified at 60 mcd in Site U1314 (Channell *et al.*, 2006) and correlates to MIS 19 in the oxygen isotopic record. The top of the Jaramillo (990 kyr) was placed at 77.7 mcd and correlates with MIS 27.

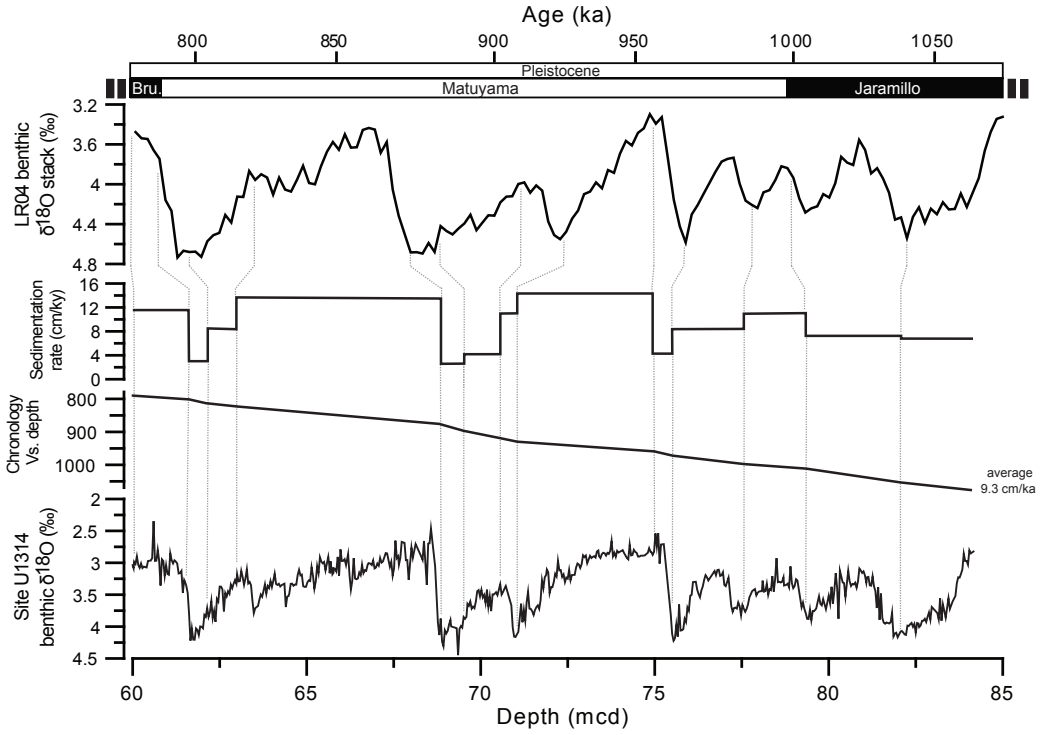

Figure 3.2. Construction of the age model was performed by correlating the benthic isotope stack LR04 with Site U1314 benthic $\delta^{18}O$. Tie points of both records are joined by dashed lines. From top to bottom: A) LR04 benthic stack; B) sedimentation rate of site 1314 after tuning; C) chronology as a function of depth in Site U1314; benthic $\delta^{18}O$ from Site U1314 as function of depth.

The final age model for the 24.16 m studied section spans an interval from ~290 kyr through the Early and Mid-Pleistocene based on 13 stratigraphic tie points (Table 3.1), yielding a temporal resolution of ~0.5 kyr. In between the tie points, sedimentation rates were assumed constant and the ages were deduced by linear interpolation. The orbitally tuned age model and corresponding linear sedimentation rates are shown in figure 3.2. The resulting sedimentation rates are moderately high (average 9.3 cm/kyr) and differ largely between glacial (1.15 cm/kyr) and interglacial (up to 27 cm/kyr), intervals indicating enhanced growth of the Gardar Drift during intervals of warmer climate. According to our geochronology, the average age resolution

is of 230 years per sample (range: ~70 to 600 years) and 1140 years (range: ~365 to 3000 years) for sample interval. The $\delta^{18}O$ records from sites 980, 983, U1313 and U1308 are all plotted versus age in figure 3.3, using their respective age-depth.

Site U1314 depth (mcd)	LR04 Time (ka)
60.10	780.619
61.79	795.244
62.16	807.358
63.12	817.649
68.55	858.636
68.92	872.225
70.99	921.458
71.88	929.571
75.01	951.451
75.50	962.858
77.60	987.871
79.41	1004.220
83.37	1058.727

Table 3.1. Tie points used in the correlation between benthic $\delta^{18}O$ from Site U1314 and benthic isotope stack LR04.

4.2. Oxygen isotopes

The stable isotope record from Site U1314 spans G-IG cycles tuned to LR04 time scale presents 6 different climate cycles (from MIS 31 to MIS 19) (Fig. 3.2). From MIS 31 to 22, each glacial/interglacial cycle has an average duration around 41 ka, while MIS 21 show a longer duration (80 ka) and an internal suborbital periodicity that breaks the stage into four isotopic interstadial periods. The benthic $\delta^{18}O$ record at Site U1314 ranges between 4.45 ‰ at 882 ka and 2.34 ‰ at 784 ka (Fig. 3.3; 3.4). Between 1069-950 ka (MIS 31-25), isotopic values difference between glacial and interglacial intervals rarely exceeded 1 ‰ (only MIS 25/26 transition, with 1.7 ‰). This trend ends abruptly above MIS 24, whit a noticeable shift toward higher benthic $\delta^{18}O$ contrast between cold and warm intervals. The total range of variation in the oxygen benthic values between glacial and interglacial periods was ~ 1.8 ‰, a equivalent value to the ~ 2 ‰ in the oxygen isotope planktonic record if we assume that the $\delta^{18}O$ signal of *N. pachyderma* sin. is affected by the global ice-volume signature and local near-surface temperature and salinity conditions (Shackleton, 1987) (Fig. 3.4). Overlapped to this long-trend term orbitally related, we observe rapid and shorter (in magnitude and duration) oscillations in the $\delta^{18}O$ record (planktonic and benthic). A clear example is the four abrupt cooling events that interrupted the warm MIS 21 period, with fluctuations in the planktonic record that exceed the 1 ‰. Also it is noticeable the fact that no large oscillations occur when benthic $\delta^{18}O$ is less than 3.5 ‰; these periods are characterized for the relative stability and the absence of any catastrophic discharge event.

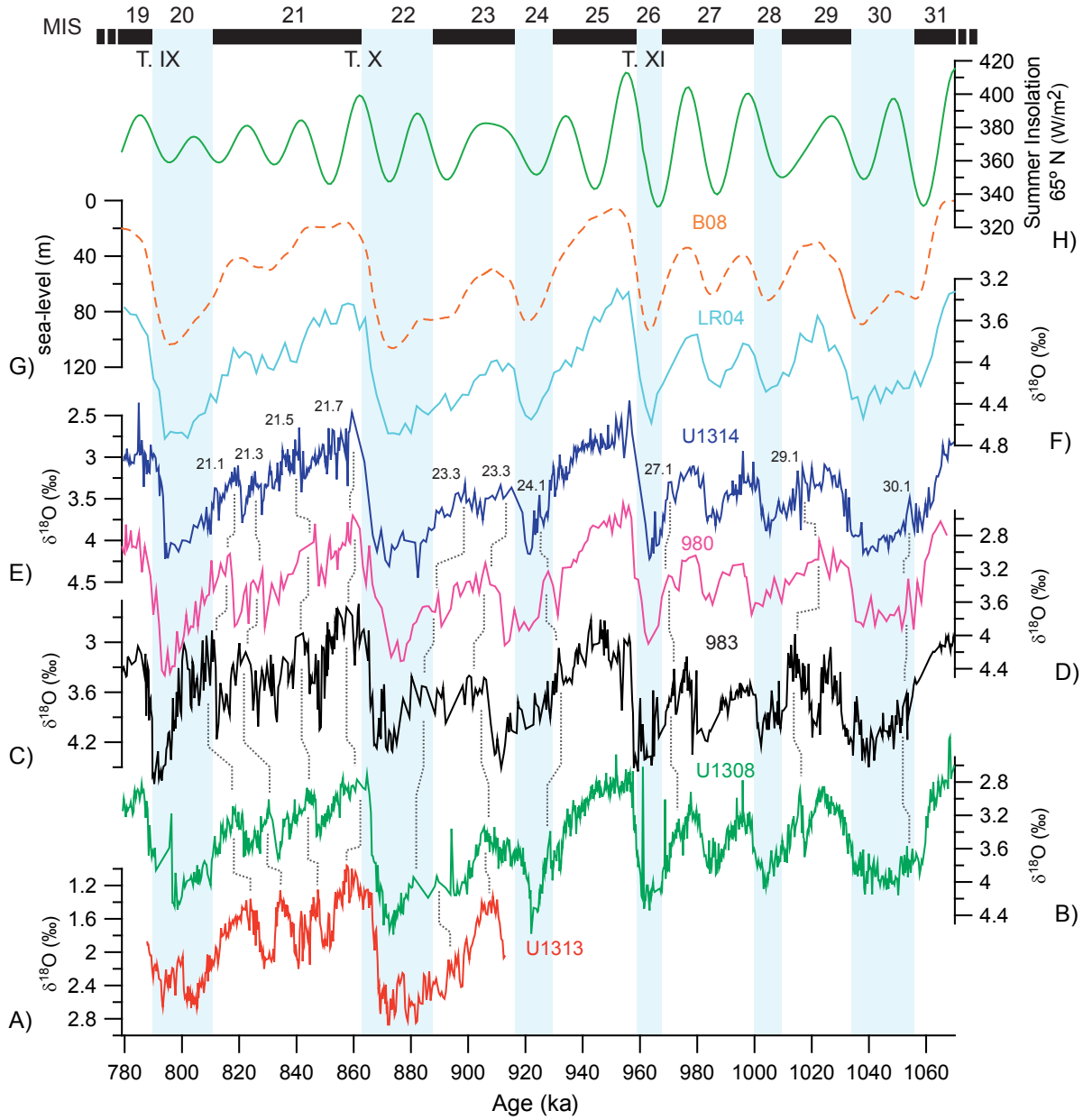

Figure 3.3. Comparison of benthic $\delta^{18}O$ records from the North Atlantic. From bottom to top: A) U1313 (Ferretti *et al.*, 2010), B) U1308 (Hodell *et al.*, 2008), C) 983 (Kleiven *et al.*, 2003), D) 980 (Flower *et al.*, 2000), E) U1314, F) benthic $\delta^{18}O$ LR04 stack (Lisiecki and Raymo, 2005), G) B08 sea-level reconstruction (Bintanja and van de Wal 2008) and H) summer insolation at 65º N (Laskar *et al.*, 2004). Vertical dashed grey lines join equivalent millennial-climate events in the North Atlantic sites. Marine Isotope Stages (MIS) are shown at the top (glacials in blue and interglacials in black).

4.3. Carbon isotopes

Benthic $\delta^{13}C$ long-term trends correlate to variations in benthic $\delta^{18}O$ variability, but with less amplitude, ranging from -1 ‰ to 1.2 ‰ (Fig. 3.4). The most striking features on the benthic $\delta^{13}C$ record are pronounced minima at Terminations associated with major IRD events and with high percentages of *N. pachyderma* sin. The largest carbon isotope shifts (~ -1‰) occurred at MIS 22 and MIS 24. Low carbon isotope values are also observed during interglacial stages, at

MIS 25 and 23, even when IRD deposition is absent and $\delta^{18}O$ variations are low, implying that rapid changes in the ventilation of the deep Northeast Atlantic span the entire 1069 to 779 kyr interval considered in this study, regardless of the background climate and ice-sheet conditions. In contrast, positive benthic $\delta^{13}C$ values were observed during the interglacials MIS 21 and of MIS 23. It is also important to note that there is a pronounced 0.15 ‰ decrease in mean ocean $\delta^{13}C$ values between after MIS 25 respect to the older section.

Site	Latitude	Longitude	Depth, m	Reference
U1314	56º36'N	27º88'W	2820	this study
980	55º29'N	14º42'W	2168	Flower et al. (2000)
983	60º23'N	23º38'W	1985	Kleiven et al. (2003)
U1308	19º53'N	24º14'W	3872	Hodell et al. (2008)
U1313	41º00'N	35º58'W	3426	Ferretti et al. (2010)

Table 3.2. Site information.

4.4. SST reconstruction

Summer SST calculated with ANN range between 17.1 and 3.2 ºC. Modern SST values for the Site U1314 at 10 m depth are around 12 ºC (Locarnini *et al.*, 2006), which is in the range of the mean summer SST calculated with ANN for the interglacial periods before MIS 26, but considerably lower, in more than 4 ºC, after MIS 25 (Fig. 3.4). Although minima SST does not vary considerably thought the studied section, slightly colder temperatures are recorded at glacial maxima of MIS 22 and 20. Paleotemperature estimate indicates that G-IG variability shifted to higher amplitude changes after MIS 25, ranging between 4-12 ºC. Moreover, frequent SST oscillations are seen on short timescales throughout the MIS 31 to 19 interval, coinciding always SST minima with IRD events

4.5. Ice-rafted debris

Fig. 3.4 shows that IRD was deposited at Gardar Drift mainly during glacial cycles (i.e. MIS 20, 22, 24, 26, 28 and 30) describing a saw-tooth steadily increases. All iceberg episodes occur when benthic $\delta^{18}O$ record surpass values of 3.5 ‰. Largest IRD events occurred at glacial Terminations 24/23, 22/21 and 20/19 and lithic discharge maximum occurred near the mid-point of the deglacial interval, as defined by the $\delta^{18}O$ record. We also observe a steady rise in the magnitude of the IRD events during the 1069 to 779 kyr periods. In contrast, little IRD input occurs during the peak interglacial maxima of MIS 19, 21, 23, 25, 27 and 29, although several IRD are located at cooler interglacial sub-stages, such as within MIS 21, 27 and 29. A notable increase in the glacial input of ice-rafted material occurred at Site U1314 since MIS 24 (~ 930 kyr). The input of ice-rafted terrigenous material during this glacial period and following glaciations was higher and lasted more time when compared to the previous glacial intervals

e.g., MIS 26-30. Maximum IRD input occurs during MIS 20 made up of two distinct peaks (at 794 and 798 kyr), that reached accumulations of about 18000 particles*cm^{-2}*kyr^{-1}.

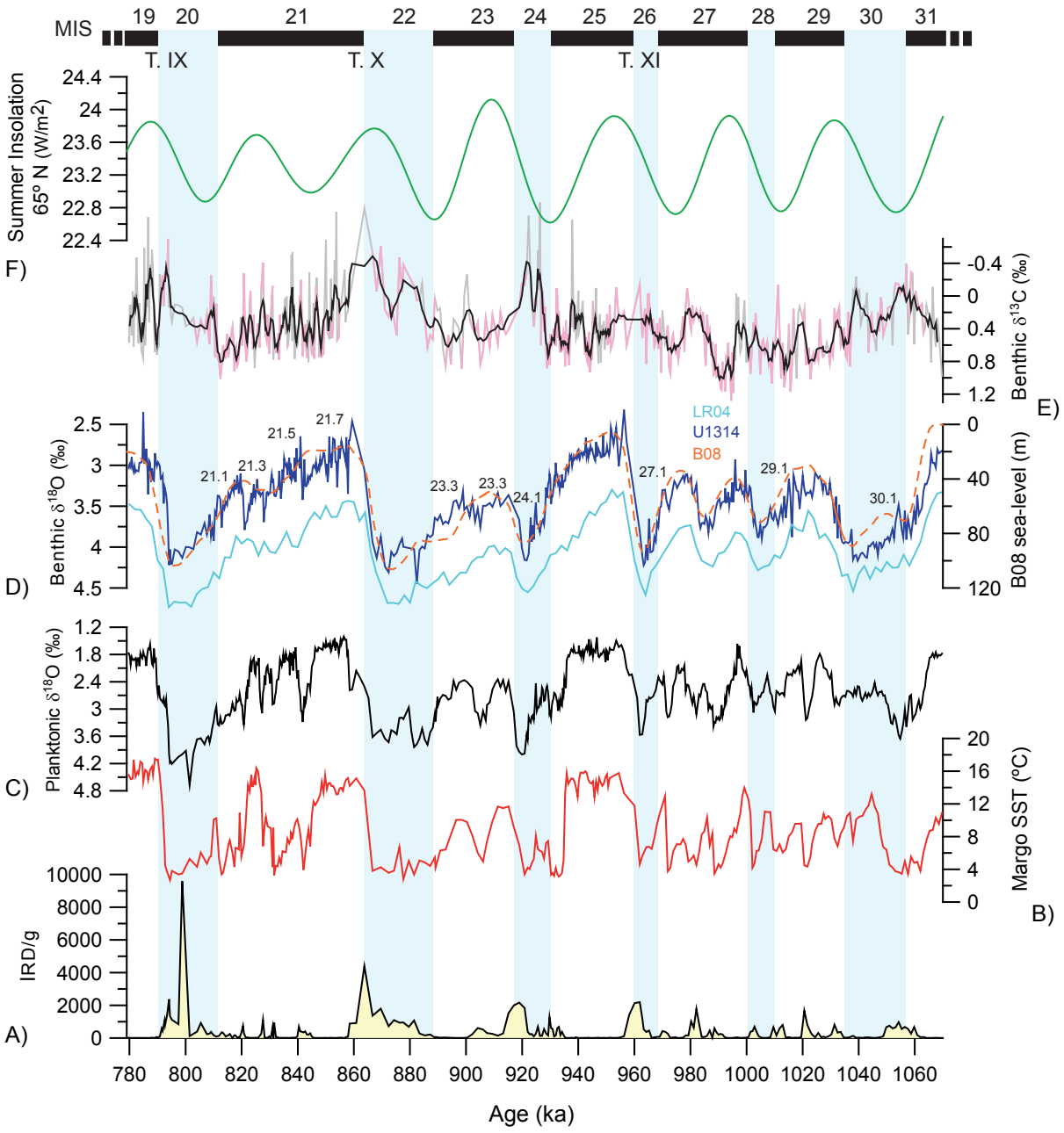

Figure 3.4. Site U1314 records from 779 to 1069 ka. From bottom to top: A) IRD/g, B) faunal-based SST, using ANN technique, C) planktonic $\delta^{18}O$, D) benthic $\delta^{18}O$ (dark blue), benthic $\delta^{18}O$ LR04 stack (Lisiecki and Raymo, 2005) (light blue) and B08 sea-level reconstruction (Bintanja and van de Wal 2008) (orange dashed line) E) benthic $\delta^{13}C$, with 5 points running average (black). Pink lines correspond with samples were *C. wuellerstorfi* individuals were picked for the stable isotope analyses, and grey lines correspond to *M. pompilloides*, values represented with corrector factor applied (see 3. Material and Methods) G) Summer insolation at 65º N (Laskar *et al.*, 2004). Vertical grey bars indicate IRD discharge events, either linked to deglaciations or to millennial-scale oscillations. Marine Isotope Stages (MIS) are shown at the top (glacials in blue and interglacials in black).

4.6. Time series analysis

Time series analysis of IRD, SST and planktonic $\delta^{18}O$ records for the time slices before MIS 25 reveals evidence for strong periodicities on Milankovitch orbital and sub-orbital timescales (Fig. 3.6). The IRD and the planktonic $\delta^{18}O$ lack long-term orbital frequencies of 100 and 41 kyr, and show pronounced spectral peaks at 21 and 10-11 kyr. The SST signal is dominated by a single strong 41 peak and two peaks at 15 and 10 kyr.

5. DISCUSSION

The MPT, the period between 940-900 kyr (MIS 25-23), has been associated with a global increase in ice-volume related to a major change in frequency of the climate cycles that evolved from 41-kyr to 100-kyr (e.g. Mudelsee and Schulz, 1997; Mudelsee and Stattegger, 1997; Pisias and Moore Jr, 1981; Prell, 1982). This bifurcation in the climate system is clearly seen in the benthic $\delta^{18}O$ record at Site U1314 along with other proxies (Fig. 3.4), and reflect a shifting environment toward a more extreme glacial conditions and greater G-IG contrast that characterizes the Earth's climate during the Late Quaternary period. Due to the changing structure of climate cycles during the MPT, we have divided our studied interval into two different time-slices in order to discuss the millennial scale climate oscillations and deep-water oceanographic changes in the North Atlantic.

5.1. Period between MIS 31 and MIS 26: low amplitude, obliquity and precession-driven G-IG variability

This period immediately predates the onset of the high amplitude 100 kyr G-IG cycles that charactarize climate changes during the Late Pleistocene (Bintanja and van de Wal, 2008; Lisiecki and Raymo, 2005). Whereas ice-sheet dynamics as recorded by the benthic $\delta^{18}O$ values is mainly driven by precession and obliquity, hydrographic changes of North Atlantic surface waters typically display a suborbital variability dominated by a 10 kyr period (Fig. 3.6).

The relatively less extreme glacial benthic $\delta^{18}O$ values reflect smaller continental ice-sheet and/or warmer deep-sea temperatures and correlate well with higher glacial pCO_2 for the MPT (Hönisch *et al.*, 2009). Glacial stages depict a symmetrical pattern, with similar gradual patterns of glacial growth and deglaciations. Transitions between G-IG stages do not show abrupt events compared to post-MIS 25 Terminations (Fig. 3.5).

Surface water conditions cyclically changed in response to southward and northward shifts of the AF, leaving colder and warmer waters at Site U1314. SST reached occasionally high temperatures, around 14 ºC, but usually remains between 10-4 ºC. This observation would be consistent with the presence of relatively cool and fresh arctic surface waters, with seasonal sea-ice cover (Sarnthein *et al.*, 2003). Nine millennial-scale climate cycles with an average

period of 10 kyr are recorded between MIS 30 and MIS 25. Each of these cycles starts with an abrupt warming event that is followed by gradual and progressive cooling to culminate with an event of iceberg discharge at the time of maximum cooling or the ensuing prominent warming. As has been proposed for climate oscillations in MIS 3, IRD events can be linked with iceberg discharges associated with episodes of ice-sheet advance towards the coastline at times of maximum cooling (Marshall and Koutnik, 2006), whereas the ensuing warming events are related with minor episodes of ice-sheet retreat that can be seen in other records all over the North Atlantic (Fig. 3.3). In particular, some of the most prominent millennial-scale warmings and the associated IRD events that precede them are clearly linked to ice-sheet decay and global decreases in ice-volume as they coincide with deglaciations at transitions between MIS 30/29, MIS 28/27, and the large deglaciation at Termination XI, between MIS 26/25, that is the most prominent IRD event and signal the onset of the 100 kyr cycles of the Late Pleistocene. In the same way the warming events not associated with major deglaciations usually take place at times of apparent interruptions of ice growth or even minor decreases in ice-volume as they usually take place at times of short inversions in the otherwise increasing benthic $\delta^{18}O$ values. (Fig. 3.5). This pattern of minor global sea-level rises is very evident at least during some of the Bond cycles of MIS 3, in which sea-level rises on the order of 10 to 30 m have been associated either to the IRD events (Heinrich events) or to the prominent warming events that follow them (Arz *et al.*, 2007; Siddall *et al.*, 2003; Sierro *et al.*, 2009). A clear exception to this pattern is observed in MIS 27.4, although almost no IRD event is recorded during this period, the warming event is not linked to ice decay but to a short event of rapid ice growth during this substage.

The relationship between the small depletions in the benthic $\delta^{18}O$ associated to Heinrich events and the subsequent interstadials with global sea-level rises has been widely debated for the last glacial period as these depletions may also be the result of deep water hydrographic changes and replacement of heavy $\delta^{18}O$ northern deep water by the lighter $\delta^{18}O$ southern water (Hodell *et al.*, 2009; Sierro *et al.*, 2009; Skinner *et al.*, 2003). The data provided in this work cannot clarify this controversy, but there are solid arguments that point to significant global sea-level rises associated to the Bond cycles (Arz *et al.*, 2007; Siddall *et al.*, 2003; Sierro *et al.*, 2009).

In order to check if these minor episodes of ice-sheet retreat are recorded in other North Atlantic benthic oxygen isotope records we compared our benthic isotope record with previously published results from Sites 980 (Raymo *et al.*, 2004), 983 (Kleiven *et al.*, 2003), U1308 (Hodell *et al.*, 2008), and with U1313 for the time interval over which these two records overlap (910-790 ka) (Ferretti *et al.*, 2010) (Fig. 3.3). Ice sheet growth after MIS 31 is interrupted by a negative excursion of 0.4 ‰ at MIS 31.1, which is correlated at Site U1308 and 983. The LR04 and B08 records also show this negative oxygen isotope excursion. Similar millennial-scale events of ice-sheet decay seem to be present in most of these benthic records at substages MIS 29.3, 29.1,

and MIS 27.1. The regional occurrence of these negative oxygen isotope excursions all over the North Atlantic does not necessarily proof they are caused by global eustatic rises, since they may be also related to deep water hydrographic changes. In some cases the magnitude of these negative oxygen isotope anomalies is on the order of 0.7 ‰ that is too high to be only associated to ice-volume since this would represent eustatic sea-level increases of 40-70 m. Instead, we suggest that besides the influence of sea-level millennial scale changes in benthic $\delta^{18}O$ partially resulted from the influence of southern water masses with different temperature and salinity (Skinner *et al.*, 2003), or isotopically light water generated by brine formation in the GIN Seas (Dokken and Jansen, 1999; Vidal *et al.*, 1998).

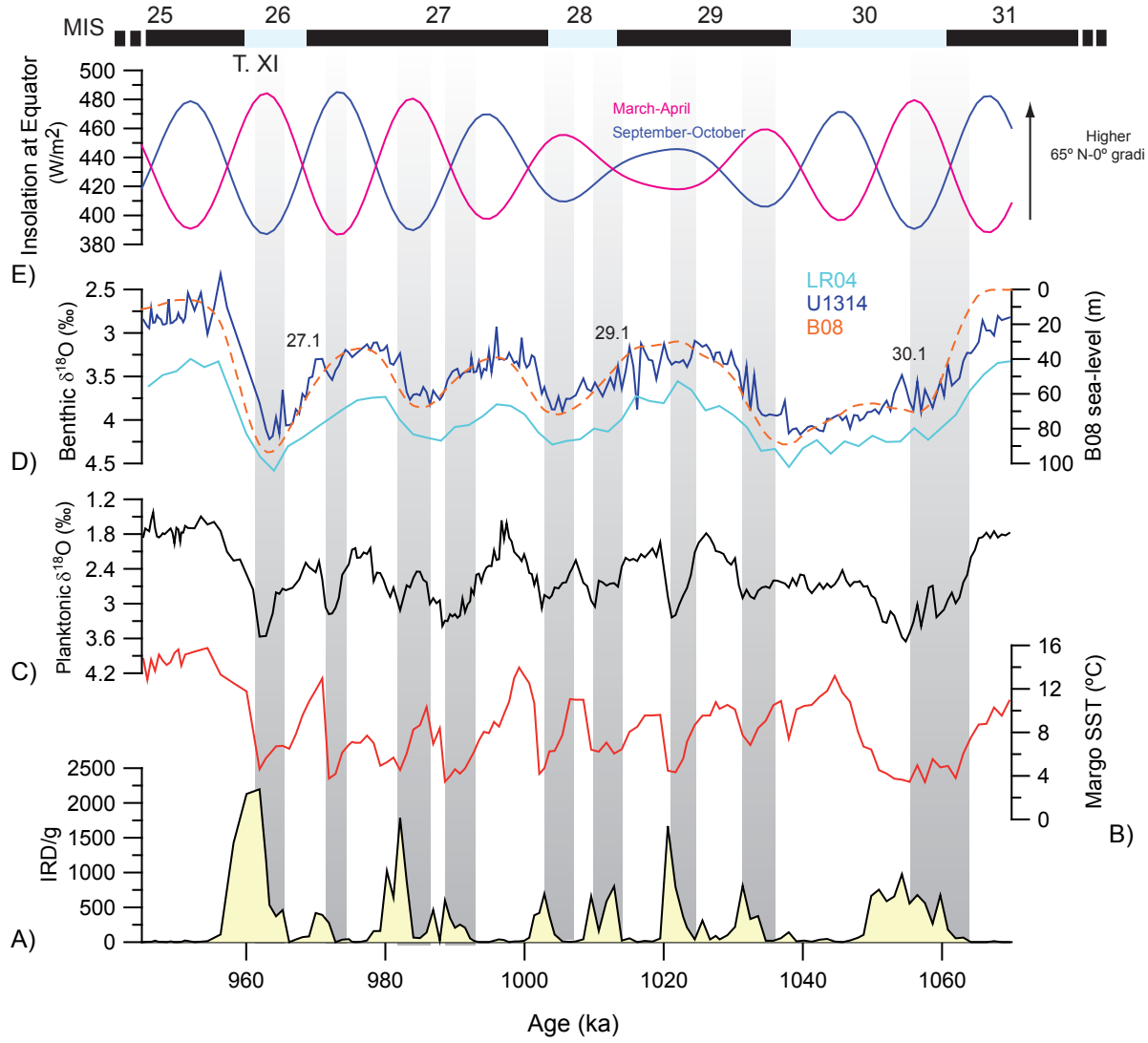

Figure 3.5. Site U1314 records between 1069 and 950 ka. From bottom to top: A) IRD/g, B) planktonic $\delta^{18}O$, C) faunal-based SST, using ANN technique, D) benthic $\delta^{18}O$ (dark blue), benthic $\delta^{18}O$ LR04 stack (Lisiecki and Raymo, 2005) (light blue) and B08 sea-level reconstruction (Bintanja and van de Wal 2008) (orange dashed line), and E) insolation at the Equator in Spring (orange solid line) and Autumn (blue dashed line) (Laskar *et al.* 2004). Vertical grey bars indicate IRD discharge events, either linked to deglaciations or to millennial-scale oscillations. Marine Isotope Stages (MIS) are shown at the top (glacials in blue and interglacials in black).

5.1.1. Origin of the millennial-scale climate changes

As may be seen in figure 3.6 power spectra for the records of sea surface proxies, such as SST, IRD and planktonic $\delta^{18}O$ is mainly concentrated on the 21 and 10 kyr, whereas global ice-volume as recorded by the benthic $\delta^{18}O$ records shows dominant periods at around 21 and 41 kyr. It is interesting the similarity between the timing of these events at Site U1314 and the millennial-scale variability of massive ice discharges seen in the Late Pleistocene sediments (e.g. Bond *et al.*, 1993; Heinrich, 1988; McManus *et al.*, 1999). One might expect that this high-frequencies did not appear at older sedimentary sequences, owing to the smaller size of the Northern Hemisphere ice-sheets, however, an increasing number of marine records at mid-and-high latitudes contain such precessional periodicity and its harmonics during the Early and Mid-Pleistocene (Bartoli *et al.*, 2006; Grützner and Higgins, 2010; Hayashi *et al.*, 2010; Raymo *et al.*, 1998; Wara *et al.*, 2000; Weirauch *et al.*, 2008), evidencing that continental ice-sheets have oscillated in a similar manner in both the 41-kyr and 100-kyr worlds. Hence, the climatic variability represented by surface proxies at Site U1314 might be driven by some component of the system that is consistent throughout the Pleistocene, well before the NHG.

The 23-kyr rhythm and its harmonics are very strong in low latitudes up to 40º N, with power diminishing northward (Ruddiman and McIntyre, 1981c; Ruddiman and McIntyre, 1984). The precessional-related cyclicity is present in different features of surface oceanography at low-latitudes, including primary productivity proxies and changes in wind intensity related to monsoonal variability (McIntyre and Molfino, 1996; McIntyre *et al.*, 1989; Molfino and McIntyre, 1990). The most accepted mechanism that originates this frequency bands at low-latitudes is an external climate forcing attributed to a twice-yearly passage of the sun across the equator during each precession cycle (Short *et al.*, 1991), that generates a signal of half the precession period at the equator. Direct consequence of this process would be the enhanced transport of heat and moisture supply via oceanic and atmospheric circulation from equatorial latitudes to the higher latitudes of the North Atlantic. This mechanism has been invoked to explain the presence of the 11 kyr cycles in oceanic sediments from mid-and-high latitudes in the North Atlantic (Ferretti *et al.*, 2010; Hagelberg *et al.*, 1994; McIntyre and Molfino, 1996; Weirauch *et al.*, 2008).

The relationship in timing between our planktonic $\delta^{18}O$, SST and IRD/g records with insolation records at the Equator in March-April and September-October (Laskar *et al.*, 2004) (Fig. 3.5) led us to speculate that changes in insolation at low latitudes may be responsible for the oceanographic and ice-sheet events described in this study. It is important to note that both equinoxes insolation maxima at equator are in phase with highest latitudinal insolation gradient between 0º-65º N. During both equinox insolation maxima at equator, the latitudinal gradient between 65º N and 0º N reaches the maximum values, leading to higher atmospheric contrast between high and low latitudes, and thus intensifying atmospheric circulation that results, in turn, in enhanced meridional moisture flux. A higher transport of warm water to

the polar regions of the northern hemisphere increases the ice-ocean moisture gradient and accelerates ice-sheet growth, and consequently, the larger the ice-sheet, the more sensitive it becomes to that excess accumulation. This will result in enhanced ice-sheet calving associated to the rapid advance of the ice margins to the coast or the shelf-break (Marshall and Koutnik, 2006). Although speculative, this mechanism would relate the major ice-rafting pulses and surface-deep ocean dynamics to an external forcing originated at low-latitudes, rather than initiating at high-latitudes and then transmitting climate changes around the globe as some models suggest (Ganopolski and Rahmstorf, 2001; Imbrie *et al.*, 1993).

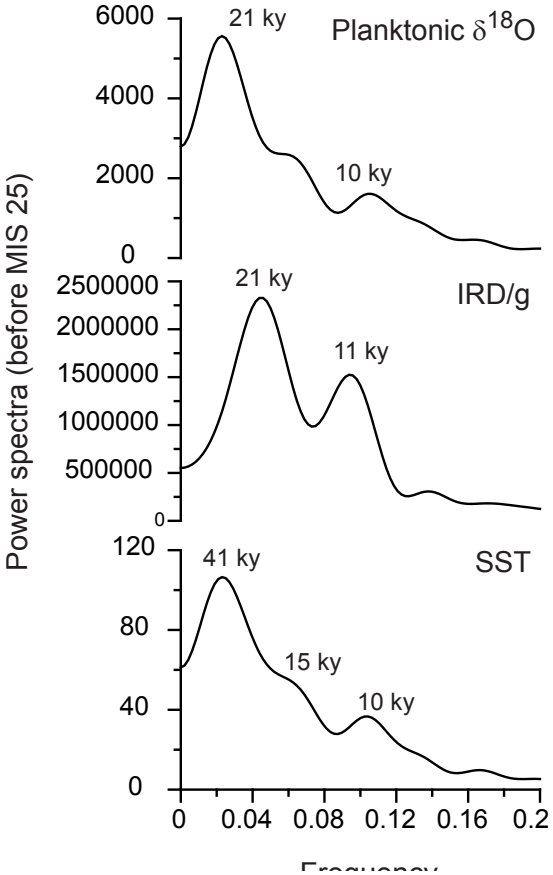

Figure 3.6. Power Spectrum of IRD/g, SST and planktonic $\delta^{18}O$ calculated by the Blackman-Tukey method for the time period before MIS 25 (~ 950 ky). The data used in the time series analysis were interpolated at 1000-year intervals. These calculations were made using *Analyseries* (Paillard *et al.*, 1996).

5.2. Period between MIS 25 and MIS 19: higher amplitude ice-volume changes

It is in MIS 25 when the typical configuration of the 100-kyr glacial cycles is initiated. The first two cycles are recognized in this work from MIS 25 to MIS 22 with a duration of ~ 100 kyr and from MIS 21 to MIS 19 that only lasted ~ 80 kyr (Fig. 3.7). Since MIS 25, a significant change occurred in the character of both surface and deep water proxy signals in the subpolar North Atlantic. We observe a positive shift in benthic $\delta^{18}O$ during glacial stages and greater G-IG amplitude variability, generally ascribed to continental ice-sheet expansion and to more severe

glaciations (Berger *et al.*, 1999; Pisias and Moore Jr, 1981). The range of glacial-to-interglacial variation in planktonic $\delta^{18}O$ values and SSTs increased markedly after MIS 25, in a way similar to the ice-volume variations (Bintanja and van de Wal, 2008; Lisiecki and Raymo, 2005), and reflect colder glacial and warmer interglacial stages than before. The faunal-based SST show an increase in glacial-interglacial peak-to-peak amplitude from 10.5 ºC during the pre-MIS 26 interval to 12.5 ºC after MIS 25, with interglacial temperatures over 16 ºC at MIS 21 and 19 (Fig. 3.7). We interpret this as a greater northward retreat of the AF to a more northerly position during interglacials than that experienced during the previous time interval, while in glacial stages it advanced to the south, bringing cold arctic waters to Site U1314 location, as occurred before MIS 25. Several authors based on faunal data from sites 980 and 984, and percentage of $C_{37:4}$ alkenone at site 983, documented a similar change in surface water conditions toward higher G-IG contrast after MIS 25 (McClymont *et al.*, 2008; Wright and Flower, 2002). This greater G-IG variability might have acted as a positive feedback by increasing the latitudinal temperature gradient that drives moisture transport to the high latitudes, and thus promoting the growth of larger ice-sheets than in the preceding time interval. The growth of northern hemisphere ice-sheets altered the shape of glacial cycles producing an asymmetric response between the deglacial and the glacial slope. Glacial progressions after MIS 25 are considerably longer than the previous glacial periods due to the new configuration of climate cycles.

We observe an amplification of the magnitude and duration of IRD events after MIS 25 (Fig. 3.7), especially in MIS 24, 22 and 20 that coincide with increased IRD deposition along the Norwegian-Greenland margins and Barents Sea after 900 kyr (Helmke *et al.*, 2003; Henrich and Baumann, 1994; Jansen *et al.*, 1988; Knies *et al.*, 2009). The increased abundance of IRD would be attributed to a pronounced ice-sheet expansion in the circum-Atlantic region, reaching fully development in thickness and height already during the Early Pleistocene (Knies *et al.*, 2009; Sejrup *et al.*, 2000). This maximum ice-sheet configuration would be consistent with our hypothesis that increased moisture transport to high latitudes after MIS 25 contributed to the development of more extensive ice-sheets, and it is compatible with paleoclimatic data and models that assume that ice-volume growth during MPT augmented bed-rock depression, leading to more unstable ice-sheets that fully melted during interglacial periods (Bintanja and van de Wal, 2008; Clark and Pollard, 1998).

5.2.1. Climate cycle from MIS 25 to MIS 21

Following MIS 25 that marks the onset of this ~ 100 kyr climate cycle, ice-sheet growth was only punctuated by some short events of lower ice-volume and a major interglacial at MIS 23.3, but the amplitude of this interglacial period was lower than that recorded during interglacial periods before MIS 25 (Fig. 3.7). Consequently, this climate cycle is in fact composed of two obliquity-driven climate cycles with glacial phases at MIS 24 and MIS 22 and the deglaciation of MIS 23.3 probably triggered by the prominent maximum in obliquity at that time.

During the pronounced interglacial period at MIS 25 SST remained high at around 14ºC for a long period of time spanning between 956 and 935 kyr. During this time period ice-volume was low or slightly increasing, however, a sharp cooling of surface waters that changed from 15º to 3 ºC in only 2 kyr, marks the onset of rapid ice-sheet growth as illustrated by the increase in the benthic $\delta^{18}O$ record. Accumulation of ice on the continents is clearly linked to a rapid southward migration of the AF at the latitude of Site U1314 and is followed in only a few kiloyears by iceberg discharge.

Three events of warmer SST were recorded during the glacial period if this climate cycle, a short, low amplitude warming event at the transition between MIS 25/24 (MIS 24.1), and two more prominent warming events at MIS 23.3 and MIS 23.1. All three events are paced by ~ 14 ka, and describe a pattern consisting in an warming phase followed by a progressive shift to cooler temperatures that ends in apparent interruptions or inversions in the trend of ice-sheet growth preceded by and IRD discharge event, consequently we relate them with ice-sheet decay events that can be seen in other North Atlantic benthic $\delta^{18}O$ records (Fig. 3.3). The depletion in $\delta^{18}O$ observed in MIS 23.3 is obviously of higher amplitude but neither SST nor the $\delta^{18}O$ data reached the typical values of the interglacial periods of MIS 25, 21 or 19.

5.2.2. Climate cycle from MIS 21 to MIS 19

This climate cycle starts with an abrupt increase in SST at Termination X that pass from 4 to 14 ºC in only 6 kyr, resulting in a rapid collapse of the ice-sheets that is recorded by a pronounced increase in the IRD/g (Fig. 3.7). SST remained relatively high during MIS 21.7 spanning from 860 to 845 ka with low ice-volume and no iceberg discharge as typically occurs during the most prominent interglacials. During this long period of time continental ice was gradually increasing as recorded by a progressive increase in the benthic oxygen isotope stack LR04, however, the onset of the glacial period is recorded by a very sharp decrease in SST at around 842 ka that is clearly associated with a rapid phase of ice-sheet growth recorded in the LR04 and our benthic $\delta^{18}O$ records by a rapid shift toward heavier values.

During this glacial period spanning from substage 21.7 to Termination IX, three millennial-scale climate oscillations are recorded in SST as recorded by the planktonic foraminifer assemblages and planktonic oxygen isotopes and the benthic oxygen and carbon isotopes. Similarly to that observed in the previous cycles, each of these millennial climate changes start with an abrupt warming event, followed by gradual cooling and increased flux of iceberg discharge and culminates with maximum IRD accumulation rate at time of maximum cooling or during the ensuing abrupt warming event. These climate fluctuations are clearly related with substages MIS 21.5, 21.3, 21.1 that have been identified and correlated across the North Atlantic Ocean (Fig. 3.3). Previous work published by Ferretti *et al.* (2010) suggested that these climatic events, associated with the precession-related frequencies (10.7 and 6 kyr)

at Site U1313, where related to the cross-equatorial heat transport toward high latitudes during both equinox insolation maxima at the equator, in a similar way to that described for the high climatic variability observed between MIS 31 and 26 at Site U1314.

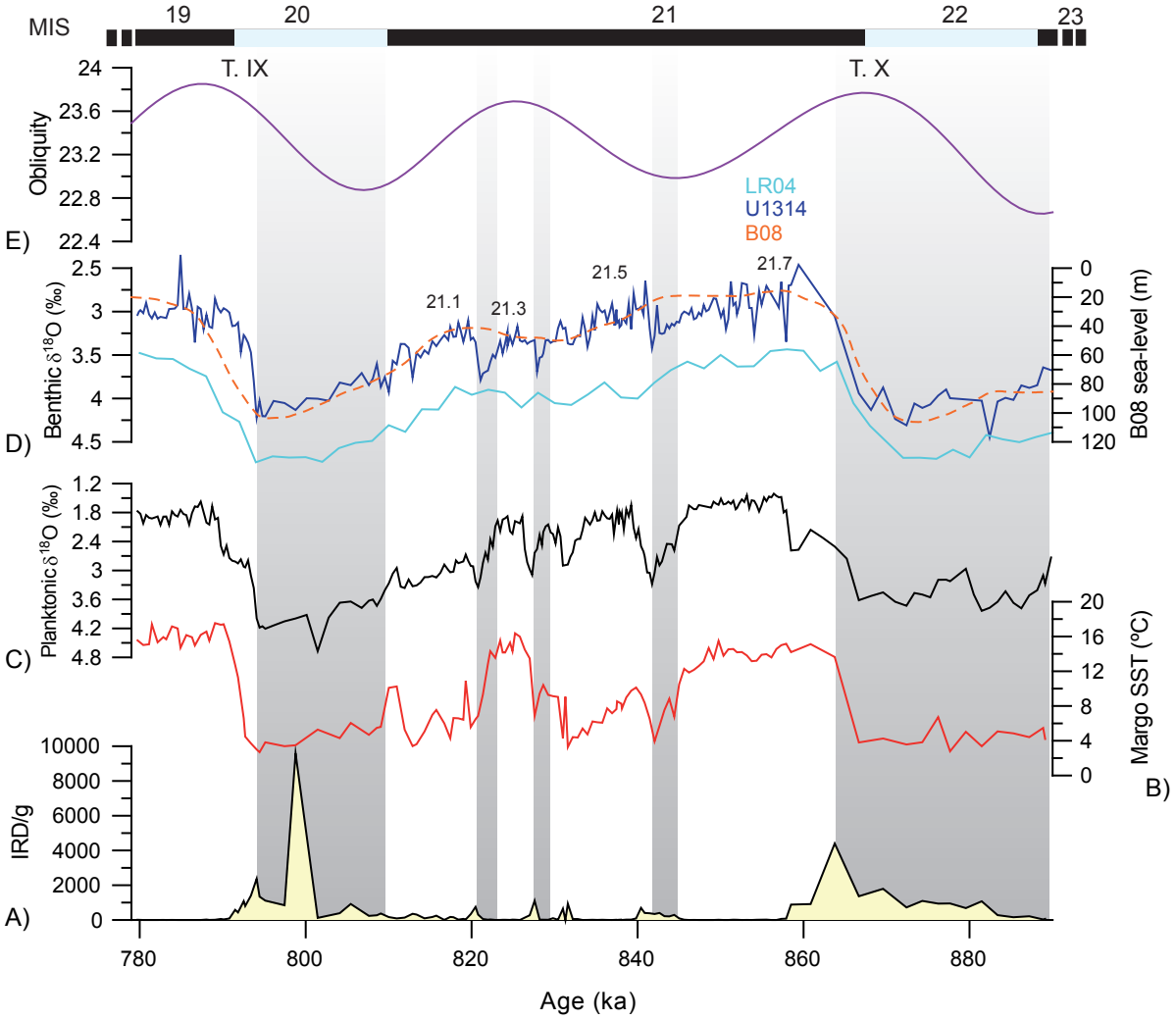

Figure 3.7. Site U1314 records between 1069 and 950 ka. From bottom to top: A) IRD/g, B) planktonic $\delta^{18}O$, C) faunal-based SST, using ANN technique, D) benthic $\delta^{18}O$ (dark blue), benthic $\delta^{18}O$ LR04 stack (Lisiecki and Raymo, 2005) (light blue) and B08 sea-level reconstruction (Bintanja and van de Wal 2008) (orange dashed line), and E) obliquity parameter (Laskar *et al.* 2004). Vertical grey bars indicate IRD discharge events, either linked to deglaciations or to millennial-scale oscillations. Marine Isotope Stages (MIS) are shown at the top (glacials in blue and interglacials in black).

A clear relationship can beestablished between abrupt warming at surface and a sharp decrease in the benthic $\delta^{18}O$, whereas a rapid increase in the benthic $\delta^{18}O$ is always associated with the phase of gradual or rapid cooling at surface. These fluctuations in the benthic $\delta^{18}O$ are also visible in all North Atlantic benthic $\delta^{18}O$ records, and at least the northernmost records typically show an asymmetric pattern, with an abrupt decrease in the $\delta^{18}O$ values at the base followed by a gradual increase in $\delta^{18}O$. In the southernmost record (Site U1313) this pattern is less evident (Fig. 3.3). The decrease of $\delta^{18}O$ at the base of these millennial fluctuations may be related with low amplitude sea-level rises due to smaller ice-sheets, deep water warming or a

higher influence of the low $\delta^{18}O$ southern deep water (Sierro *et al.*, 2009; Skinner *et al.*, 2003). In any case, the long-term increase in ice-volume from substage 21.7 to the glacial maximum in MIS 20 is punctuated by these events in which the $\delta^{18}O$ depletions in the benthic $\delta^{18}O$ record seems to reverse the otherwise increasing trend in ice-volume. The increasing discharge of icebergs during the cold phase to reach maximum values at times of maximum cooling or during abrupt warming seems to support the model results reported by Marshall and Koutnik (2006). The increasing IRD content in the sediments reflects the advance of circum-North Atlantic ice-sheet margins towards the shelf-break, resulting in high delivery of icebergs due to calving. Increased supply of moisture from low latitudes during equinox insolation maxima (Ferretti *et al.*, 2010) would promote a positive mass-balance in the ice-sheets with the consequent gradual sea-level drop. Similarly to model results, maximum delivery of icebergs is reached immediately after maximum cooling, during the phase of abrupt warming. Marshall and Koutnik (2006) found that peak iceberg flux lags maximum cooling because ice margins kept advancing to the coast 600 yr after peak cooling. During the warm phase of the climate oscillations ice margins withdraw from the coast due to ice melting under warmer summer temperatures and no icebergs were delivered to the ocean.

The cooler North Atlantic SST prevailing during the cold climate phases may have also favoured the preservation of icebergs transported from distant regions contributing to further increase the IRD content in the sediments. However, the straight relationship between IRD peaks and short depletions in the benthic $\delta^{13}C$ strongly argues in favour of episodes of ice calving as ice-sheet margins advanced towards the coast. The subsequent delivery of freshwater to the ocean reduced NADW formation that was partially replaced by the high nutrient, low $\delta^{13}C$ southern deep water.

In summary, we relate enhanced IRD with ice-sheet advance and increased ice-volume and the sudden drop in iceberg discharge to ice-sheet retreat that temporally interrupted the long-term trend of ice-sheet growth. This hypothesis cannot be tested because there are no independent records of sea-level for this time, however, we argue that the $\delta^{18}O$ depletions observed at the base of these millennial-scale climate changes can be partially related with low amplitude rises in sea-level similarly to those observed during the Bond cycles (Arz *et al.*, 2007; Siddall *et al.*, 2003; Sierro *et al.*, 2009). These $\delta^{18}O$ depletions, however, were probably amplified by the deep water hydrographic change resulting from the higher influence of LDW in the North Atlantic basin.

It is worthy to mention that the major inversion in the trend of ice-volume increase during this climate cycle occurred in MIS 21.1 that lags obliquity maximum in 6 kyr. However, this event, which is clearly visible in the benthic $\delta^{18}O$ record, is hardly distinguishable in the surface proxies, with only a small increase in SST and a low amplitude decrease in the planktonic $\delta^{18}O$ values. In contrast, a prominent increase in SST and a decrease in the planktonic $\delta^{18}O$ are recorded in MIS 21.3 exactly at the timing of the prominent obliquity maximum. Consequently,

an evident lag between maximum temperature of North Atlantic surface waters and decreasing ice-volume is recorded in this period, with the temperature record following obliquity. In fact, when looking at the SST record alone this climate cycle from MIS 21 to 19 is clearly split into two obliquity cycles of progressive cooling separated by the prominent warming event at MIS 21.3.

5.3. North Atlantic changes in thermohaline circulation at the Mid-Pleistocene Transition

The comparison of various benthic $\delta^{18}O$ records from the North Atlantic allowed us to separate the global ice-volume effect from regional deep-water hydrographic changes. The variation of the benthic $\delta^{18}O$ record from Site U1314 is parallel with those of sites U1308, 983 and 980, throughout both glacial and interglacial intervals. However, the benthic $\delta^{18}O$ values at Site 983 are systematically higher than those at Site U1314, U1308 and 980. Located at northern Gardar Drift (see Table 3.2), Site 983 is bathed today by the main core of the overflow from the GIN Seas, which consist of 70 % ISOW and varying proportions of LSW and SPMW, whereas site U1314, U1308 and 980, located south and east, are influenced by an admixture of northern source ISOW/LSW flow, and Antarctic-derived waters flowing northward from mid-latitudes, the LDW, in a proportion between 5-30 % (van Aken, 2000; Van Aken and De Boer, 1995). Lower oxygen content and salinity values makes this southern water mass clearly distinguishable from pure northern source deep-water in the modern subpolar North Atlantic (Bianchi and McCave, 2000; McCartney, 1992). This pattern shows the existence of a latitudinal gradient of the mixing ratio between two dominant water masses, one sinking in the North Atlantic and the originated in the southern ocean. We suggest that lower benthic $\delta^{18}O$ at Site U1314 respect to northern Site 983 is the result of the progressive mixing of ISOW as it travels along the eastern flank of Gardar Drift with LDW. This assumption agrees with previous $\delta^{18}O$ measurements performed on glacial and modern benthic foraminifera from the North Atlantic that exhibit a great variability, suggesting the deep waters in this basin are not homogenous, probably because they resulted from the sinking of different surface water masses at various locations (Duplessy *et al.*, 2002; Raymo *et al.*, 2004; Skinner *et al.*, 2003; Zahn and Mix, 1991)

To study changes in production and ventilation of deep ocean in the subpolar North Atlantic, we have used the $\delta^{13}C$ signal from benthic foraminifer shells, since variations in this proxy are controlled by both changes in the global ocean CO_2, nutrient content and local deep water chemistry (Boyle, 1986). At Site U1314, there are no large negative excursions in the benthic $\delta^{13}C$ signal from MIS 30 to MIS 26, only punctuated by short-lived depletions associated with glacial terminations and the millennial-scale IRD discharges mentioned above. Benthic carbon data from all subpolar North Atlantic sites show that interglacial benthic $\delta^{13}C$ in the North Atlantic were significantly lower than those observed today. Modern-like deep-

water circulation was only achieved during MIS 27, when benthic $\delta^{13}C \sim 1$ ‰ indicated a strong NADW flow (Kroopnick, 1985). Such difference between modern and Early and Mid-Pleistocene deep circulation is explained by the difference mode of deep-water production in the GIN Seas. Instead of the open ocean conditions that allow deep convection today, Henrich and Baumann (1994) proposed that cold surface conditions during Early and Mid-Pleistocene promoted enhanced sea-ice cover in the GIN Seas, limiting deep convection. Under these conditions, brine rejection under sea ice may have been the dominant mode of deep-water production, what would explain the lower $\delta^{13}C$ before MIS 26 than today.

Our finding of similar glacial and interglacial vertical nutrient profile between mid-depth sites 983, 980 and deeper U1314, suggest that, from MIS 31 to MIS 26, these sites were influenced by the low-$\delta^{13}C$ waters originated in the GIN Seas. Note that the $\delta^{13}C$ at the deepest Site, U1308, gets progressively more negative, especially during glaciations. This site is bathed today by a higher proportion of LDW and lower ISOW than northern sites (van Aken, 2000), and it has served as indicator of the mixing ratio between northern and southern sourced waters during the last glacial maximum (Curry and Oppo, 2005). The small difference of $\delta^{13}C$ between Sites U1314 and U1308 during the studied interval suggests the existence of a common water mass at both sites in the North Atlantic (Fig. 3.8). However, there is an increased nutrient gradient between Site U1314 and the deeper U1308 during MIS 30.1, 28, during high ice-volume phase within MIS 27, MIS 24 and 22, which would indicate the development of a chemocline between 2800 and 3800 m in the subpolar North Atlantic. This chemical division probably indicate the greater influence of southern source deep-waters into the deeper areas of the North Atlantic during times of reduced high latitude convection.

The major disruptions of North Atlantic thermohaline circulation occurred after MIS 25 as recorded by three pronounced minima in the benthic $\delta^{13}C$ during MIS 24, MIS 22 and MIS 20, signalling the onset of the major glaciations in the Northern Hemisphere that result in significant freshwater discharges to the areas of deep water formation in the North Atlantic. Although there are some short, low amplitude depletions in the benthic $\delta^{13}C$ associated with the millennial-scale climate fluctuations described in the previous section, the major disruptions in thermohaline circulation only took place at the time of maximum glaciation when the climate was more stable, to become specially pronounced during Terminations (Fig. 3.4). Paradoxically, during the phase of ice build-up when climate and hydrographic conditions were very unstable at surface as recorded by the millennial-scale changes in SST deep water circulation was relatively stable with continuous NADW formation that result in high benthic $\delta^{13}C$ in bottom waters.

Pronounced excursions to more negative benthic $\delta^{13}C$ values occurred in the North Atlantic during Terminations XI, X and IX (Fig. 3.4). Such large benthic $\delta^{13}C$ minima are associated with the largest peaks of IRD. This relationship suggests that during periods of major deglaciations, the convection in the GIN Seas ceased, and reduced NADW production. This caused a shoaling in the boundary between the northern and southern deep waters on the subpolar

North Atlantic. Hence, negative benthic $\delta^{13}C$ minima indicate a higher proportion of LDW during these Terminations, filling the deep North Atlantic, as is depicted by the convergent $\delta^{13}C$ values between U1314 and U1308. Conversely, the appearance of lower benthic $\delta^{13}C$ values at deep North Atlantic sites may potentially reflect not only inflow of southern source water in the deep North Atlantic but sinking of low $\delta^{13}C$ surface water formed by brine rejection under sea-ice conditions in the GIN Seas, as observed during glacial periods in ocean records of the North Atlantic (Dokken and Jansen, 1999; Raymo *et al.*, 2004; Vidal *et al.*, 1998).

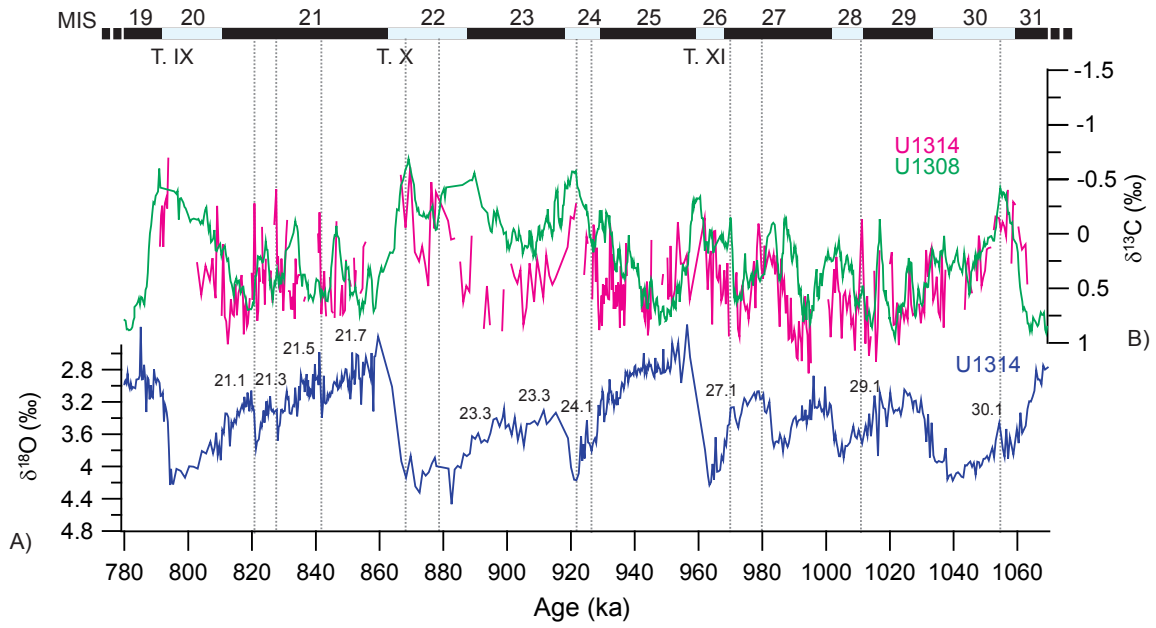

Figure 3.8. From bottom to top: A) benthic $\delta^{18}O$ from Site U1314, B) benthic $\delta^{13}C$ from Site U1314 (pink, only *C. wuellerstorfi* values shown) and U13108 (Hodell *et al.*, 2008) (red). Vertical grey dashed lines depict when the thermohaline circulation become disturbed. Marine Isotope Stages (MIS) are shown at the top (glacials in blue and interglacials in black).

After the deep-water ventilation minima reached at glacial Terminations in Site U1314, $\delta^{13}C$ values increase gradually at the onset of interglacial stages MIS 23, 21, 19, lagging the SST warming by ~ 10 kyr (Fig. 3.4), suggesting the replacement of brine waters formed in the GIN Seas or southern-source deep-waters by interglacial ISOW. As suggested by Hodell *et al.* (2009), the delay on ISOW resumption on Gardar Drift respect to the climate warming may be due to the persistent lowered surface salinity in the Labrador, Irminger and Nordic Sea, that produced components of the NADW with low benthic $\delta^{13}C$ values, and then decreased the strength and/or density of overflow to the North Atlantic. Renewed deep circulation during the following interglacial stages 23, 21 and 19, exhibits values slightly lower than modern NADW (1 ‰) (Kroopnick, 1985), indicating that deep-circulation was still less vigorous than today and there was a proportion of southern sourced water, or remnant brine entrained into water below 2000 m in the subpolar North Atlantic.

6. CONCLUSIONS

The high-resolution records at IODP Site U1314 during the 1069-779 period provide new insights in the evolution of deep-circulation changes and ice-sheets evolution in the Northern Hemisphere during the MPT. Cool surface waters but moderate ice-volume characterized the older time-slice (MIS 31-26). Deep ventilation was primarily of a northern source, favoured by the slightly-cold climate-state that concentrated salts in surface waters, and only with punctual depletions caused by rapid iceberg discharges. Millennial-scale climate oscillations consisting in abrupt warming event followed by gradual and progressive cooling punctuated ice-growth phases. These events were culminated by IRD peaks can be linked with iceberg discharges associated with episodes of ice-sheet advance towards the coastline at times of maximum cooling. The decrease of benthic $\delta^{18}O$ at the base of these millennial fluctuations may be related with low amplitude sea-level rises due to smaller ice-sheets, deep water warming or a higher influence of the low $\delta^{18}O$ southern deep water.

Higher-amplitude changes and the onset of major glaciations at ~ 940 ka (MIS 25) modified dramatically the deep circulation pattern and climate configuration in the North Atlantic. The MIS 25-19 time-slice show incipient characteristic of the Late Quaternary climate cycles, dominated by the 100 kyr cyclicity. Greater build-up of continental ice led to stronger and long-lasted iceberg discharges at glacial maxima and Terminations that transferred large amounts of freshwater from the continents to the surface ocean. Minima benthic $\delta^{13}C$ values during MIS 24, 22 and 20 documents the near-cessation of NADW production during these episodes and the northward intrusion of southern source waters. Moreover, our IRD data support the hypothesis that the MPT represents a fundamental change in ice-sheet dynamics that is consistent with the growth of thicker, more unstable ice-sheets that fully melted during interglacial periods (Bintanja and van de Wal, 2008; Clark and Pollard, 1998).

IRD, SST and planktonic $\delta^{18}O$ time series analysis show a significant concentration of variability at periods of precessional cycles and combination tones of primary precession forcing frequency (21, and 11-10 kyr). Their occurrence at times before the intensification of the NHG evidence they acted independently of the ice-volume accumulated onto continental masses. The timing and structure of the ice surges suggest they might be induced by latitudinal export of equatorial insolation forcing to high-latitudes via tropical convective process, either atmospheric or oceanic. In conclusion, our study outlines the importance of latitudinal energy and moisture gradients atmosphere-ocean-cryosphere feedback mechanisms to generating and transporting this millennial climate variability globally.

Capítulo 4

*MILLENNIAL SCALE VARIABILITY OF PLANKTONIC FORAMINIFER ASSEMBLAGES AND CHANGES IN NORTH ATLANTIC CIRCULATION DURING THE MID-PLEISTOCENE TRANSITION (1069-779 KA)**

*Este capítulo está basado en: Hernández-Almeida, I., Sierro, F.J., Filippelli, G.M., Cacho, I. and Flores, J.A. *Marine Micropaleontology* (en preparación).

RESUMEN. Los cambios en la circulación superficial del Atlántico Norte durante el Pleistoceno Inferior y Medio, entre 1069 a 779 ka, han sido reconstruidos usando el registro de asociaciones de foraminíferos planctónicos y de contenido en $CaCO_3$ de una secuencia sedimentaría recuperada en el IODP *Site* U1314 (56.36° N, 27.88° W) en el *Gardar Drift* (Atlántico Norte subpolar). Los datos obtenidos nos permiten inferir parámetros oceanográficos del pasado, como circulación superficial y productividad, y cuya comparación con registros de otros testigos profundos del océano, nos permite la reconstrucción de la variabilidad del Frente Ártico y de la hidrografía superficial durante la Transición del Pleistoceno Medio. Altas abundancias del foraminífero planctónico polar *Neogloboquadrina pachyderma* sinistrorsa (sin.), baja diversidad y productividad de carbonato biogénico, dominaron la hidrografía superficial hasta el estadio marino isotópico 26. Estas condiciones indican una expansión hacia el sureste del Frente Ártico y la subsecuente penetración de aguas superficiales polares. Las condiciones cambiaron a partir del estadio isotópico marino 25, con mayor contraste entre condiciones glaciares e interglaciares debido al retroceso del Frente Ártico, y periodos cálidos más intensos y estables. Alta diversidad, productividad carbonatada biogénica e incremento de la fauna planctónica subpolar indican la intensificación de aguas cálidas noratlánticas hacia el norte.

Palabras clave: Atlántico Norte; Pleistoceno Inferior y Medio; foraminíferos planctónicos; productividad carbonatada biogénica; Frente Ártico.

ABSTRACT. Changes in North Atlantic surface water circulation during the Early and Mid-Pleistocene, from 1069 to 779 thousands years (kyr), were reconstructed using planktonic foraminifer assemblages and $CaCO_3$ content from the sedimentary sequence recovered at the Integrated Ocean Drilling Project (IODP) Site U1314 (56.36° N, 27.88° W) in the Gardar Drift (subpolar North Atlantic). Our data set allow us to infer past oceanographic parameters, as superficial circulation and productivity, and comparison with records from other deep-ocean cores, allow reconstruction of Arctic Front (AF) variability and surface hydrography during the Mid-Pleistocene Transition (MPT). High abundances of polar planktonic foraminifer *Neogloboquadrina pachyderma* sinistrorsa (sin.), low biogenic carbonate productivity and diversity dominated surface water hydrography until Marino Isotope Stage (MIS) 26. These conditions indicate a south-eastward expansion of the AF and subsequent penetration of cold polar surface waters. Conditions changed after MIS 25, toward a higher glacial-to-interglacial contrast due to a greater retreat of the AF, with more intense and stable warm periods. High diversity, biogenic carbonate productivity, and increase subpolar planktonic fauna mark the enhanced northward advection of the North Atlantic Current (NAC).

Key words: North Atlantic; Early and Mid-Pleistocene; planktonic foraminifer; carbonate productivity; Arctic Front.

MILLENNIAL SCALE VARIABILITY OF PLANKTONIC FORAMINIFER ASSEMBLAGES AND CHANGES IN NORTH ATLANTIC CIRCULATION DURING THE MID-PLEISTOCENE TRANSITION (1069-779 KA)

1. INTRODUCTION

Detailed analyses of high-latitude North Atlantic sediment cores and paleoclimatic models have demonstrated the persistence of cyclical ice-volume variations and abrupt global climate changes throughout the Pleistocene Period. Specially intriguing is the period between 1100 and 700 kyr, known as the "Mid-Pleistocene Transition" (MPT) (Berger and Jansen, 1994b), when there was a large build up of ice-sheets in the North Hemisphere that produced higher amplitude climatic oscillations (Kleiven *et al.*, 2003; Mudelsee and Schulz, 1997; Raymo *et al.*, 1997; Raymo *et al.*, 2004; Tziperman and Gildor, 2003). This reconfiguration of the global ice-volume budget may have been associated with changes in deep-ocean circulation. In this sense, a high number of studies conducted with long-sedimentary sequences from the North Atlantic Ocean have provided paleoclimatic and paleoceanographic records that evidence strong suppression of deep-ocean ventilation during ice-sheet collapses at glacial-interglacial (G-IG) Terminations (Hodell *et al.*, 2008; Kleiven *et al.*, 2003; Raymo *et al.*, 1997; Raymo *et al.*, 2004; Venz *et al.*, 1999). The melt water produced from these icebergs discharges decreased sea surface salinity and cooled surface ocean by increasing sea-ice formation, and diminishing rates of thermohaline circulation.

Such changes in deep-ocean ventilation are directly related to migrations of the North Atlantic Arctic Front (AF), and hence, to the variability in the advection of temperate Atlantic surface waters that transport heat and moisture toward the north (Baumann *et al.*, 1995; Wright and Flower, 2002). These changing surface ocean conditions largely affected the planktonic communities, as it has been reported in several studies using micropalelontological proxies, such as coccolithophores (Marino *et al.*, 2008), diatoms (Shimada *et al.*, 2008), planktonic foraminifers (Wright and Flower, 2002) and radiolarians (Hernández-Almeida *et al.*, 2011a, submitted). Therefore, the analysis of fossil assemblages provides an effective tool for paleoceanographic reconstructions.

In the present study, we have examined in detail the relationship between planktonic foraminifer assemblages, $CaCO_3$ percentages and grain size records over the 1069-779 ka time period from Site U1314, located in a region that is particularly sensitive to migrations of the AF. The main goal is to analyse the influence of sea surface and deep water hydrography on the planktonic foraminifer assemblages as well as carbonate productivity and sediment accumulation on the Gardar Drift

2. STUDY AREA AND SITE LOCATION

Integrated Ocean Drilling Program (IODP) Site U1314 was drilled by the D/V JOIDES Resolution in the southern Gardar Drift, in the northeast Atlantic (56.36° N, 27.88° W) during IODP Expedition 306 (Fig. 4.1). Site U1314, at 2820 m water depth, is at the northern edge of the glacial North Atlantic IRD belt (Ruddiman, 1977; Ruddiman and McIntyre, 1981b) documenting direct evidence of ice rafting activity and deep current variations during the Pleistocene (Bianchi and McCave, 1999; Grützner and Higgins, 2010; Hodell *et al.*, 2009; Wang and McCave, 1990). At surface, Site U1314 is strongly influenced today by the northward flow of the North Atlantic Current (NAC). This surface water mass travels northward across the North Atlantic where it crosses the Mid-Atlantic Ridge between 53° N and 60° N. One branch turns northwestwards and travels as the Irminger Current (IC) on the western and northern side of Iceland, while the main branch flows over the Iceland-Faeroe Ridge into the Greenland, Iceland, and Norwegian (GIN) Seas (Krauss, 1986; Reynaud *et al.*, 1995). This current carries heat to the north and maintains the warm climates of central and northern Europe. Winter convection of the warm and salty Atlantic surface waters in the GIN-Seas results in the formation of North Atlantic Deep Water (NADW) that flows as the Iceland-Scotland Overflow Water (ISOW) through the Faeroe Bank channel to enter the Iceland basin (Schmitz and McCartney, 1993; Swift, 1984). Site U1314 is seasonally affected by the southward extension of cold and less saline waters of the East Greenland Current (EGC).

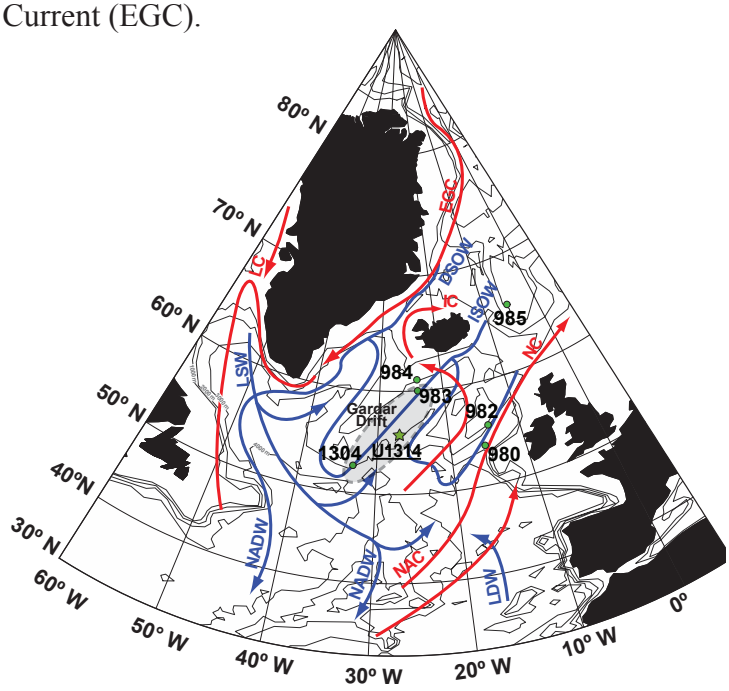

Figure 4.1. Location of IODP Site U1314 (black star: 56º21'N, 27ºW; 2820 m water depth), and other North Atlantic sites (see Table 4.1). Modern surface (red), and deep circulation (blue) in the North Atlantic (Krauss, 1986; Schmitz and McCartney, 1993). Map generated with *Ocean Data View v.3.4.3.* software (Schlitzer, 2008). East Greenland Current (EGC), Norwegian Current (NC), Labrador Current (LC), North Atlantic Current (NAC), Irminger Current (IC), Denmark Strait Overflow Water (DSOW), Iceland Scotland Overflow Water (ISOW), Labrador Sea Water (LSW), North Atlantic Deep Water (NADW), and Lower Deep Water (LDW).

The distinct oceanic front between warm saline NAC and the IC, and the cold arctic waters is known as the Artic Front (AF), that is the boundary that delimitate the maximum extent of winter sea-ice, and The cold and low salinity polar waters transported by the EGC are separated by the Polar Front (PF) from the cold but saltier arctic waters (Swift and Aagaard, 1981). The PF is close to the summer sea-ice edge, thus polar waters are perennially under the sea-ice, resulting in minima carbonate productivity (Henrich, 1998). South of the AF, calcareous productivity is more intense while and terrigenous deposition occurs widely north of the AF (Henrich *et al.*, 2002). Located in the eastern flank of the Reykjanes Ridge, the Gardar Drift, where Site U1314 was drilled, is a 1100 km long contourite deposit of pelagic material supplied by the southward flow of the Iceland Sea Overflow Water (ISOW) (Bianchi and McCave, 2000), with high-sedimentation rates during the Pleistocene (Wold, 1994).

Site	Latitude	Longitude	Location	Data	Reference
U1314	56º36'N	27º88'W	Gardar Drift	fauna, $CaCO_3$	this study
985	66º56'N	6º27'W	Iceland Plateau	fauna, $CaCO_3$	Baumann and Huber (1999)
984	61º25'N	24º04'W	Bjorn Drift	fauna, $CaCO_3$	Wright and Flower (2002) Baumann, personal communication
980	55º29'N	14º42'W	Feni Drift	fauna	Wright and Flower (2002)
982	57º30'N	15º52'W	Rockall Plateau	$CaCO_3$	Baumann and Huber (1999)

Table 4.1. Site information.

3. MATERIAL AND METHODS

The sedimentary sequence recovered at this Site U1314 varies in colour from very dark grey to light grey to hues of greenish grey, and mainly consists of predominantly nannofossil oozes enriched in biogenic and terrigenous components, and terrigenous silty clay with a varying proportion of calcareous (e.g., nannofossils, foraminifers) and siliceous organisms (e.g., diatoms and radiolarians). More detailed core description is given in Expedition 306 Scientists (Channell *et al.*, 2006).

Samples were taken every 4 cm as 2-cm thick slices between the 60 to 84.16 meters composite depth (mcd). All samples were oven-dried, weighed, and wet sieved over a 63 μm screen, and then oven-dried again. Later, the sample was dry sieved into two fractions, 63-150 μm and > 150 μm. Census counts and picking for the stable isotope analyses were carried out in the > 150 μm fraction. Full census counts were completed every other sample. Each sample was split as many times as necessary to obtain an aliquot that contains about 400 planktonic foraminifers, then species of planktonic and benthic foraminifer, mineral grains, ash, lithic fragments, radiolarians, ostracodes and planktonic foraminifer fragments were counted and relative abundances and fluxes were then calculated. Our taxonomy criteria for planktonic foraminifer specimens follows that of Bé (1977) and Hemleben *et al.* (1989). Diversity patterns of planktonic foraminifer assemblage were determined using the Shannon Weaver index

(Shannon and Weaver, 1963) This index is sensitive to both changes in the number of species and their relative abundance in the sample. High values can result from an addition of species, greater equality in abundance, or both. A more detailed discussion of this index and its use in ecological studies is provided by (Pielou, 1975).

The total carbon (TC) content of the sediment was measured every sample using a UIC Coulometrics CM150 carbon analyzer. Total organic carbon (TOC) was determined by gently removal of inorganic carbon with HCl 2M, and then measured using a Flash 2000 Combustion CHNS/O Analyzer. Calcium carbonate content was then calculated from the weight percentages of the bulk sample using the following equation:

$$CaCO_3\% = (TC\ \% - TOC\ \%) \times 8.33$$

In order to estimate carbonate dissolution a planktonic foraminifer fragmentation index (FI) was also calculated, by measuring the ratio between planktonic foraminifer fragments and whole tests. Furthermore we estimate the ratio of benthic to planktonic foraminifers B/(P+B) in the > 150 μm size fraction. In general, dissolution produces more planktonic foraminifer fragments and preferentially removes planktonic foraminifers, which leads to a higher FI and B/(P+B) ratio (Thunell, 1976).

4. CHRONOLOGY AND AGE-DEPTH MODELLING

The conversion from core depth to time was derived by direct correlation of benthic foraminifer oxygen isotope record from Site U1314 and the LR04 benthic isotope stack (Lisiecki and Raymo, 2005). All correlations were performed using the *AnalySeries 2.0.* software (Paillard, 1996). The final age model for the 24.16 m of the core section spans an interval from 779 to 1069 ka based on 13 tie points yielding a temporal resolution of 290 kyr. The final age model for the 24.16 m studied section spans an interval from ~ 290 kyr through the Early and Mid-Pleistocene based on 13 stratigraphic tie points, yielding a temporal resolution of ~ 0.5 kyr. In between the tie points sedimentation rates were assumed constant based on shipboard preliminary stratigraphy (Expedition 306 Scientists, 2006). The resulting sedimentation rates are moderately high (average 9.3 cm/ka) and differ largely between glacial (as low as 1.15 cm/kyr) and interglacial (up to 27 cm/ka) intervals, indicating enhanced growth of the Gardar Drift during intervals of warmer climate. See Hernández-Almeida *et al.* (in prep.) for further details of the age model construction.

5. RESULTS

5.1. Fauna results

The concentration of planktonic foraminifers in the sediments is higher during glacial periods, especially in MIS 20, 22, 24 and 26, when average values of 20,000 pla planktonic shells per gram of dry sediment are reached, although relatively high values are also recorded in some interglacial periods, such as in MIS 23, MIS 27 or MIS29. In general, the higher contents of planktonic foraminifers usually occur at times of high percentages of *N. pachyderma* sinistrorsa (sin.) and enhanced deposition of ice-rafted debris (IRD) during glacial periods and stadials (e.g MIS 26, 24 and 20) (Fig. 4.2).

Concerning the foraminifer assemblages the most abundant species in the period studied are *Neogloboquadrina pahyderma* sin., *Neogloboquadrina pachyderma* dextrorsa (dex.), *Globorotalia inflata*, *Globigerina bulloides*, *Globigerinita glutinata* and *Turborotalita quinqueloba*. The dominant species along the studied section is *N. pachyderma* sin. Glacial stages are highly dominated by *N. pachyderma* sin., however during the interglacial stages, it is rapidly substituted by a multispecies assemblage, where *N. pachyderma* dex. is the most abundant (from 65% to less than 1 %), followed by *G. inflata*, *G. bulloides* and *T. quinqueloba* (Fig. 4.2). *N. pachyderma* sin. shows a high variability ranging from 5 to 90 %. The lowest values are recorded at MIS 19. Throughout the interval studied an overall upcore decreasing pattern is observed during interglacial periods.

Two distinct forms of *N. pachyderma* sin have been identified following the criteria of Srinivasan and Kennett (1974) and Vilks (1974). The nonencrusted *N. pachyderma* sin. has a smooth, shiny, reticulate surface, with larger latter chambers and lobate shape. The shells of encrusted form are opaque, with a heavily encrusted crystalline surface and the morphology tends to more quadrate (see Fig. 4 in Kohfeld *et al.*, 1996). Large numbers of the encrusted forms of *N. pachyderma* sin. first appear close to the Plio/Pleistocene boundary, related to deposition of glacial detritus and absence of other cold water species, such as *N. atlantica* and nonencrusted *N. pachyderma* sin. (Huddlestun, 1984; Poore and Berggren, 1975). It is no clear if this encursted form is resulted from a process that converts nonecrusted *N. pachyderma* sin, into encrusted forms by a secondary calcification (Kohfeld *et al.*, 1996; Volkmann and Mensch, 2001), or they must be considered two different morphotypes entirely (Bergami *et al.*, 2009), but what is clear is they occupy two distinct environments. The nonencrusted form are found in the mixed layer, between 0-100 m, above the main pycnocline, whereas the encrusted morphotypes are associated to greater depths up to 300 m, with the main pycnocline (Bergami *et al.*, 2009; Kohfeld *et al.*, 1996; Stangeew, 2001). At Site U1314, encrusted individuals of *N. pachyderma* sin. appear more abundant during the last two glacial stages, at MIS 22 and 20, replacing the lobate form of this species (Fig. 4.4).

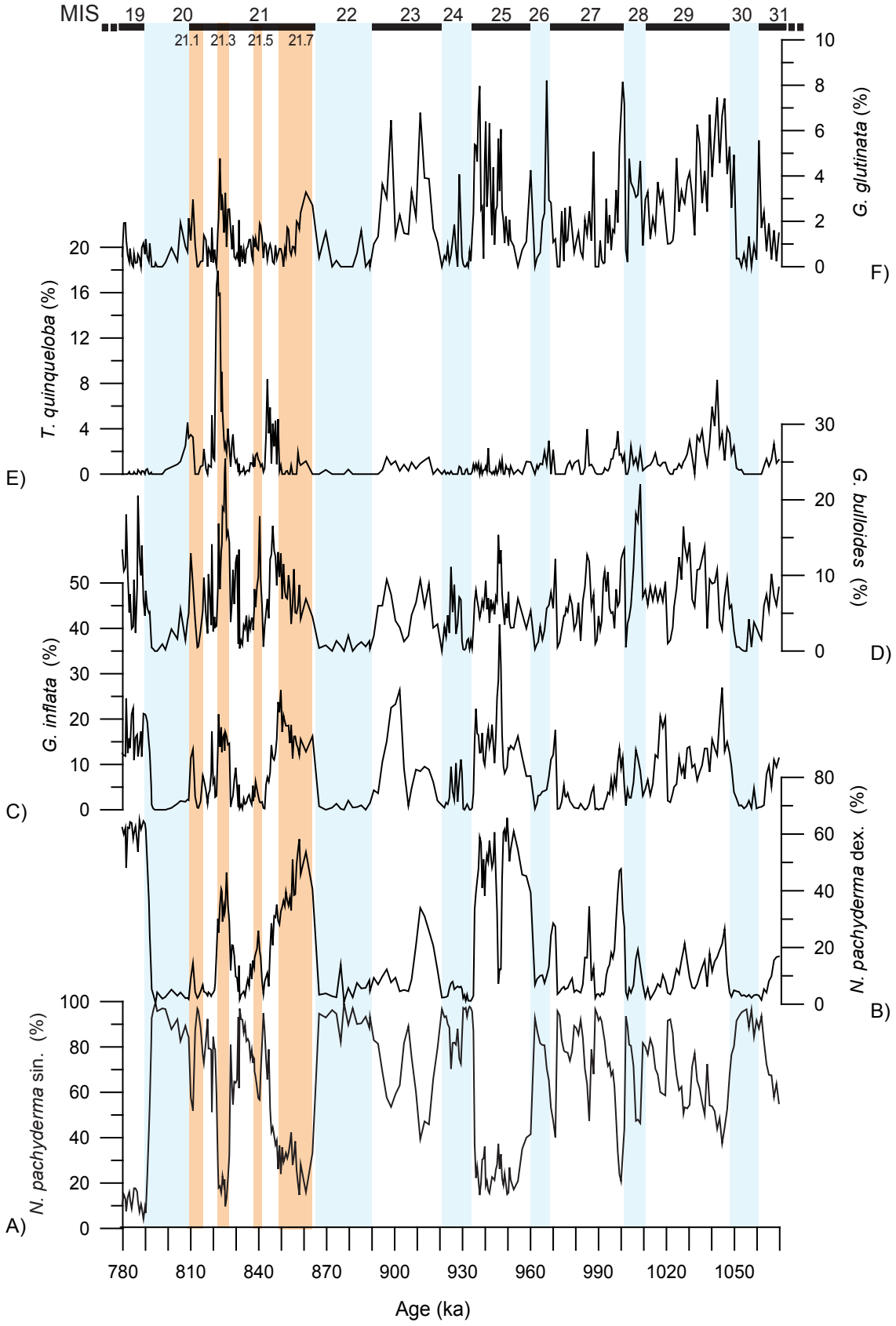

Figure 4.2. Planktonic foraminifer assemblages of Site U1314. Relative abundance of the different species, from bottom to top: A) *N. pachyderma* sin., B) *N. pachyderma* dex., C) *G. inflata*, D) *G. bulloides*, E) *T. quinqueloba* and F) *G. glutinata*. Glacial Marine Isotope Stages (MIS) are shown with blue vertical bars. Interglacial sub-stages 21.7, 21.5, 21.3 and 21.1 are shown with orange vertical bars.

The abundance record of *G. inflata* is similar to that of *N. pachyderma* dex., with values between 40 and 0 %, with a prominent peak during MIS 25. However, both species display opposite trends during MIS 21 (Fig. 4.2). The relative abundance of *G. bulloides* varies between 0 and 25%, reaching the maximum values during MIS 21. The pattern shown by this species is clearly similar to that of *N. pachyderma* dex., except during MIS 25 and 21, where they show rather opposite trends (Fig. 4.2).

Besides the most abundant species described previously, *G. glutinata*, and *T. quinqueloba* contribute in less proportion to the total assemblage. The *G. glutinata* distribution resembles that of *G. bulloides*; with values between 0 and 8%. The main feature of this curve are the low values from MIS 22 upward, and the abrupt increase from MIS 23 downward, where there are three peaks of around 8%. *T. quinqueloba* percentages are below 5 % throughout the studied section, except at MIS 29 and 21, when it reaches percentages around 18 % (Fig. 4.2).

5.2. $\delta^{18}O$ sea water

Using summer paleotemperature-estimates based on artificial neural network (ANN) technique and parallel planktonic $\delta^{18}O$ measurements carried out on *N. pachyderma* sin., a record of surface water $\delta^{18}O$ ($\delta^{18}O_{sw}$) has been calculated (Fig. 4.3). As *N. pachyderma* sin. is thought to calcify around 100 m, where the mean temperature is a remnant of the wintertime mixing, their shells would reflect the winter situation even though the calcification occurs during the summer season (Nyland *et al.*, 2006), therefore, we used winter ANN paleotemperatures in our $\delta^{18}O_{sw}$ reconstruction.$\delta^{18}O_{sw}$ was then corrected for global ocean shifts caused by ice volume changes. The global ice volume corrected seawater $\delta^{18}O_{sw}$ was calculated using a 1 ‰ whole ocean change between the LGM and the latest Holocene scaled to a 120 m sea level change using the global sea-level reconstruction by Bintanja *et al.* (2008)

It has been widely demonstrated that planktonic species do not always precipitate calcite in equilibrium. Based on the $\delta^{18}O$ measurements on seawater and *N. pachyderma* sin. tests from both seafloor grab and piston core samples from the Icelandic continental shelf, Smith *et al.* (2005) observed a $\delta^{18}O$ disequilibrium offset of 0.25 ‰. Taking into account the proximity of these samples to Site U1314, we applied a correction factor of + 0.25 ‰ to our calculated $\delta^{18}O_{sw}$. However, others authors have also observed a disequilibrium offset in the oxygen isotope composition of *N. pachyderma* sin. ~ 0.6 ‰ associated with post-gametogenic processes and thermal stratification of the water column (Nyland *et al.*, 2006; Stangeew, 2001). Contradicting studies indicate that this issue is not well constrained with a need for further study. Moreover, the reconstructed $\delta^{18}O_{sw}$ values span a range of -1.8-1.3 ‰ that exceeds the modern subpolar-subtropical $\delta^{18}O_{sw}$ gradient of 1 ‰ (Schmidt, 1999). Due to the previously commented uncertainties on *N. pachyderma* sin. vital effect, or to extreme SST low temperatures during the MPT that overestimated the $\delta^{18}O_{sw}$ values, we suggest caution when interpreting absolute down-core $\delta^{18}O_{sw}$ values.

5.3. Carbonate content and grain size

The $CaCO_3$ values from Site U1314 averaged 34.3%, with higher carbonate occurring in interglacial isotope stages and minimum during glacial stages (Figs. 4.5; 4.6). The typical glacial-to-interglacial change in carbonate percentage over 1069-779 time period was from 8 to 50 %. Highest values occurred during interglacial stage 31, 25, 21 and 19, and lowest during glacial stage 28, 26 and 22.

The fine-size fraction (< 63 wt. %) is the most abundant, with higher values during interglacial stages, always over 90 % (Fig. 4.6), while the lowest values are recorded at MIS 24 and 22 when the coarse fraction (> 63 wt. %) shows the higher values (Fig. 4.6). The $CaCO_3$ percentage record is better correlated with the fine fraction than with the coarse fraction. The highest contribution of the planktonic foraminifers to the carbonate content of the samples is observed at MIS 22, with around 180000 individuals/g (Fig. 4.6), as well as in other glacial stages, coinciding with high percentages of the coarse fraction.

5.4. Carbonate dissolution indices at Site U1314

Higher values of the planktonic fragmentation index (FI) at Site U1314 are recorded at interglacial periods with higher percentages of *N. pachyderma dex*., *G. inflata, G. bulloides* and *T. quinqueloba*, while it decreases at times of dominance of the polar species *N. pachyderma* sin., with a maximum FI of 32 % at 1002 kyr (Fig. 4.5). The B/(P+B) ratio resemble the FI record (Fig. 4.5) while the Shannon diversity (*H*) index follows the record of subpolar, temperate-water species, with higher diversity in the planktonic foraminifer assemblage during interglacial and lower during glacial stages (Fig. 4.4).

6. DISCUSSION

6.1. North Atlantic hydrographic changes

The present distribution of planktonic foraminifer assemblages clearly reflects the general hydrography of the North Atlantic. High percentages of *N. pachyderma* sin. are associated to the EGC with annual mean temperatures of 2 ºC (Pflaumann *et al.*, 2003; Tolderlund and Be, 1971). This is commonly the only species surviving in this region, giving in consequence extremely low diversity values. In contrast, *N. pachyderma* dex. and *G. inflata* are definitely linked to the warmer waters of the NAC (Hald *et al.*, 2007; Kipp, 1976; Schiebel and Hemleben, 2000). Other species such as *G. bulloides*, *G. glutinata* and *T. quinqueloba* are also present, the last species being more abundant along the region of the AF (Johannessen *et al.*, 1994). In consequence, diversity of planktonic foraminifers thriving along the NAC is higher. Site U1314 is located today along the main course of the NAC, with an average modern $\delta^{18}O_{sw}$ of 0.3 ‰ (Schmidt, 1999), and a foraminifer assemblage dominated by *N. pachyderma* dex. *G. inflata*,

G. glutinata and *G. bulloides*, with almost no *N. pachyderma* sin. (Hald *et al.*, 2007; Schiebel and Hemleben, 2000).

In this work changes of the foraminifer assemblages between 1069 and 778 kyr have been used to reconstruct the variations in the North Atlantic hydrography, in particular to explore the main oscillations of the AF that controls the northward flow of the NAC versus the arctic waters at site U1314. In order to accomplish this goal we used the abundance of *N. pachyderma* sin. as a proxy for arctic waters, while the abundance of *N. pachyderma* dex. and *G. inflata* as a proxy for the warm-water of the NAC.

As you may see in figure 4.2, high frequency fluctuations in North Atlantic surface circulation with periods of around 10 kyr prevailed prior to 960 kyr ago, although on average typically interglacial conditions similar to those found today were never reached until MIS 25 when percentages of *N. pachyderma* dex. and *G. inflata* over 70% are reached. In contrast, the influence of arctic waters with percentages of *N. pachyderma* sin. over 90 % was cyclically replaced by temperate waters that record the temporal advection of the NAC. Decreasing percentages of the only polar species found at Site U1314, *N. pachyderma* sin., evidence an AF north-west retreat and rising SST (Fig. 4.2). However, AF retreats where moderate, since *N. pachyderma* sin. percentages did not fall below 40 % within this period, indicate the limited influence of the NAC at this latitude compared to today, since relative abundances of this polar species in modern pelagic sediments are below 10 %. The reconstructed $\delta^{18}O_{sw}$ records from figure 4.3 agrees well with fauna-inferred hydrographic circulation for the MIS 31-26 interval. Our record indicates lower than modern $\delta^{18}O_{sw}$ 0.3 ‰ until MIS 26, with only brief millennial-scale positive $\delta^{18}O_{sw}$ excursions. This negative $\delta^{18}O_{sw}$ values only can readily be explained substantial freshening of the surface ocean caused by the AF location south of site U1314, and expansion of low $\delta^{18}O_{sw}$ arctic surface waters from the into the North Atlantic. Diatom assemblages records from North Atlantic sites 983 and 1304 support this interpretation, since they were dominated by the cool and low-saline waters related *Neodenticula seminae* during this period (Koç *et al.*, 1999a; Shimada *et al.*, 2008), reflecting a more southerly extension than today of the AF even during interglacials. Southern limits of the AF may have reached latitudes between 32-37º N, based on the occurrence of the diatom *N. seminae* in North Atlantic sediments (Baldauf, 1986; Ikeda *et al.*, 2000). Generalized cooled surface waters during glacial stages may have hampered surface productivity, as seen in the decrease in $CaCO_3$ values (2 %) during MIS 28 and 26, likely due to the southeastward migrations of the PF covering U1314 with year-round sea ice cover. In contrast, $CaCO_3$ values between 7-30 % at Site U1314 and presence of diatom productivity at the neighbour site 983 during MIS 30 (Koç *et al.*, 1999a) reflect some surface productivity, and suggest that the North Atlantic was free of sea-ice during this glacial stage.

Between MIS 31 and MIS 25 while global climate and ice volume was mainly driven by precession as shown by the benthic $\delta^{18}O$ record, the North Atlantic surface circulation, as

shown by the fauna and $\delta^{18}O_{sw}$ records, oscillated at 10 kyr cycles. The warmer events at 1044, 999 and 970 kyr do not necessarily occur at times at interglacial times with smaller ice-sheets, in particular the first and last of these three events took place during glacial periods, but all of them occurred at times of high insolation gradients during fall between the Equator and the high latitudes of the northern Hemisphere. In consequence, we can conclude that suborbital North Atlantic oscillations and shifts of the AF were not driven by global changes in ice-sheets dynamics.

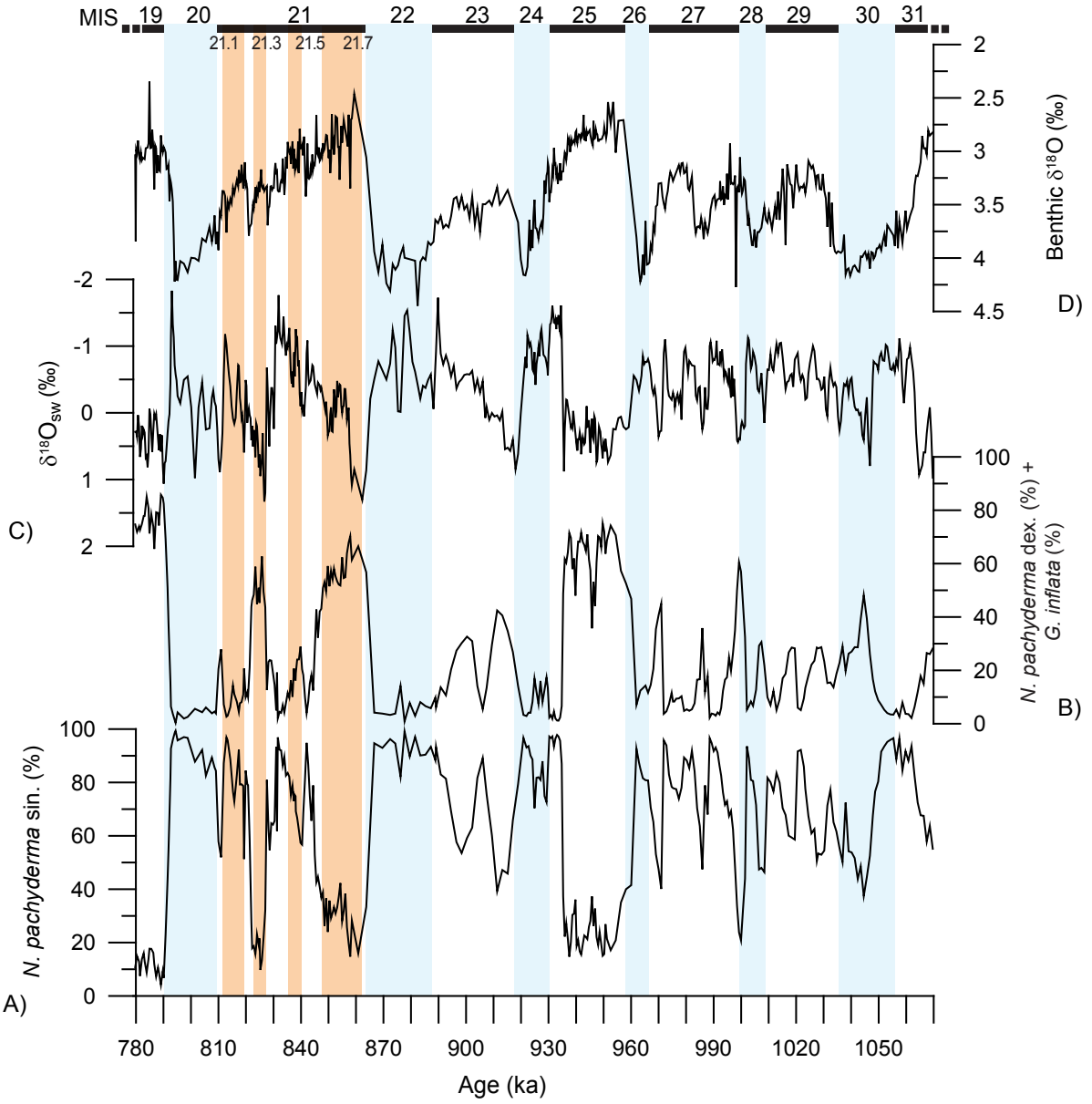

Figure 4.3. Site U1314 records from 779 to 1069 ka. From bottom to top: A) relative abundance of *N. pachyderma* sin. and B) *N. pachyderma* dex. + *G. inflata*, C) $\delta^{18}O_{sw}$ and D) benthic $\delta^{18}O$. Glacial Marine Isotope Stages (MIS) are shown with blue vertical bars. Interglacial sub-stages 21.7, 21.5, 21.3 and 21.1 are shown with orange vertical bars.

Planktonic foraminifer assemblages sharply changed at the onset of interglacial cycle of MIS 25, characterized by a long period of warm-water advection to Site U1314 with percentages of *N. pachyderma* dex. and *G. inflata* well over 70%, very similar to those reached during the Holocene, indicating SST between 10 and 14ºC (Hald *et al.*, 2007; Pflaumann *et al.*, 2003) (Fig. 4.3). This prominent and long interglacial period marks the onset of the 100 kyr G-IG cycles that characterize the Late Pleistocene. In particular, two other prominent stages with very high percentages of *N. pachyderma* dex. and *G. inflata* may be seen in MIS 21 and MIS 19 that indicate strong advection of the NAC towards the North Atlantic latitudes, similarly to that occurring today in this region. Based on the *N. pachyderma* and *G. inflata* record, two 100-kyr cycles can be recognized, starting at MIS 25 and MIS 21, respectively.

The first 100 kyr cycle started with prominent interglacial temperatures in MIS 25 and lasted for more than 20 kyr was followed by a sharp cooling event, evidenced by a pronounced increase in abundance of *N. pachyderma* sin (Fig. 4.3). This event took place at 933 kyr and reflects an abrupt southward shift of the AF. Cool arctic conditions were followed by three events of significant NAC advection towards the North Atlantic, the first one of smaller amplitude occurred during glacial stage MIS 24, while the latest two related with warmer waters are linked to two substages of MIS 23. Maximum glacial conditions during this 100 kyr cycle were recorded during MIS 22 in which arctic waters with planktonic foraminifer assemblage characterized by almost 100 % *N. pachyderma* sin. prevailed in the region for a long period of time, spanning from 885 to 862 kyr. This glacial stage is considered the most severe of the Early and Mid-Pleistocene (Head and Gibbard, 2005). Based on the high benthic $\delta^{18}O$ values (Hernández-Almeida *et al.*, in prep.), and in the diatom-barren samples at Site 983 (Koç *et al.*, 1999a), we infer that PF may have migrated southeastward bringing extremely low SST and heavy sea-ice conditions that covered the subpolar North Atlantic.

The second 100 kyr cycle started with an abrupt warming event at the onset of MIS 21, waters with dominant *N. pachyderma* sin. were rapidly replaced by waters with abundant *N. pachyderma* dex. and *G. inflata* that remained as the dominant species up to 845 kyr ago when an abrupt southward advance of the AF took place with the subsequent proliferation of *N. pachyderma* sin., that marks the onset of substage MIS 21.6. This event records the beginning of a long-term period of ice-sheets growth towards the glacial maximum that is recorded at around 800 kyr. However, a series of millennial-scale North Atlantic oscillations are recorded by the planktonic foraminifer assemblages that, in general, follow the isotope substages recognized during MIS 21. Events of enhanced northward advection of the NAC are recorded during isotope substages 21.5, two events in substage 21.3, of which the latest one is very prominent, and a low amplitude event in substage 21.1. Higher $CaCO_3$ values during this substages support the greater retreat of the AF allowing more NAC waters bathing latitudes over 60º N (Fig. 4.4). This finding is substantiated by the concomitant increase in carbonate budget in the GIN Seas (Henrich, 1989; Henrich and Baumann, 1994), what would also reflect an increased surface

water exchange between North Atlantic and Norwegian basins. Fully glacial conditions with a planktonic foraminifer assemblage dominated by *N. pachyderma* sin. prevailed from 815 to 790 kyr (MIS 20), with only a short incursion of warm-water species at around 815 kyr. Presence of significant diatom production at sites 919 and 983 (Koç and Flower, 1998; Koç *et al.*, 1999a) and $CaCO_3$ percentages of 17 % during MIS 20, indicate at least seasonal open marine conditions and PF north of 60º N during this time.

Major changes in $\delta^{18}O_{sw}$ are recorded within this interval during G-IG Terminations and millennial-scale events. Hernández-Almeida *et al.* (in prep.) suggested that IRD events at Site U1314 during the MPT were not associated with any isotopically depleted meltwater signal caused by icebergs collapse, on the basis of the lag of the $\delta^{18}O$ shift with respect to IRD deposition. Instead, lowest planktonic $\delta^{18}O$ were reached after IRD deposition. These authors interpreted this feature as a rapid reinvigoration of the AMOC. This pattern is mimicked by our $\delta^{18}O_{sw}$ record, which rapid increases after IRD events interpreted as abrupt AF shifts, and intensification of the northward flow of the NAC and replacing lower salinities surface arctic waters. We would like to remark the surface water variability during this interval. While MIS 25 is characterized with a $\delta^{18}O_{sw}$ values between 0.3 and 0.7 ‰ that could correspond with modern-like influence of warm and salty subtropical water form the south associated with a stronger NAC, MIS 23 and substages within MIS 21 show brief NAC incursions that are gradually replaced by cooler and fresher surface waters. Asymmetry shown between the period of surface circulation dominated by NAC respect to arctic waters may be to the ice-volume growth that induces to longer glaciations and short deglaciation phases during each cycle since MIS 25, respect to the time before MIS 26. Note that this gradual glaciations with no extensive sea-ice allows a more efficient moisture extraction from the subpolar ocean, and together with the increased meridional moisture flux, provides a stronger rate of precipitation over Northern Hemisphere ice sheets during glacial inceptions, allowing greater ice-build up (Gildor and Tziperman, 2000; Gildor and Tziperman, 2001).

Beside major changes in planktonic foraminifer assemblage at G-IG time-scale , represented by shifts between *N. pachyderma* sin. and *N. pachyderma* dex./*G. inflata*, there is a striking ecological succession within warm intervals that can indicate changes in properties of surface waters. *N. pachyderma* dex. reaches its maxima modern representation in the North Atlantic with enhanced warm NAC advection, specially toward longitudes > 0º E, with a clear preference for warm, stratified surface waters during summer time (Bauch and Kandiano, 2007; Fraile *et al.*, 2008; Sautter and Thunell, 1989; Schiebel and Hemleben, 2000). In contrast, although *G. bulloides* and *G. glutinata* also occupy the upper meters of the water column, their seasonal peak abundance seems to differ; these species occurs today during spring time at 60º N, following phytoplankton bloom during ice-free periods (Bé, 1977; Fraile *et al.*, 2008; Schiebel and Hemleben, 2000; Schiebel *et al.*, 2001). Accordingly, decrease of *N. pachyderma* dex. after interglacial maxima would indicate eastward shift in the flow path of the NAC toward

the Norwegian continental margin, and an incipient expansion of colder waters during late interglacial periods, like at MIS 25 and 21.1 (Fig. 4.2). Higher *G. bulloides* and *G. glutinata* levels during this progressive cooling would respond to the wind driven mixing and peaks of chlorophyll at open ocean conditions, suggesting than nutrient content played a more important role that temperature for this species.

As *G. inflata* accounts only for ~ 12 % in modern the modern North Atlantic at around 49º N, and ~ 2 % in core top fauna at 60º N (Chapman, 2010), the observed peaks larger than > 25 % of this species at 946, 902 and 849 kyr may imply a different environment that today that favoured its production (Fig. 4.2). *G. inflata* has been related to the IC at the subpolar North Atlantic (Chapman, 2010; Olson and Smart, 2004), which results from a mixture of Irminger Sea water and the warmer and saltier water transported by the NAC (Reynaud *et al.*, 1995), hence, it is possible that its proliferation was linked to strong phases of IC advection and well-mixed environment, with potentially lower nutrient levels warmer temperatures than peaks of *G. bulloides.*

Higher *T. quinqueloba* percentages generally occurs at Site U1314 between abundance peaks of *N. pachyderma* dex. and *N. pachyderma* sin., but in low abundances, revealing a shift from temperate atlantic waters to cool subpolar water masses (Fig. 4.2). This species is usually associated with the proximity of the AF (Hebbeln *et al.*, 1994; Johannessen *et al.*, 1994), hence can be interpreted as a proxy of the AF swings. Values below 2 % on average during the MIS 31-19 interval reflect the almost steady position of the AF far from the Site U1314, only the exceptions of increased *T. quinqueloba* percentages at MIS 21 substages, indicates that the AF moved back closer to the Site U1314 position.

Regional warming as a consequence of a greater retreat of AF at MIS 21, caused the increase of warmer interglacial planktonic assemblages, as it has been observed in radiolarian (Hernández-Almeida *et al.*, 2011a, submitted), coccolithophore (Marino *et al.*, 2008) and diatom assemblages (Shimada *et al.*, 2008) from several subpolar North Atlantic records. This change in surface hydrography may also have affected, *G. glutinata*, whose percentages are considerably higher before during interglacial stages before MIS 22 than after (Fig. 4.2). This species is not as opportunistic as *G. bulloides*, and is more specifically adapted to a diatom-based diet (Hemleben *et al.*, 1989; Schiebel and Hemleben, 2000). Since interval before MIS 22 is characterized by a diatom fauna dominated by *N. seminae*, a major component in prominent spring blooms in the subarctic ocean (Reid *et al.*, 2007), it is possible that disappearance of this diatom from caused by regional warming of the North Atlantic and shift to a rapid mass-dumping diatom assemblage after MIS 22 (Koç *et al.*, 1999a; Shimada *et al.*, 2008) may have diminished *G. glutinata* main source food leading to decrease its percentages after MIS 22.

6.2. Progressive increase in abundance of the *N. pachyderma* sin. "encrusted" type and changes in diversity of planktonic foraminifers

In glacial periods prior to MIS 22, which were less pronounced and relatively brief, the abundance of the encrusted form of *N. pachyderma* dex. was low, between 20 and 30%. However, a significant increase was recorded in MIS 22 and MIS 20 that represent the glacial maximum periods of the two first 100 kyr glacial cycles (Fig. 4.4). These subspheric heavily encrusted tests are linked today to low SST, at greater depths than the non-encrusted forms and they are dominant in stratified waters in north and south high-latitude oceans (Bergami *et al.*, 2009; Kohfeld *et al.*, 1996; Stangeew, 2001). In consequence, we suggest that similar conditions of low SST and strong halocline were likely achieved at MIS 22 and 20, as seen by the extremely high IRD deposition and heavy planktonic $\delta^{18}O$ values during these stages (Hernández-Almeida *et al.*, in prep.), allowed *N. pachyderma* sin. encrusted form to thrive for a few thousand years at Site U1314. Therefore, the intensification of the glacial cycles during the MPT caused an ecological adaptation in *N. pachyderma* sin., which after MIS 22 was mainly represented by the encrusted morphotype, reflecting a progressive polar water specialization in response to the onset of the 100 kyr. Similar conclusions were obtained by Kucera and Kennet (2002) for the eastern North Pacific, who documented a consistent pattern of smaller and more compact *N. pachyderma* sin. populations after 990 kyr. Hence, we conclude that temporal evolution of encrusted forms of *N. pachyderma* sin. in fossil planktonic foraminifera assemblages and apparent hemispheric synchronicity represents a useful index for interpreting Pleistocene climates.

Diversity variations in a fossil planktonic foraminifer assemblage can be also used as a proxy for surface circulation, since decreases in temperature are often accompanied by declines in species diversity (Bé, 1977; Jenkins, 1993). Higher planktonic diversity in North Atlantic environments is associated to a well established flow of the warm NAC (Balsam and Flessa, 1978; Ruddiman, 1969). Comparing the curves of species diversity (*H*) obtained for Early and Mid-Pleistocene assemblages from Site U1314 with the benthic $\delta^{18}O$ record (Hernández-Almeida *et al.*, in prep.), it is evident that intervals with relatively higher *H* correlates with increased advection of this warm current during interglacial isotopic stages 31, 29, 27, 25, 23 and 21, and diversity declines when colder surface waters with arctic origin reached the Site U1314 location (Fig. 4.4). This surface-water masses control on diversity is dictated by a SST preferences for each species and a vertical niche partitioning factor controlled by the gradients in the upper part of the water column (Rutherford *et al.*, 1999). Development of a shallow thermocline during interglacial periods yields a niche partitioning, and more species can inhabit the same region at different water depths (high *H*), while during glacial periods, thermocline is nearly absent due to the low water column temperatures with little vertical partitioning of niches (low *H*), and only polar-adapted species can proliferate. In this sense, lowest *H* coincides with highest percentages of *N. pachyderma* sin. encrusted form at MIS 22 and 20, indicating the

severity of the glaciations and extreme low SST derived of the large build-up of the ice-sheets respect to previous climatic stages.

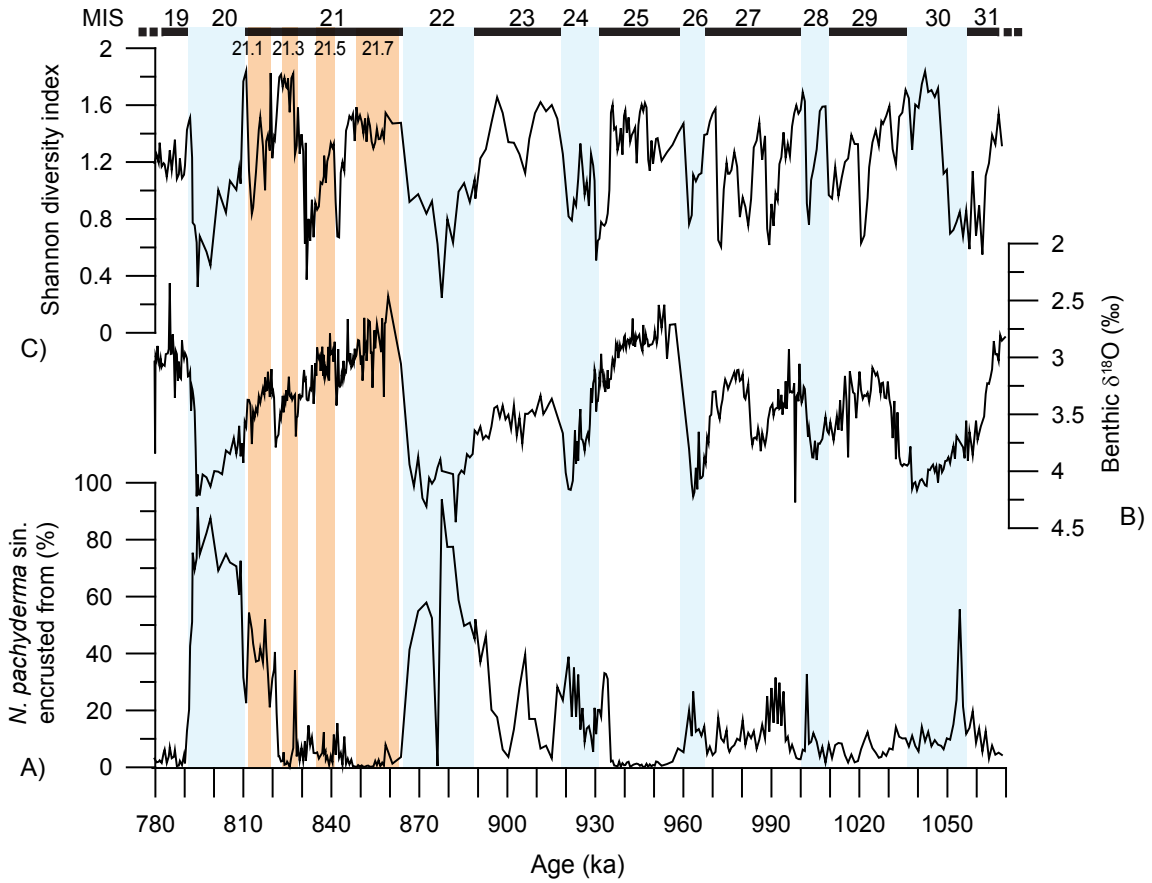

Figure 4.4. Site U1314 records from 779 to 1069 ka. From bottom to top: A) relative abundance of *N. pachyderma* sin. encrusted form, B) benthic $\delta^{18}O$ and C) Shannon diversity index (*H*). Glacial Marine Isotope Stages (MIS) are shown with blue vertical bars. Interglacial sub-stages 21.7, 21.5, 21.3 and 21.1 are shown with orange vertical bars.

6.3. Changes of biogenic carbonate settling versus bottom water advection of fine-grained carbonate

It has been demonstrated that calcium carbonate found in deep ocean sediments in the North Atlantic have two possible sources. Biogenic tests segregated by Coccoliths and Foraminifers in surface waters are settled down through the water column to finally accumulate in the sea floor, resulting in lower or higher accumulation rates depending on sea surface primary productivity. However, all particles settling through the water column are entrain and laterally advected by deep sea currents to finally deposit downstream when the current velocity decreases. Changes in carbonate accumulation rate can also be related to the enhanced or reduced flow of bottom currents. Mid Pleistocene sediments from the Gardar Drift provides an excellent record of both surface regional productivity and/or lateral particle advection by deep-currents that are function of its average speed. Besides biogenic calcite, dolomite-rich detrital carbonate

particles can also be delivered from the continents during IRD discharge events. Hernández-Almeida *et al.* (2011b, submitted) demonstrated that dolomite content in sediments from Site U1314 was punctual, and centered at IRD discharge events. Moreover, Site U1314 is located out of the North Atlantic IRD belt, and hence it is hardly influenced by the dolomite-rich IRD discharges originated in the Hudson Strait. In conclusion, we suggest that $CaCO_3$ content at Site U1314 sediments is mainly derived from biogenic carbonate production.

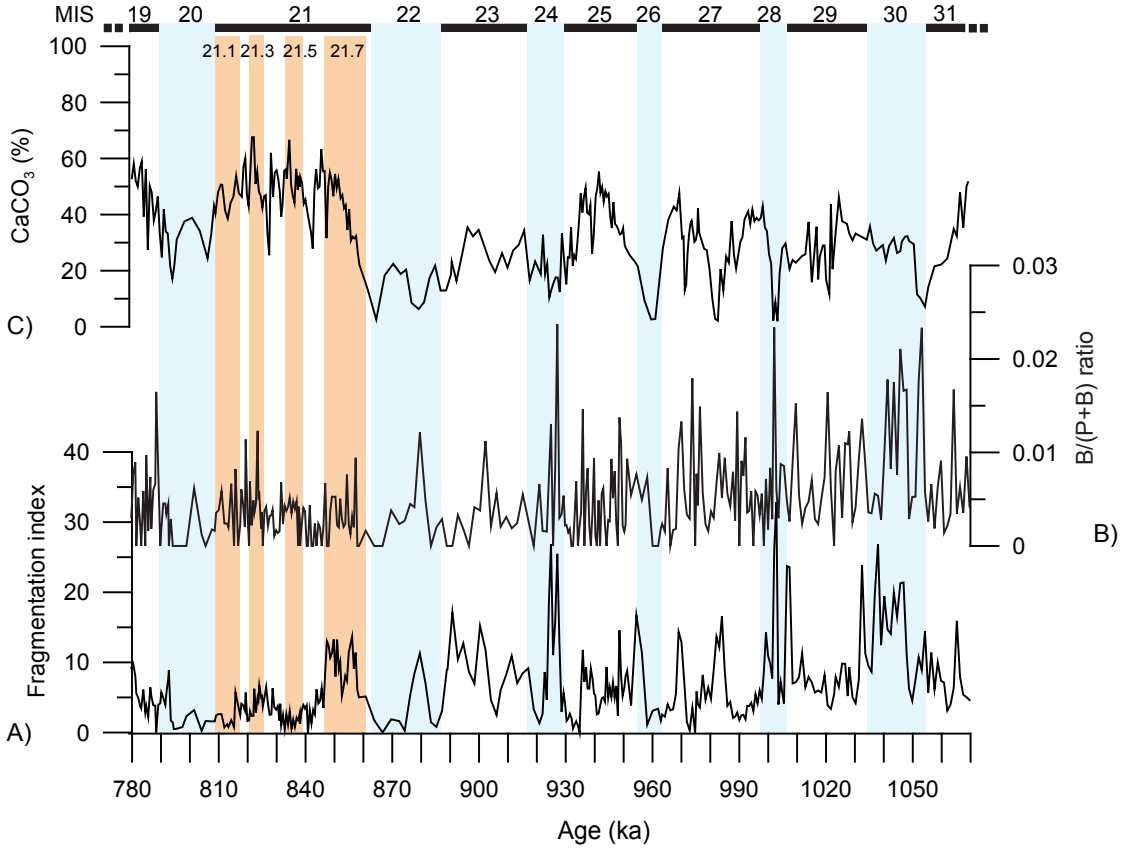

Figure 4.5. From bottom to top: A) B/B+P ratio, B) fragmentation index and C) $CaCO_3$ % from Site U1314. Glacial Marine Isotope Stages (MIS) are shown with blue vertical bars. Interglacial sub-stages 21.7, 21.5, 21.3 and 21.1 are shown with orange vertical bars.

Changes in $CaCO_3$ preservation at Site U1314 may also influence the average carbonate accumulation rate. To estimate variations in carbonate dissolution we used the FI. This index is generally lower than 40 %, that is the level when planktonic foraminifer assemblages become altered by dissolution (Miao *et al.*, 1994), reflecting a good $CaCO_3$ preservation, with no significant differences between glacial and interglacial stages. This assumption is plausible since Site U1314 is bathed by oxygen-rich, dense deep-water from the GIN Seas, which are supersaturated in carbonate ion, and it is located above the aragonite compensation depth which is presently about 3300 m in the North Atlantic (Broecker and Takahashi, 1978). This is confirmed by other studies that documented good carbonate preservation in nearby sites to U1314 (Huizhong and McCave, 1990; Hyun *et al.*, 1999; van Kreveld *et al.*, 1996). In addition, the B/(P+B) ratio was $< < 1$, which suggests that extensive calcium carbonate

dissolution did not take place in the subpolar North Atlantic between MIS 31 and 19 (Fig. 4.5).

It has been suggested that small size carbonate plankton (mainly coccolithophores) control the amplitude of carbonate records in this region as occurs in the adjacent Nordic Seas and along the Greenland margin (Andruleit and Baumann, 1998; Balestra *et al.*, 2004; Baumann and Matthiessen, 1992; Henrich and Baumann, 1994). At Site U1314, good correspondence between silt and clay fraction (< 63 μm wt. %) and $CaCO_3$ percentages suggests that carbonate bioproductivity is controlled by small planktonic organisms, presumably coccolithophores, juvenile planktonic foraminifer and small fragments. This assumption is in agreement with studies in sediment traps in the eastern North Atlantic Ocean revealing that contribution of large planktonic foraminifer (> 150 μm) to the carbonate productivity is sparse (only up to 17%) respect to the greater input of coccolithophores to the total carbonate flux (Honjo and Manganini, 1993).

The high carbonate percentages during interglacial stages reflect the higher regional average productivity associated to the enhanced northward NAC inflow, as indicated by the planktonic foraminifer assemblage characteristic of warmer conditions (*N. pachyderma* dex. increase). Input rates of clastic material delivered by icebergs, which is mainly composed by non-carbonate particles such as volcanic glass and quartz (Hernández-Almeida *et al.*, in prep.), were severely reduced during these periods, contributing to increase the biogenic carbonate content in the sediments.

In contrast, lower carbonate contents during glacial periods are linked to cold arctic-water masses affected by seasonal sea-ice cover and melt water input. The penetration of the cold arctic waters during south-eastward expansion of the AF, and the subsequent blockage of light by ice and freshwater input shed off by melting icebergs, lowered surface salinities and temperatures, rendering the environment unfavourable for most of small planktonic organisms, like coccolithophores and diatoms (Balestra *et al.*, 2010; Koç *et al.*, 1999a). Increase supply of detrital IRD by icebergs contributed to reduce the biogenic carbonate content of the sediments that decrease down to 10 % in some particular intervals dominated by IRD.

The record of carbonate content is, however, opposite to that of grain size. Higher carbonate content during interglacials is clearly associated to higher percentages of the fine-grained fraction, which is the particles smaller than 63 μm, whereas in glacial times the coarse-grained fraction is dominant but carbonate contents are widely reduced. During interglacials, deep-sea sediments from Gardar Drift mainly consist of diatoms, coccolilths, fine-grained clastic particles, and a small proportion of foraminifers and large radiolarians. Fine-grained sediments are dominant because the number of foraminifers and radiolarians per gram is very low and they are the two components that contribute to the coarse-grained fraction in the absence of IRD. The higher rate of iceberg discharge during glacial times with delivery of both fine and coarse-grained particles and the higher number of foraminifers and radiolarians per gram strongly increase sediment grain-size at these times. In particular, lithic particles per gram coarser than 150 μm increase during glacial times (Fig. 4.6).

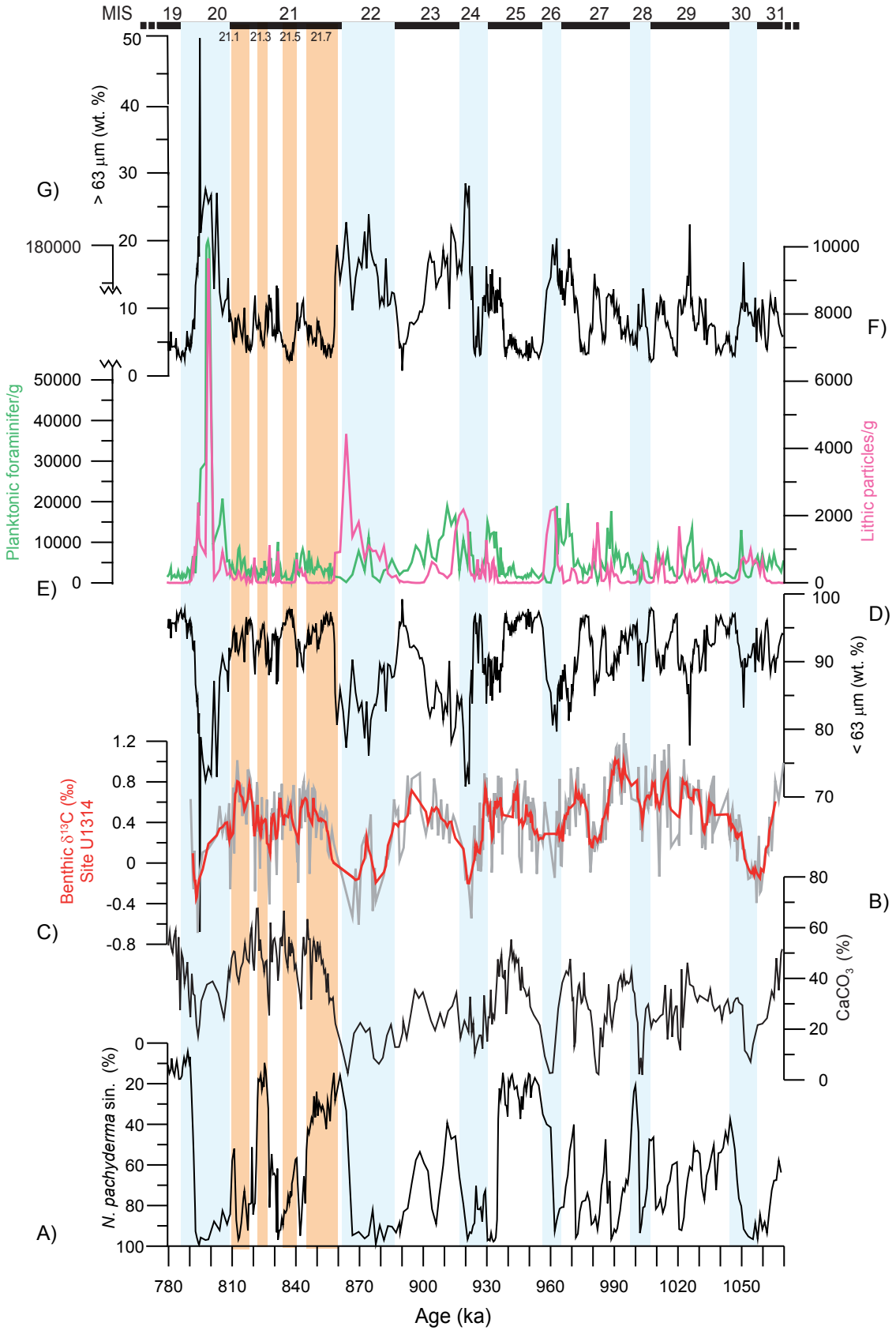

Figure 4.6 (next page). Site U1314 records from 779 to 1069 ka From bottom to top: A) relative abundance of *N. pachyderma* sin., B) $CaCO_3$ %, C) benthic $\delta^{13}C$, D) < 63 µm (wt. %), E) planktonic foraminifers (green) and IRD particles (pink) per gram) and F) > 63 µm (wt. %). Glacial Marine Isotope Stages (MIS) are shown with blue vertical bars. Interglacial sub-stages 21.7, 21.5, 21.3 and 21.1 are shown with orange vertical bars.

Several lines of evidence from Site U1314 records suggest a strong link between processes that occurs at surface waters, like water-masses changes, productivity and IRD events, and deep waters. During Early and Mid-Pleistocene IRD events in the Northern Hemisphere, thermohaline circulation was slowed-down due the lowered surface salinities in the areas of deep-convection of the GIN seas. This process is shown by lower benthic $\delta^{13}C$ at glacial times and during transitions from glacial to interglacial periods in Site U1314 (Hernández-Almeida *et al.*, in prep.). Reduction of overturning circulation produced extensive year round sea-ice cover in the North Atlantic region. The peaks in *N. pachyderma* sin. percentages coincide with lower benthic $\delta^{13}C$ and $CaCO_3$ percentages as well as increments of the sand fraction (> 63 μm wt. %) at Site U1314. The sand fraction on the southern Gardar Drift today consists of foraminifer and IRD, and is strongly diluted by silt and clay transported by ISOW (Bianchi and McCave, 2000). Our records from Site U1314 suggest that the migration of the AF and surface cooling over the entire North Atlantic may have lowered surface productivity of coccolithphores, reducing their rates of accumulation in the deep sea sediments of this region, while the planktonic foraminifers dominated by *N. pachyderma* sin. continued to proliferate. Beside this, the less vigorous deep-water flow over Gardar Drift transported and accumulated less fine-grained material, including less coccoliths that led to the relative concentration in the sediment of the coarsed-grained fraction (Fig. 4.6). In contrast, advection of atlantic waters, recognizable by abundant subpolar species (*N. pachyderma* dex., *T. quinqueloba*, *G. bulloides*, *G. inflata* and *G. glutinata*), are related to high benthic $\delta^{13}C$. During these episodes, intense NADW formation points to a stronger supply of fined-grained material by bottom currents of the ISOW to the southern end of Gardar Drift, and this material is dominated by coccoliths due to the enhanced calcium carbonate productivity in warmer surface waters. It is also important to note the lag between climate amelioration inferred from the shift from cold-to-warm fauna, and the increased in $CaCO_3$ production at Terminations MIS 26/25 and 22/21. In these cases, trend of $CaCO_3$ percentages fits more with the pattern of benthic $\delta^{13}C$ record. These calcium carbonate variations underline the importance of the ocean circulation in the sediment accumulation in the Gardar Drift, which is responsible for a strong imprint on the fine material distribution.

Selective load transport by bottom currents may explain the pattern of the planktonic foraminifer abundances. Higher numbers of planktonic foraminifers appear mainly during intermediate-to-low $CaCO_3$ percentages with high *N. pachyderma* sin. percentages, which contributes as much as 60% on average to the total planktonic foraminifer assemblage (Fig. 4.6). This reflect a higher planktonic foraminifera productivity during cold periods, when *N. pachyderma* sin. find good environmental conditions. A large part of the carbonate content of the sediments is due to the accumulation of *N. pachyderma* sin. that is very abundant at these times. Moreover, good correlation between planktonic foraminifer content and poor deep-ventilation proxies (IRD AR, > 63 μm wt. %) reflect the enrichment in coarse foraminifer and IRD particles during glacial periods with decreasing ISOW, while during interglacial periods foraminifer content decrease due to the masking by high input of fines carried by stronger deep-flow over

the Gardar Drift. The contribution of planktonic foraminifers to the carbonate fraction of the sediments is very low during these episodes. Although the carbonate content in MIS 19 or MIS 21 is around 50 %, less than 5 % is associated to foraminifers. Hence, planktonic foraminifer AR can not be considered a reliable surface paleoproductivity proxy at Site U1314.

6.4. Implications of the regional AF dynamic

We compare planktonic foraminifer and $CaCO_3$ records from Site U1314 with previously published results from other North Atlantic and Norwegian Sea (Table 4.1) sites in order to obtain a regional perspective of AF dynamics and surface water circulation pattern in this area.

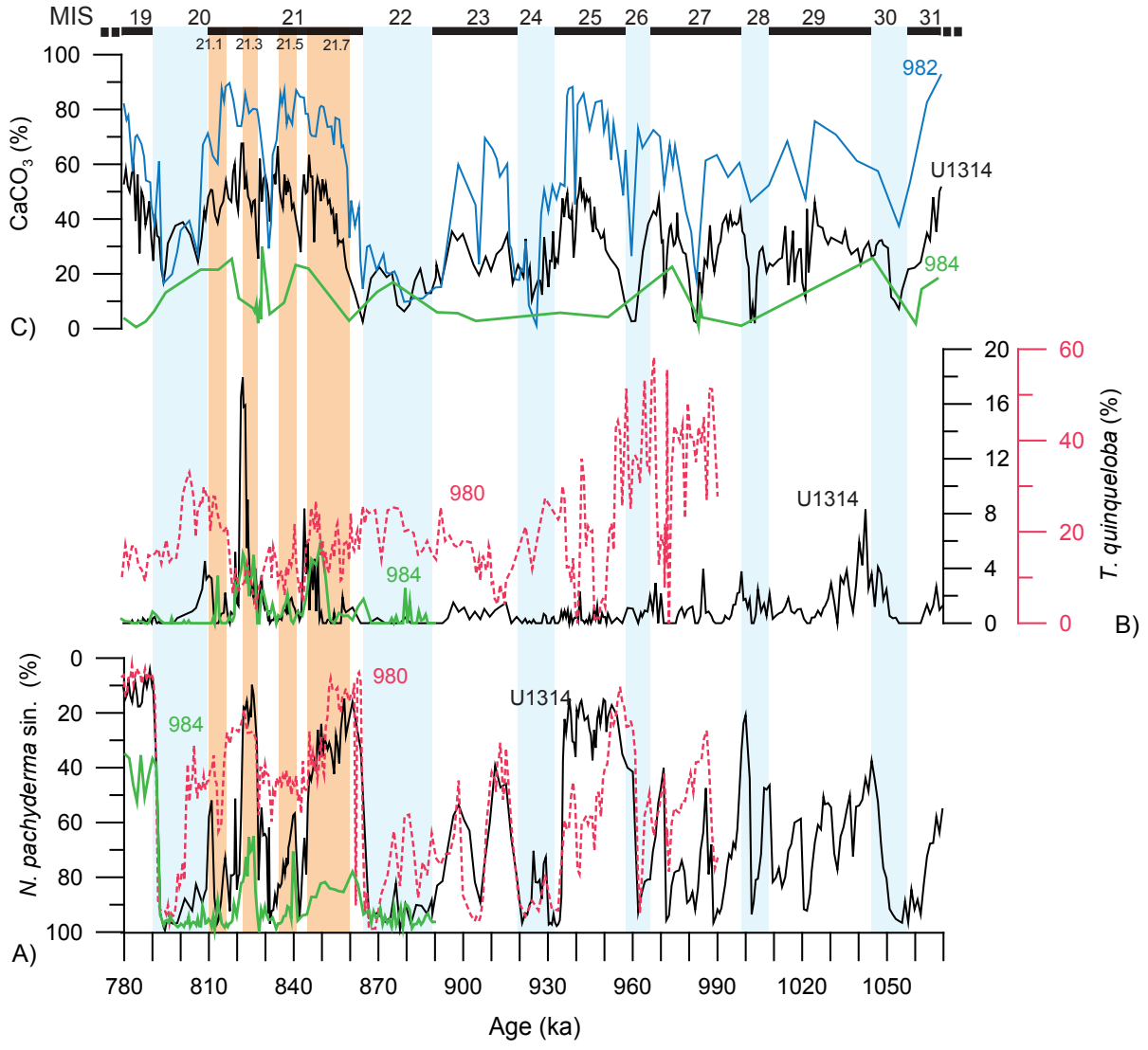

Figure 4.7. Comparison of fauna and $CaCO_3$ % record from Site U1314 with other North Atlantic Sites. From bottom to top: Relative contributions of A) *N. pachyderma* sin. and B) *T. quinqueloba*, from sites U1314 (black), 980 (dashed pink) and 984 (green) (Wright and Flower, 2002). C) $CaCO_3$ % records from sites U1314 (black), 982 (blue) and 984 (green) (Baumann personal communication; Baumann and Huber, 1999). Glacial Marine Isotope Stages (MIS) are shown with blue vertical bars. Interglacial sub-stages 21.7, 21.5, 21.3 and 21.1 are shown with orange vertical bars.

Comparing our record with $CaCO_3$ percentages from other neighbour records, we observe higher values at the eastward site 982 than at Site U1314 (average $CaCO_3$ % values 56 and 34 %, respectively), and much lower in the northern sites 984 (average 8 %) along the MIS 31 to 19 interval (Fig. 4.7). Although fauna records from neighbour sites to U1314 are limited to the 890-779 ky interval, we observe similar regional gradients in temperature. During MIS 21, while at eastward sites 980 percentages of *N. pachyderma* sin. are low and *T. quinqueloba* high, westward sites U1314 and 984 show opposite fauna trends (Baumann, personal communication; Wright and Flower, 2002). The absence of full interglacial characteristics at northern site 985, as indicated by the low $CaCO_3$ and high *N. pachyderma* sin. percentages (3.5 % and 98 %, respectively) (Baumann and Huber, 1999), reflects relatively stable positioning of the PF at around 65º N, with likely development of continuous sea-ice cover. This configuration indicates a dominant north-easterly direction of the AF towards the Faeroe Islands and an steady position of the PF, which marks the extension of the perennial sea-ice, north of 65º N. Such scenario during MIS 21 would allow northward intrusion of warm surface waters was shifted to the east, and affected to cores located in a more eastern position (Site 982 and 980), while cores located to the west (Sites U1314 and 984) would be less influence by warm water masses, as occurs today, the inflow of warm Atlantic water is compressed to the east, along the Rockall Plateau and Norwegian shelf margin while it flows northward into the Arctic Ocean basin, and subsequently, creating a strong west-east temperature gradient The existence of a narrow path of warm water flowing along westward longitudes during MIS 21 would provide necessary moisture for the growing ice-sheets (Raymo and Nisancioglu, 2003). Therefore, regional surface hydrography of the subpolar North Atlantic played and important role in the glacial inception phase and may explain the existence of large ice-sheets in this area.

7. CONCLUSIONS

The faunal record at Site U1314 enables the reconstruction of surface ocean circulation. High percentages of *N. pachyderma* sin. indicates glacial conditions with south-eastward expansion of the AF and penetration of cold arctic waters, while increased *N. pachyderma* dex., *T. quinqueloba*, *G. bulloides*, and *G. inflata* have been proven to be the best interglacial conditions indicators in the subpolar North Atlantic due to their widespread occurrence only during the advection of warm Atlantic waters by the NAC. A clear east-west SST gradient is found in the subpolar North Atlantic as the result of the position of the AF. From MIS 31 to MIS 22, AF was steady located south of Sites U1314 and 984, limiting heat flux from the North Atlantic to their positions, while eastward sites 980 and 982 where bathed for a more intense NAC flow while AF swung north-westward during interglacial periods. As the result of the steep east-west surface SST gradient, carbonate bioproductivity was lower west of the AF during this interval. Dominant northeasterly direction towards the Faeroe Islands of the AF

remains a narrow ice-free channel toward the east that allows northward heat flux transport during glacial inceptions and a maintained deep-water formation in the GIN seas during this phase. During MIS 22, most extreme surface cold conditions, with likely perennial sea-ice, occurred as consequence of the southward migration of the PF. During MIS 21 and 19, greater retreat of AF allowed a regional warming that increased carbonate bioproductivity at the Site U1314 area.

Intensification of the G-IG climate regimes after MIS 21 caused a reduction in the *N. pachyderma* sin. habitat in the subpolar North Atlantic, that shifted toward true-polar environments during the subsequent stages. Extreme SST and development of a strong halocline during IRD events at MIS 22 and 20 related to the onset of the 100 kyr climate cycles favoured development of the *N. pachyderma* sin. encrusted form. Shannon diversity index oscillations define surface circulation pattern in the North Atlantic. Periods of high diversity are characteristic of warm conditions, under the influence of Atlantic waters, which allows the establishment of a strong summer thermocline and more niche availability; while low diversity typical of cold periods and less niche-partitioning due to the small thermal gradient in the upper water column.

Comparison of surface and deep water records at Site U1314 evidence the linkage between surface-deep North Atlantic hydrography. Small-size carbonate plankton productivity (coccolithophores) and bottom-current speed/sedimentation rate of silt and clay particles (< 63 μm wt. %) controls the variability of carbonate records in this region. Highest $CaCO_3$ percentages are found during open ocean conditions that allow enhanced NAC flow that transport heat and moisture to high-latitudes. Deep-convection in the GIN seas forms a vigorous ISOW flow that accumulates more fine grained sediments over the Gardar Drift. Lowest carbonate production is found below cold arctic water masses affected by seasonal sea-ice cover and melt water input during glacial periods, which inhibited heat flux to the North Atlantic and subsequently reduced carbonate surface water bioproductivity and ventilation of the deep North Atlantic. Slower ISOW flow removed fine material, leaving a coarser foraminifer-IRD dominated residue in Gardar Drift sediments. Thus, the pronounced contrast within G-IG stages results from oceanic circulation changes: either from surface circulation governing the ice-ratted detritus supplies and the planktonic biogenic production, and from deep circulation changes with the resumption of the bottom-water formation.

Capítulo 5

*A HIGH RESOLUTION OPAL AND RADIOLARIAN RECORD FROM THE SUBPOLAR NORTH ATLANTIC DURING THE MID-PLEISTOCENE TRANSITION (1069-779 KA): PALAEOCEANOGRAPHIC IMPLICATIONS**

*Este capítulo está basado en: Hernández-Almeida, I., Bjørklund, K.R., Sierro, F.J., Filippelli, G.M., Cacho, I. and Flores, J.A., 2001a. *Palaeogeography, Palaeoclimatology, Palaeoecology* (en revisión).

RESUMEN. El registro de alta resolución de las asociaciones de radiolarios del testigo U1314 fue estudiado para reconstruir la hidrografía y los cambios climáticos en el Atlántico Norte durante la Transición del Pleistoceno Medio (1069-779 ka). Además del registro faunístico, acumulaciones absolutas de radiolarios y de ópalo biogénico total son usadas para determinar los cambios en la productividad de aguas superficiales. Los resultados indican que el Frente Ártico en el Atlántico Norte osciló repetidamente a escala glaciar/interglaciar, lo que provocó que la región del testigo estuviera bajo la influencia de aguas árticas (glaciar), y aguas atlánticas, mucho más cálidas (interglaciar). Durante periodos glaciares y eventos de descarga de material transportado por el hielo, el taxón de aguas profundas *Cycladophora davisiana* se convirtió en el máximo contribuyente de la asociación de radiolarios, sugiriendo condiciones de aguas superficiales frías, descarga de agua de fusión e intensificación de la circulación intermedia del océano. Los intervalos interglaciares estuvieron caracterizados por alta abundancia de taxones superficiales como *Pseudodyctiophimus gracilipes* y *Lithomelissa setosa*, aumento de acumulación de ópalo, y alta diversidad de radiolarios, indicando un flujo hacia el norte de aguas atlánticas superficiales hacia el área del testigo U1314. Un marcado cambio en la estructura de la asociación de radiolarios tuvo lugar después del estadio isotópico marino 22 (~ 860 ka), con grandes diferencias en la composición de especies entre periodos cálidos y fríos, probablemente en respuesta a las condiciones cambiantes del océano debido a la mayor amplitud los cambios glaciares/interglaciares debido a que la periodicidad dominante de las oscilaciones climáticas en altas latitudes pasó de 41 ka a 100 ka. Por lo tanto, se ha llegado a la conclusión que las asociaciones de radiolarios del Atlántico Norte han cambiado drásticamente junto las variaciones en la circulación superficial e intermedia en respuesta a las variaciones climáticas orbitales y milenarias que tuvieron lugar en el Pleistoceno Inferior y Medio.

Palabras clave: radiolarios; ópalo biogénico; Atlántico Norte; descarga de agua de fusión; circulación oceánica; productividad.

ABSTRACT. A high-resolution record of radiolarian assemblages from Site U1314 was studied to reconstruct hydrographic and climatic changes in the North Atlantic Ocean during the Mid-Pleistocene Transition period (1069-779 ka). Besides the faunal record, absolute accumulation of radiolarians and total biogenic opal are used to determine changes in surface water productivity. Results show that the North Atlantic Arctic Front shifted back and forth repeatedly at a glacial/interglacial timescale, bringing the site under the influence of both cold arctic (glacial), and much warmer atlantic (interglacial) waters. During glacial intervals and "ice-rafted debris" (IRD) events, the deep-dwelling taxon *Cycladophora davisiana* was the greatest contributor of the radiolarian assemblage, suggesting cold surface conditions, melt-water discharge and enhanced intermediate ocean circulation. Interglacial intervals were characterized by abundant shallow-dwelling taxa like *Pseudodyctiophimus gracilipes* and *Lithomelissa setosa*, increased opal accumulation, and higher radiolarian diversities, indicating a northward flow of warm atlantic surface waters to the Site U1314 area. A marked change in the structure of the radiolarian assemblage occurred after MIS 22 (~ 860 ka), with large taxa differences between warm and cold periods, probably in response to changing ocean conditions due to the higher amplitude of glacial/interglacial changes as the dominant periodicity of high-latitude climate oscillations shifted from 41-kyr to 100-kyr. Thus, we conclude that the radiolarian assemblage from the North Atlantic have changed drastically along with variations in the surface and intermediate-water circulation in response to orbital and millennial-scale climatic variations that occurred in the Early and Mid-Pleistocene.

Key words: radiolarian; biogenic opal; North Atlantic; melt-water discharge; ocean circulation; productivity.

A HIGH RESOLUTION OPAL AND RADIOLARIAN RECORD FROM THE SUBPOLAR NORTH ATLANTIC DURING THE MID-PLEISTOCENE TRANSITION (1069-779 KA): PALAEOCEANOGRAPHIC IMPLICATIONS

1. INTRODUCTION

Sediments in the subpolar North Atlantic Ocean have been the subject of a large number of paleoceanographic studies due to the important role of this region in modulating the global climate (Bond *et al.*, 1992; Broecker *et al.*, 1992; Heinrich, 1988; McManus *et al.*, 1994; McManus *et al.*, 1999; Oppo, 1997). Abrupt changes in the North Atlantic resulted from variations in thermohaline circulation (e.g. Ruddiman *et al.*, 1980; Shackleton *et al.*, 1983) related to extreme cooling of surface waters and enormous amounts of drifting ice (Bond *et al.*, 1992). Besides these cyclical ice-volume fluctuations, Earth's climate system show a gradual trend toward more glacial conditions between 1200 and 500 ka (Head and Gibbard, 2005), the so-called "Mid-Pleistocene Transition" (MPT), related to a shift of global glacial/interglacial cycles from 41-kyr to 100-kyr (Berger and Jansen, 1994c; Raymo and Nisancioglu, 2003; Raymo *et al.*, 2004; Ruddiman *et al.*, 1989).

Such environmental changes brought large variations in surface and deep habitats in the ocean, which consequently affected planktonic and benthic communities. Therefore, temporal evolution of fossil assemblages in the sedimentary record provides detailed paleoecological information necessary to reconstruct past climate and hydrographic conditions. Several microfossil groups have been used in paleoceanographic studies in North Atlantic sediments, such as planktonic and benthic foraminifera (Kawagata *et al.*, 2005; Venz *et al.*, 1999; Wright and Flower, 2002), diatoms (Koç *et al.*, 1993; Koç and Schrader, 1990) and coccolithophores (Marino *et al.*, 2008). We focus here alternatively on the polycystine radiolarians, Spummellaria and Nassellaria (hereafter called radiolarians), for reconstruction of the paleoceanographic conditions in the North Atlantic Ocean.

Radiolarians are widely distributed in the world ocean occupying surface and deep habitats with a broad range of physical-chemical water-mass characteristics (e.g. temperature, salinity, nutrients) (Abelmann and Gowing, 1997; Itaki, 2003; Kling and Boltovskoy, 1995). Due to this adaptive facility, radiolarians have proven an effective tool in paleonviromental reconstructions (Cortese *et al.*, 2003; Matul *et al.*, 2002; Morley, 1983; Petrushevskaya and Bjørklund, 1974). Based on this assumption, we present a new and high-resolution record of radiolarian assemblages and biosiliceous material (opal) accumulation rates from IODP Site U1314 to identify key radiolarian species and their ecological requirements, aimed at reconstructing water-mass structures and productivity regimes during glacial/interglacial cycles in the North Atlantic sediment record. In addition, we investigate the major hydrographic and climatic changes in the North Atlantic during the MPT through variations in radiolarian assemblages.

2. HYDROGRAPHY OF THE SITE LOCATION

Site U1314 (Fig. 5.1) is strongly influenced by the northward flow of the North Atlantic Current (NAC). This surface water mass travels northward across the North Atlantic where it crosses the Mid-Atlantic Ridge between 53° N and 60° N. One branch turns northwestwards and travels as the Irminger Current (IC) on the western and northern side of Iceland, mixing with the cold East Greenland Current (EGC), while the main branch flows over the Iceland-Faeroe Ridge into the Greenland, Iceland, and Norwegian (GIN) Seas (Krauss, 1986). This current carries heat to the north and maintains the warm climates of central and northern Europe. Winter convection of the warm and salty atlantic surface waters in the GIN Seas results in the formation of North Atlantic Deep Water (NADW) that flows as the Iceland-Scotland Overflow Water (ISOW) through the Faeroe Bank channel to enter the Iceland basin (Schmitz and McCartney, 1993; Swift, 1984).

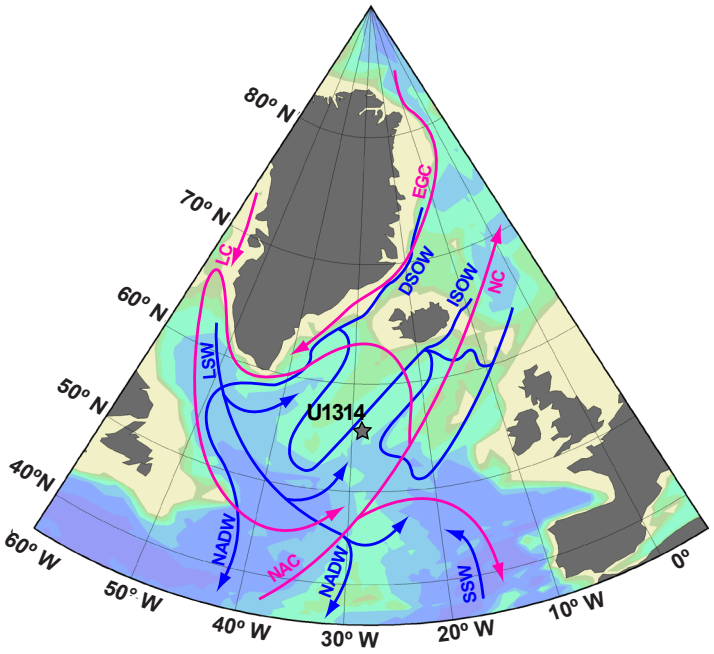

Figure 5.1. Location of IODP Site U1314 (black star: 56º21'N, 27ºW; 2820 m water depth), modern surface (pink), and deep circulation (blue) in the North Atlantic (Krauss, 1986; Schmitz and McCartney, 1993). Map generated with *Ocean Data View v.3.4.3.* software (Schlitzer, 2008). East Greenland Current (EGC), Norwegian Current (NC), Labrador Current (LC), North Atlantic Current (NAC), Denmark Strait Overflow Water (DSOW), Iceland Scotland Overflow Water (ISOW), Labrador Sea Water (LSW), North Atlantic Deep Water (NADW), and Southern Source Water (SSW).

In addition, the flow of the NAC to high-latitudes creates a complex zone of mixing between cold arctic waters and warm atlantic waters, named the Arctic Front (AF) (Swift and Aagaard, 1981). During the Pleistocene epoch, subpolar North Atlantic was affected by repeated changes in climate and water masses at a glacial/interglacial time scale (McIntyre *et al.*, 1999; McManus *et al.*, 1999; Raymo *et al.*, 2004). These variations were a consequence of

major north-south migrations of the AF, bringing the site under the influence of both cold arctic (glacial), and much warmer (interglacial) surface waters.

3. MATERIAL AND METHODS

3.1. Sediment samples and chronostratigraphy

Integrated Ocean Drilling Program (IODP) Site U1314 (2820 m) was cored by the D/V JOIDES Resolution in the southern Gardar Drift, in the subpolar North Atlantic (56.36°N, 27.88°W) during IODP Expedition 306 (Fig. 5.1). Site U1314 is located at the northern edge of the glacial North Atlantic Ice Rafted Detritus (IRD) belt (Ruddiman, 1977; Ruddiman and McIntyre, 1981b), on the east side of the Reykjanes Ridge, an area of exceptional radiolarian abundance and preservation compared to the relative scarcity in North Atlantic surface sediments (Goll and Bjørklund, 1971).

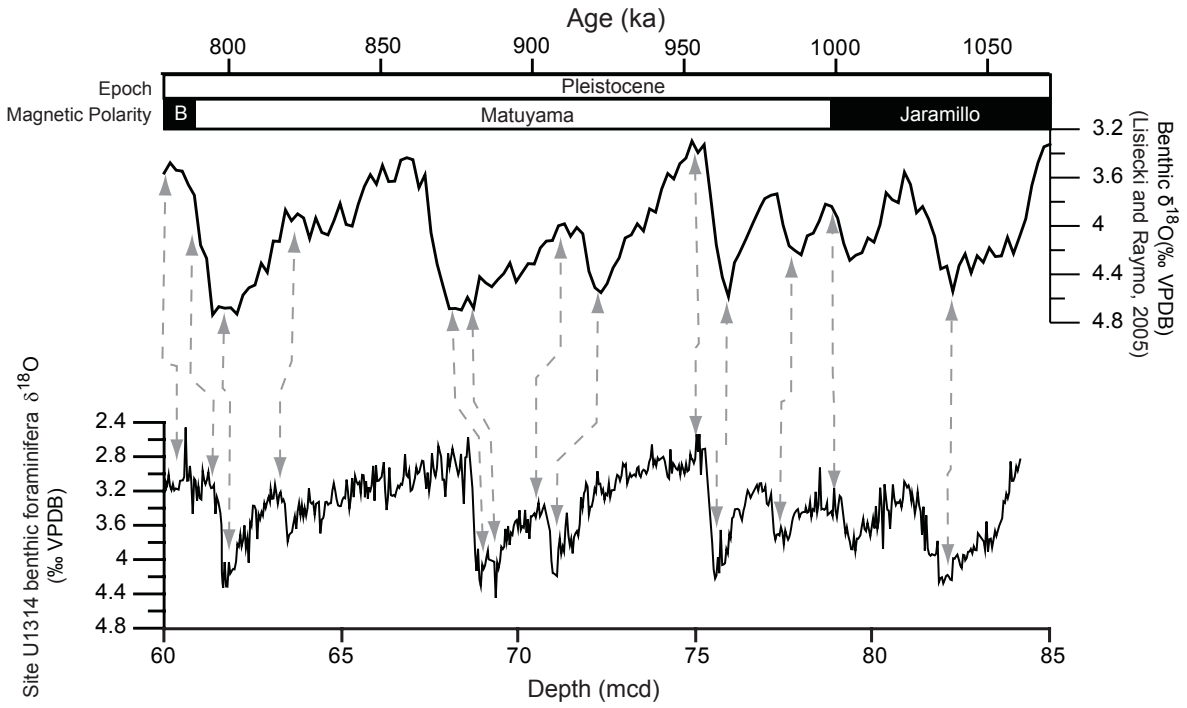

Figure 5.2. Construction of the age model was performed by correlating the benthic isotope stack of Lisiecki and Raymo (2005) (LR04) with Site U1314 benthic $\delta^{18}O$. Tie points of both records are joined by dashed lines.

The section of Site U1314 studied here comprises 24.16 m with an average sedimentation rate of about 7-7.5 cm/ka for the Pleistocene (Channell *et al.*, 2006). Lithologies consist of nannofossil oozes enriched in biogenic and terrigenous components, and terrigenous silty clay with a varying proportion of calcareous (e.g., nannofossils, foraminifers) and siliceous (e.g., sponge spicules, diatoms and radiolarians) organisms. A more detailed core description is given in Channell *et al.* (2006).

Conversion from core depth to time was derived by direct correlation of the benthic foraminiferal oxygen isotope record from Site U1314 (Hernández-Almeida *et al.*, in prep.) with the orbitally tuned benthic isotope stack of Lisiecki and Raymo (2005) (hereinafter referred to as LR04) by using *AnalySeries* 2.0 software (Paillard, 1996). Based on the 13 tie points used to correlate the reference curve LR04 with our benthic oxygen data set, the final age model for the 24.16 m of the core section spans an interval from 1069 to 779 ka, yielding a temporal resolution of 290 kyrs. Between the tie points sedimentation rates were assumed constant, based on the shipboard preliminary stratigraphy (Channell *et al.*, 2006). The orbitally tuned age model and tie points used in it are shown in figure. 5.2 and table 5.1 respectively.

Site U1314 depth (mcd)	LR04 Time (ka)
60.10	780.619
61.79	795.244
62.16	807.358
63.12	817.649
68.55	858.636
68.92	872.225
70.99	921.458
71.88	929.571
75.01	951.451
75.50	962.858
77.60	987.871
79.41	1004.220
83.37	1058.727

Table 5.1. Tie points used in the correlation between benthic $\delta^{18}O$ from Site U1314 and benthic isotope stack LR04.

3.2. Methodology

In this micropaleontological study, 299 sub-samples (2 cm thickness taken at 8-16 cm intervals) from Site U1314 were used for the radiolarian analysis. This high sample density yields a time estimate of around 1 kyr between samples. The techniques used to separate the radiolarian skeletons from the sediment follow the Goll and Bjørklund (1974) procedure. Briefly, samples were oven-dried for 24 hours, weighed (1-5 g), and then treated with 15% H_2O_2 and HCl solutions to remove the organic matter and the calcium carbonate respectively. The samples were then wet sieved (45µm mesh size), after which two types of slides were made from the residue, one to quantify the radiolarian abundance (Q-slide) and the other for species counts (faunal analysis, F-slide). In addition, a Diatom Index (DI) was determined to evaluate qualitatively diatom and terrigenous material content in our Q-slides, ranging between 1 (sporadic or absent) to 5 (extremely abundant). To prepare the Q-slides, the entire residue from each sample was transferred to a 100 ml beaker that contained 50 ml of distilled water. The solution was then well homogenised, after which a 0.2 ml sample was taken from the suspension using a micropipette and dropped onto a glass slide. The sample was then dried

and mounted with Canada balsam. The F-slides were made from the remaining residue in the beaker. Radiolarian census counts are based on at least 300 identified specimens at the lowest taxonomic level. During data generation we encountered 79 species (see Appendix A). The taxonomic level of counting was normally at the species level, but ranged from subspecies to undifferentiated family and suborder categories (*Nassellaria* indet. and *Spumellaria* indet., used mainly for juvenile stages that cannot be assigned to species). We have followed the same counting procedure that was used in Bjørklund *et al.* (1998) and Cortese *et al.* (2003), where some selected phaeodarian species were included in the counts. Therefore, the informal name radiolarians include both the selected phaeodarian species and the polycystine taxa shown in Appendix A.

Benthic foraminiferal stable isotope analyses were carried out at the University of Barcelona on a Finnigan MAT 252 mass spectrometer. Due to the scarcity of benthic foraminifera, two species were selected, *Cibicidoides wuellerstorfi* and *Melonis pompilioides*, to obtain a continuous record of oxygen and carbon isotopes. Analycal accuracy was better than 0.06 ‰ for $\delta^{18}O$, and better than 0.02‰ for $\delta^{13}C$. Calibration to the Vienna Pee Dee Belemnite (VPDB) standard scale (Coplen, 1996) was made through the NBS-19 standard.

Biogenic opal accumulation rates (AR) ($g*cm^{-2}*ka^{-1}$) were determined in 572 sub-samples (2 cm thickness taken at 4 cm intervals) following the procedure of Mortlock and Froelich (1989), using 10 ml of 2 M Na_2CO_3, although for this study final opal measuring was determined by using a Leeman Labs P950 inductively coupled plasma-atomic emission spectometer (ICP-AES) with a CETAC Corp.AT500$^+$ ultrasonic nebulizer at the Indianapolis University-Purdue University at Indianapolis. The accuracy of our analyses was evaluated by comparison to the long-term results from a consistency standard included in all biogenic opal measurements performed. The average standard deviation was 1.7 %.

3.3. Taxonomical notes

We have used the taxonomic concept by Hatakeda and Bjørklund (2009), and illustrations of the species used in the present study are given in Appendix A. Several species have been counted together due to the difficulty of an exact identification with total confidence, particularly of juvenile stages (*Lithomitra lineata* and *Lithomitra arachnea*; *Actinomma boreale* and *Actinomma leptodermum*; *Spongotrochus glacialis* and *Spongodiscus resurgens*). Therefore, these taxa are reported in this study as *L. lineata/arachnea* group, *A. leptodermum/boreale* group and *Spongotrochus glacialis*/*resurgens* group, respectively.

Additionally, species with a common tropical-subtropical affinity like *Tetrapyle octacantha*, *Pterocanium praetextum*, *Dyctiocoryne profunda*, *Spongocore puella*, *Corocalyptra craspedota*, *Lithomelissa thoracites*, *Eucyrtidium acuminatum* and *Lamprocylcas maritalis* are good indicators of warm and open ocean conditions in the North Atlantic (Goll and Bjørklund,

1971; Haslett, 1995; Matul, 1994b; Petrushevskaya and Bjørklund, 1974). These species appeared during interglacial intervals, but in low percentages too low to be of any importance as individual species. Therefore, and according to Cortese *et al.* (2003) considerations, we have grouped them as "drift fauna group".

3.4. Statistical analysis

For the diversity/statistical analysis of the radiolarian census data, radiolarian accumulation rate (RAR), and opal AR we used the *PAST* software (PAleontological STatistics; Hammer *et al.*, 2001). Radiolarian counts converted into percentages were used to calculate the Shannon-Weaver (*H*) diversity index (Shannon and Weaver, 1963). This index, based on a count of species, is sensitive both to changes in the number of species and to changes in the relative abundance of species in a sample. High values can result from an addition of species, greater equality in abundance, or both. A more detailed discussion of this index and its use in ecological studies is provided by (Pielou, 1975).

The multivariate statistics method Detrended Correspondence Analysis (DCA) was applied to our counts, because this is a suitable method for studying gradients in such data sets and to check the response to underlying environmental parameters (Hammer *et al.*, 2001). The species and samples that were used in the DCA had to meet the following criteria, as recommended by Imbrie and Kipp (1971): (1) the species had to occur as more than 1% of the total fauna in at least one sample and (2) had to occur in at least 10 samples. After this selection was applied, 26 species remained for our analysis, of which abundance curves for 18 species are shown (Fig. 5.4A-I; Fig. 5.5A-I).

Finally, in order to detect a significant underlying temporal pattern in the radiolarian population from Site U1314, we applied multivariate Mantel periodogram spectral analysis to our radiolarian data-set because this method can reveal the underlying mechanism (seasonality, astronomical, or other unknown causes) driving the dynamics of the entire fossil assemblage (Hammer, 2007). For the present study, following Hammer (2007), we used the same 26 species as for the DCA because they were regularly represented in our samples. A temporal spacing (1089 years) between data points was generated by linear interpolation and an inner product distance measure was chosen for the Mantel correlogram. Moreover, spectral analyses were performed for RAR and opal AR records to determine the dominant frequencies of both signals.

4. RESULTS

RAR generally varies inversely with the cyclicity described by the benthic oxygen isotopes from Site U1314. Pearson's *R* correlation coefficient between these two variables is -0.403 (correlation is significant at the 0.01 level), indicating that low RAR values correspond

with high benthic $\delta^{18}O$. The total radiolarian abundance ranged from barren to 30000 tests/g at Site U1314 (Fig. 5.3C, red filled). Periods of high RAR in Pleistocene sediments from the North Atlantic coincide with interglacial conditions, except during MIS 23 (Fig. 5.3C). On the other hand, glacial periods are poor in RAR and sometimes opal-barren, as also reported by Ciesielski and Bjørklund (1995).

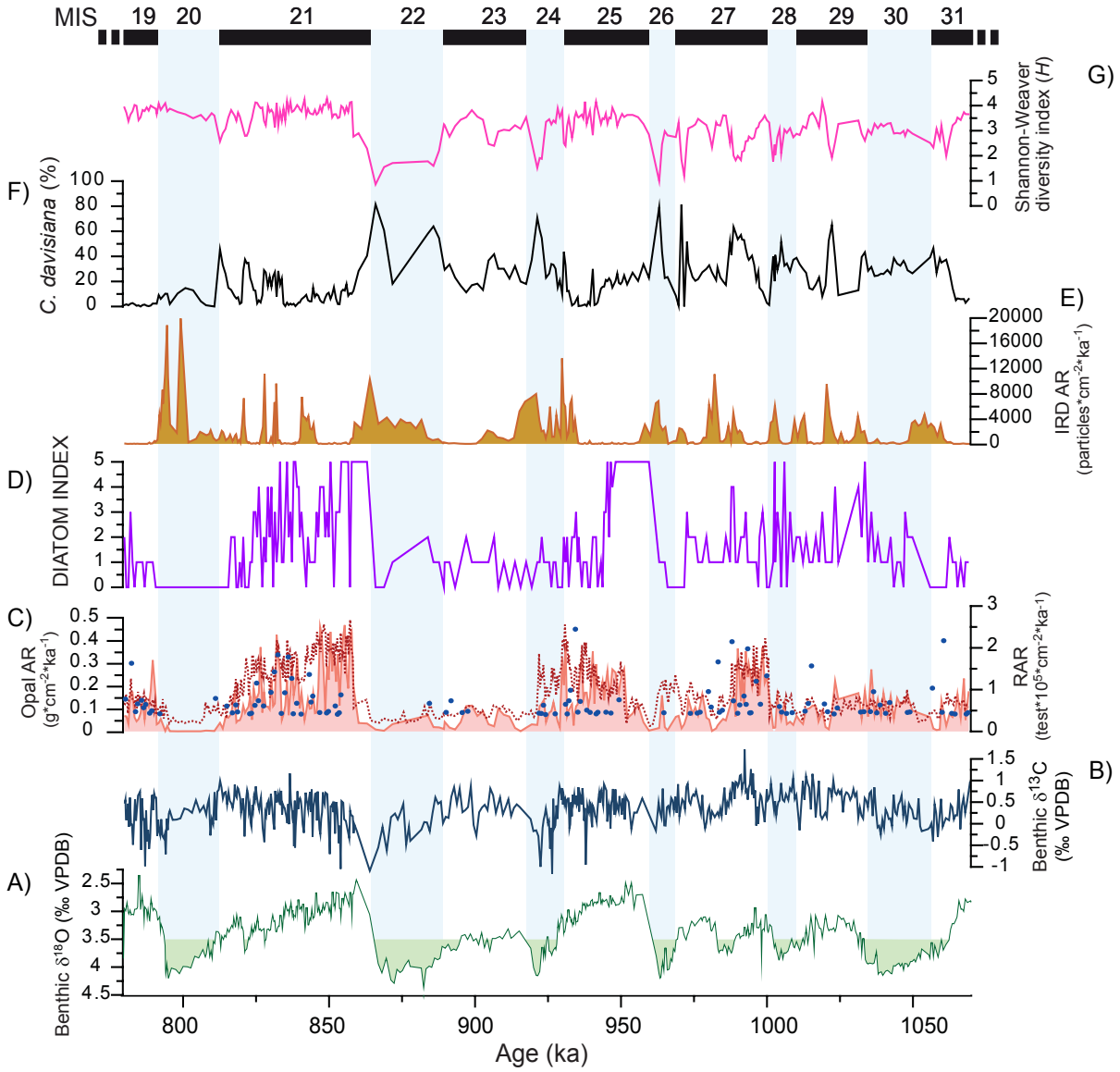

Figure 5.3. Site U1314 records from 1069 t o779 ka. From bottom to top: A) benthic $\delta^{18}O$, with green filled up to 3.5 ‰, the glacial threshold (McManus *et al.* 1999); B) benthic $\delta^{13}C$; C) RAR (red filled), opal AR (dashed red line) and phaeodarian main percentage peaks (blue dots); D) Diatom Index; E) IRD AR; F) percentage of *C. davisiana* and G) Shannon-Weaver diversity index. Marine Isotope Stages (MIS) are shown at the top (glacials in blue and interglacials in black).

The number of taxa varies between a maximum of 52 species at MIS 21, and a minimum of 7 species at MIS 22. Comparison of the RAR with opal AR at site U1314 shows that many of the opal maxima (Fig. 5.3C, dashed red line) coincide with high levels of RAR (Fig. 5.3C), and with diatom abundance, as indicated by the DI (Fig. 5.3D).

Radiolarian skeletons were well-preserved in all examined samples without any sign of significant dissolution or breakage. There are no large peaks of opal AR with low radiolarian concentrations (Fig. 5.3C) or low DI (Fig. 5.3D), which suggests a good generalized preservation of the biogenic fossils also in the <45 μm size fraction. Another proxy indicative of opal preservation is the phaeodarian abundance (Casey *et al.*, 1979b; Stadum and Ling, 1969), since their skeletons are more unstable as they contain less biogenic silica, having a porous or spongy structure, and are therefore more easily dissolved than the polycystine radiolarians (Takahashi *et al.*, 1983). In our samples, the presence of the phaeodarian taxa *Euphysetta nathorstii* and *Lirella mello* were more frequent during periods with moderate $\delta^{18}O$ values, such as during MIS 21, 25 and 27 (Fig. 5.3C, blue dots), indicating better conditions for opal preservation during interglacial intervals with moderate to high RAR and opal AR.

Of the total of 79 identified taxa of polycystine radiolarians, only the 26 species that accounted for more than 1% on average have been used in the discussion. Comparing the relative abundance curves of these dominant species, we found that most of them had a distribution pattern closely similar to total radiolarian abundance, except for *C. davisiana*. According to our faunal results, and in agreement with previous studies of the North Atlantic radiolarian fauna (Matul, 1989a; 1989b; 1994a; 1994b; Matul and Yushina, 1999), *Cycladophora daviasiana* dominates the assemblage during glacial periods (Fig. 5.4A), while *Pseudodyctiophimus gracilipes* dominates during interglacial periods (Fig. 5.4F).

Comparison of the distribution pattern of *C. davisiana* (Fig 4.3E) with the oxygen isotopic record of Site U1314 (Fig. 5.3A) revealed that most peaks of this species occurred during glacial stages or at glacial-interglacial transitions. High abundances, however, were also observed during weak interglacial stages (MIS 23) as well as in significant cool periods within prominent interglacial stages (MIS 21). Our sample spacing also shows the rapid change in abundance of *C. davisiana* at the glacial/interglacial transitions, switching from percentages close to 80 % to 20 % in less than 3 kyr (MIS 22/21, 24/23, 26/25). Additionally, high percentages of *C. davisiana* appear closely related to spikes in the IRD AR (Fig. 5.3E) and when benthic $\delta^{18}O$ values exceed 3.5 ‰ (Fig. 5.3A). The *Lithomitra lineata/arachnea* group (Fig. 5.4B) shows prominent peaks preceding or together with those of *C. davisiana* (e.g. 1056, 981, 965, 868). Likewise, *Larcopyle weddellium* and *Spongopyle osculosa* (Fig. 5.4D, C, respectively) appear to be related to the *C. davisiana* distribution (Fig. 5.4A), since they peak at IRD events (e.g. at 821, 868 and 1005 ka). Other abundant species, *Actinomma leptodermum/boreale* group, *Pseudodyctiophimus gracilipes*, *Lithomelissa setosa*, *Phorthicium clevei*, "drift fauna group", *Actinomma medianum*, *Spongotrochus glacialis/resurgens* group, *Stylochlamydium venustum*, *Larcoyple buetchslii*, *Larcospira minor*, *Botryostrobus auritus/australis* group, *Stylodictya validispina*, *Druppratractus variabilis*, *Lithocampe platycephala* (Fig. 5.4E-I; 5.5A-D), appeared mainly along interglacial intervals, although some of them showed rather diverse distribution patterns. *A. leptodermum/boreale* group showed increased abundances during MIS 22, 26, during the

transitions 20/19, 22/21, 26/25, and at sub-stages of MIS 21 (Fig. 5.4E). *L. platycephala* spikes occurred mainly during interglacial periods (Fig. 5.5H), although maxima (5-6%) are displaced toward the end of the interglacial or at benthic $\delta^{18}O$ values between 3.5 and 3 ‰ (Fig. 5.3A).

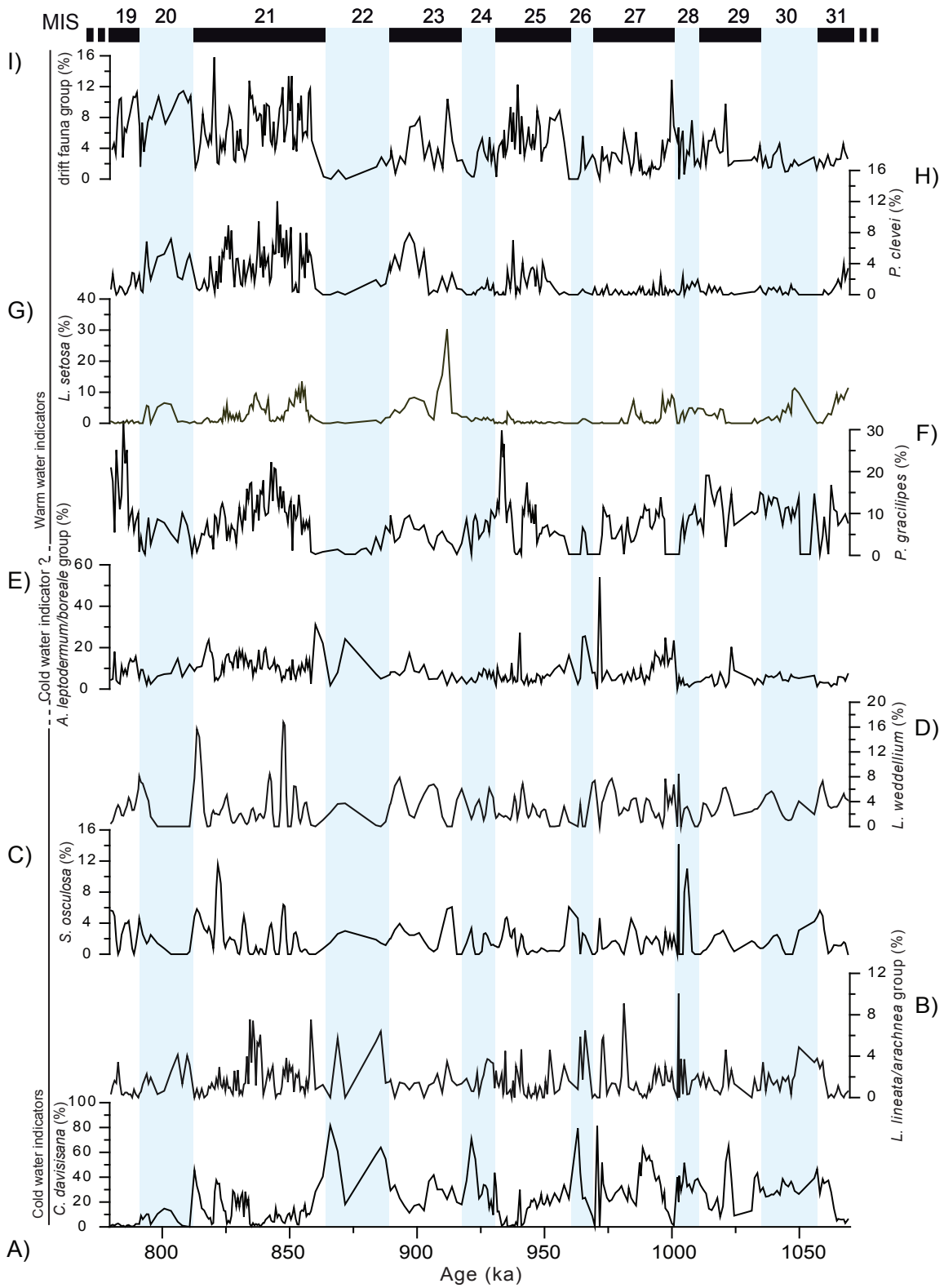

Figure 5.4. Radiolarian species representing more than 1%. Water mass affinity according to DCA represented in vertical left-side line and text. Marine Isotope Stages (MIS) are shown at the top (glacials in blue and interglacials in black).

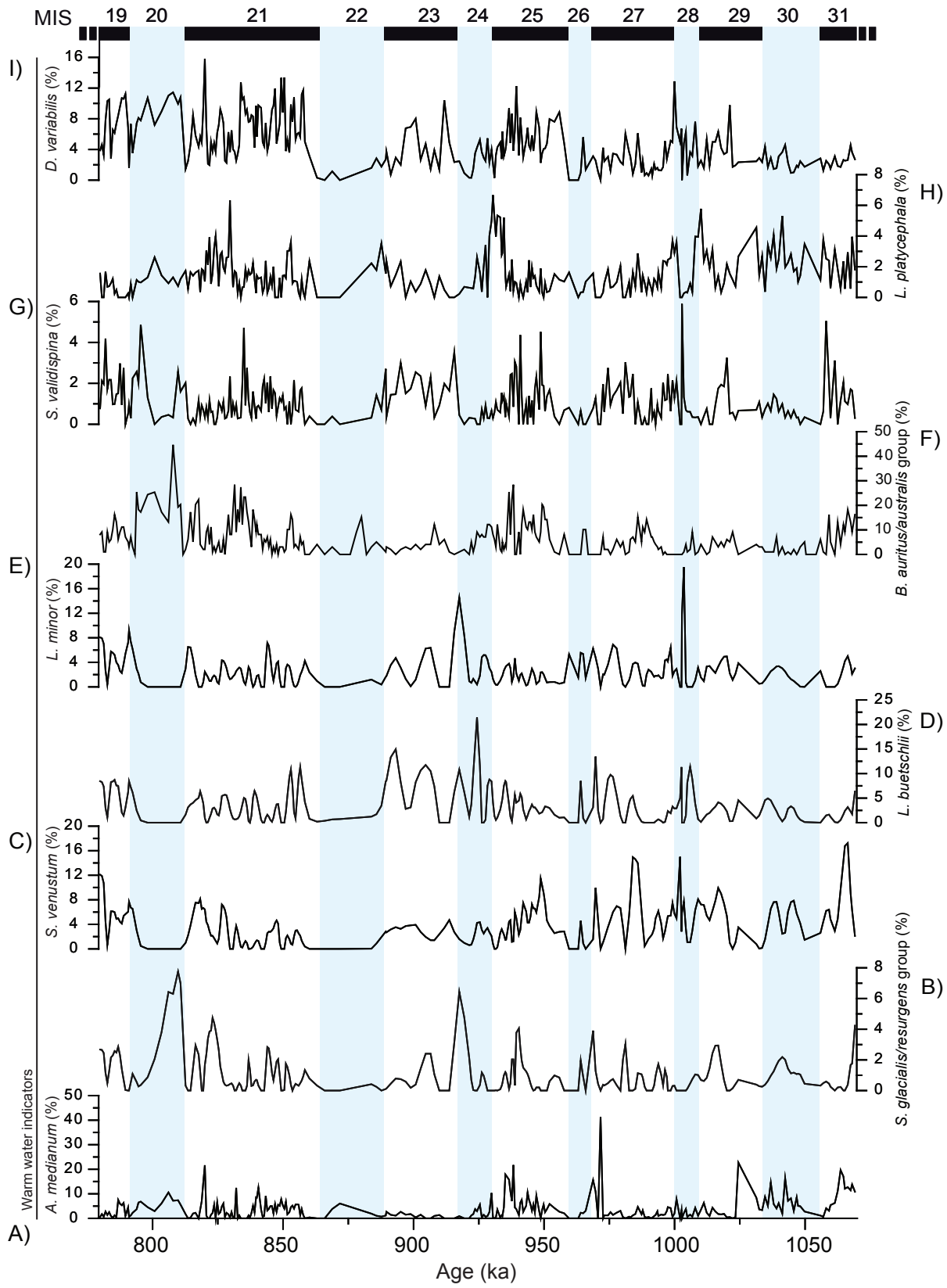

Figure 5.5. Radiolarian species representing more than 1%. Water mass affinity according to DCA represented in vertical left-side line and text. Marine Isotope Stages (MIS) are shown at the top (glacials in blue and interglacials in black).

Phaeodarians (*Lirella mello* and *Euphysetta* spp.) are little represented in our samples, and they occur normally during periods of moderate to high RAR within interglacial periods (Fig. 5.3C blue dots). The Shannon-Weaver diversity-index (*H*) shows a distribution pattern following glacial/interglacial units (Fig. 5.3G) and is negatively correlated with the distribution of the deep-living taxon *C. davisiana*. Higher *H* values were recorded during light $\delta^{18}O$ values (interglacial stages) and low percentages of *C. davisiana*, and vice versa (Fig. 5.3F-G).

The results of the DCA of the radiolarian data from Site U1314 are shown in Fig. 5.7. Axes eigenvalues (A1: 0.20; A2: 0.08; A3: 0.06) indicate the amount of variation in the dataset explained by each axis. In our DCA only Axis 1, which explain about 23 % of the total variation, is discussed, since Axes 2 and 3 have very low variance (<0.1 %) and explain only 17 % of the variation (9% and 8.1%, respectively), and therefore are of uncertain interpretation (Hammer, personal communication). Samples with higher positive Axis 1 values correspond to cold isotope stages 26 and 22. Likewise, the species *C. davisiana*, *S. osculosa* and *L. lineata/ arachnea* group that nowadays have optimum abundances in sediments below cool waters and glacial environments (e.g. Abelmann and Nimmergut, 2005; Bjørklund *et al.*, 1998; Okazaki *et al.*, 2004; Petrushevskaya and Bjørklund, 1974), are also placed at the positive side of the Axis 1. Furthermore, typical warm-condition species like *P. clevei* and *A. medianum* (Bjørklund *et al.*, 1998; Lüer, 2003) are located on the opposite side (negative values) of the Axis 1. Species that tolerate a wide range of temperature variance and also prefer mixing environments, like *P. gracilipes* (Bjørklund *et al.*, 1998), are placed in the middle of the gradient (Fig. 5.7). Based on this distribution pattern of species and samples in the DCA (Fig. 5.7), we have inferred that a combination of factors associated with changing conditions in the water column between glacial and interglacial periods (e.g. IRD input, ice-volume, nutrients, sea-surface temperature and salinity) is the underlying variable related to Axis 1, thus being responsible for gradation within the radiolarian assemblages from Site U1314.

Mantel correlogram and spectral analysis (Lomb periodogram) of the radiolarian assemblage, RAR, and opal AR records respectively, are shown in figure 5.8. Main periodicities are centered in Milankovitch orbital parameters of obliquity (~ 41 kyr), precession (~ 23 kyr), and to a lesser extent eccentricity (~ 100 kyr).

5. DISCUSSION

Using the temporal distribution of the most frequent radiolarian taxa (> 1%) at Site U1314 and the results obtained from the DCA, we have reconstructed water paleoceanographic and climatic conditions in the North Atlantic Ocean along glacial and interglacial stages. Additionally, for our ecological interpretation and radiolarian species water mass affinity, we have used published data concerning the radiolarian distribution in the surface sediments of the North Atlantic and the GIN-Seas (Bjørklund *et al.*, 1998; Cortese *et al.*, 2003; Goll

and Bjørklund, 1971; Matul, 1989a; Matul, 1994a; Matul, 1994b; Matul and Yushina, 1999; Petrushevskaya and Bjørklund, 1974).

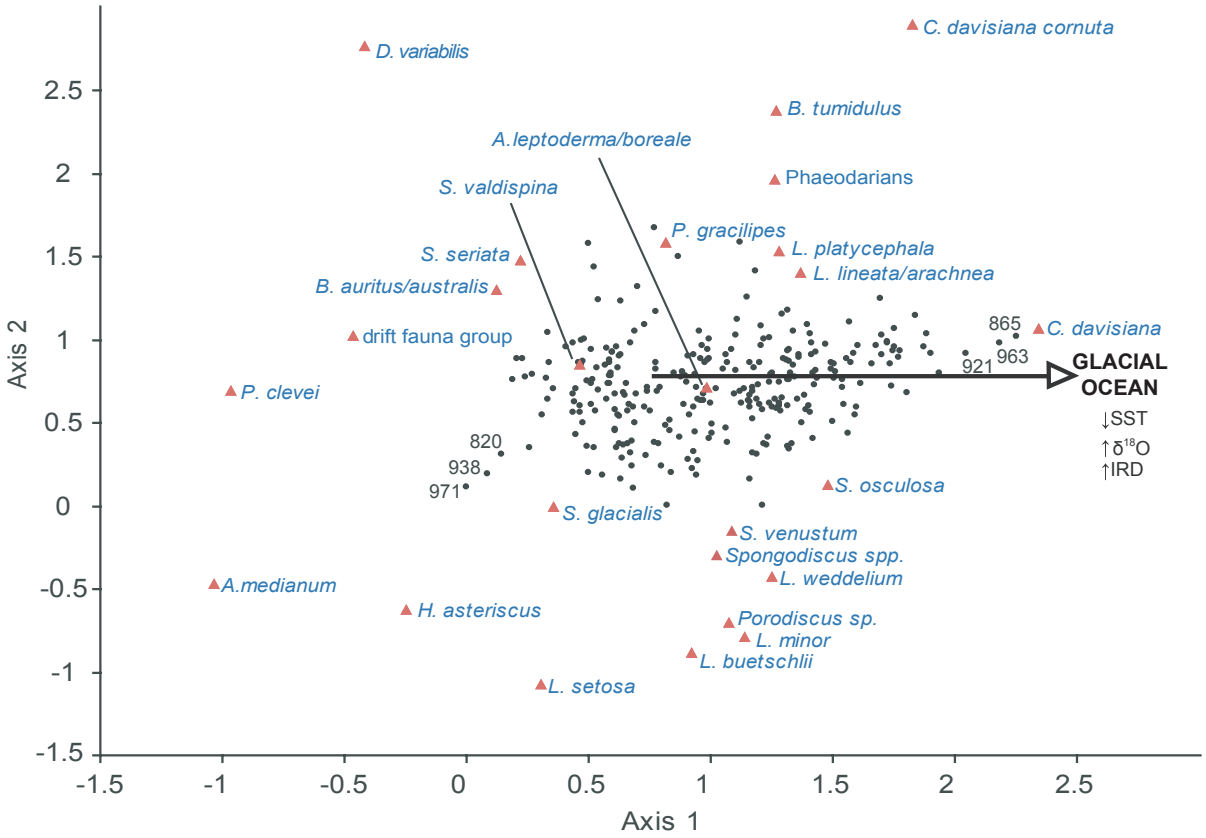

Figure 5.6. DCA diagram of the radiolarian species (red triangles) and samples (black dots) from Site U1314. Only samples occupying extreme positions along Axis 1 have been labelled with the age (ka). Arrows indicate inferred (environmental) variables.

5.1. The Glacial ocean

Glacial ocean in the subpolar North Atlantic is characterized by south-eastward shifts of the AF and expansion of cold arctic waters to meridional latitudes. These swings are accompanied by seasonal formation of sea-ice, and a more restricted distribution of the warm surface waters, NAC, in the North Atlantic, limited to a narrow flow compressed to the Norwegian continental margin (Van Nieuwenhove *et al.*, 2008). Surface and deep conditions become more dramatic during episodes of large influx of terrigenous material to the ocean triggered by periodic surges of icebergs from North Atlantic continental margins (Alley and MacAyeal, 1994; Bond *et al.*, 1992; Hemming, 2004; Moros *et al.*, 2004). Enhanced melt-water flux associated with these surges caused a great impact in thermohaline circulation by reducing convective overturning and weakening the deep convection in the GIN Seas (Maslin *et al.*, 1995; Vidal *et al.*, 1997).

This hydrographic scenario caused a large drop in surface primary productivity, as seen in the low DI values at Site U1314 and strong reduction in diatom abundance at neighbour site 983 during MIS 26, 24 and 22 (Koç *et al.*, 1999a), and led to a drastic reduction in the

radiolarian fauna. Most of radiolarian species observed at Site U1314 do not tolerate low SST that accompanied ice-sheet advances, and consequently migrated to southern latitudes. Taking into account these considerations, we suggest increasing percentages of *C. davisiana* during glacial stages and IRD discharges must be related to the reduced number of other species and development of unique conditions in the North Atlantic during these periods.

Nowhere in present day oceans *C. davisiana* abundances account for more than 5% of the total assemblage (Bjørklund and Ciesielski, 1994; Morley, 1983; Morley and Hays, 1979; Morley and Hays, 1983), except for the Okhotsk Sea, where *C. davisiana* exceeds 30 % (Abelmann and Nimmergut, 2005; Hays and Morley, 2003; Itaki *et al.*, 2008; Nimmergut and Abelmann, 2002; Okazaki *et al.*, 2004; Okazaki *et al.*, 2003a). The favourable conditions for *C. davisiana* in the Okhotsk Sea are closely related to well-ventilated, low-temperature, and oxygen-rich intermediate waters (Abelmann and Nimmergut, 2005; Itaki, 2003; Nimmergut and Abelmann, 2002) and the supply of organic matter (Abelmann and Nimmergut, 2005; Hays and Morley, 2003; Nimmergut and Abelmann, 2002; Okazaki *et al.*, 2003a). This hydrographic context occurs during periods of low surface salinities combined with extensive sea-ice (Rogachev, 2000). Hence, based on these observations, we speculate that high *C. davisiana* abundances at Site U1314 reflect prolonged periods of sea-ice cover, increased levels of sea-ice and/or iceberg melt water producing low salinity surface waters, and the establishment of a shallow temperature minimum, with relatively stable temperatures and salinities at depths below this minimum. During glacial times, convection in the GIN Seas switched from a deep to intermediate mode (Oppo and Lehman, 1993; Oppo and Lehman, 1995). Therefore, intensification of a cold oxygenized intermediate water mass, accompanied by low surface temperatures and salinities due to melt-water input during iceberg discharges, would result in a reduction of radiolarians living in surface water and a dominance of *C. davisiana* in the North Atlantic, as it is observed in the Okhotsk Sea (Abelmann and Nimmergut, 2005; Nimmergut and Abelmann, 2002). This interpretation is further supported by the shifts toward negative values in the benthic foraminiferal $\delta^{13}C$ from Site U1314 (2820 m depth) during *C. davisiana* peaks (Fig. 5.3B, F), indicating a reduction in deep water production at depths lower than 2000 m and enhanced ventilation at shallower depths (Flower *et al.*, 2000; Kleiven *et al.*, 2003; Venz *et al.*, 1999). At these times, deep water in the North Atlantic may have formed by brine rejection under sea ice on the continental shelves by processes more analogous to those observed around Antarctica today (Dokken and Jansen, 1999; Raymo *et al.*, 2004; Vidal *et al.*, 1998). Hence, as suggested by Itaki *et al.* (2009), organic matter that serves as a food source for *C. davisiana* would be released into the intermediate-water depths via a brine pumping process during winter sea-ice formation.

Hydrographic conditions inferred for high percentages of *C. davisiana* at Site U1314 are corroborated by the concomitant increases of the polar foraminifera *Neogloboquadrina pachyderma* sinistrorsa (sin.) at Site 980 and 984, for the time interval over which these two

records overlap (1000-779 ka) (Wright and Flower, 2002). In North Atlantic marine sediments, rapid increases in the abundance of *N. pachyderma* sin. correspond to a major reduction in planktonic foraminifer abundance, linked with changes in primary productivity, and changes in temperature and/or salinity related to AF fluctuations and massive iceberg discharges (Bond *et al.*, 1992; Bond and Lotti, 1995; Johannessen *et al.*, 1994; Pflaumann *et al.*, 2003). Hence, we suggest that high percentages of *C. davisiana* significance in Early and Mid-Pleistocene sediments at Site U1314 would be analogue to that of the polar planktonic foraminifera *N. pachyderma* sin. in the North Atlantic.

A detailed examination of the relationship between glacial-interglacial conditions and *C. davisiana* peaks, reveals that high abundances of the species occurred when benthic $\delta^{18}O$ values were around 3.5 ‰ and the highest abundances coincide with $\delta^{18}O$ more than 4‰ (Fig. 5.3A, F), as previously noted by Ciesielski and Bjørklund (1995). This observation is supported by correlation between Axis 1 samples scores and benthic $\delta^{18}O$ values (Table 5.2); the higher oxygen isotope values, radiolarian assemblage is more dominated by species located at right side of Axis 1, like *C. davisiana*. The boundary of 3.5‰ in benthic $\delta^{18}O$ for increased *C. davisiana* populations is the same threshold as proposed by McManus *et al.* (1999) as the minimum ice-volume required to trigger large instabilities in the North Atlantic ice-sheets. Therefore, *C. davisiana* abundance fluctuations seem to be dependant on a gradual ice growth that weakens deep-convection and triggers catastrophic IRD events, when benthic $\delta^{18}O$ values exceed 3.5‰ (Fig. 5.3A, E-F). This close relationship between *C. davisiana* and high benthic $\delta^{18}O$ values also showed up in the position of *C. davisiana* along the Axis 1 of the DCA (Fig. 5.7), next to the samples with heaviest oxygen isotopic values. Rapid depletions came along with large reductions in the *C. davisiana* populations near stage transitions (Fig. 5.3F) (e.g., stages 22/21, 24/23, 26/25), which would indicate rapid loss of the continental ice-volume during deglaciation that facilitates the resumption of LNADW versus the intermediate circulation.

	RAR	Benthic $\delta^{18}O$	IRD AR
Axis 1	**-0.223**	**0.458**	**0.348**

Table 5.2. Correlation matrix between Axis 1 from DCA and Site U1314 proxies. The bold values correspond to significant correlations at $p < 0.01$ level.

Ubiquity of *C. davisiana* in glacial Early and Mid-Pleistocene sediments is a common feature in the North Atlantic, since high percentages of this species have been also observed in other neighbour sites 114, 609 and 646 (Benson, 1972; Ciesielski and Bjørklund, 1995). In this sense, it is striking that lower than expected *C. davisiana* percentages during MIS 20 at Site U1314 and former sites (Fig. 5.3F), were also observed in the Okhotsk Sea (Matul *et al.*, 2009). Since *C. davisiana* relative abundance patterns appear to be synchronized worldwide (Morley and Hays, 1979; Morley *et al.*, 1982), this similarity between North Pacific and the

North Atlantic oceans may represent an environmental change at global scale.

Larcopyle weddellium and *Spongopyle osculosa* have been listed as intermediate-deep species in several regions (Abelmann and Gowing, 1997; Casey *et al.*, 1979b; Kling and Boltovskoy, 1995; McMillen and Casey, 1978). At Site U1314, both taxa appear frequently associated with the high *C. davisiana* percentages that also characterize the IRD events. Molina-Cruz (1977a) observed high percentages of *Spongurus* sp. (=*L. weddellium*) associated with *C. davisiana* in coastal and cool waters of the southeast Pacific during episodes of low radiolarian productivity due to very high rates of terrigenous supply. In the same sense, Dow (1978) reported that *S. osculosa* is also highly correlated with high percentages of *C. davisiana* and IRD in the Pleistocene sediments of the Indian Ocean. Okazaki *et al.* (2004) related *S. osculosa* to unfavourable conditions in the surface waters of the Okhotsk Sea due to seasonal formation of sea-ice (low sea surface salinities and temperatures). Environments described by previous authors therefore suggest conditions very similar to those when IRD was discharged at Site U1314, meaning a water column more suitable for the development of deep-dwellers, due to fresher surface water, causing stratification of the upper water layer.

On the other hand**,** the *Lithomitra lineata/arachnea* group (Fig. 5.4B) shows discrete percentages along the studied period, although several significant peaks (3-9%) appear close to the IRD peak together with high *C. davisiana* abundances (e.g. at 1056, 981, 965, 868). Hass *et al.* (2001) and Molina-Cruz (1991) also reported *L. lineata* together with *C. davisiana* and continental terrigenous supply, and depicted this assemblage as an indicator of a clear arctic environment, influenced mainly by sea-ice conditions and related to southward migrations of the AF in a short time-scale. Petrushevskaya and Bjørklund (1974) concluded that the cosmopolitan species *L. lineata* preferentially inhabits deep waters in cold water regions, together with *Artostrobus annulatus* and *C. davisiana*, as observed in our samples. Moreover, Petrushevskaya (1971a) included *L. arachnea* in her list of species with positive preservation potential, so its increase during IRD and glacial periods may be due to its high resistance to dissolution. Therefore, the *L. lineate/arachnea* group peaks in our samples may indicate cooling conditions during the progressive southward expansion of the AF.

Following *C. davisiana* peaks, at cold and deglacial events, once the adverse conditions for the development of shallow species ended (extensive sea-ice conditions) *Actinomma boreale* and *A. leptodermum* bloomed (Swanberg and Eide, 1992). Numerous authors have reported high abundances of the *A. leptodermun*/*boreale* group (Bjørklund *et al.*, 1998; Hass *et al.*, 2001; Molina-Cruz and Bernal-Ramirez, 1996; Petrushevskaya and Bjørklund, 1974; Swanberg and Eide, 1992) in the Greenland and Iceland Seas related to arctic or cold atlantic surface waters, and hence, they seem to be adapted to cold-water conditions. Therefore, increased abundances of the *A. leptodermun*/*boreale* group during cool and transitional periods suggest arctic or cold atlantic environments with open oceanic conditions.

5.2. The Interglacial ocean

Since total biogenic opal and the radiolarian content are generally used to infer ocean productivity, variability in the radiolarian assemblage can also be a good proxy to for monitoring changes in surface water processes. *P. gracilipes* and *L. setosa* are small-sized nassellaria strongly linked to warm water masses in the Norwegian Sea (Cortese *et al.*, 2003) under conditions of high primary productivity and eutrophic conditions (Yamashita *et al.*, 2002). *P. gracilipes* (Fig. 5.4F) and *L. setosa* (Fig. 5.4G) show a distribution pattern that is parallel to those of RAR and DI (Fig. 5.3C-D). Accordingly, both species are directly related with increased primary productivity associated with increased influence of the warm NAC and water column water mixing (Swanberg and Eide, 1992; Takahashi, 1997)

In the same sense, occurrence of shallow water (upper 200 m) and temperate conditions species *P. clevei* (= *P. pylonium*), *S. glacialis/resurgens* group, *L. buetchslii*, *S. venustum*, *S. glacialis/resurgens* group, *L. minor*, *Botryostrobus auritus/australis* group, *A. medianum*, *Stylodictya validispina* (Abelmann and Nimmergut, 2005; Boltovskoy *et al.*, 1996; Hass *et al.*, 2001; Hays and Morley, 2003; Lüer, 2003; Matul *et al.*, 2002; McMillen and Casey, 1978; Okazaki *et al.*, 2004; Samtleben *et al.*, 1995) during interglacial periods (MIS 31, 29, 27, 25, 21) would indicate a northward position of the AF and stronger transport of the NAC, which brings warm waters to high latitudes and originates the high productivity conditions in the area of Site U1314 (Bjørklund *et al.*, 1998; Goll and Bjørklund, 1971; Hatakeda and Bjørklund, 2009; Matul, 1989b; Matul, 1994a; Matul and Yushina, 1999). A similar response is shown by *Druppatractus variabilis* (=*Druppratractus cf. pyriformis*) (Fig. 5.5I), considered a surface-dweller of warm-waters in the Gulf of California, where it reaches high abundances with development of oceanic fronts (Molina-Cruz, 1988; Molina-Cruz *et al.*, 1999).

S. venustum (Fig. 5.5C) and *S. glacialis/resurgens* group (Fig. 5.5B), both indicative of open ocean conditions (Okazaki *et al.*, 2003a), show some peaks during low RAR (e.g. at 917 and 904 ka). This can be explained by the high adaptability to adverse surface conditions, like low temperature and salinity with strong seasonal changes (Nimmergut and Abelmann, 2002). Moreover, *S. glacialis/resurgens* group, *S. venustum*, and other radiolarians belonging to Spongodiscidae family (*Spongodiscus* sp., *Porodiscus* sp. and *S. validispina*) are particularly resistant (Boltovskoy *et al.*, 1993a; Takahashi and Honjo, 1983), allowing easier identification of incomplete shells, thus increasing considerably their abundances in our samples.

L. platycephala occurs during cool periods, according to the benthic $\delta^{18}O$ values. This species inhabits subarctic waters in the modern Iceland and Greenland seas, in the mixing area of arctic and atlantic waters (Bjørklund *et al.*, 1998; Cortese *et al.*, 2003; Molina-Cruz and Bernal-Ramirez, 1996). Consequently, *L. platycephala* in our samples is related to the southward migration of arctic waters during the beginning of glaciations.

As discussed previously, *C. davisiana* generally accounts for less than 5% in the modern

North Atlantic and in surface sediments (Bjørklund *et al.*, 1998; Petrushevskaya and Bjørklund, 1974); we can therefore assume that samples with the lowest percentages of *C. davisiana* at Site U1314 correspond with fully developed interglacial conditions similar to present day ocean, with a resumed deep convection in the Nordic Seas that ventilates the North Atlantic at all depths (Venz *et al.*, 1999). In contrast, *C. davisiana* abundances exceeding 20% in some samples located within interglacial stages may correspond to significant cool periods within robust interglacial stages (at 821 and 827) or weak interglacial stages (at 906, 970, 988 and 1022). This is further confirmed by the absence of *L. setosa* (< 1 %) and high percentages of *S. venustum* (up to 11 %), which tolerates a wide range of temperatures and salinities (Abelmann and Nimmergut, 2005; Nimmergut and Abelmann, 2002), as during early MIS 25. This suggests that some input of cold and low salinity waters reached the area of Site U1314 during this interglacial stage and increased the percentages of *S. vensutum* and *C. davisiana*, causing a decrease in *L. setosa* abundance.

Finally, we interpret increased values of "drift fauna group" during interglacial as enhanced NAC episodes that transport them to the subpolar North Atlantic. These species are intruders from tropical waters and can probably not live and reproduce at latitudes as high as 58º N (Bjørklund and Kruglikova, 2003; Cortese *et al.*, 2003). Consequently, they drifted passively up to the Site U1314 location and do not represent "in-situ" radiolarian production.

5.3. Changes in radiolarian and opal accumulation at Site U1314

Global ocean distribution of radiolarians, as in other important opaline plankton groups (diatoms and silicoflagellates), is dependent on several major environmental parameters, although several authors have highlighted the close affinity of this group to food availability among other factors (Boltovskoy *et al.*, 1996; De Wever *et al.*, 1994b; Petrushevskaya and Bjørklund, 1974). Determination of RAR, in combination with opal AR, may serve as a first-order approximation of past levels of surface productivity, but with some limitations because of possible differential dissolution problems at the sediment water interface (Broecker and Peng, 1982; Takahashi, 1994). Nevertheless, decrease in bulk sediment porosity during IRD deposition would reduce water content, and hence would limit exchange with silica unsaturated bottom waters and better preserve opal microfossils (Nave *et al.*, 2007). In addition, penetrations of silica-rich southern source waters far into the high northern latitudes during decreased relative glacial production of NADW (Marchitto *et al.*, 2002) would help for major opal preservation in North Atlantic sediments. Consequently, we discard opal dissolution as a mechanism for the lower RAR observed at IRD events.

Opal generally accumulates in sediments when diatom and radiolarian production is high, and therefore the primary signal related to opal production is quite relevant in view of the paleoceanographic utilization of opal accumulation data, where emphasis is placed on

production rather than on preservation processes (Cortese *et al.*, 2004). Our opal AR, conforms well to the general pattern of the RAR and the DI at Site 1314 (Fig. 5.3C-D), suggesting that both signals reflect large-scale changes in the amount of microfossil silicate in our core. However, a point-by-point comparison of both records shows that they are not totally equivalent (Pearson's correlation coefficient R= 0.67, Fig. 5.6). This is not surprising since RAR values exclude all opal particles smaller than 45 μm (our sieve mesh size), and fragments or opal produced by diatoms and sponge spicules are both considered as significant components of total opal (Leinen, 1985).

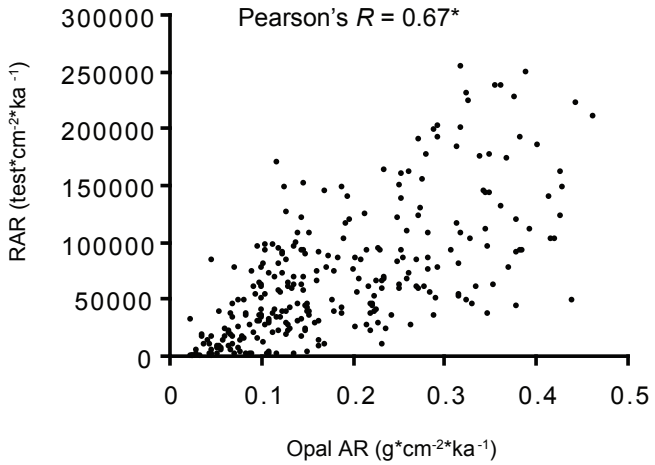

Figure 5.7. Correlation between RAR and opal AR. * Correlation is significant at p < 0.01 level.

RAR and opal AR signals co-vary in accordance with the climatic background (Fig. 5.3C), in a way similar to contemporary conditions. Today, the Reykjanes Ridge area located southeast of the AF, has an annual mean sea surface temperature of 9º-10º C, and is an area of maximal accumulation of radiolarian skeletons (up to 30000 individuals per gram of sediment) in surface sediments from the North Atlantic region (Goll and Bjørklund, 1971; Matul, 1989a). Hence, we can assume that the samples with the highest radiolarian productivity in our study were similarly located south of the AF or near the region of mixing between the warm atlantic and cold arctic waters, as suggested by Molina-Cruz and Bernal-Ramirez (1996). Moreover, according to Aksu and Mudie (1985), high dissolved silica fluxes from the Arctic Ocean (Codispoti, 1979) and increased SST in the North Atlantic during interglacial stages would increase radiolarian and diatom production as well the preservation of opal in the sedimentary record (Berger, 1970b; Nave *et al.*, 2007; Takahashi, 1991).

During IRD peaks, radiolarian shells are scarce indicating a period with decreased fertility in the upper water layers (Herguera, 1992; Takahashi, 1991). We interpret this as reduced opal and radiolarian production rates associated with the climate-induced southward migration of the AF, bringing to the Site U1314 location water with low SST, as well as reduced light due to extended ice cover, and accompanying stratification by melt-water input (Aksu *et al.*, 1992; Morley, 1983; Scharek *et al.*, 1994). Additionally, transfer of arctic waters rich in dissolved

silica to the North Atlantic would be restricted due to the partial or total freezing of the Arctic Ocean, limiting nutrient input to the Site U1314 area (Aksu and Mudie, 1985). These results are in agreement with those of Thomas *et al.* (1995) and Nave *et al.* (2007), who reported similar reduced surface productivity during Heinrich Events in the North Atlantic (50º - 62º N), on the basis of benthic foraminifera and diatom-based proxies, respectively. Under these unfavourable environmental conditions, only cold-adapted radiolarian species like *C. davisiana* can survive (Bjørklund and Ciesielski, 1994; Morley *et al.*, 1987; Morley, 1983; Morley and Hays, 1983). RAR are considerably low during these periods, and *C. davisiana* is not an important opal carrier (Jacot Des Combes and Abelmann, 2009), what explain the low opal AR values during critical glacial periods. Opal production was likely restricted to short periods in ice-free areas of the North Atlantic and Nordic Seas during summer (Pflaumann *et al.*, 2003), similar to biological productivity episodes in the modern Arctic Ocean (Bjørklund and Kruglikova, 2003; Itaki, 2003).

Important reductions in the radiolarian content during glacial times since 950 ka, were also observed in the Northwest Pacific (Morley and Dworetzky, 1991). This suggests a cooling trend and onset of major ice-sheets that could have diminished glacial ocean productivity in the Northern Hemisphere (Berger *et al.*, 1993a; Berger and Jansen, 1994c).

Additionally, since the Gardar Drift is a contourite drift formed by accumulation of sediment carried by the northeastern branch of the NADW, the ISOW (Bianchi and McCave, 2000), we can expect some size-sorting by bottom currents at Site U1314. Interglacial stages with low benthic $\delta^{18}O$ values and null IRD deposition at Site U1314 correspond with periods of enhanced ventilation of the deep North Atlantic, as indicated the high benthic $\delta^{13}C$ values ISOW, correspond with higher opal plankton productivity (Fig. 5.3A-C). Episodes of enhanced ISOW flow correspond with enhanced silt and clay deposition over the southern end of Gardar Drift (Bianchi and McCave, 1999). Hence, we suggest that increases of RAR and opal AR during interglacial periods are the result of enhanced transport of fine sediment by ISOW, being this material dominated biogenic particles derived of increased planktonic productivity in surface warmer waters. In contrast, during cold periods with weakened ISOW flow because of melt-water input at deep-convection sites, fine biogenic sedimentation was strongly diluted by periodic and episodic influxes of ice-rafted material from the surrounding land masses. Thus, the pronounced contrast in RAR and opal AR within G-IG stages results from oceanic circulation changes: either from surface circulation governing the ice-rafted detritus supplies and the planktonic biogenic production; and from deep circulation changes with the reactivation of the ISOW flow.

5.4. Mid-Pleistocene Transition: impact on the radiolarian fauna

The interval investigated is within the period known as the Mid-Pleistocene Transition

(MPT), characterized by a shift of global glacial/interglacial cycles from 41-kyr to 100-kyr (e.g. Berger and Jansen, 1994c; Ruddiman *et al.*, 1989). This shift in the dominant cyclicity triggered several large-scale climatic-events; e.g. global ice mass increase (Mudelsee and Schulz, 1997), drastic cooling and aridification in Africa (deMenocal, 1995), and large ice-sheet advances in the North and South Atlantic Ocean (Ferretti *et al.*, 2005; Raymo *et al.*, 1997). Likewise, clear radiolarian-based evidence shows change in the sea-surface temperature after MIS 26 toward cooler conditions (Matul *et al.*, 2009; Morley and Dworetzky, 1991; Wang and Abelmann, 2002; Wang *et al.*, 2000). According to faunal and isotopic data from Site U1314, we have identified two time-periods in our sedimentary record with different dominant cycles.

In the period from 1069 to 860 ka, the distribution of the RAR was characterized by frequent low-amplitude fluctuations (Fig. 5.3C), where adverse surface conditions (extensive sea-ice and IRD discharges) were not always accompanied by minimum values of radiolarian abundance and diversity, suggesting milder conditions, or an ocean that was only seasonally partly ice-covered and allowed a certain amount of plankton productivity. This interval is characterized by a radiolarian assemblage continuously dominated by the cold and deep-dweller *C. davisiana* (27 % on average) (Fig. 5.4A), but co-occurring with shallow-dwellers, like *P. gracilipes* and *L. setosa* (Fig. 5.4F-G). This planktonic fauna and flora suggests a cold environment with relatively stable water masses at Site U1314, even during interglacials, as a result of an AF that was southward of its present position. Dominance (> 60 %) of the cold-water diatom *Neodenticula seminae* (Shimada *et al.*, 2008) and high concentrations of $C_{37:4}$ alkenones (McClymont *et al.*, 2008) in the North Atlantic until MIS 21 support the inference made from our radiolarian data that cooler and fresher waters prevailed at Site U1314 during this interval. This also indicates the absence of extreme contrast between glacial and interglacial periods, due to the rapid fluctuation of the volume of continental ice-masses discharged to the North Atlantic following the 41-kyr Milankovitch obliquity cycles, without the time necessary for building up a great continental ice-sheet (Mudelsee and Schulz, 1997).

After ~ 860 ka ago, higher amplitude changes are recorded in the benthic $\delta^{18}O$ signal. MIS 22 represents the first interval of substantial sea-level fall due to the glacioeustatic effect of continental ice build-up (Ferretti *et al.*, 2005), consistent with the onset of the larger-amplitude 100-kyr Milankovitch eccentricity cycles during the Brunhes Chron (Mudelsee and Schulz, 1997). At Site U1314, the onset of the large-amplitude 100 ka cycles is manifested in the heavy benthic isotope values recorded during MIS 22, the highest for the last 1.1 Myr, and the massive growth of the ice rafting activity (Fig. 5.3A, E) suggests more severe glacial conditions. Glacial MIS 22 also represents a marked decrease in the accumulation of radiolarians, producing a greater contrast in glacial/interglacial planktonic production.

Likewise, a shift in the faunal composition can also be appreciated from about 850 ka upward. Upcore of MIS 21, the main cold taxon, *C. davisiana* underwent a large shift toward lower values (9 % on average), while Shimada *et al.* (2008) observed a rapid disappearance of

N. seminae from the North Atlantic diatom community, indicating an increase in the abundance of warm water diatoms. This scenario suggests a progressive northwest retreat of the AF, that culminated after 610 ka (MIS 16), to almost the same position that it occupies today (Wright and Flower, 2002), and hence an intensification of the northward flow of warm subtropical water, as reflected by the increased numbers of warm-water radiolarian species (e.g. Fig. 5.4I) after 850 ka. Moreover, higher opal and RAR values (Fig. 5.3C) after MIS 22 may indicate increased nutrient supply from land and continental shelves (Kitamura and Kawagoe, 2006) during large amplitude sea level fluctuations in glacial cycles after 890 ka (up to 33m) (Prell, 1982; Ruddiman *et al.*, 1989), leading to higher primary productivity (Broecker, 1982) and more efficient export flux of surface biosiliceous production (Shimada *et al.*, 2008).

5.5. Diversity Index

Radiolarian diversity tracks decreasing ecosystem complexity with depth; in other words, there are more niches for radiolarians in shallow waters than in deep waters (McMillen and Casey, 1978). Hence, the *H* pattern at Site U1314 reflects water column "habitability", which in turn depends on the climatic background. During interglacial periods, we observe numerous shallow water species, some of them microhervibores or with host-symbionts, such as *Didymocyrtis tetrathalamus*, *Eucyrtidium* spp., *Heliodiscus asteriscus*, *Peridium* sp., *Pterocanium praetextum*, *Tetrapyle octacantha* and *Ommatartus tetralamhus* (Takahashi *et al.*, 2003). In contrast, during glacial periods, proliferation of shallow dwellers is hampered by harsh conditions such as sea ice and large salinity and temperature changes (Hays and Morley, 2003; Morley and Hays, 1983), leading to enhancement of percentages of the deep-dweller *C. davisiana*, which feeds mainly on phytodetritus provided by the brine pump system (Abelmann and Nimmergut, 2005; Anderson, 1983; Itaki *et al.*, 2009). These results agree with the findings of Bjørklund *et al.* (1998) for the GIN Seas, who described the highest species richness for polycystine radiolarians in the warm atlantic domain, while the lowest species number was found in the colder arctic and polar domains. In the same way, the *H* pattern of radiolarians in the North Atlantic is very similar to that described by planktonic foraminifera: showing higher *H* values with the shifting of the warm Gulf Stream surface currents into the North Atlantic (Balsam and Flessa, 1978; Ruddiman, 1969).

5.6. Time series and variance spectra

In order to show the dominant signals controlling the radiolarian assemblage structure, RAR, and opal AR, different techniques of spectral analysis (see Results) were used to study the variability of the three paleoceanographic records.

A prominent peak at 40 samples indicates a recurrence of taxa over a 7 kyr period (Fig. 5.8A). The power spectrum generated from the discrete Fourier transform of the Mantel

correlogram shows two spectral peaks, at 6 and 14, reflecting an obliquity-dominated (~ 48 kyr) and precessional signal (~ 20 kyr) over the 289 kyr period, respectively (Fig. 5.8B). The offset of 7 kyr in the obliquity frequency found in the radiolarian assemblage indicates that this spectral peak may not be related in a simple direct way to the suggested periodicity, and that further considerations which we have not identified in this study may influence the radiolarian assemblage periodicity. Likewise, spectral analysis of the RAR and opal AR record reveals a significant obliquity-related response (~ 45 kyr and ~ 47 kyr respectively) and precessional signal (~ 23 kyr and ~ 27 kyr respectively) (Fig. 5.8C-D). Therefore, frequencies driving RAR, opal AR and radiolarian assemblage signals coincide with the dominant Earth´s solar orbit during the MPT, obliquity and precession (Mudelsee and Schulz, 1997; Mudelsee and Stattegger, 1997), and indicating that the quasi-periodic oscillations observed in the variations of all bio-silica records at Site U1314 are largely controlled by these orbital parameters. Moreover, the periodogram from the RAR record also shows a third dominant cyclicity (~ 100 kyr) (Fig. 5.8C), and opal AR shows cyclicity centered at ~ 121 kyr and ~ 83 kyr (Fig. 5.8D), both related to eccentricity and reflecting the incipient climatic transformation at the MPT (Berger *et al.*, 1993a). Coherence between the dominant periodicity of the bio-silica records from Site U1314 indicates that climate changes driven by orbital parameters affect indistinctively the radiolarian group and all other opaline siliceous organisms (e.g. diatoms, silicoflagellates and sponge spicules), independently of their different ecologies.

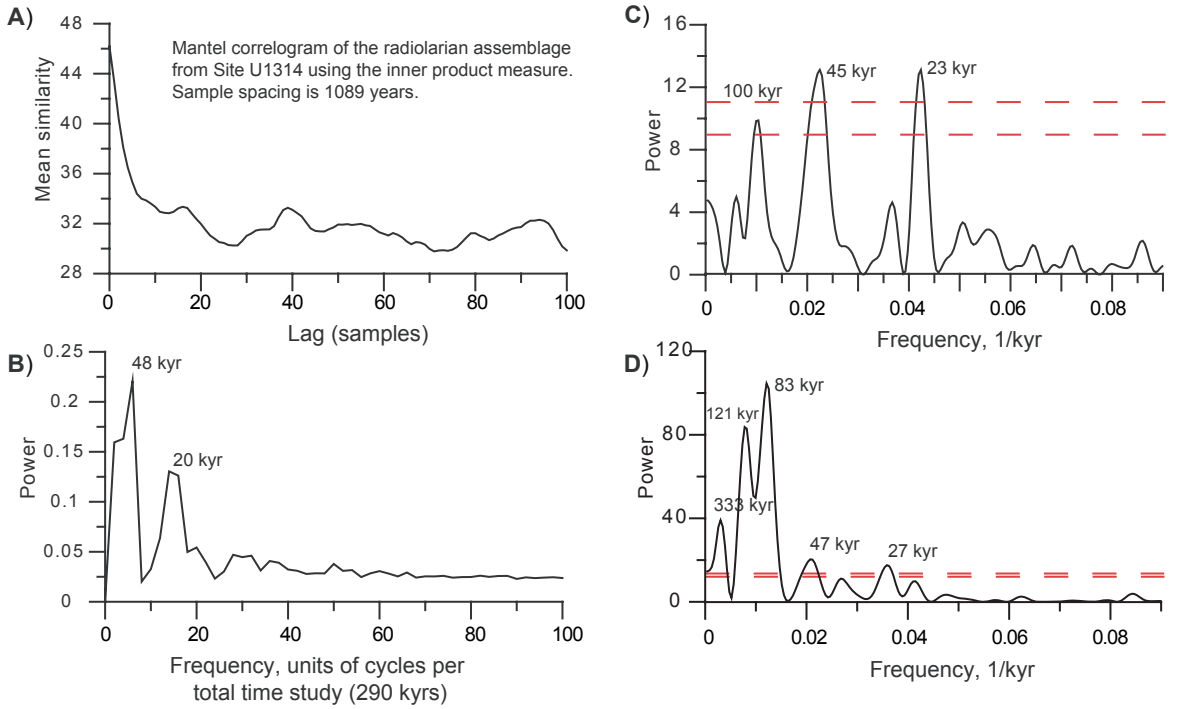

Figure 5.8. A) Mantel correlogram of the multispecies time series for the interval 1069-779 ka using inner product measure (sample spacing is 1089 year) and B) time spectra using the discrete Fourier transform of the Mantel correlogram. See Hammer (2007) for procedure description. Spectral analysis (Lomb periodogram) of the different paleoceanographic records from Site U1314: C) RAR and D) opal AR for the same interval. Numbers above peaks denote respective periodicities. The 0.01 and 0.05 significance levels ('white noise lines') are shown as red dashed lines.

6. CONCLUSIONS

The biogenic silica data set from Site U1314 provides a detailed record of surface oceanographic conditions (radiolarian assemblages) and surface productivity conditions (biogenic silica deposition) for the Early and Mid-Pleistocene (1069-779 ka) in the North Atlantic.

Temporal evolution of radiolarian assemblage composition and results from DCA show that the hydrographic and climatic context had a major influence on the radiolarian assemblage, yielding a clear glacial/interglacial faunal succession. During glacial periods *C. davisiana* dominated the radiolarian fauna because of the relatively low-surface temperatures and the episodically low surface salinities caused by ice melting and the increase in the IRD delivery, which restricted the radiolarian productivity and diversity (*H*). In contrast, during interglacial periods, warm and shallow water dwellers (e.g. *P. gracilipes*, *L. setosa*, *S. glacialis/ resurgens* group and *S. venustum*) proliferate due to the open water conditions provided by the vicinity of the warm atlantic waters and the ice-sheet retreat, which is conducive to higher surface water productivity and higher *H*. Furthermore, occasional occurrence of species with tropical-subtropical affinity ("drift fauna group") is related to a northeastward transport by the warm atlantic surface waters to the Site U1314 position; therefore do not represent "in-situ" production.

The temporal pattern of the RAR runs parallel with the DI and opal AR patterns, suggesting that radiolarians as a whole can be considered a productivity indicator in Pleistocene samples of the North Atlantic. Radiolarian and opal paleofluxes show significant fluctuations along the sedimentary record according to the climate-induced latitudinal migration of the AF and associated changes that took place in the water column; increased RAR and opal values during interglacials indicate intense water mixing and active NAC flow in the North Atlantic, that decrease during glacial periods, when severe surface conditions (low SST and sea-ice cover) and stratification by melt-water input during ice-rafting episodes occurred.

Additionally, bottom currents play an important role on fine grain material sedimentation at Site U1314. Enhanced ISOW flow during interglacial periods results in an increase in accumulation of fine biogenic particles produced at surface, while less vigorous deep-water flow over Gardar Drift during melt-water events transported and accumulated less fine-grained material, including less opal plankton, that led to the relative concentration in the sediment of the coarsed-grained fraction. Therefore, the pronounced contrast in RAR and opal AR within G-IG stages results from a combination of surface and deep oceanic circulation changes: either from surface circulation governing the ice-ratted detritus supplies and the planktonic biogenic production; and from deep circulation changes with the reactivation of the ISOW flow.

The temporal variation of the radiolarian assemblage along the Site U1314 record shows a drastic change at MIS 22 (~ 860 ka). Before this time the deep-dwelling taxon *C. davisiana* co-

existed with shallow dwellers, e.g. *P. gracilipes* and *L. setosa*, indicating a milder environment without such extreme seasonal conditions and not so severe glacial conditions, with dominance of the 41-kyr glacial cyclicity. Since ~ 860 ka more severe glacial conditions, due to increased global ice-volume, caused a strong reduction in the North Atlantic thermohaline circulation (Mudelsee and Stattegger, 1997). Isotopic and faunal records at Site U1314 do show higher amplitude variations in response to these new environmental conditions. The radiolarian assemblage shows a higher contrast between glacial and interglacial periods. Cold and deep-dwellers dominated during glacial periods and IRD discharge. In contrast, interglacial periods are characterized by an increase in shallow-dwellers that represent enhanced opal and radiolarian production during introduction of warm atlantic waters and water mixing.

Spectral analyses (Mantel periodograms) of the radiolarian assemblage reveal dominant periodicities of ~ 48 kyr and ~ 20 kyr, which could be related to the Milankovitch cycles of obliquity and precession, respectively dominant during the MPT. RAR and opal AR records exhibit a coherent response to the whole radiolarian assemblage, with a more significant obliquity and precessional -related cyclicity, and showing an incipient eccentricity signal, which represents the prelude of the high-amplitude cycles typical during the Late Pleistocene.

PLATE 1

1-4. *Actinomma boreale* Cleve, 1899

1. Hole C; core 7; section 5; cm 146-148 (64.46 mcd)

2-3. Hole B; core 9; section 2; cm 124-126 (77.84 mcd)

4. Hole C; core 8; section 6; cm 30-32 (75.20 mcd)

5-8. *Actinomma leptodermum leptodermum* (Jørgensen, 1900)

Hole C; core 7; section 5; cm 146-148 (64.46 mcd)

9-11. *Actinomma medianum* Nigrini, 1967

9-10. Hole C; core 8; section 4; cm 98-100 (72.88 mcd)

11. Hole C; core 8; section 5; cm 2-4 (73.42 mcd)

12. *Actinomma popofskii* (Petrushevskaya, 1967)

Hole C; core 8; section 6; cm 30-32 (75.20 mcd)

13. *Actinomma trinacrium* Haeckel, 1862

Hole C; core 7; section 5; cm 146-148 (64.46 mcd)

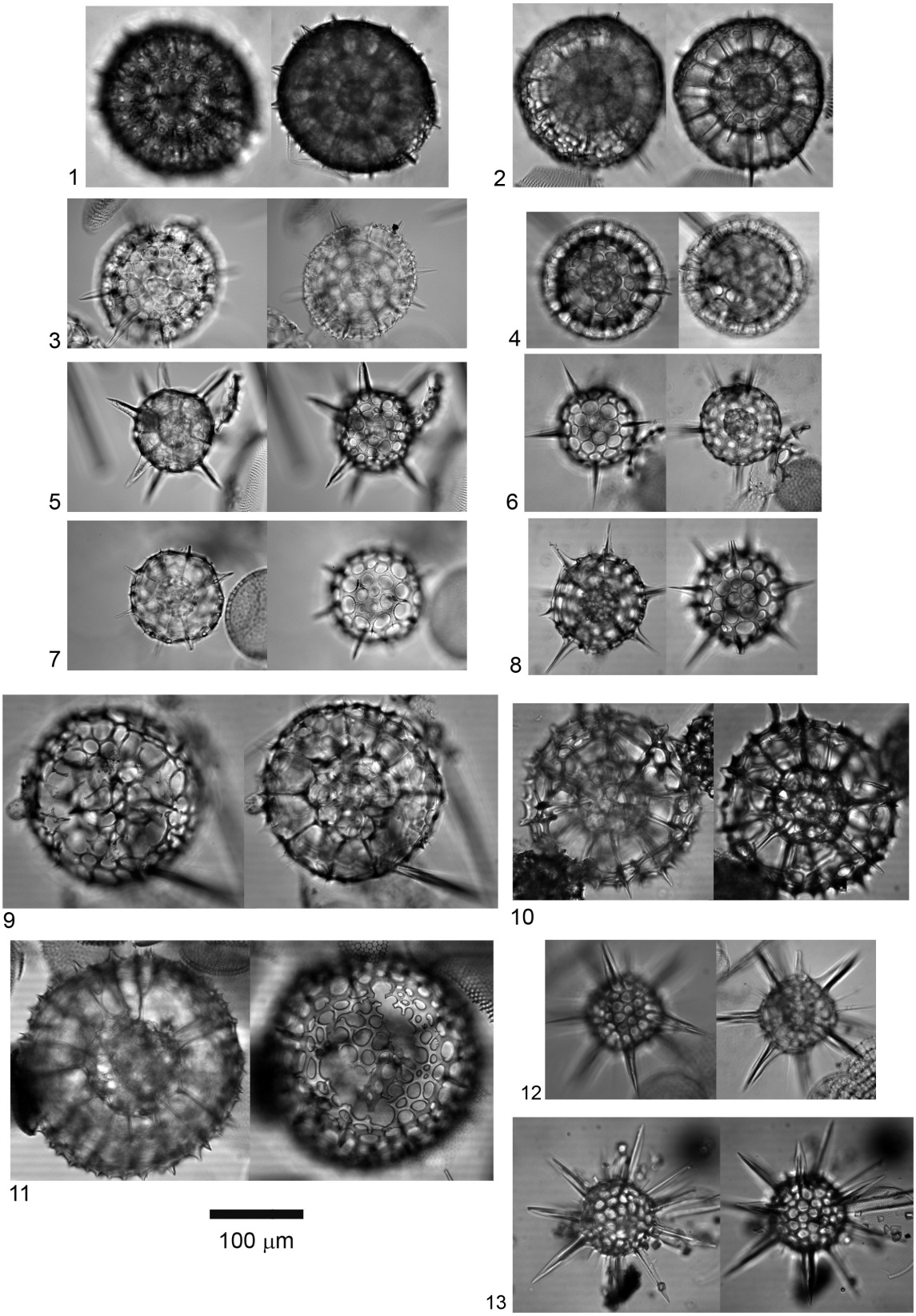
1
2
3
4
5
6
7
8
9
10
11
12
13
100 μm

PLATE 2

1-3. *Druppatractus variabilis* Dumitrica, 1973

Hole B; core 9; section 2; cm 124-126 (77.84 mcd)

4. *Dictyocoryne profunda* Ehrenberg, 1860

Hole C; core 8; section 5; cm 2-4 (73.42 mcd)

5-6. *Heliodiscus asteriscus* Haeckel, 1887

Hole B; core 7; section 6; cm 38-40 (61.88 mcd)

7-8. *Larcopyle buetschlii* Dreyer, 1889

7. Hole C; core 8; section 2; cm 146-148 (70.36 mcd)

8. Hole B; core 9; section 2; cm 124-126 (77.84 mcd)

9-14. *Larcopyle weddellium* Lazarus et al, 2005

Hole C; core 8; section 2; cm 146-148 (70.36 mcd)

15-19. *Larcospira minor* (Jørgensen, 1900)

15. Hole B; core 9; section 2; cm 124-126 (77.84 mcd)

16-19. Hole C; core 8; section 2; cm 146-148 (70.36 mcd)

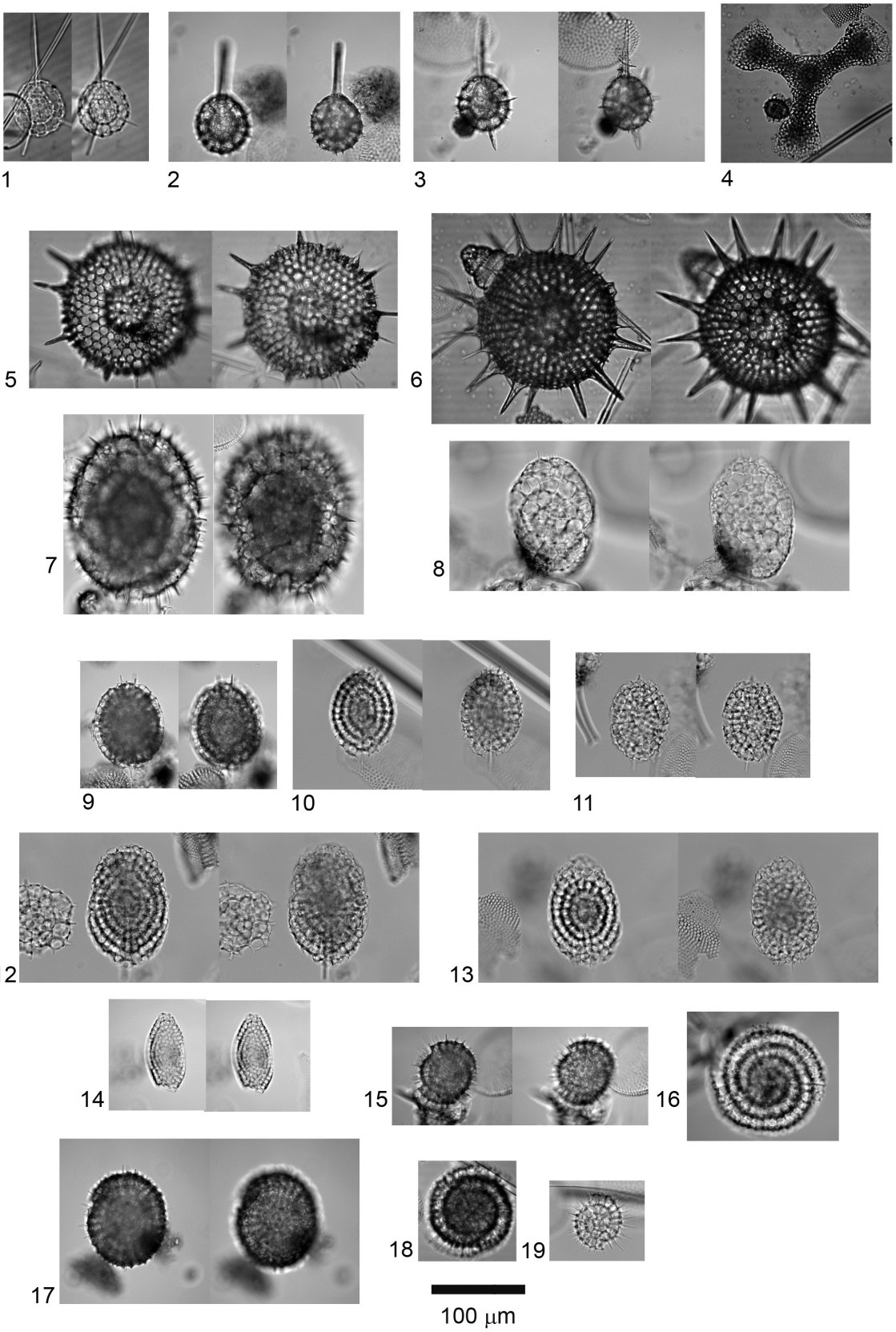
1
2
3
4
5
6
7
8
9
10
11
12
13
14
15
16
17
18
19
100 μm

PLATE 3

1-5. *Phorticium clevei* (Jørgensen, 1900)

Hole C; core 8; section 4; cm 98-100 (72.88 mcd)

6-9. *Porodiscus* sp. 1

Hole C; core 8; section 4; cm 98-100 (72.88 mcd)

10. *Spongocore puella* Haeckel, 1887

Hole C; core 7; section 5; cm 146-148 (64.46 mcd)

11-12. *Spongodiscus* sp. Takahashi and Honjo, 1981

Hole C; core 8; section 2; cm 146-148 (70.36 mcd)

13-15. *Spongopyle osculosa* Dreyer, 1889

13-14. Hole C; core 8; section 2; cm 146-148 (70.36 mcd)

15. Hole C; core 7; section 5; cm 146-148 (64.46 mcd)

16-19. *Spongotrochus glacialis/resurgens* group Popofsky, 1908

Hole C; core 8; section 4; cm 98-100 (72.88 mcd)

20. *Stylatractus* sp. 1

Hole C; core 7; section 5; cm 146-148 (64.46 mcd)

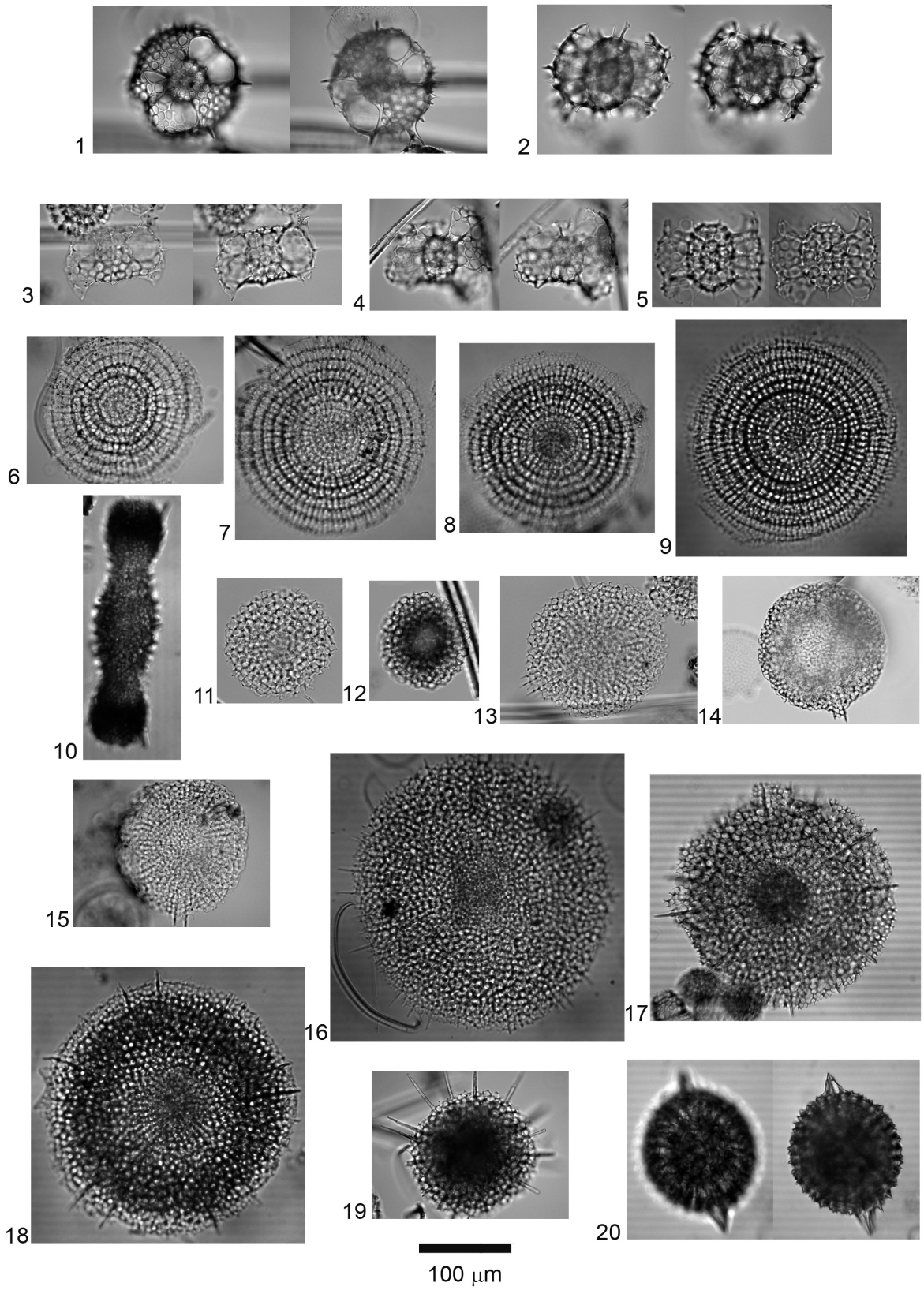
1
2
3
4
5
6
7
8
9
10
11
12
13
14
15
16
17
18
19
20
100 μm

PLATE 4

1-6. *Stylochlamydium venustum* (Bailey, 1856)

1-3. Hole C; core 8; section 2; cm 146-148 (70.36 mcd)

4-6. Hole C; core 8; section 4; cm 98-100 (72.88 mcd)

7-9. *Stylodictya validispina* Jørgensen, 1905

7-8. Hole C; core 7; section 5; cm 146-148 (64.46 mcd)

9. Hole C; core 8; section 4; cm 98-100 (72.88 mcd)

10. *Tetrapyle octacantha* Müller, 1858

Hole C; core 8; section 2; cm 146-148 (70.36 mcd)

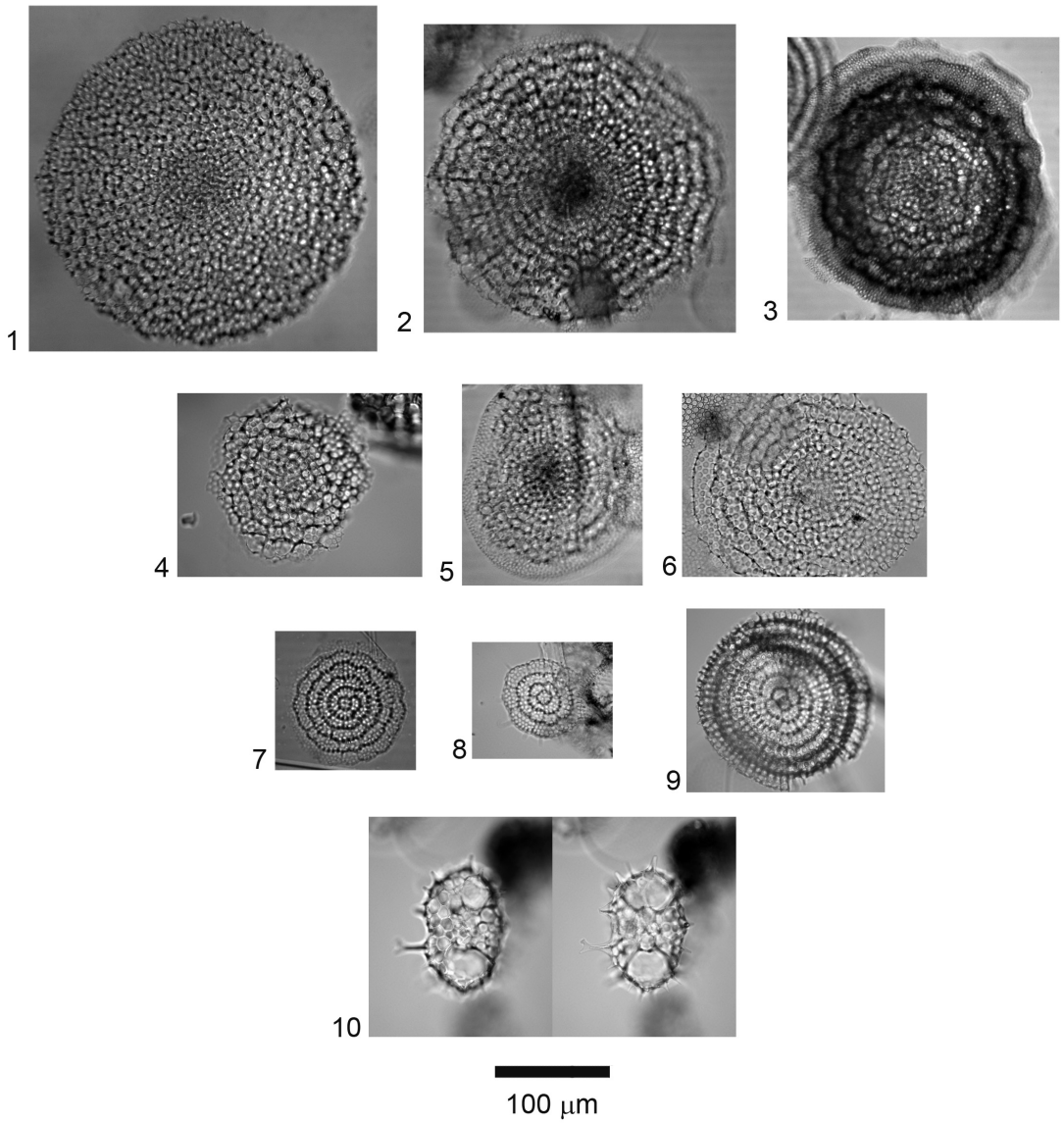
1
2
3
4
5
6
7
8
9
10
100 μm

PLATE 5

1-3. *Artostrobus annulatus* (Bailey, 1856)

1. Hole C; core 8; section 2; cm 146-148 (70.36 mcd)

2-3. Hole C; core 8; section 5; cm 2-4 (73.42 mcd)

4. *Artostrobus joergenseni* Petrushevskaya, 1967

Hole C; core 8; section 4; cm 98-100 (72.88 mcd)

5. *Botryocampe inflata* (Bailey, 1856)

Hole C; core 8; section 5; cm 2-4 (73.42 mcd)

6-7. *Botryostrobus auritus/australis* (Ehrenberg) group Nigrini, 1977

Hole B; core 9; section 2; cm 124-126 (77.84 mcd)

8. *Botryostrobus tumidulus* (Bailey, 1856)

Hole C; core 7; section 5; cm 146-148 (64.46 mcd)

9-10. *Cornutella profunda* Ehrenberg, 1854

Hole C; core 8; section 4; cm 98-100 (72.88 mcd)

11. *Corocalyptra craspedota* (Jørgensen, 1900)

Hole A; core 8; section 6; cm 2-4 (69.17 mcd)

12-18.*Cycladophora davisiana* (Ehrenberg, 1862)

12-16. Hole B; core 9; section 2; cm 124-126 (77.84 mcd)

17-18. Hole C; core 8; section 2; cm 146-148 (70.36 mcd)

19. *Eucyrtidium acuminatum* (Ehrenberg, 1844)

Hole C; core 8; section 4; cm 98-100 (72.88 mcd)

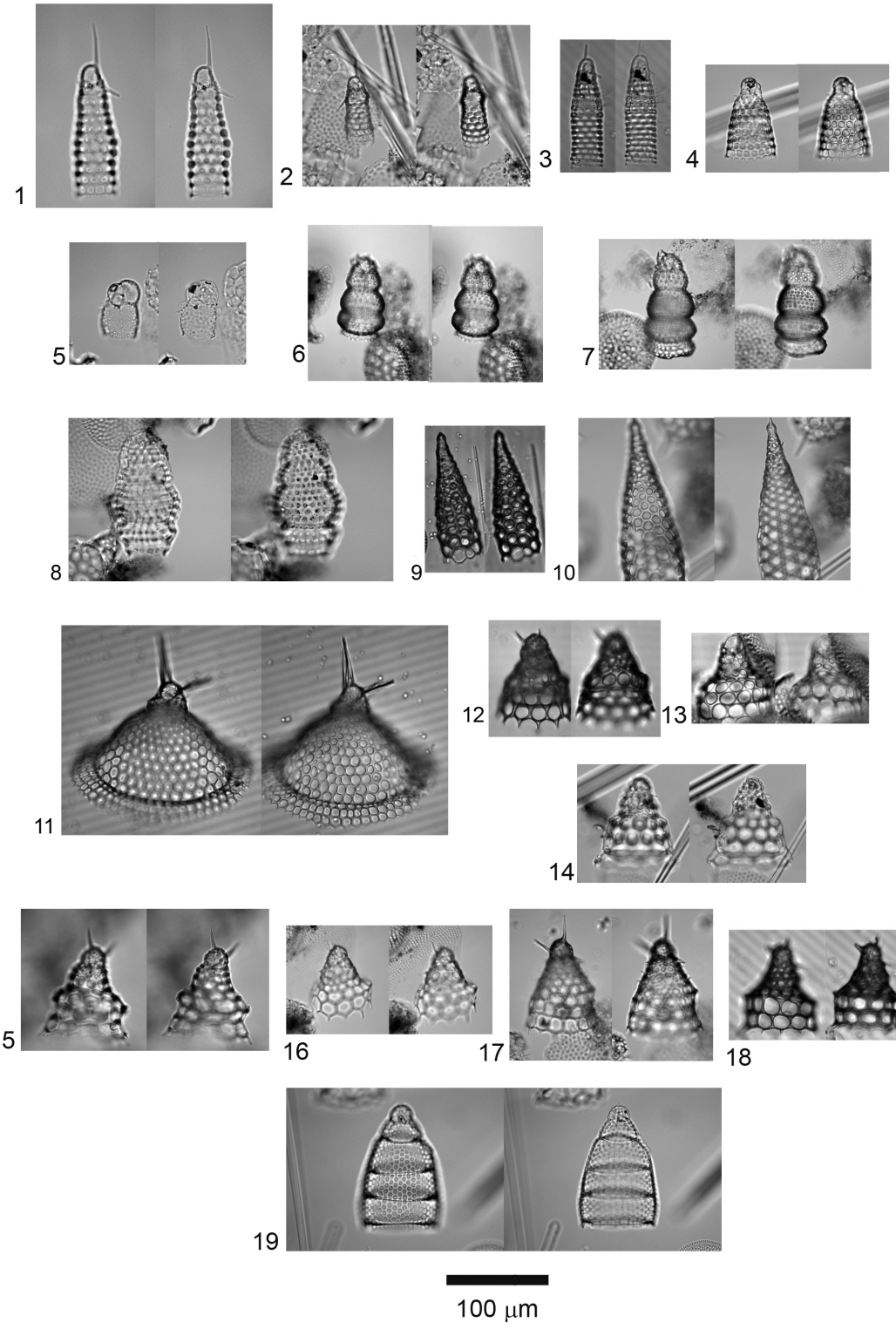
1
2
3
4
5
6
7
8
9
10
11
12
13
14
15
16
17
18
19
100 μm

PLATE 6

1-3. *Lithocampe platycephala* (Ehrenberg, 1873)

Hole C; core 8; section 4; cm 98-100 (72.88 mcd)

4-8. *Lithomelissa setosa* Jørgensen, 1900

4-6. Hole C; core 8; section 2; cm 146-148 (70.36 mcd)

7-8. Hole C; core 8; section 4; cm 98-100 (72.88 mcd)

9-14. *Lithomitra lineata*/*arachnea* group (Ehrenberg, 1839)

9. Hole C; core 8; section 2; cm 146-148 (70.36 mcd)

10-14. Hole C; core 7; section 5; cm 146-148 (64.46 mcd)

15. *Lithostrobus cuspidatus* (Bailey, 1856)

Hole B; core 9; section 1; cm 126-128 (76.36 mcd)

16. *Peripyramis circumtexta* Haeckel, 1887

Hole C; core 8; section 2; cm 146-148 (70.36 mcd)

17-23. *Pseudodictyophimus gracilipes* (Bailey, 1856)

17-19. Hole C; core 8; section 5; cm 2-4 (73.42 mcd)

20-23. Hole C; core 8; section 5; cm 2-4 (73.42 mcd)

24-27. *Stichocorys seriata* Jørgensen, 1905

Hole C; core 8; section 4; cm 98-100 (72.88 mcd)

28. *Euphysetta nathorstii* Cleve, 1899

Hole C; core 8; section 4; cm 98-100 (72.88 mcd)

29. *Lirella melo* (Cleve, 1899)

Hole C; core 8; section 2; cm 146-148 (70.36 mcd)

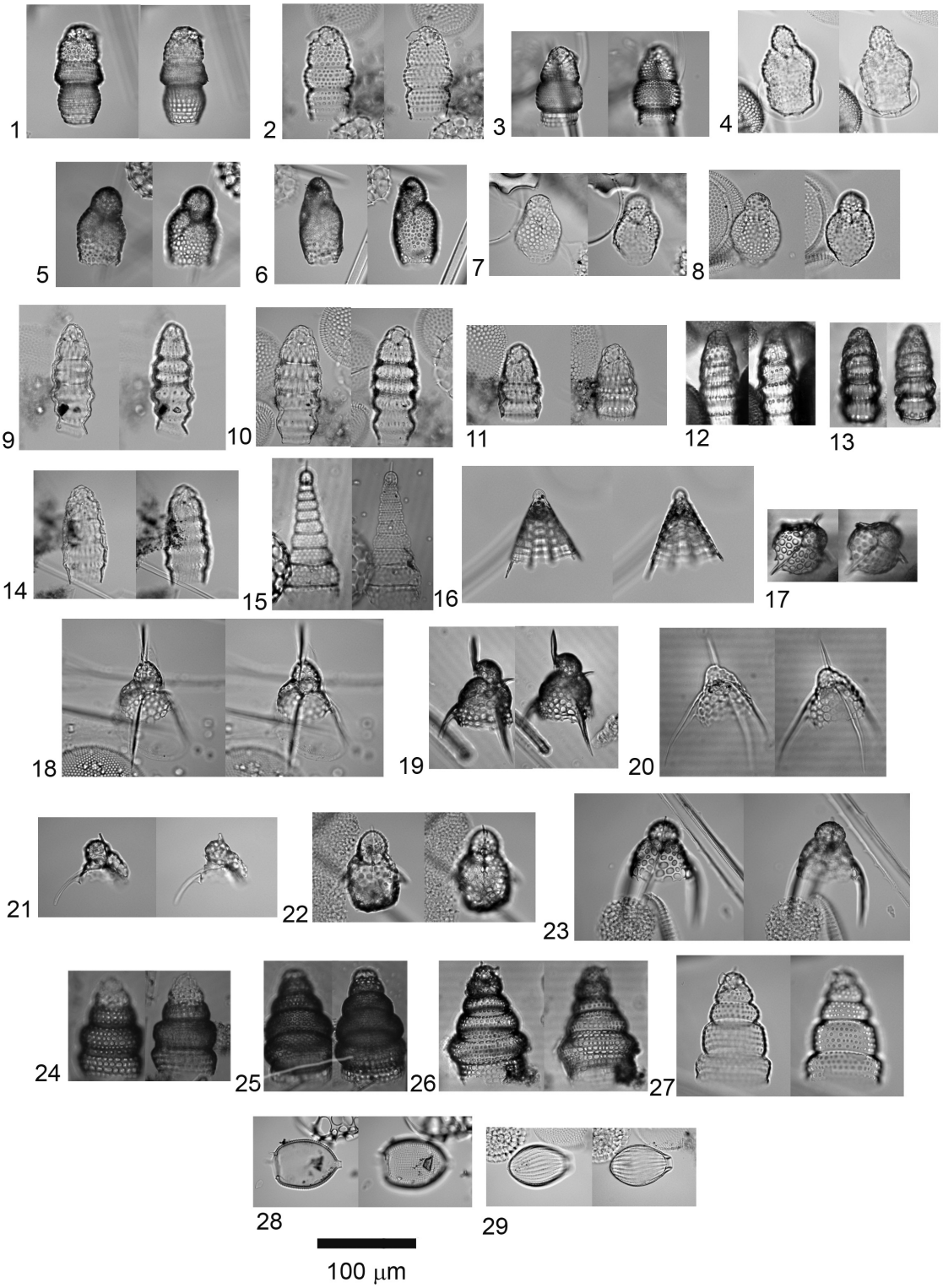
1
2
3
4
5
6
7
8
9
10
11
12
13
14
15
16
17
18
19
20
21
22
23
24
25
26
27
28
29
100 µm

Capítulo 6

*CARACTERIZACIÓN E INTERPRETACIÓN DE LAS CAPAS RICAS EN DETRÍTICOS EN SEDIMENTOS DEL SITE U1314 (ATLÁNTICO NORTE) DURANTE LOS ESTADIOS ISOTÓPICOS MARINOS 21-19 (~ 830-779 KA)**

*Este capítulo está basado en: Hernández-Almeida, I., Sierro, F.J., Suarez, M., Filippelli, G.M. and Flores, A., 2011b. *Geogaceta* (en revisión).

RESUMEN. Muestras de testigos extraídos en el IODP *Site* U1314, localizado en la formación Gardar Drift (Atlántico Norte subpolar), fueron estudiados para determinar que procesos controlan la sedimentación terrígena continental en esta área, e identificar la fuente de dicho material lítico. Para este propósito, hemos realizado un estudio geoquímico y mineralógico a través de digestión total de sedimento y difracción de rayos X, y un estudio micropaleontológico y litológico en la fracción gruesa (>150 μm) entre ~ 830-779 ka (estadios isotópicos marinos 21-19). Con este enfoque, hemos sido capaces de determinar que cuarzo, plagioclasa, filosilicatos, fragmentos líticos de tamaño arena (principalmente cuarzo y material volcánico), y algo de dolomita, fueron liberados al océano durante secuencias episódicas de avance/retroceso de los casquetes de hielo continental, mientras que la calcita biogénica y el feldespato dominaron la sedimentación durante periodos cálidos. Carbonato detrítico rico en dolomita es escaso en nuestras muestras, indicando una expansión limitada del casquete de hielo de Laurentia hacia el estrecho de Hudson, o que alternativamente, los icebergs producidos en esta región no sobrevivieron al transporte hasta el área del testigo U1314. Esta observación indicaría que otros casquetes más cercanos han servido como fuente de material transportado por el hielo, denominado *ice-rafted debris* (IRD), durante descargas masivas de los icebergs.

Palabras clave: IRD; Atlántico Norte; geoquímica; mineralogía; sedimento; carbonato detrítico rico en dolomita.

ABSTRACT. Samples from IODP Site U1314, drilled in the Gardar Drift formation (subpolar North Atlantic), were studied to determine which processes mainly rule terrigenous sedimentation from continents in this area and to fingerprint the source of such lithic material. For this purpose, we performed a geochemical and mineralogical study using bulk sediment digestion and X-ray diffraction, and a lithological and micropaleontological study in the coarse fraction component (> 150 μm) between ~ 830-779 ka (Marine Isotope Stages 21-19). With this approach, we were able to determine that quartz, plagioclase, phyllosilicates, coarse lithic fragments (mainly quartz and volcanic material), and some trace dolomite were released to the ocean during episodic ice-sheet advance/retreat sequences, while biogenic calcite and feldspar dominated sedimentation during warmer periods. Detrital dolomite-rich carbonate is rare in our samples, indicating a limited surging of Laurentide ice-sheet off Hudson Strait, or alternatively, that icebergs produced from this area did not survive transport to Site U1314. This observation indicates that more proximal ice-sheets may have served as source for the ice-rafted debris (IRD) released during massive discharge of icebergs.

Key-words: IRD; North Atlantic; geochemical; mineralogical; bulk sediment; detrital dolomite-rich carbonate.

CARACTERIZACIÓN E INTERPRETACIÓN DE LAS CAPAS RICAS EN DETRÍTICOS EN SEDIMENTOS DEL SITE U1314 (ATLÁNTICO NORTE) DURANTE LOS ESTADIOS ISOTÓPICOS MARINOS 21-19 (~ 830-779 KA)

1. INTRODUCCIÓN

Diversos estudios de los sedimentos oceánicos profundos en el Atlántico Norte han puesto de manifiesto la existencia de capas con alto contenido en material detrítico de tamaño grueso (> 63 μm), presumiblemente transportado por *icebergs,* el cual se denomina *ice-rafted debris* (IRD) (p. ej., Broecker *et al.*, 1992; Heinrich, 1988). Este material detrítico se encuentra en mayor proporción en el cinturón subpolar entre 40º-55º N (Ruddiman, 1977), asociado a episodios de máxima extensión de las masas de hielo continental hacia el sur y posterior fusión (Broecker *et al.*, 1992; Heinrich, 1988), acompañados de una fuerte disminución de temperaturas superficiales en el Atlántico Norte (Bond *et al.*, 1992). Estos eventos catastróficos son de vital importancia en reconstrucciones paleoceanográficas, ya que están asociados con drásticos cambios en los patrones de circulación oceánica superficial y profunda (van Kreveld *et al.*, 2000).

Si bien muchos estudios paleoceanográficos se han centrado en la observación de capas detríticas en el Atlántico durante el Pleistoceno superior y especialmente en el último periodo glaciar (p. ej. Bond *et al.*, 1992; Grousset *et al.*, 1993), poco es conocido acerca de la naturaleza de los IRD para periodos glaciares más antiguos en el Pleistoceno, debido principalmente a la escasez de registros sedimentarios de alta resolución para este periodo cerca del cinturón de IRD en el Atlántico Norte. Por ello, para reconstruir los patrones de circulación e interacciones hielo-océano en el pasado es necesaria una mejor comprensión de la distribución espacio-temporal de estos eventos y del origen del material detrítico.

2. MATERIALES Y MÉTODOS

Las muestras estudiadas en este trabajo pertenecen al IODP *Site* U1314, recuperado en la parte sur de la formación *Gardar Drift*, en el Atlántico Norte (56.36° N, 27.88° W, 2820 m), durante la expedición oceanográfica 306 del *Integrated Ocean Drilling Program* (IODP) (Fig. 6.1). La edad de la sección estudiada, que comprende desde los 60 a los 64,76 m de longitud del testigo, fue obtenida a través de la correlación de la curva isotópica global de Lisiecki y Raymo (2005) con el registro de $\delta^{18}O$ bentónico del *Site* U1314 (Hernández-Almeida *et al.*, in prep.). Según este modelo de edad, el intervalo estudiado abarca entre 830 y 779 ka.

Para identificar las capas de IRD en el *Site* U1314 hemos usado varios de los parámetros más utilizados para definir este tipo de eventos, como son la susceptibilidad magnética, la abundancia de granos líticos tamaño arena (IRD) respecto a foraminíferos planctónicos (IRD/

planctónicos) y la abundancia del foraminífero planctónico polar *Neogloboquadrina pachyderma* sinistrorsa (sin.). El análisis de las propiedades y composición de estas capas de IRD se ha realizado a través de la determinación de la distribución mineralógica tipo por difracción de rayos X, obtenida mediante el análisis semicuantitativo de 59 muestras, espaciadas cada 8 cm, aproximadamente. Las muestras seleccionadas se molieron manualmente en mortero de ágata y se analizaron por difracción de rayos X utilizando un difractómetro Siemens D8 Advance que emite radiación de cobre K_{α}. Las condiciones de trabajo fueron: velocidad de barrido de 1º/ min, 30 mA y 40 kv y zona explorada de 2 a 65º de 2Θ. También se analizó la concentración elemental, a la misma resolución que el análisis semicuantitativo, mediante una digestión total del sedimento siguiendo el método 3051A establecido por Link *et al*. (1998). Con este análisis se obtuvieron concentraciones totales de Ca, Al, Sr, Mg, entre otros elementos. Estos análisis se realizaron en un espectrómetro Leeman Labs P950 con ICP y un nebulizador ultrasónico CETAC Corp. AT500^{+} acoplado en la IUPUI, en Indianápolis (EEUU). Finalmente, se realizó un estudio litológico y micropaleontológico de forma sistemática cada 4 cm, mediante el recuento e identificación de los fragmentos de roca, minerales y foraminíferos planctónicos en la fracción > 150 µm con lupa binocular. Por otro lado, la susceptibilidad magnética fue medida a bordo a intervalos de 5 cm (más detalles en Channell *et al.,* 2006).

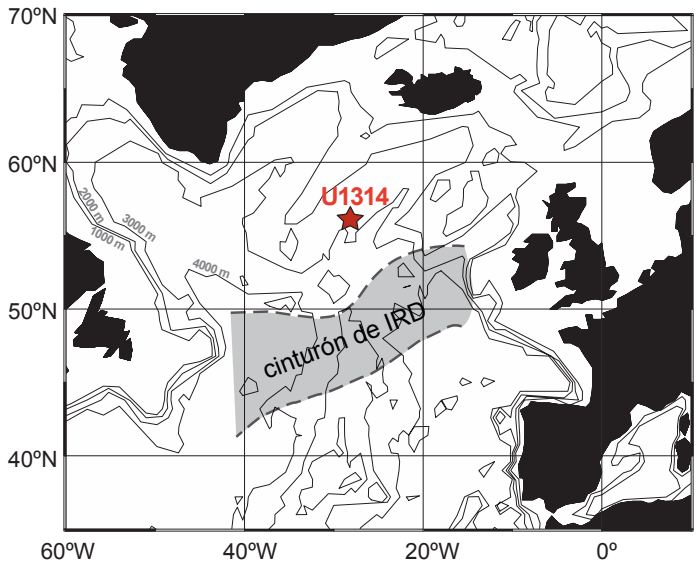

Figura 6.1. Localización del IODP *Site* U1314 (56.36° N, 27.88° W, 2820 m) en el Atlántico Norte subpolar. El área sombreada se corresponde con la máxima deposición de IRD durante el Último Máximo Glacial (Ruddiman, 1977).

3. RESULTADOS

Durante el periodo MIS 21-19 la relación IRD/planctónicos aumenta coincidiendo con valores altos en la abundancia relativa del foraminífero planctónico *N. pachyderma* sin. y bajos en la relación Ca/Al. La composición mineralógica de los IRD es de cuarzo, plagioclasa, filosilicatos y dolomita, con contribuciones puntuales de feldespato potásico (feld K). En

general, las cantidades de todos estos minerales detríticos incrementan durante períodos fríos en consonancia con el aumento de la relación IRD/planctónicos. Una clara excepción es el feld K, que aparece asociado a la abundancia de calcita, aumentando incluso durante periodos con baja relación IRD/planctónicos y baja susceptibilidad magnética. En los recuentos de componentes líticos de la fracción arena también hay altos valores de cuarzo, acompañados de abundante material volcánico (basalto y vidrio volcánico) (Fig. 6.2).

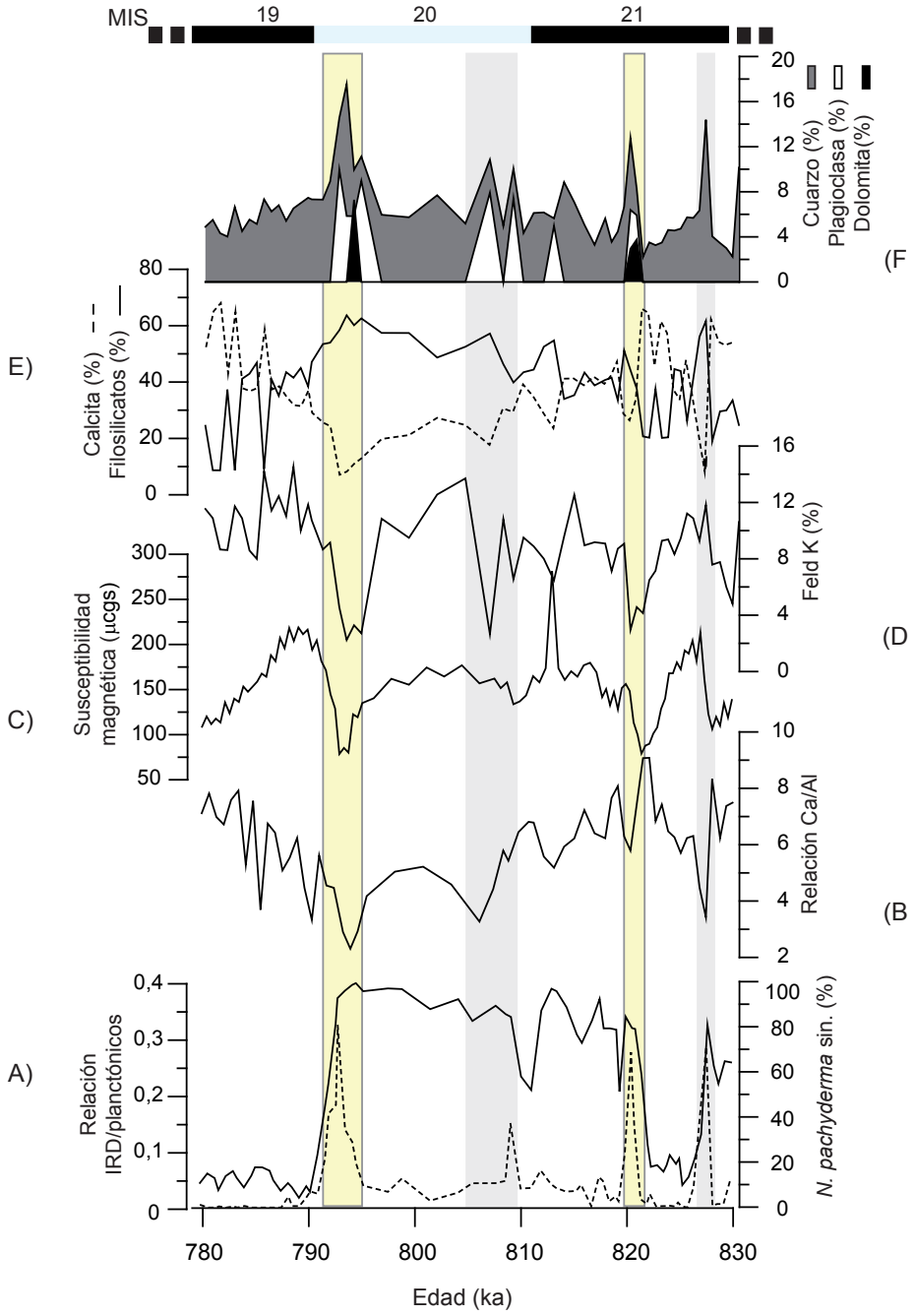

Figura 6.2. De abajo a arriba: A) contribución relativa de *N. pachyderma* sin. (línea continua), relación IRD/ planctónicos (línea discontinua). B) Ratio Ca/Al. (C) Susceptibilidad magnética. Distribución mineralógica (en %): D) feld K, E) calcita (línea discontinua) y filosilicatos (línea continua), F) dolomita (negro), plagioclasa (blanco), cuarzo (gris oscuro). Las áreas sombreadas horizontales se corresponden con los principales eventos de descarga de IRD, con dolomita (amarillo) y sin dolomita (gris claro). Estadios isotópicos marinos están indicados en la parte de arriba (azul glacial, negro interglacial).

4. DISCUSIÓN

La figura 6.2A muestra una clara correlación entre los picos de IRD/planctónicos y valores altos en el porcentaje del foraminífero planctónico polar *N. pachyderma* sin., un indicador de paleotemperatura relacionado con bajas temperaturas superficiales en el océano, proximidad del frente Ártico y de hielo marino estacional (Johannessen *et al.*, 1994). La coincidencia de máximos de la relación IRD/planctónicos con mínimos de temperatura superficial indicaría episodios de inestabilidad en los casquetes de hielo que rodean el Atlántico Norte, que causarían la descarga de gran cantidad de material terrígeno y aguas de fusión frías y poco salinas. Estas condiciones superficiales permitirían un avance hacia el sur del frente Ártico y del límite del hielo marino. El descenso en la relación Ca/Al indica una fuerte reducción en la producción biogénica carbonatada (foraminíferos planctónicos y cocolitóforos) como consecuencia de estas condiciones adversas en la parte superior de la columna de agua (Fig. 6.2B). El *Site* U1314, pese a estar al norte de la zona de máxima acumulación de IRD (Ruddiman, 1977), registra valores altos de la relación IRD/planctónicos (Fig. 6.2A), principalmente debido a la proximidad de este *Site* a los casquetes de hielo de Groenlandia, Escandinavia, Europa e Islandia (Fig. 6.1).

Al contrario que en estudios previos, llevados a cabo en el cinturón de IRD (Heinrich, 1988; Ruddiman, 1977), la susceptibilidad magnética no aumenta en relación con el aporte de IRD (Fig. 6.2C). En este estudio, las variaciones de susceptibilidad están más correlacionadas con los aumentos de feld K que tienen lugar durante periodos con baja acumulación de IRD (Figs. 6.2C, D), y se relacionan con la presencia de basaltos de grano fino ricos en feld K y minerales titanomagnéticos procedentes de la zona de Islandia y dorsal de Reykjanes. De acuerdo con Ruddiman y Bowles (1976), estas partículas son transportadas por corrientes de fondo intensas y depositadas a lo largo de la dorsal de Reykjanes durante periodos más cálidos y con circulación profunda más intensa, en los que también aumenta la productividad biogénica carbonatada, como indica el aumento simultáneo de calcita y de la relación Ca/Al. Aunque relacionado principalmente con períodos cálidos, una parte del feld K tiene una procedencia continental ligada a las descargas de icebergs, como ocurre durante el evento de IRD en ~ 827 ka.

La presencia ocasional de dolomita coincidiendo con los incrementos en la relación IRD/planctónicos, en 794 y 820 ka, marca el depósito de carbonatos detríticos (Fig. 65.2F). En latitudes más meridionales la presencia de dolomita en sedimentos marinos se asocia a carbonatos Paleozoicos de Norteamérica (región de Canadá y Labrador) erosionados y transportados por el casquete de hielo de Laurentia (Broecker *et al.*, 1992; Grousset *et al.*, 1993). Estudios previos han mostrado que estas avenidas no comenzaron de hasta ~ 640 ka (Hodell *et al.*, 2008), coincidiendo con el aumento del volumen de hielo global, y en especial en Norteamérica, tras la reconfiguración del sistema climático durante la Transición del Pleistoceno medio (Clark y Pollard, 1998). Nuestras investigaciones indican que o bien los icebergs procedentes de Norteamérica ya transportaban dolomita antes de ~ 640 ka, o bien que la dolomita observada

en el Site U1314 tiene otra procedencia. La simultaneidad de picos de dolomita con otros componentes minerales como cuarzo, plagioclasa y filosilicatos, siendo probablemente illita y clorita los más abundantes (Grousset *et al*., 1982), y con los de fragmentos líticos (principalmente cuarzo, basalto y vidrio volcánico) de la fracción > 150 μm puede indicar una fuente común de material terrígeno (Fig. 6.2E, F). La similitud de la composición de estas capas ricas en terrígenos del *Site* U1314 con la de los sedimentos superficiales de Groenlandia, Islandia e Islas Feroe (Grousset *et al.*, 1982), hace suponer que estas son las áreas fuentes más probables, junto con pequeños afloramientos de dolomita existentes al noreste de Groenlandia y norte de Europa (Grousset *et al.*, 1993). Esto es corroborado además por el estudio de Andrews (2008), en el que asoció la composición mineralógica de varias capas ricas en detríticos con edades entre 10 y 40 ka, identificadas en testigos del estrecho de Dinamarca, con áreas fuente muy similares a las propuestas para nuestro testigo.

5. CONCLUSIONES

La correlación de máximos en la relación IRD/planctónicos con altos porcentajes del foraminífero planctónico polar *N. pachyderma* sin. indica el avance hacia el sur del frente Ártico y la desestabilización de los casquetes de hielo que rodean el Atlántico Norte subpolar. Durante estos periodos hay una fuerte reducción en la producción biogénica carbonatada debido a las adversas condiciones superficiales de frío y hielo. La baja susceptibilidad magnética durante los eventos IRD indica una composición mineralógica diferente respecto al mismo tipo de eventos en latitudes más meridionales. El aumento de feld K, calcita y de la relación Ca/Al coincidiendo con descensos en la fauna polar y el aumento de la susceptibilidad magnética indica una intensificación de las corrientes de fondo que transportan material volcánico de grano fino rico en titanomagnéticos y recuperación de la productividad biogénica carbonatada durante períodos cálidos.

Las áreas fuente más probables para el cuarzo, plagioclasa, filosilicatos y los fragmentos líticos observados en la fracción > 150 μm, son Groenlandia, Islandia e Islas Feroe. La presencia de dolomita en nuestras muestras indica que, o bien los icebergs procedentes de Norteamérica ya transportaban dolomita antes de ~ 640 ka, o bien que los niveles de dolomita en el testigo U1314 proceden de pequeños depósitos de dolomita del noreste de Groenlandia y norte de Europa, más cercanos a nuestro testigo.

Capítulo 7

TÉCNICAS GEOQUÍMICAS EN EL TESTIGO U1314 Y SU APLICACIÓN PALECEANOGRÁFICA

RESUMEN. El estudio de la geoquímico del sedimento (Fe, Ca, Al, Mn, P, Ba, Sr, Zn, Mg, Ti) y de la relación Mg/Ca en *N. pachyderma* sin. en muestras del testigo U1314, ha permitido una mejor compresión de los procesos sedimentológicos e hidrográficos en esta región durante el Pleistoceno, desde el MIS 31 al 19 (1070-779 ka). En base al estudio estadístico de la composición elemental del sedimento y su comparación con otros paleoindicadores del testigo U1314, se han establecido diferentes grupos, los cuales nos permiten formular hipótesis acerca de las condiciones paleoclimáticas y paleoceanográficas que controlan la sedimentación profunda en el Atlántico Norte. La interpretación de los datos geoquímicos ha sido complementada con información mineralógica de una parte de la sección, que nos permite realizar una aproximación sobre las probables áreas fuente de sedimento. Además, hemos realiazdo una estimación de las paleotemperaturas a partir de la relación Mg/Ca.

Durante los períodos glaciares, reducción en la formación de aguas profundas en latitudes altas del Atlántico Norte provocó una menor advección de agua noratlántica superficiales y una migración hacia el sur del frente ártico (*Arctic Front*, AF). Por ello, la sedimentación oceánica durante estos períodos procede de la erosión de las masas continentales adyacentes y su depósito durante episodios de fusión de casquetes de hielo. El aumento de elementos como Ba, Mg y Zn se debe al transporte de material continental al océano durante periodos de fusión de icebergs. El descenso de elementos de carácter biogénico (Ca, Sr, P) se explica por la baja productividad superficial durante estos episodios, limitada por las bajas temperaturas del océano y la estratificación superficial por aporte de aguas de fusión. La ralentización de la circulación profunda durante estos eventos limitó considerablemente la acumulación de elementos transportados por corrientes de fondo, como el Ti y Fe. Durante períodos interglaciares, el aumento de flujo de aguas cálidas hacia altas latitudes y la desestratificación de la columna de agua reactiva la productividad biogénica, con lo que aumentan Ca, Sr, P y Mn, este último precipitando como una fase del carbonato biogénico de la concha de foraminíferos planctónicos y cocolitóforos. La intensificación de la circulación termohalina aumenta el transporte de material detrítico basáltico de grano fino rico en minerales titanomagnéticos, desde las provincias volcánicas de Islandia, dorsal de Reykjanes e Islas Feroe, hacia el sur. Por lo tanto, la secuencia sedimentaria del Pleistoceno del testigo U1314 representa una sucesión de cambios en la naturaleza de las áreas fuente de sedimento a consecuencia de los variaciones climáticas y oceanográficas que tuvieron lugar durante ese periodo.

La estimación de temperaturas a partir de la relación Mg/Ca muestra incrementos a continuación de los máximos de descarga de IRD, lo que podría ser interpretado como una acumulación sub-superficial de calor y posterior liberación a la superficie, que aceleraría el retroceso de las masas de hielo continental en el Atlántico Norte

Palabras clave: Pleistoceno; Atlántico Norte; geoquímica; elemento; sedimento; biogénico; paleotemperatura; Mg/Ca.

ABSTRACT. The geochemical study of sediments (Fe, Ca, Al, Mn, P, Ba, Sr, Zn, Mg, Ti) and Mg/Ca of *N. pachyderma* sin. from samples from Site U1314, have allowed a better understanding of the sedimentological and hydrographic processes in this region during the Pleistocene from MIS 31 to 19 (1079-779 ka). Using a statistical approach of the elemental composition of the sediment, we have identified different groups, which allow us to establish a hypothesis about the paleoclimatic and paleoceanographic conditions controlling deep sedimentation in the North Atlantic. Interpretation of geochemical data has been accompanied by mineralogical information from a section of our core, which enables to identify the sediment source. Moreover, we have performed a paleotemperature estimates based on Mg/Ca ratio.

During glacial periods, reduction in the deep-water formation in high latitudes in the North Atlantic caused a lower advection of atlantic surface waters and a southward migration of the Arctic Front (AF). Sedimentation during these periods is mainly autochthonous, derivates from the erosion of adjacent continental masses and later deposition during ice-sheet melting. Increasing concentrations of Ba, Mg and Zn is due to the transport of continental material to the ocean delivered by ice-rafting activity. Decrease in biologically-related elements (Ca, Sr, P) is linked to the low surface productivity during these episodes, limited by the low ocean temperatures and surface waters stratification by meltwater input. Deep-circulation slow-down during these events limited Ti and Fe transport and accumulation by bottom-currents. During interglacial periods, enhanced warm water flow toward high latitudes and column-water de-stratification reactivate biogenic productivity, increasing Ca, Sr, P and Mn, this last element precipitating as a phase in lattice biogenic carbonate in planktonic foraminifera and coccolithophores. Intensification of the thermohaline circulation increased transport of fine-grained basaltic material transport rich in titanomagnetic minerals, from volcanic provinces of Iceland, Reykjanes Ridge and Faeroe Islands toward the south. Thus, Mid-Pleistocene sedimentary sequence at Site U1314 shows a succession of changes in the nature of sediment source due to climatic and oceanographic variations during this period.

Paleotemperature estimates based on Mg/Ca ratio show increases following IRD peaks, which could be interpreted as a sub-surface accumulation of heat and subsequent release to the surface that would accelerate the ice-sheet retreat in the North Atlantic.

Keywords: Pleistocene; North Atlantic; geochemistry; element; sediment; biogenic; paleotemperature; Mg/Ca.

TÉCNICAS GEOQUÍMICAS EN EL TESTIGO U1314 Y SU APLICACIÓN PALEOCEANOGRÁFICA

1. INTRODUCCIÓN

El Atlántico Norte subpolar ha sido objeto de numerosas investigaciones desde el punto de vista paleoceanográfico, usando multitud de técnicas basadas en geoquímica de isótopos estables, evidencias micropaleontológicas y sedimentológicas. Sin embargo, son escasos los trabajos con base geoquímica llevados a cabo en sedimentos profundos de esta región. Existen estudios sobre la composición geoquímica de sedimentos superficiales de la región del Atlántico Norte oriental (dorsal de Reykjanes, Islas Feroe, Islandia y zona de fractura de Charlie-Gibbs), pero sólo se realizaron en sedimentos correspondientes al Cuaternario más reciente (Grousset *et al.*, 1982; Grousset and Parra, 1982; Latouche and Parra, 1976; Latouche and Parra, 1979; Parra *et al.*, 1981)

Dada la gran variabilidad espacio temporal de los procesos hidrodinámicos que tienen lugar en el Atlántico Norte, y la gran diversidad de fuentes de material que suplen a la sedimentación hemipelágica de la zona, determinar estos parámetros aporta valiosa información a la hora de realizar reconstrucciones sedimentológicas. En este estudio se ha realizado un análisis estadístico de los datos geoquímicos generados con la determinación de la composición elemental en sedimentos del Pleistoceno (MIS 31-19), los cuales han sido después comparados con otros paleoindicadores con el fin de detectar patrones de variabilidad en el conjunto de datos. Con esta técnica se pretende determinar que áreas fuente y/o agentes de transporte están involucrados en la sedimentación profunda en el Atlántico Norte y su variación a escala glaciar-interglacial.

Por otro lado, también hemos realizado una reconstrucción de paleotemperaturas usando la relación entre contenido en magnesio en carbonatos biogénicos y temperaturas, para la que hemos utilizado individuos del foraminífero planctónico *Neogloboquadrina pachyderma* sin. Este estudio se centra en los cambios en la temperatura superficial que tienen lugar durante las deglaciaciones que siguen a los periodos de descarga de IRD, el cual ha sido objeto análisis en los últimos años por las implicaciones que tiene en la recuperación de la AMOC tras periodos de intenso enfriamiento (Hulbe *et al.*, 2004; Jonkers *et al.*, 2010a; Moros *et al.*, 2002; Peck *et al.*, 2006; Rasmussen and Thomsen, 2004; Shaffer *et al.*, 2004).

2. MATERIALES Y MÉTODOS

El material estudiado procede del testigo U1314, recuperado en la formación *Gardar Drift*, en el Atlántico Norte (56.36° N, 27.88° W, 2820 m) (ver Capítulo 2, página 15). La metodología analítica empleada fue la de Link *et al.* (1998) para determinar la composición elemental y la

de Filippelli y Delaney (1996), modificada de Ruttenberg (1992) para la extracción secuencial de P (ver pág. X; Anexos 6 y 7). Posteriormente, los resultados de los análisis geoquímicos del sedimento se han representado y estudiado de dos maneras:

1) A través de un análisis factorial en modo R con una rotación "varimax normalizada", realizado con el programa *SPSS* sobre el log10 de los datos de la composición elemental. Asimismo, se han calculado los coeficientes de correlación entre los elementos. Esta técnica permite reducir el número de variables y detectar estructuras en las relaciones entre las variables resultantes.

2) Examinando la variación temporal de los factores y comparándolos con otros paleoindicadores del testigo U1314 (isótopos estables, acumulación de IRD en la fracción gruesa, ópalo, carbonato cálcico), con el fin de validar la interpretación de los diferentes factores.

La metodología seguida para el análisis del Mg/Ca en la concha de *N. pachyderma* sin. están detallados en la página 30 del Capítulo 2 y en el Anexo 5.

3. RESULTADOS

La Tabla 7.1 muestra el resultado del análisis estadístico de la composición elemental de los sedimentos profundos del Atlántico Norte. Se han obtenido tres factores principales, los cuales explican un 83 % de la varianza. El factor 1 explica 34,9 % de la varianza, y las cargas más altas de este factor se observan en los elementos Ca, Sr, P y Mn. En el factor 2, que explica el 33 % de la varianza y está definido por los elementos Fe, Ti, Al, Mg y Zn. El factor 3, el cual explica el 15 % de la varianza, en el que los elementos Ba, Zn y Mg presentan las cargas más altas. También se ha realizado una calibración ambiental mediante la comparación entre las cargas de los tres factores con distintos paleoindicadores para corroborar nuestras interpretaciones (Tabla 7.2). El factor 1 está positivamente correlacionado con el porcentaje de $CaCO_3$ y con la acumulación de ópalo, y negativamente correlacionado con la acumulación de IRD. El factor 2 únicamente está correlacionado con la susceptibilidad magnética, y el factor 3 con la acumulación de IRD.

Diversos estudios sobre la ecología de *N. pachyderma* sin. han concluido que su composición isotópica refleja condiciones por debajo de la termoclina, a 150 m de profundad (Nürnberg, 1995; Simstich *et al.*, 2003), por lo tanto hemos asumido que la relación Mg/Ca de la concha de esta especie refleja temperaturas a una profundidad similar. El registro de la relación Mg/Ca en la especie *N. pachyderma* sin. varía entre 0.6 y 1.7 mmol*mol^{-1} y muestra un patrón similar a la señal de $\delta^{18}O$ en la misma especie y el porcentaje de $CaCO_3$. La estimación de la paleotemperatura está basada en la calibración de Nürnberg *et al*. (1996a), la cual está optimizada para reconstrucciones en altas latitudes. Las temperaturas obtenidas varían entre 1.0 y 11.5 ºC (Fig. 7.2), por lo tanto menores que las estimadas usando funciones de transferencia sobre la asociación de foraminíferos planctónicos, y menores que las actuales temperaturas

registradas en el área del testigo U1314, de cerca de 10 ºC (Locarnini *et al.*, 2006). Esto se puede deber a que hay un margen de error debido a la ecuación de calibración utilizada, o a que simplemente las temperaturas durante el Pleistoceno Inferior y Medio eran inferiores a las actuales. Las temperaturas más altas se registran durante periodos interglaciales y justo después de los eventos de descargas de IRD.

Varimax normalizado			
Elemento	Factor		
	1	2	3
Fe	-0,291	**0,832**	-0,116
Al	-0,645	**0,645**	0,212
Ca	**0,794**	-0,265	-0,219
Mg	-0,063	**0,875**	**0,396**
Ti	0,091	**0,907**	0,198
Sr	**0,909**	-0,259	-0,026
Ba	-0,182	0,088	**0,905**
P	**0,757**	0,383	-0,037
Mn	**0,954**	-0,056	-0,112
Zn	-0,094	**0,564**	**0,605**
	34,945	33,089	15,029

Porcentaje de la varianza

Tabla 7.1. Cargas de los diferentes factores obtenidos con el análisis factorial en modo R, usando la rotación varimax normalizada. Valores en negrita marcan los elementos más significativos en cada factor.

	Factor 1	Factor 2	Factor 3
% $CaCO_3$	**0,78**	-0,43	-0,18
TA ópalo	**0,34**	-0,22	-0,18
TA IRD	-0,53	-0,02	**0,31**
$\delta^{13}C$ Bentónico	**0,26**	-0,01	-0,21
Susceptibilidad magnética	0,15	**0,60**	-0,28

Tabla 7.2. Matriz de correlación entre los factores y diferentes registros del testigo U1314.

4. DISCUSIÓN

4.1. Composición elemental del sedimento

La interpretación geoquímica para determinar tanto el origen o área fuente de los distintos elementos del testigo U1314 se ha basado en la distribución de las cargas de los factores obtenidos del análisis de componentes principales y su correlación con otros indicadores paleoceanográficos ya presentados en esta Tesis.

4.1.1. Factor 1: Sedimentación pelágica y transporte lateral por las corrientes de fondo de componentes biogénicos

La buena correlación de elementos con mayor carga en este primer factor (Ca, Sr, P y

Mn) con indicadores biogénicos ($CaCO_3$, ópalo), y su correlación negativa con la acumulación de IRD, parece indicar que estos elementos están ligados a cambios en los niveles de productividad superficial, controlados por la variabilidad climática glaciar-interglaciar (Tabla 7.2; Fig. 7.1A-E).

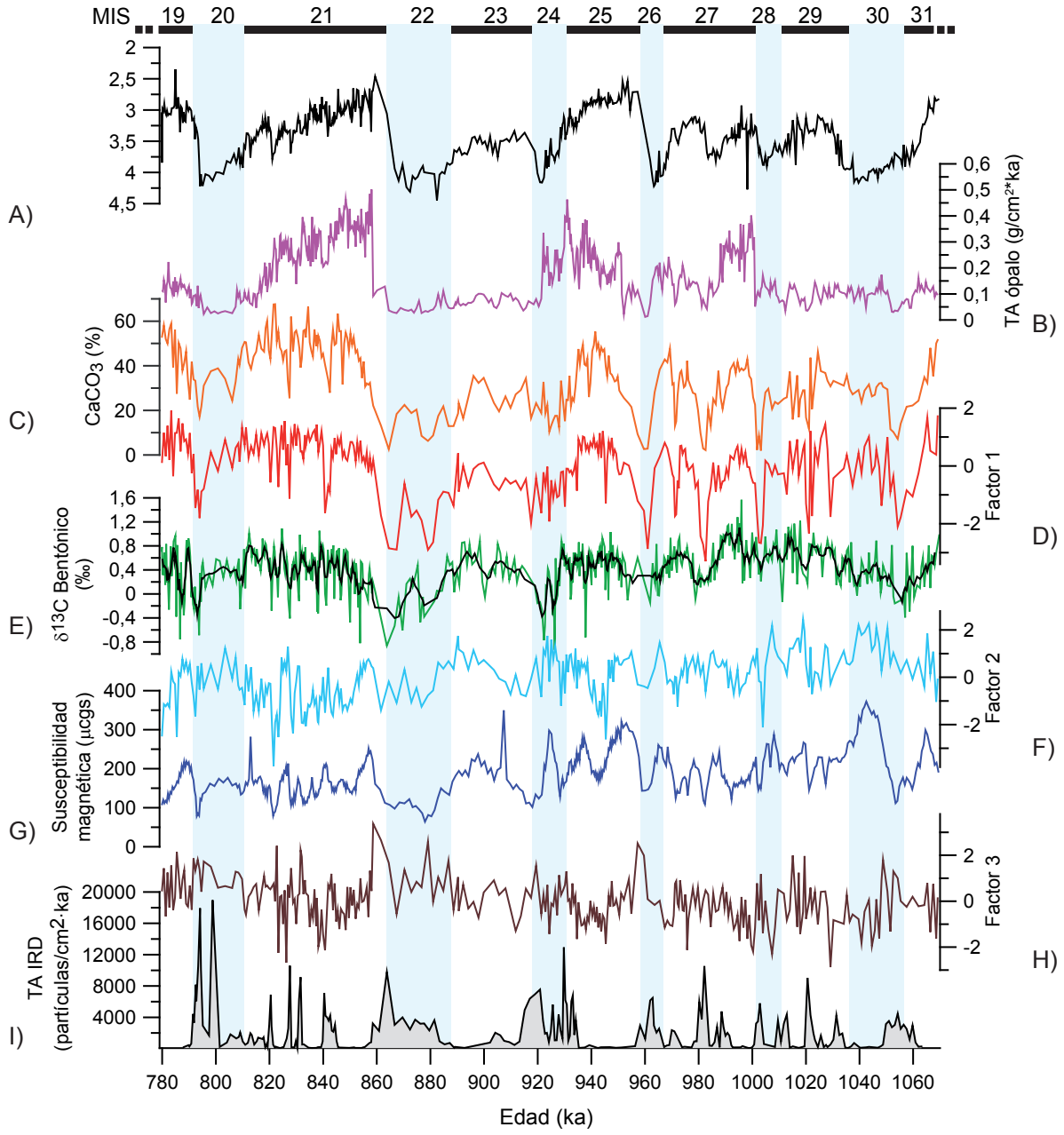

Figura 7.1. Registros del testigo U1314 entre 1060 y 779 ka y las cargas de los factores obtenidos del análisis factorial en modo R de la composición elemental del sedimento. Desde abajo hacia arriba: A) tasa de acumulación de IRD (partículas/cm²*ka), B) factor 3, C) susceptibilidad magnética, D) factor 2, E) $\delta^{13}C$ bentónico, F) factor 1, G) porcentaje de $CaCO_3$, H) tasa de acumulación de ópalo (g/cm²*ka) y I) $\delta^{18}O$ bentónico. Las barras verticales azules indican los estadios marinos isotópicos glaciares.

El calcio y el estroncio, son elementos comúnmente asociados a la productividad biogénica carbonatada de foraminíferos y cocolitóforos (Emiliani, 1955; Thomson and Bowen, 1969), y presentan un patrón muy parecido, con valores altos durante periodos interglaciares y bajos durante glaciares. Sin embargo, la correlación entre estos dos elementos tan sólo es del $R^2 = 0{,}58$ (Fig. 7.2A). Esto es debido a que el material detrítico volcanogénico que caracteriza el sur de Islandia e Islas Feroe es una fuente de feldespatos ricos en Sr, no ligado a carbonatos biogénicos (Grousset and Parra, 1982). Estos feldespatos ricos en Sr están distribuidos a lo largo de una dirección norte-sur al ser transportados por las mismas corrientes de fondo que redistribuyen los sedimentos ricos en Ti y Fe durante periodos con intensa circulación termohalina (Parra *et al.*, 1981). Por lo tanto, mientras que los elevados valores de Ca durante períodos interglaciares pueden considerarse puramente biogénicos derivados del aumento de la productividad superficial durante el avance de las masas de agua cálida de la NAC a estas latitudes, el origen del Sr presenta una doble procedencia. Por un lado puede tener un origen biogénico, asociado a la producción carbonatada superficial, y por otro detrítico, asociado a los feldespatos de las zonas volcánicas de Islandia y Feroe y redistribuidos por la ISOW (*Iceland-Scotland Overflow Water*), la corriente de fondo dominante en esta zona.

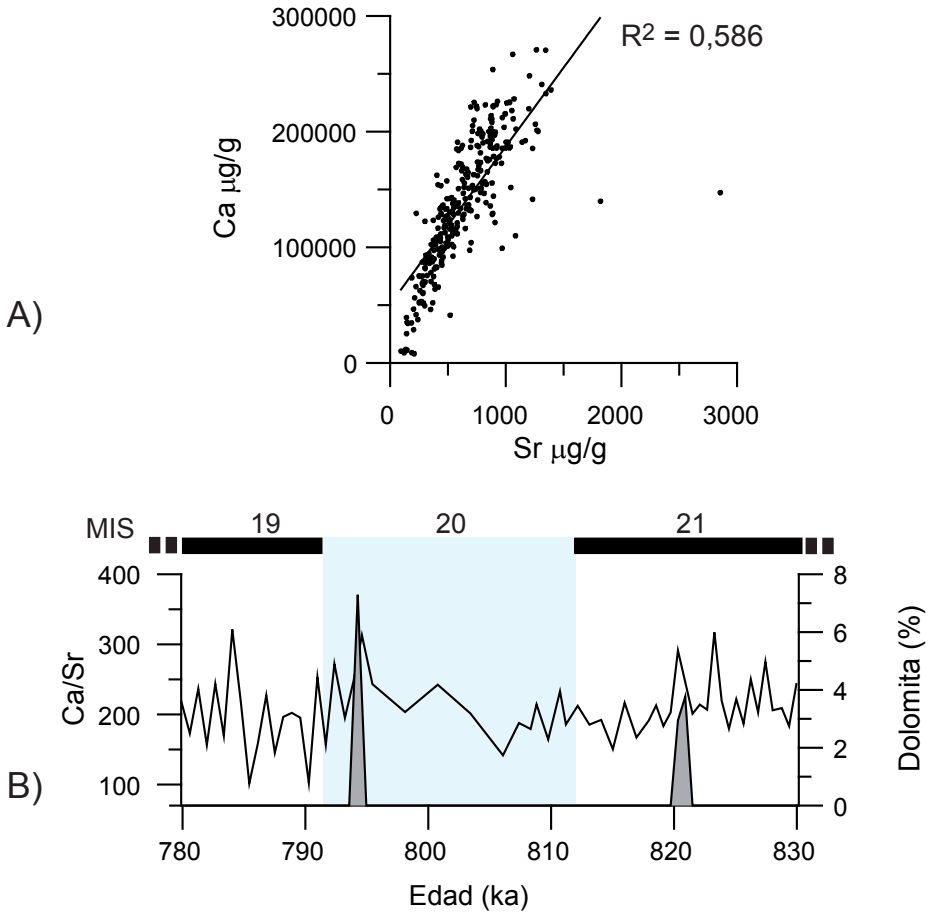

Figura 7.2. Desde abajo hacia arriba: A) contenido en dolomita (%) (área gris) y relación Ca/Sr para el periodo 830-779 ka y B) correlación entre el contenido en Ca (µg/g) y en Sr (µg/g) para sedimentos del testigo U1314. La barra vertical azul indica el estadio isotópico glaciar 20.

La existencia de diferentes fuentes de Sr explica la variabilidad de la relación Ca/Sr durante periodos interglaciares, influenciada por el transporte de feldespatos volcanogénicos hacia el sur, lo que invalida la relación de Ca/Sr como indicador de eventos de descarga de IRD (Fig. 7.2B). Esta relación ha sido usada como indicador de eventos Heinrich en el Atlántico Norte en zonas con menor acumulación de material volcánico (e.g. Hodell *et al.*, 2008), partiendo de la base de que gran parte del material detrítico de origen continental que se libera al océano es carbonato detrítico (dolomita), el cual presenta altos valores de la relación Ca/Sr debido al descenso de Sr por la baja acumulación de carbonato biogénico durante estos eventos y alto Ca por la gran cantidad de dolomita presenta en estas capas de IRD. En nuestro caso, la existencia de una fuente secundaria de Sr no biogénica hace que la relación Ca/Sr varíe de forma considerable aún en la ausencia de material dolomítico, con lo cual la relación Ca/Sr no puede ser considerada como indicador fiable de la presencia de dolomita en el testigo U1314.

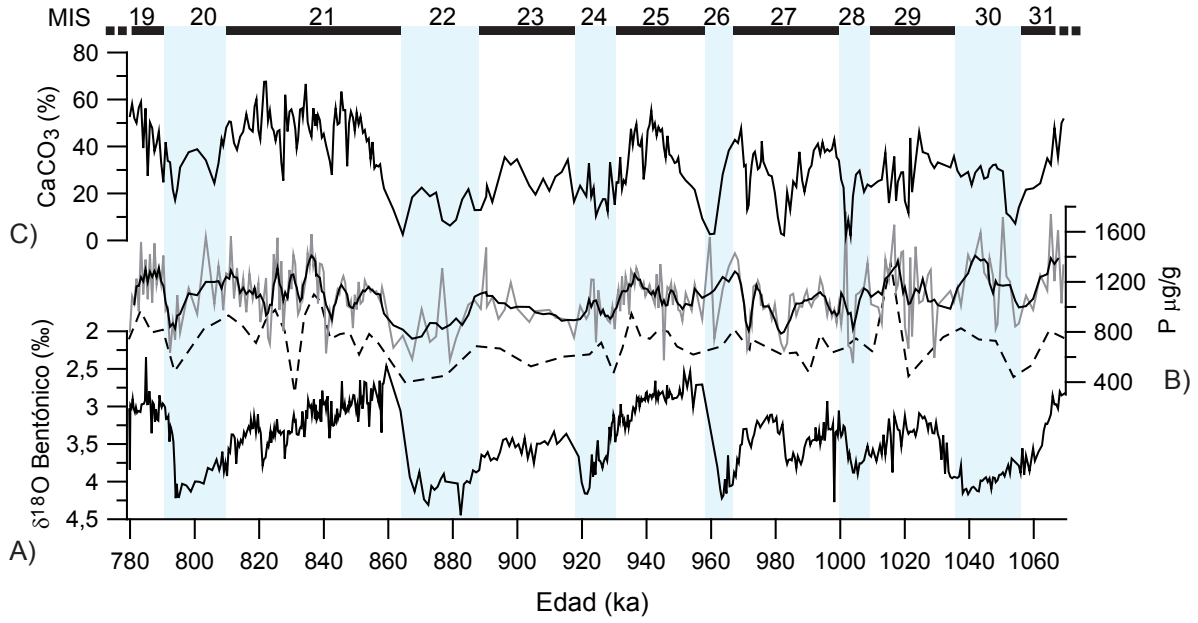

Figura 7.3. Desde abajo hacia arriba: A) registro del $\delta^{18}O$ bentónico, B) registro del P total (µg/g) (línea gris, línea negra valore medio cada 3 puntos) obtenido de los análisis de composición elemental, y P reactivo (µg/g) (suma de P *orgánico, autogénico/biogénico y adsorbido) obtenido de la extracción secuencial de P y C) porcentaje de* $CaCO_3$, en el testigo U1314 entre 1060 y 779 ka. Las barras verticales azules indican los estadios marinos isotópicos glaciares.

El fósforo es un elemento limitante para la productividad biológica, y la concentración de este elemento en el sedimento está asociada normalmente a la actividad biológica y/o a la materia orgánica (Boström *et al.*, 1972). Por esto, las elevadas concentraciones de P durante periodos interglaciares indican aumento de la productividad en las aguas superficiales del Testigo U1314. Sin embargo, el P también puede tener un origen terrígeno (Filippelli and Delaney, 1996), el examen detallado de las diferentes fases del P mediante extracción secuencial revela una mayor proporción de P relacionado con la actividad biológica, incluyendo P orgánico, autogénico/biogénico y adsorbido (denominados en conjunto como P reactivo). Estos

componentes reactivos aumentan durante periodos interglaciares, junto con otros indicadores de productividad, como el % $CaCO_3$, lo que indicaría un aumento en la producción exportada y enterramiento de materia orgánica durante estos periodos (Fig. 7.3).

El Mn muestra una distribución ligada a episodios con sedimentación biogénica dominante (factor 1) y bajo contenido de terrígenos (factores 2 y 3). Esta estrecha relación del Mn con la productividad superficial se explica por la co-precipitación de una fase contaminante rica en Mn dentro de los caparazones carbonatados (cocolitóforos y foraminíferos) (Boyle, 1983a; Pena *et al.*, 2005; Thomson *et al.*, 1986). Resultados de Mn/Ca obtenidos de los datos elementales de limpieza reductiva en foraminíferos planctónicos sugieren la existencia de recrecimientos de Mn en las conchas (Fig. 7.4). La correlación de estos aumentos en la relación Mn/Ca y en la concentración de Mn total indican la existencia de recrecimientos de Mn en la calcita biogénica asociados a procesos diagenéticos (Boyle, 1983a). Una fuente probable para el Mn es el material volcánico de la cuenca de Islandia, el cual es rico en este elemento (Grousset *et al.*, 1982), y que sería extraído del agua del mar y preservado junto con la calcita biogénica (Van Der Weijden *et al.*, 1970).

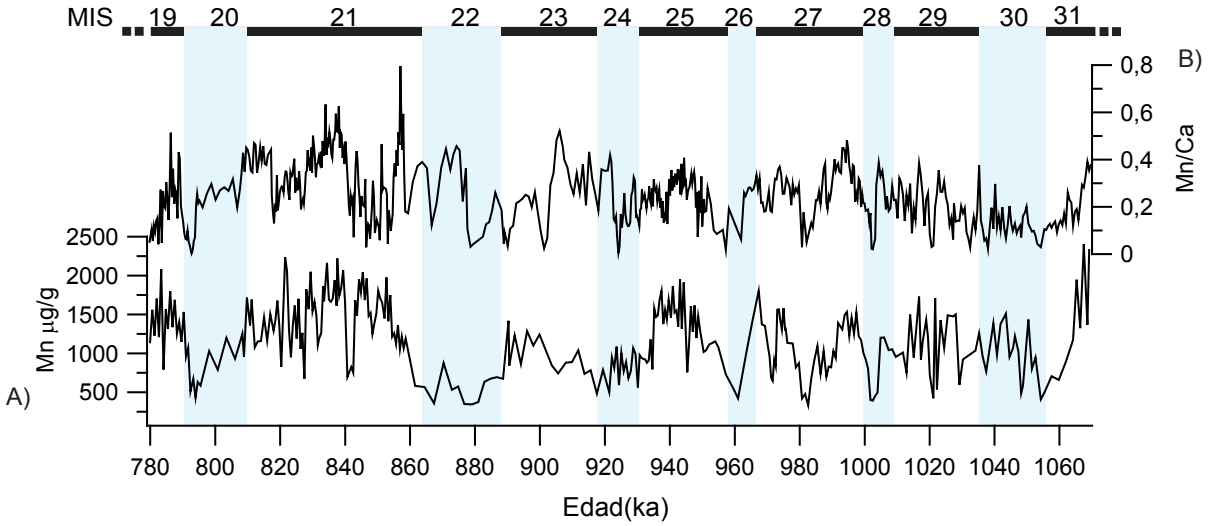

Figura 7.4. Desde abajo hacia arriba: A) registro del contenido en Mn (µg/g) obtenido de los análisis de composición elemental, y B) relación del Mn/Ca (línea discontinua) *obtenida de los datos elementales de limpieza reductiva en foraminíferos planctónicos,* en el testigo U1314 entre 1060 y 779 ka. Las barras verticales azules indican los estadios marinos isotópicos glaciares.

Aunque es evidente que el incremento de estos elementos esta asociado de una forma u otra al aumento de la productividad primaria inducida por el calentamiento de las aguas superficiales, la distribución de material biogénico concentrado durante periodos interglaciares está también asociado a la circulación oceánica profunda. Durante episodios con alto $\delta^{13}C$ bentónico, el intenso flujo del ISOW transporta gran cantidad de material de grano fino hacia el *Gardar Drift*, el cual es mayoritariamente carbonato cálcico de grano fino (cocolitos) producido por el aumento de la productividad primaria superficial con la llegada de aguas cálidas a la

zona. De este modo, el marcado contraste entre estadios glaciares e interglaciares resulta de los cambios en la circulación oceánica, ya sea por la circulación superficial que controla los aportes de material detrítico durante episodios de fusión de hielo continental y por el aumento de la productividad planctónica con la advección de aguas cálidas, o por los cambios en la circulación profunda que controlan la acumulación de material fino en el *Gardar Drift*.

4.1.2. Factor 2: Transporte y sedimentación profunda de componentes no biogénicos

El aumento de los elementos Ti, Fe, Al, Mg y Zn en el factor 2 refleja la composición típica de los sedimentos oceánicos en la zona de la dorsal de Reykjanes, cuya distribución está controlada por los procesos hidrodinámicos profundos en la región (Horowitz, 1974; Horowitz and Cronan, 1976). En sedimentos superficiales de la región del Atlántico Norte oriental, estos elementos se distribuyen a lo largo de un gradiente noreste-suroeste a lo largo de la dorsal de Reykjanes, con una distribución muy parecida a la de la esmectita (Grousset and Parra, 1982; Grousset and Chesselet, 1986; Latouche and Parra, 1976). Altas concentraciones de elementos como Ti y Fe parecen estar asociadas a material volcánico de tamaño limo (escoria, ceniza volcánica, minerales pesados y vidrio volcánico) y/o ligado a esmectitas, derivadas de Islandia y de Islas Feroe (Hyun *et al.*, 1999; Latouche and Parra, 1976). Por lo tanto el aumento en la concentración de elementos relacionados con el factor 2 indicaría un transporte de los mismos desde la cuenca de Islandia por corrientes nefeloides asociadas a la intensificación de la ISOW durante periodos interglaciares. Así mismo, la correlación entre el factor 2 y la susceptibilidad magnética viene a corroborar este patrón de distribución (Tabla 7.2; Fig. 7.1F-G). Al contrario que en eventos Heinrich que tienen lugar en algunas zonas de máxima acumulación de IRD, entre ~ 40º y 50º N (e.g. Grousset *et al.*, 2000; Heinrich, 1988), los eventos tipo Heinrich registrados en el testigo U1314 son claramente identificables por los bajos valores de susceptibilidad magnética. Esto demuestra una diferente composición de las capas detríticas, y por lo tanto, una diferente procedencia del material. Mientras que las capas de IRD de la parte central del Atlántico Norte se caracterizan por altos contenidos en rocas volcánicas básicas y ultrabásicas, con altos valores magnéticos, y proceden del margen nororiental de Norte América (Nueva Escocia, Terranova, etc.) y de la costa occidental de Groenlandia (Thouveny *et al.*, 2000), la situación es muy diferente inmediatamente al sur de Islandia. En esta zona, el material dominante es limo volcánico de grano fino rico en titanomagnéticos y depositado en zonas de alta acumulación, como la formación *Gardar Drift*, durante periodos de alta circulación en el fondo oceánico (Kissel *et al.*, 1999). Por el contrario, una menor velocidad en la corriente de fondo, debido a la interrupción en la ventilación profunda con origen en los mares Nórdicos, reduce el transporte de material rico en titanomagnéticos, y junto con el incremento en el depósito de capas detríticas ricas en cuarzo, producen el descenso en los valores de susceptibilidad magnética observado durante los periodos glaciares.

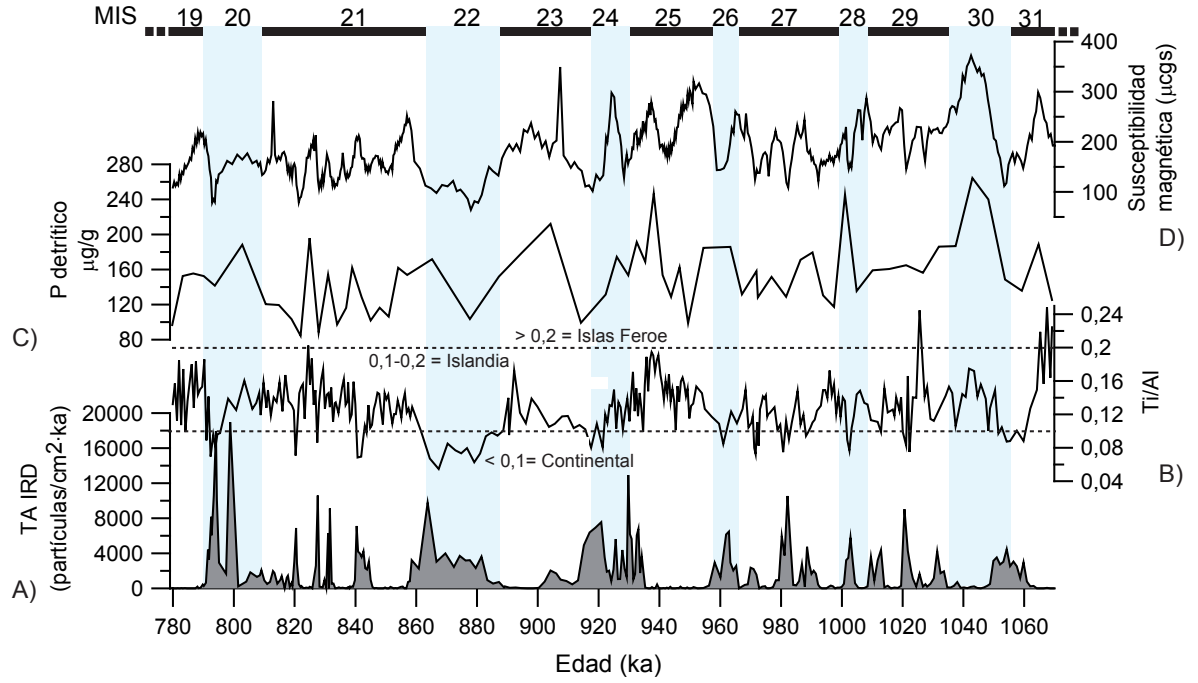

Figura 7.5. Desde abajo hacia arriba: A) registro de la tasa de acumulación de IRD (partículas/cm^2*ka), B) relación Ti/Al, valores < 0,1 corresponderían sedimentos continentales, valores entre 0,1-0,2 corresponden con basaltos procedentes de Islandia y valores > 0,2 a *basaltos de las Islas Feroe* (Hyun y Kim, 1999), C) P detrítico (µg/g) obtenido de la extracción secuencial de P y D) susceptibilidad magnética en el testigo U1314 entre 1060 y 779 ka. Las barras verticales azules indican los estadios marinos isotópicos glaciares.

El alto contenido en Al en toda la secuencia sedimentaria del testigo 1314 es principalmente debido a la gran cantidad de ceniza volcánica y otros detritos basálticos presentes en la zona debido a la proximidad con Islandia, cuya alteración produce gran cantidad de arcillas ricas en Al, principalmente illita (Chester and Messiha-Hanna, 1970; Horowitz, 1974). Además, el aumento de material detrítico de origen continental durante descargas de IRD eleva la cantidad de Al respecto a otros constituyentes que tienen su única fuente en el material basáltico del océano, como el Ti (Fig. 7.5A). Por esta razón, la relación Ti/Al refleja con bastante precisión la ciclicidad climática glaciar-interglaciar y es un criterio sólido a la hora de discriminar con precisión la procedencia de los sedimentos en cada momento. De acuerdo con Hyun y Kim (1999), relaciones Ti/Al < 0,1 indicarían un aporte de sedimento predominantemente continental que tiene lugar durante periodos glaciares, mientras que valores mayores son debidos a un mayor aporte de material basáltico de grano fino transportado por la ISOW durante periodos interglaciares (Fig. 7.5B). Una variabilidad temporal similar en la relación Ti/K fue obtenida por Grützner et al (2010) usando análisis de XRF en sedimentos del testigo U1314 que demuestra un mismo patron de cambio en las fuentes de sedimento (basáltica/ácida) que la mostrada por la relación Ti/Al. Además, la relación Ti/Al también nos ayuda a discriminar el origen de las partículas basálitcas ricas en Ti. Valores > 0,2 en la relación Ti/Al, como los observados durante el MIS 19 y 31, indican que estos basaltos proceden en parte del suroeste de las Islas Feroe,

formados durante una fase volcánica anterior a la de Islandia (Grousset *et al.*, 1982; Waagstein, 1988), y por ello con mayor contenido en Ti (Fig. 7.5B).

El leve aumento de la carga del P en el factor 2, el cual se relaciona con elementos presentes en el material basáltico del fondo oceánico, se explica por el aumento de la producción de montmorillonita rica en P detrítico, debido a la alteración de los basaltos durante periodos interglaciares (Latouche and Parra, 1976) y su posterior transporte junto con los otros elementos magnéticos por corrientes de fondo (Fig. 7.5C-D).

Por lo tanto, el la variabilidad de los elementos con mayor peso en el factor 2, al igual que los del factor 1, subraya la importancia de la circulación oceánica profunda en la acumulación de sedimento de grano fino en el *Gardar Drift*. Llama la atención la baja correlación del factor 2 con la señal del $\delta^{13}C$ bentónico (Tabla 7.2). Este se debe a que durante los episodios de aumento de transporte de material fino por el ISOW durante interglaciares, los elementos más abundantes son los relacionados al factor 1, indicador de productividad biogénica, y por lo tanto diluyen la abundancia de los elementos del factor 2, que son también transportados y depositados en el *Gardar Drift* por el ISOW.

4.1.3. Factor 3: Aporte de material continental

El agrupamiento de elementos como Ba, Zn y Mg en el factor 3, es similar a lo observado por Grousset *et al.* (1982), que relacionó estos elementos con la presencia de minerales arcillosos (illita y clorita) y la descarga de material ácido continental transportado por el hielo, como indica su correlación únicamente con la tasa de acumulación de IRD y su correlación inversa con elementos biogénicos (Tabla 7.2; Fig. 7.1H-I). Aunque el Ba ha sido usado como un indicador de paleoproductividad en diferentes ambientes oceánicos (e.g. Dymond *et al.*, 1992; Kasten *et al.*, 2001), las mayores concentraciones de Ba en el testigo U1314 se encuentran en torno a episodios de alta acumulación de IRD y con altos valores de Al, y en cambio descienden cuando aumenta la abundancia de otros indicadores de paleoproductividad ya contrastados (TA radiolarios, ópalo, $CaCO_3$). Por todo ello, la concentracion de Ba no parece estar ligada a la productividad, sino todo lo contrario. Hyun *et al.* (1999) tampoco encontraron claras evidencias de cantidades significativas de Ba ligadas a productividad biogénica en el océano en sedimentos del testigo 983, muy cercano al testigo U1314, debido al alto contenido en aluminosilicatos que dificultaba su determinación. El patrón de distribución de este elemento en sedimentos superficiales en la cuenca de Irminger y de Islandia describe un gradiente norte-sur, relacionado al aporte de material continental durante episodios de fusión de hielo en periodos fríos (Grousset *et al.*, 1982). De acuerdo con Nesbitt *et al.* (1980), el Ba es liberado durante procesos de meteorización continental e incorporado por arcillas secundarias a través de procesos de intercambio y adsorcion, para luego ser transportado al océano mediante la erosión del material continental. Por lo tanto, aumentos de Ba en nuestras muestras estarían asociados al depósito de IRD durante periodos glaciares.

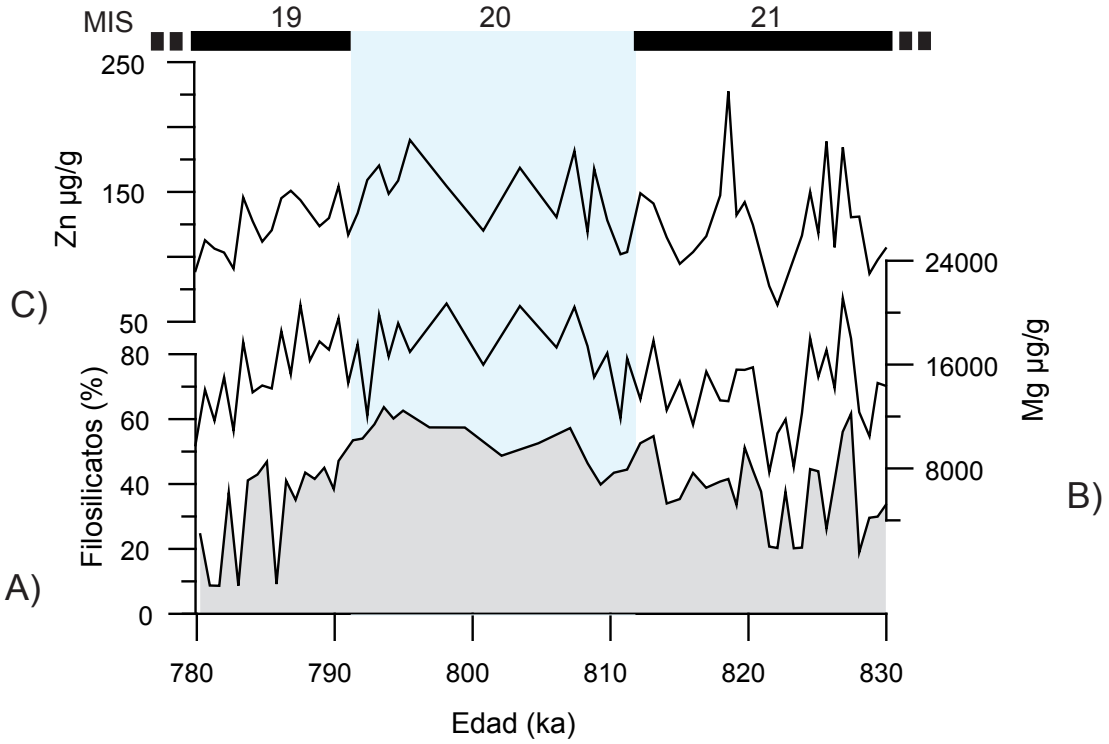

Figura 7.6. Desde abajo hacia arriba: A) Porcentaje de filosilicatos (área gris), B) registro de Mg (µg/g) y C) Zn (µg/g) para el periodo 830-779 ka. La barra vertical azul indica el estadio marino isotópicos glaciares 20.

La presencia de elevados niveles de Mg en sedimentos oceánicos del Atlántico Norte ha sido frecuentemente ligado a la presencia de dolomita procedente de descargas de IRD (e.g. Hodell *et al.*, 2008; Scourse *et al.*, 2000). Sin embargo, basándonos en la distribución mineralógica obtenida para el periodo ~830-779 ka, nosotros no observamos ninguna relación aparente entre las concentraciones de Mg y de dolomita en el testigo U1314. La presencia de valores elevados de Mg puede proceder del material basáltico que abunda en la región o por la alteración del mismo. Sedimentos ricos en Mg han sido documentados en la región de la dorsal de Reykjanes y la dorsal Meso-Atlántica, caracterizadas por el alto contenido en minerales arcillosos y otros aluminosilicatos neo-formados de la alteración de rocas basálticas (Horowitz and Cronan, 1976). En nuestro caso, la buena correlación entre las curvas de contribución relativa de filosilicatos y la concentración de Mg para el período ~830-779 ka parece indicar que algún tipo de arcilla es con toda probabilidad una de las fuentes más importantes de Mg en el testigo U1314 (Fig. 7.6A-B). En este sentido, numerosos autores han documentado la abundancia durante períodos glaciares de la asociación arcillosa rica en Mg, clorita-illita, en regiones frías del Atlántico Norte (Biscaye, 1965; Bout-Roumazeilles *et al.*, 1999; Fagel *et al.*, 1996). Estos filosilicatos serían transportados al océano durante episodios de descarga de IRD procedentes de provincias ácidas de Groenlandia y norte de Europa (Grousset and Parra, 1982), lo cual explicaría el aumento de Mg en los sedimentos glaciares del testigo U1314. Del mismo modo que el Mg, el Zn concentrado en minerales de arcillas formados por la alteración de

cenizas volcánicas sería transportado al fondo oceánico por corrientes turbidíticas y/o formando parte del detrito continental liberado durante la fusión de icebergs (Bout-Roumazeilles *et al.*, 1997; Damuth, 1978).

4.2. Estimación de paleotemperaturas usando la relación Mg/Ca

La simultanead de incrementos en la temperatura estimada a partir de la relación Mg/Ca y en el contenido de calcita con descensos en el $\delta^{18}O$ en foraminíferos planctónicos a continucación del máximo de descarga de IRD, indicaría un aumento de las temperaturas superficiales. Este calentamiento podría haber contribuido a aumentar la fusión y retroceso de las masas de hielo continental durante el inicio del interglacial. Registros recientes de análisis de Mg/Ca y calcita, en combinación con otros indicadores reflejan condiciones similares, con un calentamiento abrupto durante las descargas de icebergs en periodos fríos (Hulbe *et al.*, 2004; Jonkers *et al.*, 2010a; Moros *et al.*, 2002; Peck *et al.*, 2006; Rasmussen and Thomsen, 2004; Shaffer *et al.*, 2004). Este calentamiento siguiendo el máximo de IRD explicaría el rápido retroceso de los casquetes de hielo del Atlántico Norte, resultado del incremento de temperaturas sub-superficiales que liberan calor atrapado bajo la superficie del océano y favorecería la recuperación de la AMOC. Este mecanismo podría estar ya funcionando en regiones del océano Ártico (Carmack *et al.*, 1995; Grotefendt *et al.*, 1998; Holland *et al.*, 2008), donde el rápido adelgazamiento de los glaciares ha sido explicado como el resultado de la intensificación del calentamiento del océano sub-superficial durante las últimas décadas.

Dado que la relación Mg/Ca indica la temperatura de calcificación y las temperaturas calculadas a partir de la asociación de foraminíferos planctónicos corresponderían a condiciones más superficiales, las diferencias entre ambos registros se podrían deber a que ambas señales reflejan diferentes profundidades. La diferencia también se puede estar influenciada por la baja sensibilidad de la calibración de Mg/Ca a las bajas temperaturas (Kozdon *et al.*, 2009).

Algunos modelos han propuesto que este rápido calentamiento durante el retroceso de las masas de hielo puede deberse a una liberación súbita de calor subsuperficial, acumulado durante un periodo de estratificación debido al aporte de aguas con baja salinidad o de formación de hielo marino (Alvarez-Solas *et al.*, 2010; Bakke *et al.*, 2009; Shaffer *et al.*, 2004). La explicación propuesta por estos modelos implicaría un flujo continuado de aguas cálidas sub-superficiales hacia el norte (Rasmussen and Thomsen, 2004). Aunque creemos que este mecanismo no desencadena los eventos de descarga de IRD durante las secuencias de avance/retroceso de los casquetes de hielo continental, relacionados con el balance de la acumulación de hielo (Marshall and Koutnik, 2006), si que pensamos que podrían acelerar la ruptura de las plataformas de hielo durante fases de deglaciación al liberar gran cantidad de energía sub-superficial, y explicaría el rápido calentamiento de las aguas que observamos después del pico de IRD.

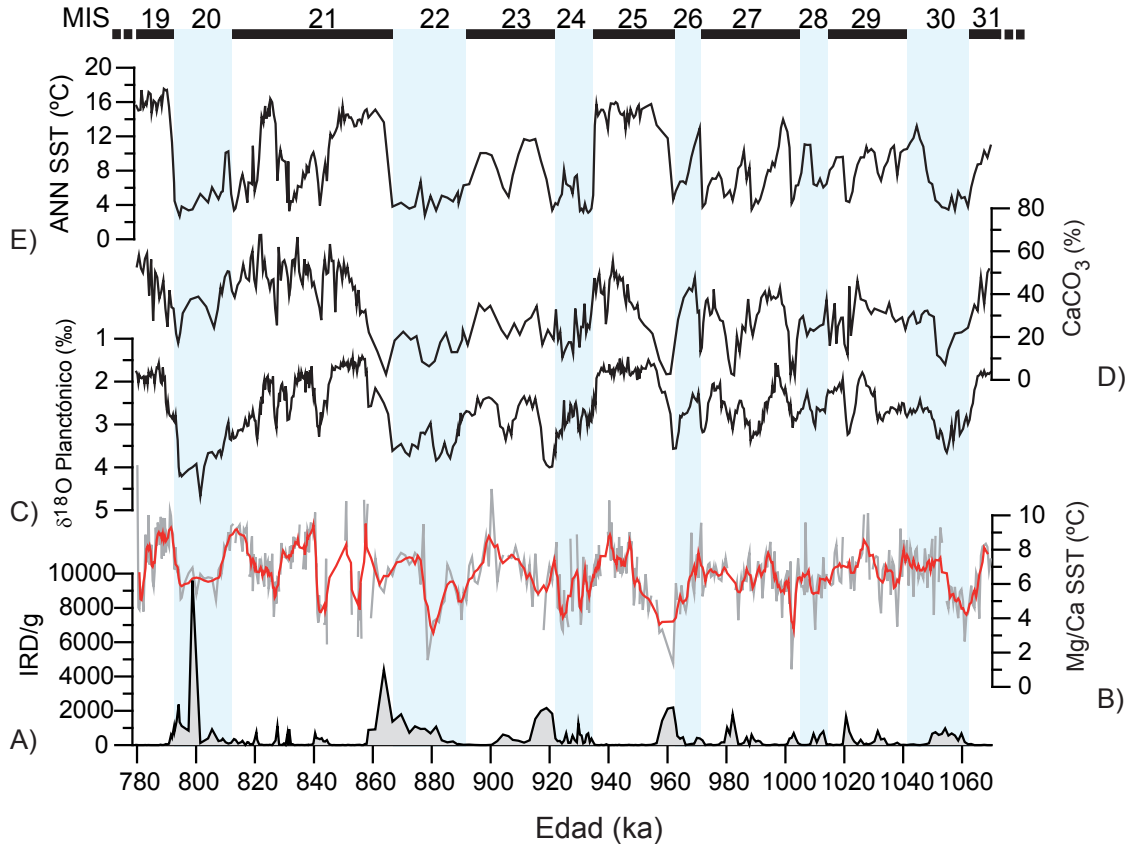

Figura 7.7. Desde abajo hacia arriba: A) IRD/g, B) reconstrucción de temperaturas a partir de la relación Mg/Ca (en rojo, media de cinco puntos), C) $\delta^{18}O$ planctónico, D) $CaCO_3$ (%), y E) reconstrucción de temperaturas a partir de la funciones de transferencia.

Sin embargo, a pesar del progreso alcanzado en los últimos años en las calibraciones y técnicas de limpieza utilizadas en reconstrucciones de paleotemperaturas a a través de la relación Mg/Ca (e.g. Elderfield and Ganssen, 2000; Lea *et al.*, 1999; Nürnberg *et al.*, 1996a; Pena *et al.*, 2005; von Langen *et al.*, 2005), existen todavía importantes incertidumbres en el uso de *N. pachyderma* sin. en latitudes altas del Atlántico Norte debido a la marcada diferencia de las propiedades de las masas de agua superficiales de esta región. Nürnberg (1995) observó en su estudio de relación Mg/Ca en conchas de *N. pachyderma* sin. valores muy altos en condiciones de hielo marino perenne, mientras que Lea *et al.* (1999) y Meland *et al.*(2006) sugirieron que descensos en el pH del océano o influencia de aguas árticas y polares con bajos valores de ion carbonato podrían producir valores anormalmente altos en la relación Mg/Ca.

En conclusión, a pesar de que las paleotemperaturas reconstruidas a partir de la relación Mg/Ca en *N. pachyderma* sin. en nuestro testigo indican un calentamiento siguiendo la máxima descarga de IRD, sugerimos que estos resultados sean tomados con cautela debido a las múltiples incertidumbres que rodean esta técnica de estimación de paleotemperaturas en regiones árticas.

5. CONCLUSIONES

La composición elemental de los sedimentos del testigo U1314 refleja los cambios en el origen de las partículas; biogénico, del fondo oceánico o continental, y por lo tanto también indican variaciones en el modo de transporte; actividad de corrientes de fondo o fusión de hielo continental. Una clara sucesión de periodos con aumento en la productividad oceánica e incrementos en los eventos de descarga por *icebergs* se puede identificar en el testigo U1314 a escala glaciar-interglaciar. Periodos de alta productividad superficial y de reactivación de la circulación profunda, indicados por el aumento de valores del factor 1, tiene lugar durante etapas interglaciares. Durante estos periodos climáticos óptimos, se observa un descenso en el flujo de IRD causado por la reducción del tamaño de las masas de hielo continental del Atlántico Norte, y que permitieron un aumento del transporte de aguas atlánticas cálidas que favorecieron la productividad superficial y mayor transporte de material fino por corrientes de fondo más intensas. Este patrón pone de manifiesto la interconexión de la circulación oceánica superficial y profunda, en la acumulación de sedimento de grano fino en el *Gardar Drift*.

El análisis de la composición elemental también nos ha permitido diferenciar varias fuentes de material terrígeno y medios de transporte. Altos valores de los elementos relacionados con el factor 2 (Ti, Fe, Mg, Al y Zn) indican que un material terrígeno oceánico enriquecido en estos elementos fue transportado hacia la posición del testigo U1314 por corrientes nefeloides asociadas a la intensificación de la ISOW durante periodos interglaciares. Por el contrario, el aumento de elementos relacionados con el factor 3 (Ba, Mg y Zn) y descenso en la relación Ti/Al reflejan periodos con mayor extensión de los casquetes de hielo en el Atlántico Norte, con fusiones episódicas del hielo y aporte de material continental rico en arcillas.

La estimación de paleotemperaturas a partir de la relación Mg/Ca en *N. pachyderma* sin. muestra rápidos calentamientos después del máximo de descarga de IRD. Esto reflejaría un incremento de temperaturas sub-superficiales que, al ser liberado de forma súbita después del colapso del casquete de hielo, aceleraría el retroceso las masas de hielo en el Atlántico Norte. Sin embargo, la existencia de incertidumbres en la calibración de las temperaturas obtenidas con este método, en las técnicas de limpieza y otros factores que pueden afectar a la relación Mg/Ca, nos lleva a tomar con cautela estos resultados.

Capítulo 8

CONCLUSIONES

CONCLUSIONES

El estudio en alta resolución de la sucesión micropaleontológica, isotópica, sedimentológica y geoquímico del testigo U1314, ha demostrado la existencia de una variabilidad climática y oceanográfica en el Atlántico Norte, relacionada con secuencias de avance y retroceso de las masas de hielo continental en esta región. Las principales conclusiones derivadas de los objetivos que se plantearon al comienzo de este estudio son las siguientes:

• Hemos realizado un estudio en alta resolución del $\delta^{18}O$ de las conchas de los foraminíferos bentónicos, que sincronizado con la curva de referencia de volumen de hielo global LR04, nos ha permitido elaborar una cronología para los sedimentos de la sección estudiada de nuestro testigo, la cual comprende desde 1069 hasta 779 ka (MIS 31-19). Todos los indicadores utilizados en el testigo U1314 muestran importantes variaciones climáticas orbitales (glacial-interglacial) y suborbitales. Uno de los rasgos más característicos del periodo estudiado es el cambio en la amplitud de los eventos climáticos antes y después del MIS 25.

• El registro de isótopos estables en foraminíferos bentónicos nos ha permitido reconstruir los cambios en la evolución de las masas de hielo y la circulación profunda en el Hemisferio Norte. Durante el periodo comprendido entre el MIS 31 y 26, los cambios de volumen de hielo acumulado en los continentes son moderados, existe una formación constante de aguas profundas en los mares Nórdicos que permite una buena ventilación profunda del Atlántico Norte, sólo interrumpida brevemente por rápidas descargas de icebergs. El rasgo más llamativo de este intervalo es la existencia de eventos climáticos milenarios que interrumpen la fase de crecimiento de las masas de hielo de los estadios isotópicos glaciales. Estos eventos comienzan con un calentamiento abrupto seguido de un enfriamiento gradual que finaliza con un pico de descarga de IRD, el cual ha sido interpretado como el avance de los casquetes de hielo hacia la línea de costa y posterior ruptura. El descenso en el $\delta^{18}O$ de los foraminíferos bentónicos en la base de estas oscilaciones milenarias podría estar relacionado con leves ascensos del nivel del mar, calentamiento de las aguas profundas y/o a mayor influencia de aguas profundas con $\delta^{18}O$ más bajo procedentes del Hemisferio Sur.

• El análisis espectral de los registros de IRD, reconstrucción de temperaturas superficiales y $\delta^{18}O$ de foraminíferos planctónicos muestra una ciclicidad dominante asociada a las frecuencias de precesión y hemi-precesión (21 y 11-10 ka). La coincidencia de ciclicidad con las variaciones de insolación durante los equinoccios en el ecuador, que a su vez corresponden a máximos en el gradiente latitudinal de insolación, parece indicar que el mayor transporte de vapor de agua durante los periodos de máxima insolación en bajas latitudes ha jugado un papel fundamental en el ritmo de crecimiento de las masas de hielo continental del Atlántico Norte y su posterior colapso al llegar a la línea de costa. La existencia de una marcada variabilidad climática milenaria previa a la intensificación de la glaciación del Hemisferio Norte indica

que los mecanismos que controlan estas oscilaciones de alta frecuencia son independientes del volumen de hielo acumulado en los continentes. Basándonos en su ritmo y estructura, estos eventos parecen ser estar controlados por las variaciones de insolación en el ecuador durante los equinoccios, exportada hacia altas latitudes por procesos convectivos tropicales. Este proceso pone de manifiesto la importancia de los gradientes latitudinales de energía y vapor de agua en los sistemas atmósfera, océano y criosfera, que generan y transportan esta variabilidad climática a otras regiones de la Tierra.

- Los fuertes cambios observados en la asociación de foraminíferos planctónicos responden a la variabilidad de masas de agua superficiales en el Atlántico Norte, controlada por la posición del Frente Ártico. Durante periodos cálidos y mayor presencia de aguas atlánticas, especies subpolares y transicionales, como *Neogloboquadrina pachyderma* dex., *Globorotalia inflata*, *Globigerina bulloides* y *Globigerinita glutinada*, son las más abundantes, mientras que durante periodos fríos en los que la circulación superficial está dominada por aguas árticas, la especie principal es *Neogloboquadrina pachyderma* sin., con porcentajes en torno al 90 %. También hemos observado que la forma más incrustada y robusta de *N. pachyderma* sin. es mucho más abundante durante los estadios glaciares 22 y 20, más intensos y con temperaturas superficiales más bajas. Igualmente, la posición del Frente Ártico respecto a nuestro testigo ha sido estimada a través de abundancia de *Turborotalita quinqueloba,* la cual aumenta cuanto más cerca se encuentre el frente.

- Las asociaciones de foraminíferos planctónicos también han permitido la reconstrucción de paleotemperaturas empleando la técnica de redes neuronales artificiales. Los resultados demuestran una variabilidad orbital y suborbital muy marcada, especialmente en el intervalo entre el estadio isotópico marino 31 y 26. A su vez, combinando las paleotemperaturas con los isótopos de oxígeno de foraminíferos planctónicos, hemos reconstruido el $\delta^{18}O$ del agua del mar, el cual está relacionado con la variabilidad de aguas árticas versus atlánticas en la región.

- En el estudio de la asociación de radiolarios, se han identificado 79 especies, muchas las cuales han demostrado reflejar con precisión las condiciones superficiales del océano. Los porcentajes de la especie *Cycladophora davisiana* aumentan durante periodos de crecimiento de volumen de hielo continental y menor temperatura superficial, y durante los eventos de descarga de IRD. Este dominio se debe a que *C. davisiana* vive por debajo de la zona fótica y a su adaptación a condiciones de baja salinidad y formación de hielo marino. La diversidad de especies aumenta durante periodos de mayor influencia de aguas atlánticas y aumento de la productividad superficial. La asociación cambia drásticamente, siendo especies adaptadas a condiciones de alta productividad primaria, como *Lithomelissa setosa* y *Pseudodictyophimus gracilipes*.

- A través del estudio de las asociaciones de foraminíferos planctónicos y radiolarios, hemos reconstruido la variabilidad de la circulación superficial del Atlántico Norte. Durante el periodo anterior al MIS 25, la mayor abundancia de especies de foraminíferos planctónicos

y radiolarios adaptados a condiciones frías, como *Neogloboquadrina pachyderma* sin. y *Cycladophora davisiana*, respectivamente, indica que las condiciones de las aguas superficiales estuvieron condicionadas por la posición semi-estable del Frente Ártico al sureste del testigo U1314, y en consecuencia una hidrografía superficial dominada por masas de agua árticas frías y de baja salinidad. Esta disposición del Frente Ártico provocó que el transporte hacia altas latitudes de aguas atlánticas superficiales, más cálidas y salinas, fuera limitado y desplazado hacia el margen continental de Noruega. Un menor aporte de vapor de agua hacia zonas de formación de aguas profundas en los mares Nórdicos debido a esta configuración hidrográfica pudo haber sido la causa del crecimiento limitado de los casquetes de hielo en el Hemisferio Norte durante el Pleistoceno Inferior respecto a estadios isotópicos posteriores.

- El comienzo de glaciaciones más intensas y cambios climáticos de mayor amplitud hacia el MIS 25, modificó de forma dramática los patrones de circulación profunda y el clima en el Atlántico Norte. El intervalo entre el MIS 25 y el 19 muestra el incipiente desarrollo de ciclos climáticos de 100 ka de duración, que se asemejan más a los del Pleistoceno Superior. El mayor crecimiento de las masas de hielo continental provocó deglaciaciones más intensas que tuvieron un fuerte impacto en la circulación profunda. Valores mínimos de $\delta^{13}C$ en foraminíferos bentónicos durante los MIS 24, 22 y 20 son el resultado de una fuerte reducción en la producción de la NADW y mayor transporte hacia el norte de LDW. A partir del MIS 21, un mayor retroceso del Frente Ártico durante periodos de descenso de volumen de hielo, permitió un mayor transporte de aguas cálidas superficiales hacia el norte, lo que provocó cambios más marcados en la fauna del Atlántico Norte y una mayor diversidad de especies.

- Las variaciones en el contenido de carbonato cálcico y ópalo biogénico parecen responder a cambios en la productividad primaria superficial junto con variaciones en la circulación de aguas profundas. El retroceso hacia el norte del frente y la mayor entrada de aguas cálidas noratlánticas durante periodos interglaciales tiene como resultado una mayor productividad primaria, y por lo tanto mayor acumulación de carbonato cálcico y ópalo biogénico. La mayor producción de aguas profundas durante estos periodos desencadenó un elevado transporte y acumulación de partículas biogénicas de tamaño fino producidas en superficie. Por el contrario, durante periodos de avance hacia el sureste del Frente Ártico y episodios de fusión y descarga de icebergs, las temperaturas superficiales más bajas y la formación de hielo estacional restringen la productividad primaria, que junto con la ralentización de la circulación profunda en el Atlántico Norte, producen una menor acumulación de material fino y una mayor concentración de material de grano arena (detritus transportados por icebergs y foraminíferos > 63 μm).

- El estudio geoquímico y mineralógico del material del testigo U1314 nos ha permitido inferir las posibles áreas fuentes del material y los mecanismos que lo han transportado. Los minerales de cuarzo, plagioclasa, filosilicatos, y los fragmentos líticos observados en la fracción > 150 μm parecen proceder de los márgenes de Groenlandia, Islandia e Islas Feroe, arrancados

del sustrato continental durante periodos de avance de los casquetes de hielo y transportados al océano durante la posterior fusión. La presencia esporádica de dolomita en nuestras muestras indica que, o bien los icebergs procedentes de Norteamérica ya transportaban dolomita antes de ~ 640 ka, o bien que los niveles de dolomita en el testigo U1314 proceden de pequeños depósitos de dolomia al noreste de Groenlandia y norte de Europa, más cercanos a nuestro testigo. La composición elemental del sedimento refleja las diferentes fuentes y medios de transporte implicados; durante periodos interglaciares con circulación termohalina más intensa, hay un aumento de elementos asociados a la productividad superficial (Ca, Sr, Mn, P), lo que corrobora el control parcial de la circulación profunda en la acumulación de partículas biogénicas en el *Gardar Drift* y una mayor productividad primaria en esta región. Durante estos periodos también hay una mayor acumulación de elementos asociados a material terrígeno oceánico de grano fino (Ti, Fe, Mg, Al y Zn), transportado por corrientes nefeloides asociadas a la intensificación de la circulación termohalina. Por el contrario, el aumento de elementos asociados a arcillas (Ba, Mg y Zn) indicaría una mayor extensión de los casquetes de hielo en el Atlántico Norte y posterior fusión que liberaría el material continental rico en esas arcillas.

- La estimación de paleotemperaturas a partir de la relación Mg/Ca en *N. pachyderma* sin. muestra rápidos calentamientos después del máximo de descarga de IRD. Esto reflejaría un incremento de temperaturas sub-superficiales que al ser liberado de forma súbita después del colapso del casquete de hielo, aceleraría el retroceso las masas de hielo en el Atlántico Norte. Sin embargo, la existencia de incertidumbres en la calibración de las temperaturas obtenidas con este método, en las técnicas de limpieza y otros factores que pueden afectar a la relación Mg/Ca, nos lleva a tomar con cautela estos resultados.

CONCLUSIONS

The study of a high resolution micropaleontological, isotopic, mineralogical and geochemical succession from Site U1314, has demonstrated the existence of a climatic and oceanographic variability in the North Atlantic, related with advance/retreat ice-sheet sequences in this region. The main conclusions derived from the objectives exposed at the beginning of this study are the following:

- We have performed a high-resolution benthic foraminifer $\delta^{18}O$ study that has been synchronized with the benthic global stack LR04 in order to elaborate a chronology for the sediments of the studied section of our site, which ranges from 1069 to 779 ka (MIS 31-19). All proxies used at Site U1314 show a marked orbital (glacial-interglacial) and suborbital climate variability. One of the most characteristic features of the study period is the change in the amplitude of climatic changes before and after MIS 25.

- Benthic stable isotopes records have enabled us to reconstruct changes in the ice-sheets and deep-circulation in the Northern Hemisphere. In the period between MIS 31 and 26, ice-volume change is moderate, and deep-ventilation is generally good due to a constant deep-water formation rate in the GIN Seas, only interrupted by rapid iceberg discharges. The most important feature during this interval is the existence of millennial-scale climate events that punctuated the ice-growth phase during glacial stages. These events start with an abrupt warming followed by a gradual cooling that is culminated with an IRD discharge event, which has been interpreted as an ice-sheet advance toward the coast line and calving. The decrease in the benthic $\delta^{18}O$ signal at the base of these millennial oscillations could be related to sea-level rises, deep-water warming or to greater influence of southern deep waters in the North Atlantic.

- Spectral analysis of IRD, paleotemperature reconstruction, and planktonic $\delta^{18}O$ show cyclicities centered at precessional and half-precessional frequencies (21 and 11-10 kyr). The coincidence these dominant cyclicities in surface proxies with insolation variations during equinoxes at the Equator, which in turn correspond to maxima in the latitudinal gradient of insolation, may suggests that intensification of cross-equatorial moisture transport during insolation maxima at the Equator play an important role in ice-sheet growth in circum-Atlantic continents and subsequent calving when they reach the coast-line. Occurrence of millennial-climate events before the intensification of Northern Hemisphere Glaciation indicates that mechanisms controlling these high-frequency oscillations are independent of the ice-volume accumulated onto continental masses. The timing and structure of the ice surges suggest they might be induced by latitudinal export of equatorial insolation forcing to high-latitudes via tropical convective processes. In conclusion, our study outlines the importance of latitudinal gradients of energy and moisture through the atmosphere-ocean-cryosphere system to generating

and transporting this millennial climate variability to other Earth regions.

• Abrupt changes in planktonic foraminifer assemblages reflect the strong variability of surface water masses in the North Atlantic, controlled by the position of the AF. During warm periods and higher influence of atlantic waters, subpolar and transitional species, such as *Neogloboquadrina pachyderma* dex., *Globorotalia inflata*, *Globigerina bulloides* and *Globigerinita glutinada*, are the most abundant, while during cold periods whit the surface hydrography dominated by arctic waters, the most important species is *Neogloboquadrina pachyderma* sin., with percentages around 90 %. We also have observed that *N. pachyderma* sin. encrusted form is more abundant during glacial periods 22 and 20, more intense and with lower surface temperatures. Moreover, the AF position was estimated through the abundance of *Turborotalita quinqueloba*, which increases when the front is closer.

• We have also performed a paleotemperature reconstructions based on planktonic foraminifer assemblage using artificial neural networks technique. Results show a marked orbital and suborbital variability, especially during the interval between MIS 31-26. Additionally, combining faunal based paleotemperatures with planktonic oxygen isotope, we have reconstructed the $\delta^{18}O$ of sea water, which is related to the arctic versus atlantic waters variability in this region.

• In the study of the radiolarian assemblage, we have identified 79 species, many of them reflect accurately conditions of surface ocean. Percentages of *Cycladophora davisiana* increase during periods of ice-sheet growth and lowered surface temperaturas, and IRD discharge events. This domain is because *C. davisiana* lives below the photic zone and it is adapted to low salinity and sea-ice formation conditions. Species diversity increases during periods with higher influence of atlantic waters and surface primary productivity. Radiolarian assemblage changed drastically, and species adapted to former ocean conditions became more abundant.

• Through the study of planktonic foraminifer and radiolarian assemblages, we have inferred surface circulation variability of the North Atlantic. During the time interval before MIS 25, higher abundance of cold-adapted species of planktonic foraminifer and radiolarian, such as *Neogloboquadrina pachyderma* sin. and *Cycladophora davisiana*, respectively, indicate that surface circulation was controlled by the steady position of the AF south-east of Site U1314, and consequently, dominated by cold and low salinity arctic waters. The AF layout caused a reduced advection toward high latitudes of warm and saline atlantic waters, restricted to the Norwegian continental margin. A lower moisture supply toward deep-water formation areas in the GIN Seas might have limited ice-sheet growth in the North Atlantic during the Early Pleistocene respect to younger isotopic stages.

• Higher-amplitude changes and the onset of major glaciations since MIS 25 modified dramatically the deep circulation pattern and climate configuration in the North Atlantic. The MIS 25-19 time-slice show the incipient characteristics of the Late Pleistocene climate cycles,

dominated by the 100 kyr cyclicity. Greater build-up of continental ice led to stronger and long-lasted iceberg discharges at glacial maxima and Terminations that had a large impact in deep circulation. Minima benthic $\delta^{13}C$ values during MIS 24, 22 and 20 documents the near-cessation of NADW production during these episodes and the northward intrusion of LDW. A greater AF retreat during ice-volume decay periods allowed enhanced warm surface waters transport toward high-latitudes, which caused marked fauna changes in the North Atlantic and higher species diversity.

• Variability of calcium carbonate and biogenic opal content in the sediments seems to respond to changes in surface primary productivity together with variations of deep water circulation. The northward AF retreat and high northward advection of warm atlantic waters during interglacial periods results in an increase in primary productivity, and hence, in calcium carbonate and biogenic opal accumulation rates. Higher production rate of deep waters during these periods accumulates more fine biogenic particles produced at surface. In contrast, at times of southeast advance of the AF and iceberg discharge events, SST decreased and seasonal sea-ice formation inhibits primary productivity, that together with less vigorous deep-water flow in the North Atlantic, accumulated less fine-grained material, that led to the relative concentration in the sediment of the coarsed-grained fraction (IRD and planktonic foraminifera > 63 μm).

• The geochemical and mineralogical study of sediments from U1314 has enabled us to infer sediment sources and transport mechanisms. Quartz, plagioclase, phyllosilicates and lithic fragments observed in the > 150 μm fraction may point to a Greenland, Iceland or Faroe Island origin, eroded from the continents during ice-sheet advance and released into the ocean during subsequent melting. The sporadic occurrence of dolomite in our samples indicate that either icebergs from North America transported dolomite up to Site U1314 location before ~ 640 ka, or that it comes from small dolomite deposits from Northeast Greenland and North Europe, closer to our Site. Sediment elemental composition reflects different sources and mechanisms transport; during interglacial periods with strong thermohaline circulation, there is an increase in elements related to surface productivity (Ca, Sr, Mn, P), that corroborates partial control of deep circulation in accumulation of biogenic particles over Gardar Drift together with enhanced primary productivity in the region. During these periods there is also a higher accumulation of elements related to fine terrigenous oceanic material (Ti, Fe, Mg, Al y Zn), transported by nepheloid currents associated to the intensification of the thermohaline circulation. On the contrary, the increased of elements associated with clays (Ba, Mg y Zn) would indicate an ice-sheet expansion in the North Atlantic followed by melting that would release this clay-rich continental material to the ocean.

• Paleotemperature estimates base on Mg/Ca ratio of *N. pachyderma* sin. show rapid warmings following the IRD peak. This would reflect a sub-surface temperature increase that would sudden released after ice-sheet collapse, which would accelerate ice-sheet retreat in the North Atlantic. However, the existence of uncertainties in the calibration of temperatures

obtained with this method, in the cleaning techniques and other factors affecting the Mg/Ca ration, thus, recommend taking these results with caution.

BIBLIOGRAFÍA

BIBLIOGRAFÍA

Abelmann, A. and Gowing, M.M., 1997. Spatial distribution pattern of living polycystine radiolarian taxa - baseline study for paleoenvironmental reconstructions in the Southern Ocean (Atlantic sector). Marine Micropaleontology, 30(1-3): 3-28.

Abelmann, A. and Nimmergut, A., 2005. Radiolarians in the Sea of Okhotsk and their ecological implication for paleoenvironmental reconstructions. Deep Sea Research Part II: Topical Studies in Oceanography, 52(16-18): 2302-2331.

Aksu, A.E. and Mudie, P.J., 1985. Late Quaternary stratigraphy and paleoecology of northwest Labrador Sea. Marine Micropaleontology, 9(6): 537-557.

Aksu, A.E., Mudie, P.J., de Vernal, A. and Gillespie, H., 1992. Ocean-atmosphere responses to climatic change in the Labrador Sea: Pleistocene plankton and pollen records. Palaeogeography, Palaeoclimatology, Palaeoecology, 92(1-2): 121-138.

Alley, R.B. and MacAyeal, D.R., 1994. Ice-rafted Debris Associated with Binge/Purge Oscillations of the Laurentide Ice Sheet. Paleoceanography, 9(4): 503-511.

Alvarez-Solas, J. *et al.*, 2010. Links between ocean temperature and iceberg discharge during Heinrich events. Nature Geosciences, 3(2): 122-126.

Anderson, O.R., 1983. Radiolaria. Springer, New York, 355 pp.

Andruleit, H.A. and Baumann, K.-H., 1998. History of the Last Deglaciation and Holocene in the Nordic seas as revealed by coccolithophore assemblages. Marine Micropaleontology, 35(3-4): 179-201.

Arz, H.W., Lamy, F., Ganopolski, A., Nowaczyk, N. and Pätzold, J., 2007. Dominant Northern Hemisphere climate control over millennial-scale glacial sea-level variability. Quaternary Science Reviews, 26(3-4): 312-321.

Bakke, J. *et al.*, 2009. Rapid oceanic and atmospheric changes during the Younger Dryas cold period. Nature Geosciences, 2(3): 202-205.

Baldauf, J.G., 1986. Diatom biostratigraphic and palaeoceanographic interpretations for the middle to high latitude North Atlantic Ocean. Geological Society, London, Special Publications, 21(1): 243-252.

Balestra, B., Ziveri, P., Baumann, K.-H., Troelstra, S. and Monechi, S., 2010. Surface water dynamics in the Reykjanes Ridge area during the Holocene as revealed by coccolith assemblages. Marine Micropaleontology, 76(1-2): 1-10.

Balestra, B., Ziveri, P., Monechi, S. and Troelstra, S., 2004. Coccolithophorids from the Southeast Greenland Margin (Northern North Atlantic): production, ecology and the surface sediment record. Micropaleontology, 50(Suppl_1): 23-34.

Balsam, W.L. and Flessa, K.W., 1978. Patterns of planktonic foraminiferal abundance and diversity in surface sediments of the western North Atlantic. Marine Micropaleontology, 3(3): 279-294.

Barendregt, R.W. and Irving, E., 1998. Changes in the extent of North American ice sheets

during the late Cenozoic. Canadian Journal of Earth Sciences, 35(5): 504-509.

Barry, R.G. and Chorley, R.J., 2003. Atmosphere, weather and climate. Routledge, New York, 472 pp.

Bartoli, G., Sarnthein, M. and Weinelt, M., 2006. Late Pliocene millennial-scale climate variability in the northern North Atlantic prior to and after the onset of Northern Hemisphere glaciation. Paleoceanography, 21: PA4205.

Bauch, D., Carstens, J. and Wefer, G., 1997. Oxygen isotope composition of living *Neogloboquadrina pachyderma* (sin.) in the Arctic Ocean. Earth and Planetary Science Letters, 146(1-2): 47-58.

Bauch, H.A., 1994. Significance of variability in Turborotalita quinqueloba (Natland) test size and abundance for paleoceanographic interpretations in the Norwegian-Greenland Sea. Marine Geology, 121(1-2): 129-141.

Bauch, H.A., Erlenkeuser, H., Jung, S.J.A. and Thiede, J., 2000. Surface and deep water changes in the subpolar North Atlantic during Termination II and the Last Interglaciation. Paleoceanography, 15(1): 76-84.

Bauch, H.A. and Kandiano, E.S., 2007. Evidence for early warming and cooling in North Atlantic surface waters during the last interglacial. Paleoceanography, 22(1): PA1201.

Baumann, K.-H. and Huber, R., 1999. Sea-surface gradients between the North Atlantic and the Norwegian Sea during the last 3.1 m.y.: comparison of Sites 982 and 985. In: M.E. Raymo, E. Jansen, P. Blum and T.D. Herbert (Editors), Proc. ODP, Sci. Results, 162. Ocean Drilling Program, College Station, TX, pp. 179-190.

Baumann, K.-H. *et al.*, 1995. Reflection of Scandinavian Ice Sheet Fluctuations in Norwegian Sea Sediments during the Past 150,000 Years. Quaternary Research, 43(2): 185-197.

Baumann, K.H. and Matthiessen, J., 1992. Variations in surface water mass conditions in the Norwegian Sea: Evidence from Holocene coccolith and dinoflagellate cyst assemblages. Marine Micropaleontology, 20(2): 129-146.

Bé, A.H.W., 1977. An ecological, zoogeographic and taxonomic review of recent planktonic foraminifera. In: A.T.S. Ramsay (Editor), Oceanic Micropaleontology. Academic Press, London pp. 1-100.

Bé, A.W.H. and Tolderlund, D.S., 1971. Distribution and ecology of living planktonic foraminifera in surface waters of the Atlantic and Indian Oceans. In: B.M. Funnel and W.R. Riedel (Editors), Micropaleontology of the Oceans. Cambridge Univ. Press, Cambridge, pp. 105-149.

Belanger, P.E., Curry, W.B. and Matthews, R.K., 1981. Core-top evaluation of benthic foraminiferal isotopic ratios for paleo-oceanographic interpretations. Palaeogeography, Palaeoclimatology, Palaeoecology, 33(1-3): 205-220.

Benson, R.N., 1972. Radiolaria, Leg XII, Deep Sea Drilling Project. In: A.S. Laughton *et al.* (Editors), Initial Reports of the Deep Sea Drilling Project. U.S. Goverment Printing Office, Washington, D.C., pp. 1085-1113.

Bergami, C., Capotondi, L., Langone, L., Giglio, F. and Ravaioli, M., 2009. Distribution of living planktonic foraminifera in the Ross Sea and the Pacific sector of the Southern Ocean (Antarctica). Marine Micropaleontology, 73(1-2): 37-48.

Berger, A., Li, X.S. and Loutre, M.F., 1999. Modelling northern hemisphere ice volume over the last 3 Ma. Quaternary Science Reviews, 18(1): 1-11.

Berger, W.H., 1970a. Planktonic Foraminifera: Selective solution and the lysocline. Marine Geology, 8(2): 111-138.

Berger, W.H., 1970b. Biogenous deep-sea sediments: Fractionation by deep-sea circulation. Geological Society of America Bulletin, 81(5): 1385-1402.

Berger, W.H., Bickert, T., Jansen, E., Wefer, G. and Yasuda, M., 1993a. The central mystery of the Quaternary Ice Age. Oceanus, 36: 53–56.

Berger, W.H. and Jansen, E., 1994a. Mid-Pleistocene climate shift-The Nansen connection. In: O.M. Johannessen, R.D. Muench and J.E. Overland (Editors), The Polar Oceans and their Role in Shaping the Global Environment. AGU, Washington D.C., pp. 295-311.

Berger, W.H. and Jansen, E., 1994b. Mid-Pleistocene climate shift: the Nansen connection. In: T. Johannessen, R.D. Muench and J.E. Overland (Editors), The Polar Oceans and Their Role in Shaping the Global Environment: The Nansen Centennial Volume. AGU, Geophysical Monographs Washington D.C.

Berger, W.H. and Jansen, E., 1994c. Mid-Pleistocene climate shift: the Nansen connection. In: O.D. Johannessen, R.D. Muench and J.E. Overland (Editors), The Polar Oceans and Their Role in Shaping the Global Environment: The Nansen Centennial Volume. AGU, Geophysical Monographs. AGU, Washington, D.C., pp. 295–311.

Bianchi, G.G. and McCave, I.N., 1999. Holocene periodicity in North Atlantic climate and deep-ocean flow south of Iceland. Nature, 397(6719): 515-517.

Bianchi, G.G. and McCave, I.N., 2000. Hydrography and sedimentation under the deep western boundary current on Björn and Gardar Drifts, Iceland Basin. Marine Geology, 165(1-4): 137-169.

Bintanja, R. and van de Wal, R.S.W., 2008. North American ice-sheet dynamics and the onset of 100,000-year glacial cycles. Nature, 454(7206): 869-872.

Biscaye, P.E., 1965. Mineralogy and sedimentation of recent deep-sea clay in Atlantic Ocean and adjacent seas and oceans. Geological Society of America Bulletin, 76(7): 803-832.

Bjørklund, K.R. and Ciesielski, P.F., 1994. Ecology, morphology, stratigraphy, and the paleoceanographic significance of *Cycladophora davisiana davisiana*. Part I: Ecology and morphology. Marine Micropaleontology, 24(1): 71-88.

Bjørklund, K.R., Cortese, G., Swanberg, N. and Schrader, H.J., 1998. Radiolarian faunal provinces in surface sediments of the Greenland, Iceland and Norwegian (GIN) Seas. Marine Micropaleontology, 35(1-2): 105-140.

Bjørklund, K.R. and Kruglikova, S.B., 2003. Polycystine radiolarians in surface sediments in the Arctic Ocean basins and marginal seas. Marine Micropaleontology, 49(3): 231-273.

Bolton, C.T. *et al.*, 2010. Millennial-scale climate variability in the subpolar North Atlantic Ocean during the late Pliocene. Paleoceanography, 25(4): PA4218.

Boltovskoy, D., Alder, V.A. and Abelmann, A., 1993a. Radiolarian sedimentary imprint in Atlantic equatorial sediments: Comparison with the yearly flux at 853 m. Marine Micropaleontology, 23(1): 1-12.

Boltovskoy, D., Kling, S.A., Takahashi, K. and Bjørklund, K., 2010. World atlas of distribution of recent Polycystina (Radiolaria). Palaeontologia Electronica, 13(3): 18A, 230.

Boltovskoy, D., Uliana, E. and Wefer, G., 1996. Seasonal variation in the flux of microplankton and radiolarian assemblage compositions in the Northeastern tropical Atlantic at 2,195 m. Limnology and Oceanography, 41(4): 615-635.

Bond, G. *et al.*, 1993. Correlations between climate records from North Atlantic sediments and Greenland ice. Nature, 365(6442): 143-147.

Bond, G. *et al.*, 1992. Evidence for massive discharges of icebergs into the North Atlantic ocean during the last glacial period. Nature, 360: 245-249.

Bond, G. *et al.*, 2001. Persistent Solar Influence on North Atlantic Climate During the Holocene. Science, 294(5549): 2130-2136.

Bond, G. *et al.*, 1997. A Pervasive Millennial-Scale Cycle in North Atlantic Holocene and Glacial Climates. Science, 278(5341): 1257-1266.

Bond, G.C. and Lotti, R., 1995. Iceberg discharges into the North Atlantic on millennial time scales during the last glaciation. Science, 267(5200): 1005-1010.

Boström, K., Joensuu, O., Valdés, S. and Riera, M., 1972. Geochemical history of South Atlantic Ocean sediments since Late Cretaceous. Marine Geology, 12(2): 85-121.

Bout-Roumazeilles, V., Cortijo, E., Labeyrie, L. and Debrabant, P., 1999. Clay mineral evidence of nepheloid layer contributions to the Heinrich layers in the northwest Atlantic. Palaeogeography, Palaeoclimatology, Palaeoecology, 146(1-4): 211-228.

Bout-Roumazeilles, V., Debrabant, P., Labeyrie, L., Chamley, H. and Cortijo, E., 1997. Latitudinal control of astronomical forcing parameters on the high-resolution clay Mineral distribution in the 45°–60° N range in the North Atlantic Ocean during the past 300,000 years. Paleoceanography, 12(5): 671-686.

Boyle, E.A., 1983a. Manganese carbonate overgrowths on foraminifera tests. Geochimica et Cosmochimica Acta, 47(10): 1815-1819.

Boyle, E.A., 1986. Paired carbon isotope and cadmium data from benthic foraminifera: Implications for changes in oceanic phosphorus, oceanic circulation, and atmospheric carbon dioxide. Geochimica et Cosmochimica Acta, 50(2): 265-276.

Boyle, E.A. and Keigwin, L., 1987. North-Atlantic thermohaline circulation during the past 20,000 years linked to high-latitude surface-temperature. Nature, 330(6143): 35-40.

Broecker, W., Bond, G., Klas, M., Clark, E. and McManus, J., 1992. Origin of the northern Atlantic's Heinrich events. Climate Dynamics, 6(3): 265-273.

Broecker, W.S., 1971. A kinetic model for the chemical composition of sea water. Quaternary

Research, 1(2): 188-207.

Broecker, W.S., 1982. Ocean chemistry during glacial time. Geochimica et Cosmochimica Acta, 46(10): 1689-1705.

Broecker, W.S., Bond, G., Klas, M., Bonani, G. and Wolfli, W., 1990. A Salt Oscillator in the Glacial Atlantic? 1. The Concept. Paleoceanography, 5(4): 469-477.

Broecker, W.S. and Denton, G.H., 1990. The role of ocean-atmosphere reorganizations in glacial cycles. Quaternary Science Reviews, 9(4): 305-341.

Broecker, W.S. and Peng, T.H., 1982. Tracers in the sea. Eldigio Press, Palisades, N.Y.

Broecker, W.S. and Takahashi, T., 1978. The relationship between lysocline depth and in situ carbonate ion concentration. Deep-Sea Research, 25: 65-95.

Burns, S.J., Fleitmann, D., Matter, A., Kramers, J. and Al-Subbary, A.A., 2003. Indian Ocean Climate and an Absolute Chronology over Dansgaard/Oeschger Events 9 to 13. Science, 301(5638): 1365-1367.

Cacho, I. *et al.*, 1999. Dansgaard-Oeschger and Heinrich Event Imprints in Alboran Sea Paleotemperatures. Paleoceanography, 14(6): 698-705.

Carmack, E.C., Macdonald, R.W., Perkin, R.G., McLaughlin, F.A. and Pearson, R.J., 1995. Evidence for warming of Atlantic water in the Southern Canadian Basin of the Arctic Ocean: Results from the Larsen-93 Expedition. Geophys. Res. Lett., 22(9): 1061-1064.

Casey, R.E. *et al.*, 1979b. Radiolarian ecology and the development of the radiolarian component in Holocene sediments, Gulf of Mexico and adjacent seas with potential paleontological applications. Transactions of the Gulf Coast Association of Geological Societies 29: 228-237.

Ciesielski, P.F. and Bjørklund, K.R., 1995. Ecology, morphology, stratigraphy, and the paleoceanographic significance of *Cycladophora davisiana davisiana*. Part II: Stratigraphy in the North Atlantic (DSDP Site 609) and Labrador Sea (ODP Site 646B). Marine Micropaleontology, 25(1): 67-86.

Clark, P.U. *et al.*, 2006. The middle Pleistocene transition: characteristics, mechanisms, and implications for long-term changes in atmospheric pCO2. Quaternary Science Reviews, 25(23-24): 3150-3184.

Clark, P.U. and Pollard, D., 1998. Origin of the Middle Pleistocene Transition by Ice Sheet Erosion of Regolith. Paleoceanography, 13(1): 1-9.

Clarke, G.K., Marshall, S.J., Hillaire-Marcel, C., Bilodeau, G. and Veiga-Pires, C., 1999. A glaciological perspective on Heinrich events. In: P.U. Clark, R.S. Webb and L.D. Keigwin (Editors), Mechanisms of Global Climate Change at Millennial Time Scales. AGU Geophysical Monograph 112, Washington D.C., pp. 243–262.

CLIMAP Project Members, 1976. The Surface of the Ice-Age Earth. Science, 191(4232): 1131-1137.

Codispoti, L.A., 1979. Arctic Ocean processes in relation to the dissolved silicon content of the Atlantic. Marine Science Communications, 5(6): 361-381.

Conkright, M. *et al.*, 1998. World Ocean Atlas 1998, version 2. National Oceanic and Atmospheric Administration.

Coplen, T.B., 1996. More uncertainty than necessary. Paleoceanography, 11(4): 369-370.

Cortese, G., Bjørklund, K.R. and Dolven, J.K., 2003. Polycystine radiolarians in the Greenland-Iceland-Norwegian Seas: species and assemblage distribution. Sarsia, 88: 65-88.

Cortese, G., Dolven, J.K., Bjørklund, K.R. and Malmgren, B.A., 2005. Late Pleistocene-Holocene radiolarian paleotemperatures in the Norwegian Sea based on artificial neural networks. Palaeogeography, Palaeoclimatology, Palaeoecology, 224(4): 311-332.

Cortese, G., Gersonde, R., Hillenbrand, C.-D. and Kuhn, G., 2004. Opal sedimentation shifts in the World Ocean over the last 15 Myr. Earth and Planetary Science Letters, 224(3-4): 509-527.

Curry, W.B. and Oppo, D.W., 2005. Glacial water mass geometry and the distribution of $\delta^{13}C$ of ΣCO2 in the western Atlantic Ocean. Paleoceanography, 20: PA1017.

Channell, J.E.T. *et al.*, 2006. Site U1314 summary. In: J.E.T. Channell *et al.* (Editors), Proc. IODP, 303/306. College Station TX (Integrated Ocean Drilling Program Management International, Inc.).

Chapman, M.R., 2010. Seasonal production patterns of planktonic foraminifera in the NE Atlantic Ocean: Implications for paleotemperature and hydrographic reconstructions. Paleoceanography, 25(1): PA1101.

Chester, R. and Messiha-Hanna, R.G., 1970. Trace element partition patterns in North Atlantic deep-sea sediments. Geochimica et Cosmochimica Acta, 34(10): 1121-1128.

Damuth, J.E., 1978. Echo character of the Norwegian-Greenland Sea: Relationship to Quaternary sedimentation. Marine Geology, 28(1-2): 1-36.

Dansgaard, W., Johnsen, S.J., Clausen, H.B. and Langway, J.C.C., 1971. Climatic record revealed by the Camp Century ice core. In: K.K. Turekian (Editor), Late Cenozoic Glacial Ages. Yale University Press, New Haven, pp. 37-56.

de Wever, P., Azema, J. and Fourcade, E., 1994a. Radiolarians and Radiolarites: primary production, diagenesis and paleogeography. Bulletin des Centres de Recherches Exploration-Production, Elf Aquitaine, 18(1): 315-379.

De Wever, P., Azéma, J. and Fourcade, E., 1994b. Radiolaires et radiolarites: productivité primaire, diagenèse et paléogéographie. Bulletin des Centres de Recherches Exploration-Production Elf Aquitaine, 18(1): 315-379.

deMenocal, P., Ortiz, J., Guilderson, T. and Sarnthein, M., 2000. Coherent high- and low-latitude climate variability during the Holocene warm period. Science, 288(5474): 2198-2202.

deMenocal, P.B., 1995. Plio-Pleistocene african climate. Science, 270(5233): 53-59.

Dennell, R., 2004. Hominid dispersals and Asian biogeography during the Lower and Early Middle Pleistocene, c. 2.0-0.5 Mya. Asian Perspectives, 43(2): 205-226.

Denton, G.H., 2000. Does an asymmetric thermohaline–ice-sheet oscillator drive 100 000-yr glacial cycles? Journal of Quaternary Science, 15(4): 301-318.

Denton, G.H. *et al.*, 2010. The Last Glacial Termination. Science, 328(5986): 1652-1656.

Dickson, R.R. and Brown, J., 1994. The production of North Atlantic Deep Water: Sources, rates, and pathways. J. Geophys. Res., 99(C6): 12319-12341.

Dokken, T.M. and Jansen, E., 1999. Rapid changes in the mechanism of ocean convection during the last glacial period. Nature, 401(6752): 458-461.

Dow, R.L., 1978. Radiolarian distribution and the late pleistocene history of the Southeastern Indian Ocean. Marine Micropaleontology, 3(3): 203-227.

Duplessy, J.-C., Labeyrie, L. and Waelbroeck, C., 2002. Constraints on the ocean oxygen isotopic enrichment between the Last Glacial Maximum and the Holocene: Paleoceanographic implications. Quaternary Science Reviews, 21(1-3): 315-330.

Duplessy, J.C. *et al.*, 1988. Deepwater source variations during the last climatic cycle and their impact on the global deepwater circulation. Paleoceanography, 3(3): 343–360.

Dymond, J., Suess, E. and Lyle, M., 1992. Barium in Deep-Sea Sediment: A Geochemical Proxy for Paleoproductivity. Paleoceanography, 7(2): 163–181.

Elderfield, H. and Ganssen, G., 2000. Past temperature and $\delta^{18}O$ of surface ocean waters inferred from foraminiferal Mg/Ca ratios. Nature, 405(6785): 442-445.

Emiliani, C., 1955. Mineralogical and chemical composition of the tests of certain pelagic foraminifera. Micropaleontology, 1(4): 377-380.

Expedition 306 Scientists, 2006. Site U1314. In: J.E.T. Channell *et al.* (Editors), Proc. IODP, 303/306. College Station TX (Integrated Ocean Drilling Program Management International, Inc.).

Fagel, N., Robert, C. and Hillaire-Marcel, C., 1996. Clay mineral signature of the NW Atlantic Boundary Undercurrent. Marine Geology, 130(1-2): 19-28.

Ferretti, P., Crowhurst, S.J., Hall, M.A. and Cacho, I., 2010. North Atlantic millennial-scale climate variability 910 to 790 ka and the role of the equatorial insolation forcing. Earth and Planetary Science Letters, 293(1-2): 28-41.

Ferretti, P., Shackleton, N.J., Rio, D. and Hall, M.A., 2005. Early-Middle Pleistocene deep circulation in the western subtropical Atlantic: southern hemisphere modulation of the North Atlantic Ocean. In: M.J. Head and P.L. Gibbard (Editors), Early-Middle Pleistocene Transitions: The Land-Ocean Evidence. Geological Society, London, pp. 131-145.

Filippelli, G.M. and Delaney, M.L., 1996. Phosphorus geochemistry of equatorial Pacific sediments. Geochimica et Cosmochimica Acta, 60(9): 1479-1495.

Flower, B.P. *et al.*, 2000. North Atlantic Intermediate to Deep Water Circulation and Chemical Stratification During the Past 1 Myr. Paleoceanography, 15(4): 388-403.

Fraile, I., Schulz, M., Mulitza, S. and Kucera, M., 2008. Predicting the global distribution of planktonic foraminifera using a

dynamic ecosystem model. Biogeosciences, 5: 891-911.

Ganopolski, A. and Rahmstorf, S., 2001. Rapid changes of glacial climate simulated in a coupled

climate model. Nature, 409(6817): 153-158.

Gildor, H. and Tziperman, E., 2000. Sea ice as the glacial cycles' Climate switch: role of seasonal and orbital forcing. Paleoceanography, 15(6): 605-615.

Gildor, H. and Tziperman, E., 2001. A sea ice climate switch mechanism for the 100-kyr glacial cycles. J. Geophys. Res., 106(C5): 9117-9133.

Goll, R.M. and Bjørklund, K.R., 1971. Radiolaria in surface sediments of the North Atlantic Ocean. Micropaleontology, 17(4): 434-454.

Goll, R.M. and Bjørklund, K.R., 1974. Radiolaria in Surface Sediments of the South Atlantic. Micropaleontology, 20(1): 38-75.

Grootes, P.M., Stuiver, M., White, J.W.C., Johnsen, S. and Jouzel, J., 1993. Comparison of oxygen isotope records from the GISP2 and GRIP Greenland ice cores. Nature, 366(6455): 552-554.

Grotefendt, K., Logemann, K., Quadfasel, D. and Ronski, S., 1998. Is the Arctic Ocean warming? Journal of Geophysical Research, 103(C12): 27679-27687.

Grousset, F., Latouche, C. and Parra, M., 1982. Late Quaternary sedimentation between the Gibbs Fracture and the Greenland Basin: Mineralogical and geochemical data. Marine Geology, 47(3-4): 303-330.

Grousset, F. and Parra, M., 1982. Contribution of mineralogical and geochemical data to the study of northeast atlantic deep quaternary sediments: trace-elements as bottom-current indicators. Sedimentary Geology, 31(1): 49-61.

Grousset, F.E. and Chesselet, R., 1986. The Holocene sedimentary regime in the northern Mid-Atlantic Ridge region. Earth and Planetary Science Letters, 78(2-3): 271-287.

Grousset, F.E., Pujol, C., Labeyrie, L., Auffret, G.r. and Boelaert, A., 2000. Were the North Atlantic Heinrich events triggered by the behavior of the European ice sheets? Geology, 28(2): 123-126.

Grützner, J. and Higgins, S.M., 2010. Threshold behaviour of millennial scale variability in deep water hydrography inferred from a 1.1 Ma long record of sediment provenance at the southern Gardar Drift. Paleoceanography, 25(4): PA4204.

Haeuselmann, P., Granger, D.E., Jeannin, P.-Y. and Lauritzen, S.-E., 2007. Abrupt glacial valley incision at 0.8 Ma dated from cave deposits in Switzerland. Geology, 35(2): 143-146.

Hagelberg, T.K., Bond, G. and deMenocal, P., 1994. Milankovitch Band Forcing of Sub-Milankovitch Climate Variability during the Pleistocene. Paleoceanography, 9(4): 545-558.

Hald, M. *et al.*, 2007. Variations in temperature and extent of Atlantic Water in the northern North Atlantic during the Holocene. Quaternary Science Reviews, 26(25-28): 3423-3440.

Hammer, Ø., 2007. Spectral analysis of a Plio-Pleistocene multispecies time series using the Mantel periodogram. Palaeogeography, Palaeoclimatology, Palaeoecology, 243(3-4): 373-377.

Hammer, Ø., Harper, D.A.T. and Ryan, P.D., 2001. PAST: Paleontological Statistics Software Package for Education and Data Analysis. Palaeontologia Electronica, 4(1).

Haslett, S.K., 1995. Pliocene-Pleistocene radiolarian biostratigraphy and palaeoceanography of the North Atlantic. Geological Society, London, Special Publications, 90(1): 217-225.

Hass, C. *et al.*, 2001. The potential of synoptic plankton analyses for paleoclimatic investigations: Five plankton groups from the Holocene Nordic Seas. In: P. Schäfer, W. Ritzrau, M. Schlüter and J. Thiede (Editors), The northern North Atlantic: A changing environment. Springer, Berlin, pp. 291-318.

Hatakeda, K. and Bjørklund, K.R., 2009. Polycystine radiolarian assemblages from IODP Expedition 306 Site U1313 and Site U1314, a preliminary result. News of Osaka Micropaleontologists, Special Volume, 14: 91-108.

Hayashi, T. *et al.*, 2010. Millennial-scale iceberg surges after intensification of Northern Hemisphere glaciation. Geochem. Geophys. Geosyst., 11(9): Q09Z20.

Hays, J.D. and Morley, J.J., 2003. The Sea of Okhotsk: A Window on the Ice Age Ocean. Deep Sea Research Part I: Oceanographic Research Papers, 50(12): 1481-1506.

Head, M.J. and Gibbard, P.L., 2005. Early-Middle Pleistocene transitions: an overview and recommendation for the defining boundary. Geological Society, London, Special Publications, 247(1): 1-18.

Hebbeln, D., Dokken, T., Andersen, E.S., Hald, M. and Elverhoi, A., 1994. Moisture supply for northern ice-sheet growth during the Last Glacial Maximum. Nature, 370(6488): 357-360.

Heinrich, H., 1988. Origin and consequences of cyclic ice rafting in the Northeast Atlantic Ocean during the past 130,000 years. Quaternary Research, 29(2): 142-152.

Helmke, J.P., Bauch, H.A. and Erlenkeuser, H., 2003. Development of glacial and interglacial conditions in the Nordic seas between 1.5 and 0.35 Ma. Quaternary Science Reviews, 22(15-17): 1717-1728.

Hemleben, C., Spindler, M. and Anderson, O.R., 1989. Modern planktic foraminifera. Springer Verlag, New York, 363 pp.

Hemming, S.R., 2004. Heinrich events: Massive late Pleistocene detritus layers of the North Atlantic and their global climate imprint. Rev. Geophys., 42: RG1005.

Hemming, S.R., 2007. Paleoceanography, physical and chemical proxies: Terrigenous Sediments. In: S.A. Elias (Editor), Encyclopedia of Quaternary Science. Elsevier, Oxford, pp. 1776-1785.

Henrich, R., 1989. Glacial/Interglacial cycles in the Norwegian Sea: sedimentology, paleoceanographyu and evolution of Late Pliocene to Quaternary Northern Hemisphere climate. In: O. Eldholm, J. Thiede, E. Taylor and e. al. (Editors), Proceedings of the ODP. Ocean Drilling Program, College Station, Texas, pp. 189-232.

Henrich, R., 1998. Dynamics of Atlantic water advection to the Norwegian-Greenland Sea - a time-slice record of carbonate distribution in the last 300 ky. Marine Geology, 145(1-2):

95-131.

Henrich, R., Baumann, K.-H., Huber, R. and Meggers, H., 2002. Carbonate preservation records of the past 3 Myr in the Norwegian-Greenland Sea and the northern North Atlantic: implications for the history of NADW production. Marine Geology, 184(1-2): 17-39.

Henrich, R. and Baumann, K.H., 1994. Evolution of the Norwegian Current and the Scandinavian Ice Sheets during the past 2.6 m.y.: evidence from ODP Leg 104 biogenic carbonate and terrigenous records. Palaeogeography, Palaeoclimatology, Palaeoecology, 108(1-2): 75-94.

Herguera, J.C., 1992. Deep-sea benthic foraminifera and biogenic opal: Glacial to postglacial productivity changes in the western equatorial Pacific. Marine Micropaleontology, 19(1-2): 79-98.

Hernández-Almeida, I. *et al.*, 2011a, submitted. A high resolution opal and radiolarian record from the subpolar North Atlantic during the Mid-Pleistocene Transition (779-1069 ky): palaeoceanographic implications. Palaeogeography, Palaeoclimatology, Palaeoecology.

Hernández-Almeida, I., Sierro, F.J., Cacho, I. and Flores, J.A., in prep. Impact of suborbital climate changes in the North Atlantic on ice-sheets dynamics at the Mid-Pleistocene Transition.

Hernández-Almeida, I., Sierro, F.J., Suarez, M., Filippelli, G.M. and Flores, A., 2011b, submitted. Caracterización e interpretación de las capas ricas en detríticos en sedimentos del Site U1314 (Atlántico Norte) during los estadios isotópicos marinos 21-19 (830-779 ka). Geogaceta.

Heslop, D., Dekkers, M.J. and Langereis, C.G., 2002. Timing and structure of the mid-Pleistocene transition: records from the loess deposits of northern China. Palaeogeography, Palaeoclimatology, Palaeoecology, 185(1-2): 133-143.

Hodell, D.A., Channell, J.E.T., Curtis, J.H., Romero, O.E. and Röhl, U., 2008. Onset of "Hudson Strait" Heinrich events in the eastern North Atlantic at the end of the middle Pleistocene transition (~640 ka)? Paleoceanography, 23(4): 1-16.

Hodell, D.A. *et al.*, 2009. Surface and deep-water hydrography on Gardar Drift (Iceland Basin) during the last interglacial period. Earth and Planetary Science Letters, 288(1-2): 10-19.

Holland, D.M., Thomas, R.H., de Young, B., Ribergaard, M.H. and Lyberth, B., 2008. Acceleration of Jakobshavn Isbrae triggered by warm subsurface ocean waters. Nature Geosciences, 1(10): 659-664.

Hönisch, B., Hemming, N.G., Archer, D., Siddall, M. and McManus, J.F., 2009. Atmospheric Carbon Dioxide Concentration Across the Mid-Pleistocene Transition. Science, 324(5934): 1551-1554.

Honjo, S. and Manganini, S.J., 1993. Annual biogenic particle fluxes to the interior of the North Atlantic Ocean; studied at 34°N 21°W and 48°N 21°W. Deep Sea Research Part II: Topical Studies in Oceanography, 40(1-2): 587-607.

Horowitz, A., 1974. The geochemistry of sediments from the northern Reykjanes Ridge and the Iceland--Faroes Ridge. Marine Geology, 17(2): 103-122.

Horowitz, A. and Cronan, D.S., 1976. The geochemistry of basal sediments from the North Atlantic Ocean. Marine Geology, 20(3): 205-228.

Huddlestun, P.F., 1984. Planktonic Foraminiferal Biostratigraphy, Deep Sea Drilling Project Leg 81. In: D.G. Roberts *et al.* (Editors), Initial Reports. DSDP, 81. U.S. Government Printing Office, Washington D.C., pp. 429-438.

Huizhong, W. and McCave, I.N., 1990. Distinguishing climatic and current effects in mid-Pleistocene sediments of Hatton and Gardar Drifts, NE Atlantic. Journal of the Geological Society, 147(2): 373-383.

Hulbe, C.L., MacAyeal, D.R., Denton, G.H., Kleman, J. and Lowell, T.V., 2004. Catastrophic ice shelf breakup as the source of Heinrich event icebergs. Paleoceanography, 19, PA1004.

Hyun, S. and Kim, S.-R., 1999. Geochemical study for provenance and paleoceanography on ODP Site 907 sediments of the North Atlantic Ocean. Geosciences Journal, 3(2): 95-106.

Hyun, S., Ortiz, J.D., Raymo, M.E. and Taira, A., 1999. Low-frequency oscillations in site 983 sediment: relationship between carbonate and productivity proxies. Proceedings of the ODP Scientific Results, 162: 197−207.

Ikeda, A., Okada, H. and Koizumi, I., 2000. Data report: late Miocene to Pleistocene diatoms from the Blake Ridge, Site 997. In: C.K. Paull, R. Matsumoto, P.J. Wallace and W.P. Dillon (Editors), Proceedings ODP, Scientific Results. Ocean Drilling Program, College Station, TX, pp. 365-376.

Imbrie, J. *et al.*, 1993. On the Structure and Origin of Major Glaciation Cycles 2. The. Paleoceanography, 8(6): 699-735.

Imbrie, J. *et al.*, 1992. On the Structure and Origin of Major Glaciation Cycles 1. Linear Responses to Milankovitch Forcing. Paleoceanography, 7(6): 701-738.

Imbrie, J. and Kipp, N.G., 1971. A new micropaleontological method for quantitative paleoclimatology. Application to a late Pleistocene Caribbean core. In: K.K. Turekian (Editor), The Late Cenozoic glacial ages. Yale University Press, New Haven, pp. 71-131.

IPCC, 2001. Contribution of working group I, II and III to the third assessment report of the Intergovernmental Panel on Climate Change, Cambridge.

Itaki, T., 2003. Depth-related radiolarian assemblage in the water-column and surface sediments of the Japan Sea. Marine Micropaleontology, 47(3-4): 253-270.

Itaki, T., Khim, B.-K. and Ikehara, K., 2008. Last glacial-Holocene water structure in the southwestern Okhotsk Sea inferred from radiolarian assemblages. Marine Micropaleontology, 67(3-4): 191-215.

Itaki, T. *et al.*, 2009. Late Pleistocene stratigraphy and palaeoceanographic implications in

northern Bering Sea slope sediments: evidence from the radiolarian species *Cycladophora davisiana*. Journal of Quaternary Science, 24(8): 856-865.

Jacot Des Combes, H. and Abelmann, A., 2009. From species abundance to opal input: Simple geometrical models of radiolarian skeletons from the Atlantic sector of the Southern Ocean. Deep Sea Research Part I: Oceanographic Research Papers, 56(5): 757-771.

James, R., 2005. Marine biogeochemical cycles. Elsevier/The Open University, Oxford, 130 pp.

Jansen, E., Bleil, U., Henrich, R., Kringstad, L. and Slettemark, B., 1988. Paleoenvironmental Changes in the Norwegian Sea and the Northeast Atlantic During the Last 2.8 m.y.: Deep Sea Drilling Project/Ocean Drilling Program Sites 610, 642, 643 and 644. Paleoceanography, 3(5): 563–581.

Jenkins, D.G., 1993. The evolution of the Cenozoic southern high- and mid-latitude planktonic foraminiferal faunas. In: J.P. Kennett and D.A. Warnke (Editors), The Antarctic Paleoenvironment: a Perspective on Global Change. Antarctic Research Series. American Geophysics Union, Washington, DC, pp. 175-194.

Jenkins, G.M. and Watts, D.G., 1968. Spectral analysis and its applications. Holden-Day, San Francisco, 525 pp.

Johannessen, T., Jansen, E., Flatoy, A. and Ravelo, A.C., 1994. The relationship between surface water masses, oceanographic fronts and paleoclimatic proxies in surface sediments of the Greenland, Iceland, Norwegian seas. In: R. Zahn, T.F. Pedersen, M.A. Kaminski and L. Labeyrie (Editors), Carbon cycling in the glacial ocean: constraints on the oceans's role in global change. Springer-Verlag, Berlin, pp. 61-85.

Johnson, G.L. and Schneider, E.D., 1969. Depositional ridges in the North Atlantic. Earth and Planetary Science Letters, 6(6): 416-422.

Jonkers, L., Brummer, G.-J.A., Peeters, F.J.C., van Aken, H.M. and De Jong, M.F., 2010a. Seasonal stratification, shell flux, and oxygen isotope dynamics of left-coiling N. pachyderma and T. quinqueloba in the western subpolar North Atlantic. Paleoceanography, 25(2): PA2204.

Jonkers, L. et al., 2010b. A reconstruction of sea surface warming in the northern North Atlantic during MIS 3 ice-rafting events. Quaternary Science Reviews, 29(15-16): 1791-1800.

Jouzel, J. *et al.*, 2007. Orbital and Millennial Antarctic Climate Variability over the Past 800,000 Years. Science, 317(5839): 793-796.

Kasten, S., Haese, R.R., Zabel, M., Rühlemann, C. and Schulz, H.D., 2001. Barium peaks at glacial terminations in sediments of the equatorial Atlantic Ocean--relicts of deglacial productivity pulses? Chemical Geology, 175(3-4): 635-651.

Kawagata, S., Hayward, B.W., Grenfell, H.R. and Sabaa, A., 2005. Mid-Pleistocene extinction of deep-sea foraminifera in the North Atlantic Gateway (ODP sites 980 and 982). Palaeogeography, Palaeoclimatology, Palaeoecology, 221(3-4): 267-291.

Kawase, M. and Sarmiento, J.L., 1986. Circulation and nutrients in middepth Atlantic waters.

J. Geophys. Res., 91(C8): 9749-9770.

Kellogg, T.B., 1977. Paleoclimatology and paleo-oceanography of the Norwegian and Greenland Seas: The last 450,000 years. Marine Micropaleontology, 2: 235-249.

Kennett, J.P., Cannariato, K.G., Hendy, I.L. and Behl, R.J., 2000. Carbon isotopic evidence for methane hydrate Instability during Quaternary interstadials. Science, 288(5463): 128-133.

Kipp, N.G., 1976. New transfer function for estimating past sea-surface conditions from sea-bed distribution of planktonic foraminiferal assemblages in the North Atlantic. In: R.M. Cline and J.D. Hays (Editors), Investigations of Late Quaternary Palaeoceanography and Palaeoclimatology. Geolgical Society of America, Boulder, pp. 3-42.

Kissel, C. *et al.*, 1999. Rapid climatic variations during marine isotopic stage 3: magnetic analysis of sediments from Nordic Seas and North Atlantic. Earth and Planetary Science Letters, 171(3): 489-502.

Kitamura, A. and Kawagoe, T., 2006. Eustatic sea-level change at the Mid-Pleistocene climate transition: new evidence from the shallow-marine sediment record of Japan. Quaternary Science Reviews, 25(3-4): 323-335.

Kleiven, H.F., Jansen, E., Curry, W.B., Hodell, D.A. and Venz, K., 2003. Atlantic Ocean thermohaline circulation changes on orbital to suborbital timescales during the mid-Pleistocene. Paleoceanography, 18.

Kling, S.A., 1978. Radiolaria. In: B.U. Haq and A. Boersma (Editors), Introduction to Marine Micropaleontology. Elsevier, New York, pp. 203–244.

Kling, S.A. and Boltovskoy, D., 1995. Radiolarian vertical distribution patterns across the Southern California current. Deep Sea Research Part I: Oceanographic Research Papers, 42(2): 191-231.

Knies, J. *et al.*, 2009. The Plio-Pleistocene glaciation of the Barents Sea-Svalbard region: a new model based on revised chronostratigraphy. Quaternary Science Reviews, 28(9-10): 812-829.

Koç, N. and Flower, B., P., 1998. High-resolution Pleistocene diatom biostratigraphy and paleoceanography of site 919 from the Irminger Basin. In: A.D. Saunders, H.C. Larsen and S.W. Wise (Editors), Proceedings of the Ocean Drilling Program, Scientific Results. Ocean Drilling Program, College Station, TX.

Koç, N., Hodell, D., A., Kleiven, H. and Labeyrie, L., 1999a. High-resolution Pleistocene diatom biostratigraphy of site 983 and correlations with isotope stratigraphy. In: M.E. Raymo, E. Jansen, P. Blum and T.D. Herbert (Editors), Proceedings of the Ocean Drilling Program, Scientific Results. Ocean Drilling Program, College Station, TX.

Koç, N., Hodell, D.A., Kleiven, H. and Labeyrie, L., 1999b. High-resolution Pleistocene diatom biostratigraphy of Site 983 and correlations with isotope stratigraphy. In: M.E. Raymo, E. Jansen, P. Blum and T.D. Herbert (Editors), ODP Scientific Results. Ocean Drilling Program, College Station, pp. 51-62.

Koç, N., Jansen, E. and Haflidason, H., 1993. Paleoceanographic reconstructions of surface ocean conditions in the Greenland, Iceland and Norwegian seas through the last 14 ka based on diatoms. Quaternary Science Reviews, 12(2): 115-140.

Koç, N. and Schrader, H., 1990. Surface Sediment Diatom Distribution and Holocene Paleotemperature Variations in the Greenland, Iceland and Norwegian Sea. Paleoceanography, 5(4): 557–580.

Kohfeld, K.E., Fairbanks, R.G., Smith, S.L. and Walsh, I.D., 1996. *Neogloboquadrina pachyderma* (sinistral coiling) as Paleoceanographic Tracers in Polar Oceans: Evidence from Northeast Water Polynya Plankton Tows, Sediment Traps, and Surface Sediments. Paleoceanography, 11(6): 679-699.

Kozdon, R., Eisenhauer, A., Weinelt, M., Meland, M.Y. and Nürnberg, D., 2009. Reassessing Mg/Ca temperature calibrations of *Neogloboquadrina pachyderma* (sinistral) using paired $\delta^{44/40}$Ca and Mg/Ca measurements. Geochem. Geophys. Geosyst., 10(3): Q03005.

Krauss, W., 1986. The North Atlantic Current. J. Geophys. Res., 91(C4): 5061-5074.

Kroopnick, P.M., 1985. The distribution of ^{13}C of ΣCO_2 in the world oceans. Deep Sea Research Part A. Oceanographic Research Papers, 32(1): 57-84.

Kucera, M. and Kennett, J.P., 2002. Causes and consequences of a middle Pleistocene origin of the modern planktonic foraminifer *Neogloboquadrina pachyderma* sinistral. Geology, 30(6): 539-542.

Kucera, M., Rosell-Melé, A., Schneider, R., Waelbroeck, C. and Weinelt, M., 2005a. Multiproxy approach for the reconstruction of the glacial ocean surface (MARGO). Quaternary Science Reviews, 24(7-9): 813-819.

Kucera, M. *et al.*, 2005b. Reconstruction of sea-surface temperatures from assemblages of planktonic foraminifera: multi-technique approach based on geographically constrained calibration data sets and its application to glacial Atlantic and Pacific Oceans. Quaternary Science Reviews, 24(7-9): 951-998.

Larrasoaña, J.C., Roberts, A.P., Rohling, E.J., Winklhofer, M. and Wehausen, R., 2003. Three million years of monsoon variability over the northern Sahara. Climate Dynamics, 21(7): 689-698.

Laskar, J. *et al.*, 2004. A long-term numerical solution for the insolation quantities of Â the Â Earth. A&A, 428(1): 261-285.

Latimer, J.C. and Filippelli, G.M., 2001. Terrigenous Input and Paleoproductivity in the Southern Ocean. Paleoceanography, 16(6): 627-643.

Latouche, C. and Parra, M., 1976. Mineralogie et geochimie des sediments quaternaires de l'Ocean atlantique nord-oriental (Mer de Novege -- Golfe de Cascogne) -- Essais d'interpretations sedimentologiques. Marine Geology, 22(1): 33-69.

Latouche, C. and Parra, M., 1979. La sedimentation au Quaternaire recent dans le "Northwest Atlantic Mid-Ocean Canyon" - Apport des donnees mineralogiques et geochimiques. Marine Geology, 29(1-4): 137-164.

Lea, D.W., Martin, P.A., Pak, D.K. and Spero, H.J., 2002. Reconstructing a 350 ky history of sea level using planktonic Mg/Ca and oxygen isotope records from a Cocos Ridge core. Quaternary Science Reviews, 21(1-3): 283-293.

Lea, D.W., Mashiotta, T.A. and Spero, H.J., 1999. Controls on magnesium and strontium uptake in planktonic foraminifera determined by live culturing. Geochimica et Cosmochimica Acta, 63(16): 2369-2379.

Leinen, M., 1985. Techniques for determining opal in deep-sea sediments: A comparison of radiolarian counts and x-ray diffraction data. Marine Micropaleontology, 9(5): 375-383.

Leuschner, D.C. and Sirocko, F., 2000. The low-latitude monsoon climate during Dansgaard-Oeschger cycles and Heinrich Events. Quaternary Science Reviews, 19(1-5): 243-254.

Link, D.D., Kingston, H.M. and Walter, P.J., 1998. Development and validation of the new EPA microwave-assisted leach method 3051A. Environmental Science and Technology, 32: 3628-3632.

Lisiecki, L.E. and Raymo, M.E., 2005. A Pliocene-Pleistocene stack of 57 globally distributed benthic $\delta^{18}O$ records. Paleoceanography, 20: PA1003.

Lisitzin, A.P., 1972. Sedimentation in the world ocean. Society of economic paleontologist and mineralogists. Special publication, 17, 218 pp.

Locarnini, R.A., Mishonov, A.V., Antonov, J.I., Boyer, T.P. and Garcia, H.E., 2006. World Ocean Atlas 2005, Volume 1: Temperature. U.S. Government Printing Office, Washington D.C.

Lüer, V., 2003. Quaternary Radiolarians from offshore Eastern New Zealand, Southwestern Pacific (ODP Leg 181, Site 1123): importance for correlation and identification of climatic changes, University of Bremen, Bremen, 103 pp.

MacAyeal, D.R., 1993a. Binge/Purge Oscillations of the Laurentide Ice Sheet as a Cause of the North Atlantic Heinrich Events. Paleoceanography, 8(6): 775–784.

MacAyeal, D.R., 1993b. A low-order model of the Heinrich event cycle. Paleoceanography, 8(6): 767-773.

Malmgren, B.A., Kucera, M., Nyberg, J. and Waelbroeck, C., 2001. Comparison of Statistical and Artificial Neural Network Techniques for Estimating Past Sea Surface Temperatures from Planktonic Foraminifer Census Data. Paleoceanography, 16(5): 520-530.

Marchitto, T.M., Jr., Oppo, D.W. and Curry, W.B., 2002. Paired benthic foraminiferal Cd/Ca and Zn/Ca evidence for a greatly increased presence of Southern Ocean Water in the glacial North Atlantic. Paleoceanography, 17(3): 1038.

Marino, M., Maiorano, P. and Lirer, F., 2008. Changes in calcareous nannofossil assemblages during the Mid-Pleistocene Revolution. Marine Micropaleontology, 69(1): 70-90.

Marshall, S.J. and Koutnik, M.R., 2006. Ice sheet action versus reaction: Distinguishing between Heinrich events and Dansgaard-Oeschger cycles in the North Atlantic. Paleoceanography, 21: PA2021.

Maslin, M.A. and Ridgwell, A.J., 2005. Mid-Pleistocene revolution and the 'eccentricity myth'. Geological Society, London, Special Publications, 247(1): 19-34.

Maslin, M.A., Shackleton, N.J. and Pflaumann, U., 1995. Surface water temperature, salinity, and density changes in the Northeast Atlantic during the Last 45,000 Years: Heinrich Events, deep water formation, and climatic rebounds. Paleoceanography, 10(3): 527–544.

Matul, A., Abelmann, A., Nürnberg, D. and Tiedemann, R., 2009. Stratigraphy and major paleoenvironmental changes in the Sea of Okhotsk during the last million years inferred from radiolarian data. Oceanology, 49(1): 93-100.

Matul, A., G., 1989a. Radiolarian distribution in the surface sediment layer in the north Atlantic. Oceanology, 29(6): 992-998.

Matul, A., Yushina, I.G. and Emelyanov, E.M., 2002. On the Late Quaternary paleohydrological parameters of the Labrador Sea based on radiolarians. Oceanology, 42(2): 262-266.

Matul, A.G., 1989b. Radiolarian distribution in the surface sediment layer in the north Atlantic. Oceanology, 29(6): 992-998.

Matul, A.G., 1994a. Late Quaternary paleoceanology of the North Atlantic based on radiolaria analysis data. Oceanology, 34(4): 550-555.

Matul, A.G., 1994b. On the problem of paleoceanological evolution of the Reykjanes Ridge region (North Atlantic) during the last deglaciation based on the study of radiolarian. Oceanology, 34(6): 806-814.

Matul, A.G. and Yushina, I.G., 1999. Radiolarians in North Atlantic sediment. In: R.F. Spielhagen, M.S. Barash, G.I. Ivanov and J. Thiede (Editors), German-Russian Cooperation: Biogeographic and biostratigraphic investigations On selected sediment cores from the Eurasian continental margin and marginal seas to analyze the Late Quaternary climatic variability. Ber. Polarforsch.

Mayewski, P.A. *et al.*, 2004. Holocene climate variability. Quaternary Research, 62(3): 243-255.

McCartney, M.S., 1992. Recirculating components to the deep boundary current of the northern North Atlantic. Progress In Oceanography, 29(4): 283-383.

McCave, I.N. and Tucholke, B.E., 1986. Deep current controlled sedimentation in the western North Atlantic. In: P.R. Vogt and B.E. Tucholke (Editors), The western North Atlantic region. Geological Society of America, Boulder, pp. 451-468

McClymont, E.L., Rosell-Melé, A., Haug, G.H. and Lloyd, J.M., 2008. Expansion of subarctic water masses in the North Atlantic and Pacific oceans and implications for mid-Pleistocene ice sheet growth. Paleoceanography, 23: PA4214.

McCorkle, D.C., Keigwin, L.D., Corliss, B.H. and Emerson, S.R., 1990. The influence of microhabitats on the carbon isotopic composition of deep-sea benthic foraminifera. Paleoceanography, 5(2): 161-185.

McIntyre, A. and Molfino, B., 1996. Forcing of Atlantic Equatorial and Subpolar Millennial

Cycles by Precession. Science, 274(5294): 1867-1870.

McIntyre, A., Ruddiman, W.F., Karlin, K. and Mix, A.C., 1989. Surface Water Response of the Equatorial Atlantic Ocean to Orbital Forcing. Paleoceanography, 4(1): 19-55.

McIntyre, K., Delaney, M.L. and Ravelo, A.C., 2001. Millennial-Scale Climate Change and Oceanic Processes in the Late Pliocene and Early Pleistocene. Paleoceanography, 16(5): 535-543.

McIntyre, K., Ravelo, A.C. and Delaney, M.L., 1999. North Atlantic Intermediate Waters in the Late Pliocene to Early Pleistocene. Paleoceanography, 14(3): 324–335.

McManus, J.F. *et al.*, 1994. High-resolution climate records from the North Atlantic during the last interglacial. Nature, 371(6495): 326-329.

McManus, J.F., Oppo, D.W. and Cullen, J.L., 1999. A 0.5-Million-Year Record of Millennial-Scale Climate Variability in the North Atlantic. Science, 283(5404): 971-975.

McMillen, K.J. and Casey, R.E., 1978. Distribution of living polycystine radiolarians in the Gulf of Mexico and Caribbean Sea, and comparison with the sedimentary record. Marine Micropaleontology, 3(2): 121-145.

McNabb, J., 2005. Hominins and the Early-Middle Pleistocene transition: evolution, culture and climate in Africa and Europe. In: M.J. Head and P.L. Gibbard (Editors), Early-Middle Pleistocene Transitions: The Land-Ocean Evidence. Geological Society, London, pp. 287-304.

Medina-Elizalde, M. and Lea, D.W., 2005. The Mid-Pleistocene Transition in the Tropical Pacific. Science, 310(5750): 1009-1012.

Meland, M.Y., Jansen, E. and Elderfield, H., 2005. Constraints on SST estimates for the northern North Atlantic/Nordic Seas during the LGM. Quaternary Science Reviews, 24(7-9): 835-852.

Meland, M.Y. *et al*., 2006. Mg/Ca ratios in the planktonic foraminifer Neogloboquadrina pachyderma (sinistral) in the northern North Atlantic/Nordic Seas. Geochem. Geophys. Geosyst., 7(6): Q06P14.

Miao, Q., Thunell, R.C. and Anderson, D.M., 1994. Glacial-Holocene Carbonate Dissolution and Sea Surface Temperatures in the South China and Sulu Seas. Paleoceanography, 9(2): 269-290.

Milankovitch, M., 1941. Canon of insolation and the ice-age problem. Royal Serbian Sciences Special Publication. Section of Mathematical and Natural Sciences, 33: 633.

Molfino, B. and McIntyre, A., 1990. Precessional Forcing of Nutricline Dynamics in the Equatorial Atlantic. Science, 249(4970): 766-769.

Molina-Cruz, A., 1977a. Radiolarian assemblages and their relationship to the oceanography of the subtropical southeastern Pacific. Marine Micropaleontology, 2: 315-352.

Molina-Cruz, A., 1984. Radiolaria as indicators of upwelling processes: The Peruvian connection. Marine Micropaleontology, 9(1): 53-75.

Molina-Cruz, A., 1988. Late Quaternary oceanography of the mouth of the Gulf of California:

the Polycystine connection. Paleoceanography, 3(4): 447-459.

Molina-Cruz, A., 1991. Holocene palaeo-oceanography of the northern Iceland Sea, indicated by Radiolaria and sponge spicules. Journal of Quaternary Science, 6(4): 303-312.

Molina-Cruz, A. and Bernal-Ramirez, R.G., 1996. Distribution of Radiolaria in surface sediments and its relation to the oceanography of the Iceland and Greenland Seas. Sarsia, 81: 315-328.

Molina-Cruz, A., Welling, L. and Caudillo-Bohorquez, A., 1999. Radiolarian distribution in the water column, southern Gulf of California, and its implication in thanatocoenose constitution. Marine Micropaleontology, 37(2): 149-171.

Morley, J., Pisias, N. and Leinen, M., 1987. Late Pleistocene Time Series of Atmospheric and Oceanic Variables Recorded in Sediments from the Subarctic Pacific. Paleoceanography, 2(1): 49-62.

Morley, J.J., 1983. Identification of density-stratified waters in the late-Pleistocene North Atlantic: A faunal derivation. Quaternary Research, 20(3): 374-386.

Morley, J.J. and Dworetzky, B.A., 1991. Evolving Pliocene-Pleistocene climate: A North Pacific perspective. Quaternary Science Reviews, 10(2-3): 225-237.

Morley, J.J. and Hays, J.D., 1979. Cycladophora davisiana: a stratigraphic tool for Pleistocene North Atlantic and interhemispheric correlation. Earth and Planetary Science Letters, 44(3): 383-389.

Morley, J.J. and Hays, J.D., 1983. Oceanographic conditions associated with high abundances of the radiolarian *Cycladophora davisiana*. Earth and Planetary Science Letters, 66: 63-72.

Morley, J.J., Hays, J.D. and Robertson, J.H., 1982. Stratigraphic framework for the late Pleistocene in the northwest Pacific Ocean. Deep Sea Research Part A. Oceanographic Research Papers, 29(12): 1485-1499.

Moros, M. *et al.*, 2002. Were glacial iceberg surges in the North Atlantic triggered by climatic warming? Marine Geology, 192(4): 393-417.

Moros, M. *et al.*, 2004. Sea surface temperatures and ice rafting in the Holocene North Atlantic: climate influences on northern Europe and Greenland. Quaternary Science Reviews, 23(20-22): 2113-2126.

Mortlock, R.A. and Froelich, P.N., 1989. A simple method for the rapid determination of biogenic opal in pelagic marine sediments. Deep Sea Research Part A. Oceanographic Research Papers, 36(9): 1415-1426.

Mudelsee, M. and Schulz, M., 1997. The Mid-Pleistocene climate transition: onset of 100 ka cycle lags ice volume build-up by 280 ka. Earth and Planetary Science Letters, 151(1-2): 117-123.

Mudelsee, M. and Stattegger, K., 1997. Exploring the structure of the mid-Pleistocene revolution with advanced methods of time-series analysis. Geologische Rundschau, 86(2): 499-511.

Muttoni, G. *et al.*, 2003. Onset of major Pleistocene glaciations in the Alps. Geology, 31(11): 989-992.

Muttoni, G., Scardia, G. and Kent, D.V., 2010. Human migration into Europe during the late Early Pleistocene climate transition. Palaeogeography, Palaeoclimatology, Palaeoecology, 296(1-2): 79-93.

Nave, S. *et al.*, 2007. Primary productivity response to Heinrich events in the North Atlantic Ocean and Norwegian Sea. Paleoceanography, 22.

Nesbitt, H.W., Markovics, G. and price, R.C., 1980. Chemical processes affecting alkalis and alkaline earths during continental weathering. Geochimica et Cosmochimica Acta, 44(11): 1659-1666.

Nigrini, C. and Moore, T.C., Jr., 1979. A guide to modern Radiolaria. Special Publication, 16. Cushman Foundation for Foraminiferal Research.

Nimmergut, A. and Abelmann, A., 2002. Spatial and seasonal changes of radiolarian standing stocks in the Sea of Okhotsk. Deep Sea Research Part I: Oceanographic Research Papers, 49(3): 463-493.

Nürnberg, D., 1995. Magnesium in tests of *Neogloboquadrina pachyderma* sinistral from high northern and southern latitudes. Journal of Foraminiferal Research, 25(4): 350-368.

Nürnberg, D., Bijma, J. and Hemleben, C., 1996a. Assessing the reliability of magnesium in foraminiferal calcite as a proxy for water mass temperatures. Geochimica et Cosmochimica Acta, 60(5): 803-814.

Nyland, B.F., Jansen, E., Elderfield, H. and Andersson, C., 2006. *Neogloboquadrina pachyderma* (dex. and sin.) Mg/Ca and $\delta^{18}O$ records from the Norwegian Sea. Geochem. Geophys. Geosyst., 7(10): Q10P17.

O'Regan, H.J., Bishop, L.C., Lamb, A., Elton, S. and Turner, A., 2005. Large mammal turnover in Africa and the Levant between 1.0 and 0.5 Ma. In: M.J. Head and P.L. Gibbard (Editors), Early-Middle Pleistocene Transitions: The Land-Ocean Evidence. Geological Society, London, pp. 231-249.

Oeschger, H., Beer, J., Siegenthaler, U. and Stauffer, B., 1984. Late glacial climate history from ice cores. In: J.E. Hansen and T. Takahashi (Editors), Climate Porcesses and Cliamte Sensitivity. American Geophysical Union, Washington D.C., pp. 299-306.

Okazaki, Y., Takahashi, K., Itaki, T. and Kawasaki, Y., 2004. Comparison of radiolarian vertical distributions in the Okhotsk Sea near the Kuril Islands and in the northwestern North Pacific off Hokkaido Island. Marine Micropaleontology, 51(3-4): 257-284.

Okazaki, Y. *et al.*, 2003a. Radiolarians under the seasonally sea-ice covered conditions in the Okhotsk Sea: flux and their implications for paleoceanography. Marine Micropaleontology, 49(3): 195-230.

Olson, H.C. and Smart, C.W., 2004. Pleistocene climatic history reflected in planktonic foraminifera from ODP Site 1073 (Leg 174A), New Jersey margin, NW Atlantic Ocean. Marine Micropaleontology, 51(3-4): 213-238.

Oppo, D., 1997. Millennial Climate Oscillations. Science, 278(5341): 1244-1246.

Oppo, D.W. and Fairbanks, R.G., 1987. Variability in the deep and intermediate water circulation of the Atlantic Ocean during the past 25,000 years: Northern Hemisphere modulation of the Southern Ocean. Earth and Planetary Science Letters, 86(1): 1-15.

Oppo, D.W., Horowitz, M. and Lehman, S.J., 1997. Marine core evidence for reduced deep water production during Termination 2 followed by a relatively stable substage 5e. Paleoceanography, 12(1): 51-63.

Oppo, D.W., Keigwin, L.D., McManus, J.F. and Cullen, J.L., 2001. Persistent Suborbital Climate Variability in Marine Isotope Stage 5 and Termination II. Paleoceanography, 16(3): 280-292.

Oppo, D.W. and Lehman, S.J., 1993. Mid-Depth Circulation of the Subpolar North Atlantic During the Last Glacial Maximum. Science, 259(5098): 1148-1152.

Oppo, D.W. and Lehman, S.J., 1995. Suborbital Timescale Variability of North Atlantic Deep Water During the Past 200,000 Years. Paleoceanography, 10(5): 901–910.

Oppo, D.W., McManus, J.F. and Cullen, J.L., 1998. Abrupt climate events 500,000 to 340,000 years ago: Evidence from subpolar North Atlantic sediments. Science, 279(5355): 1335-1338.

Overpeck, J.T. and Cole, J.E., 2006. Abrupt change in Earth's climate system. Annual review of environment and resources, 31(1): 1-31.

Paillard, D.L., L. Yiou, P., 1996. Macintosh program performs time-series analysis. Eos Trans. AGU, 77: 379.

Palombo, M.R., 2009. A scenario of human dispersal in the northwestern Mediterranean throughout the Early to Middle Pleistocene. Quaternary International, 223-224: 179-194.

Parra, M., Puechmaille, C. and Carruesco, C., 1981. Strontium as a marker of the origin of biogenic and terrigenous materials and as a hydrodynamic tracer in the deep-sea North Atlantic area. Chemical Geology, 34(1-2): 91-102.

Parrenin, F. and Paillard, D., 2003. Amplitude and phase of glacial cycles from a conceptual model. Earth and Planetary Science Letters, 214(1-2): 243-250.

Peck, V.L., Hall, I.R., Zahn, R. and Elderfield, H., 2008. Millennial-scale surface and subsurface paleothermometry from the northeast Atlantic, 55-8 ka BP. Paleoceanography, 23(3): PA3221.

Peck, V.L. *et al.*, 2006. High resolution evidence for linkages between NW European ice sheet instability and Atlantic Meridional Overturning Circulation. Earth and Planetary Science Letters, 243(3-4): 476-488.

Pena, L.D., Calvo, E., Cacho, I., Eggins, S. and Pelejero, C., 2005. Identification and removal of Mn-Mg-rich contaminant phases on foraminiferal tests: Implications for Mg/Ca past temperature reconstructions. Geochem. Geophys. Geosyst., 6: Q09P02.

Petrushevskaya, M.G., 1971a. Spumellarian and Nasselarian Radiolaria in the plankton and

bottom sediments of the Central Pacific. In: B.M. Funnel and W.R. Riedel (Editors), Micropaleontology of Oceans. Cambridge University Press, Cambridge, pp. 309-317.

Petrushevskaya, M.G. and Bjørklund, K.R., 1974. Radiolarians in Holocene sediments of the Norwegian-Greenland Seas. Sarsia, 57(4): 33-46.

Pflaumann, U., Duprat, J., Pujol, C. and Labeyrie, L.D., 1996. SIMMAX: A modern analog technique to deduce Atlantic sea surface temperatures from planktonic foraminifera in deep-sea sediments. Paleoceanography, 11(1): 15-35.

Pflaumann, U. *et al.*, 2003. Glacial North Atlantic: Sea-surface conditions reconstructed by GLAMAP 2000. Paleoceanography, 18(3): 1065.

Pielou, E.C., 1975. Ecological diversity. Wiley, New York, 165 pp.

Pisias, N.G. and Moore Jr, T.C., 1981. The evolution of Pleistocene climate: A time series approach. Earth and Planetary Science Letters, 52(2): 450-458.

Poore, R.Z. and Berggren, W.A., 1975. Late Cenozoic planktonic foraminiferal biostratigraphy and paleoclimatology of Hatton-Rockall Basin; DSDP Site 116. Journal of Foraminiferal Research, 5(4): 270-293.

Potts, R. and Deino, A., 1995. Mid-Pleistocene Change in Large Mammal Faunas of East Africa. Quaternary Research, 43(1): 106-113.

Prell, W.L., 1982. Oxygen and carbon isotope stratigraphy for the Quaternary of Hole 502B: evidence for two modes of isotopic variability. In: W.L. Prell and J.L. Gardner (Editors), Initial Reptorts. Deep Sea Drilling Project, pp. 455–464.

Prins, M.A. *et al.*, 2002. Ocean circulation and iceberg discharge in the glacial North Atlantic: Inferences from unmixing of sediment size distributions. Geology, 30(6): 555-558.

Rahmstorf, S., 2002. Ocean circulation and climate during the past 120,000 years. Nature, 419(6903): 207-214.

Rasmussen, T.L. and Thomsen, E., 2004. The role of the North Atlantic Drift in the millennial timescale glacial climate fluctuations. Palaeogeography, Palaeoclimatology, Palaeoecology, 210(1): 101-116.

Raymo, M.E., Ganley, K., Carter, S., Oppo, D.W. and McManus, J., 1998. Millennial-scale climate instability during the early Pleistocene epoch. Nature, 392(6677): 699-702.

Raymo, M.E. and Nisancioglu, K., 2003. The 41 kyr world: Milankovitch's other unsolved mystery. Paleoceanography, 18: 1011.

Raymo, M.E., Oppo, D.W. and Curry, W., 1997. The Mid-Pleistocene Climate Transition: A Deep Sea Carbon Isotopic Perspective. Paleoceanography, 12(4): 546-559.

Raymo, M.E. *et al.*, 2004. Stability of North Atlantic water masses in face of pronounced climate variability during the Pleistocene. Paleoceanography, 19: PA2008.

Reid, P.C. *et al.*, 2007. A biological consequence of reducing Arctic ice cover: arrival of the Pacific diatom *Neodenticula seminae* in the North Atlantic for the first time in 800000 years. Global Change Biology, 13(9): 1910-1921.

Reynaud, T.H., Weaver, A.J. and Greatbatch, R.J., 1995. Summer mean circulation of the

northwestern Atlantic Ocean. J. Geophys. Res., 100(C1): 779-816.

Rogachev, K.A., 2000. Recent variability in the Pacific western subarctic boundary currents and Sea of Okhotsk. Progress in Oceanography, 47(2-4): 299-336.

Rohling, E. and Cooke, S., 2003. Stable oxygen and carbon isotopes in foraminiferal carbonate shells. In: B.K.S. Gupta (Editor), Modern Foraminifera. Springer Netherlands, pp. 239-258.

Rosenthal, Y., Boyle, E.A. and Slowey, N., 1997b. Temperature control on the incorporation of magnesium, strontium, fluorine, and cadmium into benthic foraminiferal shells from Little Bahama Bank: Prospects for thermocline paleoceanography. Geochimica et Cosmochimica Acta, 61(17): 3633-3643.

Ruddiman, W.F., 1969. Recent Planktonic Foraminifera: Dominance and Diversity in North Atlantic Surface Sediments. Science, 164(3884): 1164-1167.

Ruddiman, W.F., 1977. Late Quaternary deposition of ice-rafted sand in the subpolar North Atlantic (lat 40º to 65ºN). Geological Society of America Bulletin, 88(12): 1813-1827.

Ruddiman, W.F., 2001. Earth's climate; past and future. W. H. Freeman, New York 465 pp.

Ruddiman, W.F., 2003. Orbital insolation, ice volume, and greenhouse gases. Quaternary Science Reviews, 22(15-17): 1597-1629.

Ruddiman, W.F. and McIntyre, A., 1981b. The mode and mechanism of the last deglaciation: Oceanic evidence. Quaternary Research, 16(2): 125-134.

Ruddiman, W.F. and McIntyre, A., 1981c. Oceanic Mechanisms for Amplification of the 23,000-Year Ice-Volume Cycle. Science, 212(4495): 617-627.

Ruddiman, W.F. and McIntyre, A., 1984. Ice-age thermal response and climatic role of the surface Atlantic Ocean, 40ºN to 63ºN. Geological Society of America Bulletin, 95(4): 381-396.

Ruddiman, W.F., McIntyre, A., Niebler-Hunt, V. and Durazzi, J.T., 1980. Oceanic evidence for the mechanism of rapid northern hemisphere glaciation. Quaternary Research, 13(1): 33-64.

Ruddiman, W.F., Raymo, M.E., Martinson, D.G., Clement, B.M. and Backman, J., 1989. Pleistocene evolution: Northern hemisphere ice sheets and North Atlantic Ocean. Paleoceanography, 4(4): 353-412.

Rutherford, S., D'Hondt, S. and Prell, W., 1999. Environmental controls on the geographic distribution of zooplankton diversity. Nature, 400(6746): 749-753.

Ruttenberg, K.C., 1992. Development of a sequential extraction method for different forms of phosphorus in marine sediments. Limnology and Oceanography, 37(7): 1460-1482.

Ruttenberg, K.C. and Berner, R.A., 1993. Authigenic apatite formation and burial in sediments from non-upwelling, continental margin environments. Geochimica et Cosmochimica Acta, 57(5): 991-1007.

Samtleben, C. *et al.*, 1995. Plankton in the Norwegian-Greenland Sea: from living communities to sediment assemblages —an actualistic approach. Geologische Rundschau, 84(1):

108-136.

Sarnthein, M., Pflaumann, U. and Weinelt, M., 2003. Past extent of sea ice in the northern North Atlantic inferred from foraminiferal paleotemperature estimates. Paleoceanography, 18(2): 25-1 - 25-8.

Sarnthein, M. *et al.*, 2000. Fundamental modes and abrupt changes in North Atlantic circulation and climate over the last 60 ky-concepts, reconstruction and numerical modeling. In: P. Schäfer, W. Ritzrau, M. Schlüter and J. Thiede (Editors), The Northern Atlantic: A Changing Environment. Springer, Berlin, pp. 365-410.

Sato, T., Kameo, K. and Mita, I., 1999. Validity of the latest Cenozoic calcareous nannofossil datums and its application to the tephrochronology,. Earth Science, 53(4): 265-274.

Sautter, L.R. and Thunell, R.C., 1989. Seasonal succession of planktonic foraminifera; results from a four-year time-series sediment trap experiment in the Northeast Pacific. Journal of Foraminiferal Research, 19(4): 253-267.

Scourse, J.D., Hall, I.R., McCave, I.N., Young, J.R. and Sugdon, C., 2000. The origin of Heinrich layers: evidence from H2 for European precursor events. Earth and Planetary Science Letters, 182(2): 187-195.

Scharek, R. *et al.*, 1994. The transition from winter to early spring in the eastern Weddell Sea, Antarctica: Plankton biomass and composition in relation to hydrography and nutrients. Deep Sea Research Part I: Oceanographic Research Papers, 41(8): 1231-1250.

Schefuß, E., Schouten, S., Jansen, J.H.F. and Sinninghe Damste, J.S., 2003. African vegetation controlled by tropical sea surface temperatures in the mid-Pleistocene period. Nature, 422(6930): 418-421.

Schiebel, R. and Hemleben, C., 2000. Interannual variability of planktic foraminiferal populations and test flux in the eastern North Atlantic Ocean (JGOFS). Deep Sea Research Part II: Topical Studies in Oceanography, 47(9-11): 1809-1852.

Schiebel, R., Waniek, J., Bork, M. and Hemleben, C., 2001. Planktic foraminiferal production stimulated by chlorophyll redistribution and entrainment of nutrients. Deep-Sea Research I, 48: 721- 740.

Schlitzer, R., 2008. Ocean Data View, http://odv.awi.de.

Schmidt, G.A., 1999. Forward Modeling of Carbonate Proxy Data from Planktonic Foraminifera Using Oxygen Isotope Tracers in a Global Ocean Model. Paleoceanography, 14(4): 482-497.

Schmieder, F., von Dobeneck, T. and Bleil, U., 2000. The Mid-Pleistocene climate transition as documented in the deep South Atlantic Ocean: initiation, interim state and terminal event. Earth and Planetary Science Letters, 179(3-4): 539-549.

Schmitz, W.J., Jr. and McCartney, M.S., 1993. On the North Atlantic Circulation. Rev. Geophys., 31(1): 29-49.

Schulz, H., von Rad, U. and Erlenkeuser, H., 1998. Correlation between Arabian Sea and Greenland climate oscillations of the past 110,000 years. Nature, 393(6680): 54-57.

Sejrup, H.P. *et al.*, 2000. Quaternary glaciations in southern Fennoscandia: evidence from southwestern Norway and the northern North Sea region. Quaternary Science Reviews, 19(7): 667-685.

Shackleton, N., J., Berger, A. and Peltier, W., R., 1990. An alternative astronomical calibration of the lower Pleistocene timescale based on ODP Site 677. Transactions of the Royal Society of Edinburgh: Earth Sciences, 81: 251-261.

Shackleton, N.J., 1987. Oxygen isotopes, ice volume and sea level. Quaternary Science Reviews, 6(3-4): 183-190.

Shackleton, N.J., Imbrie, J. and Hall, M.A., 1983. Oxygen and carbon isotope record of East Pacific core V19-30: implications for the formation of deep water in the late Pleistocene North Atlantic. Earth and Planetary Science Letters, 65(2): 233-244.

Shackleton, N.J. and Pisias, N.G., 1985. Atmospheric carbon dioxide, orbital forcing, and climate. In: E.T. Sundquist and W.S. Broecker (Editors), The Carbon cycle and atmospheric CO2 : natural variations, Archean to present. American Geophysical Union, Washington, D.C.

Shaffer, G., Olsen, S.M. and Bjerrum, C.J., 2004. Ocean subsurface warming as a mechanism for coupling Dansgaard-Oeschger climate cycles and ice-rafting events. Geophys. Res. Lett., 31(24): L24202.

Shannon, C.E. and Weaver, W., 1963. The mathematical theory of communication. University of Illinois Press, 144 pp.

Shimada, C., Sato, T., Toyoshima, S., Yamasaki, M. and Tanimura, Y., 2008. Paleoecological significance of laminated diatomaceous oozes during the middle-to-late Pleistocene, North Atlantic Ocean (IODP Site U1304). Marine Micropaleontology, 69(2): 139-150.

Short, D.A., Mengel, J.G., Crowley, T.J., Hyde, W.T. and North, G.R., 1991. Filtering of milankovitch cycles by earth's geography. Quaternary Research, 35(2): 157-173.

Siddall, M. *et al.*, 2003. Sea-level fluctuations during the last glacial cycle. Nature, 423(6942): 853-858.

Sierro, F.J. *et al.*, 2009. Phase relationship between sea level and abrupt climate change. Quaternary Science Reviews, 28(25-26): 2867-2881.

Simstich, J., Sarnthein, M. and Erlenkeuser, H., 2003. Paired $\delta^{18}O$ signals of *Neogloboquadrina pachyderma* (s) and *Turborotalita quinqueloba* show thermal stratification structure in Nordic Seas. Marine Micropaleontology, 48(1-2): 107-125.

Skinner, L.C., Shackleton, N.J. and Elderfield, H., 2003. Millennial-scale variability of deep-water temperature and $\delta^{18}O_{dw}$ indicating deep-water source variations in the Northeast Atlantic, 0–34 cal. ka BP. Geochem. Geophys. Geosyst., 4(12): 1098.

Smith, L.M. *et al.*, 2005. Temperature reconstructions for SW and N Iceland waters over the last 10 cal ka based on $\delta^{18}O$ records from planktic and benthic Foraminifera. Quaternary Science Reviews, 24(14-15): 1723-1740.

Srinivasan, M.S. and Kennett, J.P., 1974. Secondary calcification of the planktonic foraminifer

Neogloboquadrina pachyderma as a climatic index. Science, 186(4164): 630-632.

Stadum, C.J. and Ling, H.-Y., 1969. Tripylean Radiolaria in Deep-Sea Sediments of the Norwegian Sea. Micropaleontology, 15(4): 481-489.

Stangeew, E., 2001. Distribution and isotopic composition of living planktonic foraminifera *N. pachyderma* (sinistral) and *T. quinqueloba* in the high latitude North Atlantic, Christian-Albrechts-Universität zu Kiel, Kiel, Germany, 98 pp.

Swanberg, N.R. and Eide, L.K., 1992. The radiolarian fauna at the ice edge in the Greenland Sea during summer, 1988. Journal of Marine Research, 50: 297-320.

Swift, J.H., 1984. The circulation of the Denmark Strait and Iceland-Scotland overflow waters in the North Atlantic. Deep Sea Research Part A. Oceanographic Research Papers, 31(11): 1339-1355.

Swift, J.H. and Aagaard, K., 1981. Seasonal transitions and water mass formation in the Iceland and Greenland seas. Deep Sea Research Part A. Oceanographic Research Papers, 28(10): 1107-1129.

Takahashi, K., 1991. Radiolaria: flux, ecology, and taxonomy in the Pacific and Atlantic. In: S. Honjo (Editor), Ocean Biocenosis, Series No. 3. Woods Hole Oceanographic Institution Press, pp. 1-303.

Takahashi, K., 1994. From modern flux to paleoflux: assessment from sinking assemblages to thanatocoenosis. In: R. Zahn, T.F. Pedersen, M.A. Kaminski and L. Labeyrie (Editors), Carbon Cycling in the Glacial Ocean: Constraints on the Ocean‘s Role in Global Change Global Environmental Change. Springer-Verlag, Berlin, pp. 413-424.

Takahashi, K., 1997. Time-series fluxes of Radiolaria in the eastern subarctic Pacific Ocean. News of Osaka Micropaleonotlogists, Special Volume(10): 299-309.

Takahashi, K. and Honjo, S., 1983. Radiolarian skeletons: size, weight, sinking speed, and residence time in tropical pelagic oceans. Deep Sea Research Part A. Oceanographic Research Papers, 30(5): 543-568.

Takahashi, K., Hurd, D.C. and Honjo, S., 1983. Phaeodarian Skeletons: Their Role in Silica Transport to the Deep Sea. Science, 222(4624): 616-618.

Takahashi, O., Mayama, S. and Matsuoka, A., 2003. Host-symbiont associations of polycystine Radiolaria: epifluorescence microscopic observation of living Radiolaria. Marine Micropaleontology, 49(3): 187-194.

Thomas, E., Booth, L., Maslin, M. and Shackleton, N.J., 1995. Northeastern Atlantic Benthic Foraminifera During the Last 45,000 Years: Changes in Productivity Seen from the Bottom Up. Paleoceanography, 10(3): 545-562.

Thomson, G. and Bowen, V.T., 1969. Analysis of coccolith ooze in the deep tropical

Atlantic. Journal of Marine Research, 57(1): 32-38.

Thomson, J. *et al.*, 1986. The behaviour of manganese in Atlantic carbonate sediments. Geochimica et Cosmochimica Acta, 50(8): 1807-1818.

Thouveny, N. *et al.*, 2000. Rock magnetic detection of distal ice-rafted debries: clue for the

identification of Heinrich layers on the Portuguese margin. Earth and Planetary Science Letters, 180(1-2): 61-75.

Thunell, R.C., 1976. Optimum indices of calcium carbonate dissolution, in deep-sea sediments. Geology, 4(9): 525-528.

Toggweiler, J.R., Russell, J.L. and Carson, S.R., 2006. Midlatitude westerlies, atmospheric CO2, and climate change during the ice ages. Paleoceanography, 21(2): PA2005.

Tolderlund, D.S. and Be, A.W.H., 1971. Seasonal distribution of planktonic foraminifera in the western North Atlantic. Micropaleontology, 17(3): 297-329.

Toucanne, S. *et al.*, 2009. A 1.2 Ma record of glaciation and fluvial discharge from the West European Atlantic margin. Quaternary Science Reviews, In Press, Corrected Proof.

Trauth, M.H., Larrasoaña, J.C. and Mudelsee, M., 2009. Trends, rhythms and events in Plio-Pleistocene African climate. Quaternary Science Reviews, 28(5-6): 399-411.

Tziperman, E. and Gildor, H., 2003. On the mid-Pleistocene transition to 100-kyr glacial cycles and the asymmetry between glaciation and deglaciation times. Paleoceanography, 18(1): 1001.

van Aken, H.M., 2000. The hydrography of the mid-latitude northeast Atlantic Ocean: I: The deep water masses. Deep Sea Research Part I: Oceanographic Research Papers, 47(5): 757-788.

Van Aken, H.M. and De Boer, C.J., 1995. On the synoptic hydrography of intermediate and deep water masses in the Iceland Basin. Deep Sea Research Part I: Oceanographic Research Papers, 42(2): 165-189.

Van Der Weijden, C.H., Schuiling, R.D. and Das, H.A., 1970. Some geochemical characteristics of sediments from the North Atlantic Ocean. Marine Geology, 9(2): 81-99.

van Kreveld, S. *et al.*, 2000. Potential links between surging ice sheets, circulation changes, and the Dansgaard-Oeschger cycles in the Irminger Sea, 60-18 Kyr. Paleoceanography, 15(4): 425-442.

van Kreveld, S.A., Knappertsbusch, M., Ottens, J., Ganssen, G.M. and van Hinte, J.E., 1996. Biogenic carbonate and ice-rafted debris (Heinrich layer) accumulation in deep-sea sediments from a Northeast Atlantic piston core. Marine Geology, 131(1-2): 21-46.

Van Nieuwenhove, N., Bauch, H.A. and Matthiessen, J., 2008. Last interglacial surface water conditions in the eastern Nordic Seas inferred from dinocyst and foraminiferal assemblages. Marine Micropaleontology, 66(3-4): 247-263.

Venz, K.A., Hodell, D.A., Stanton, C. and Warnke, D.A., 1999. A 1.0 Myr Record of Glacial North Atlantic Intermediate Water Variability from ODP Site 982 in the Northeast Atlantic. Paleoceanography, 14(1): 42-52.

Vidal, L. *et al.*, 1997. Evidence for changes in the North Atlantic Deep Water linked to meltwater surges during the Heinrich events. Earth and Planetary Science Letters, 146(1-2): 13-27.

Vidal, L., Labeyrie, L. and van Weering, T.C.E., 1998. Benthic $\delta^{18}O$ eecords in the North Atlantic

over the last glacial period (60-10 kyr): evidence for brine formation. Paleoceanography, 13(3): 245-251.

Vilks, G., 1974. The distribution of planktonic foraminifera in the sediments and water of the northwest passage and northern Baffin Bay: a tool for paleoceanographic synthesis. Geological Survey of Canada, 1(74-30): 109-121.

Visbeck, M.H., Hurrell, J.W., Polvani, L. and Cullen, H.M., 2001. The North Atlantic Oscillation: Past, present, and future. Proceedings of the National Academy of Sciences of the United States of America, 98(23): 12876-12877.

Volkmann, R. and Mensch, M., 2001. Stable isotope composition $\delta^{18}O$, $\delta^{13}C$ of living planktic foraminifers in the outer Laptev Sea and the Fram Strait. Marine Micropaleontology, 42(3-4): 163-188.

von Langen, P.J., Pak, D.K., Spero, H.J. and Lea, D.W., 2005. Effects of temperature on Mg/Ca in neogloboquadrinid shells determined by live culturing. Geochem. Geophys. Geosyst., 6.

Waagstein, R., 1988. Structure, composition and age of the Faeroe basalt plateau. Geological Society, London, Special Publications, 39(1): 225-238.

Wang, H. and McCave, I.N., 1990. Distinguishing climatic and current effects in mid-Pleistocene sediments of Hatton and Gardar Drifts, NE Atlantic. Journal of the Geological Society, 147(2): 373-383.

Wang, R. and Abelmann, A., 2002. Radiolarian responses to paleoceanographic events of the southern South China Sea during the Pleistocene. Marine Micropaleontology, 46(1-2): 25-44.

Wang, R., Abelmann, A., Li, B. and Zhao, Q., 2000. Abrupt variations of the radiolarian fauna at Mid-Pleistocene climate transition in the South China Sea. Chinese Science Bulletin, 45(10): 952-955.

Wara, M.W., Ravelo, A.C. and Revenaugh, J.S., 2000. The Pacemaker Always Rings Twice. Paleoceanography, 15(6): 616-624.

Weirauch, D., Billups, K. and Martin, P., 2008. Evolution of millennial-scale climate variability during the mid-Pleistocene. Paleoceanography, 23: PA3216.

Wold, C.N., 1994. Cenozoic Sediment Accumulation on Drifts in the Northern North Atlantic. Paleoceanography, 9(6): 917-941.

Wright, A.K. and Flower, B.P., 2002. Surface and deep ocean circulation in the subpolar North Atlantic during the mid-Pleistocene revolution. Paleoceanography, 17(4).

Yamashita, H., Takahashi, K. and Fujitani, N., 2002. Zonal and vertical distribution of radiolarians in the western and central Equatorial Pacific in January 1999. Deep Sea Research Part II: Topical Studies in Oceanography, 49(13-14): 2823-2862.

Zachos, J., Pagani, M., Sloan, L., Thomas, E. and Billups, K., 2001. Trends, rhythms, and aberrations in global climate 65 Ma to present. Science, 292(5517): 686-693.

Zahn, R. and Mix, A.C., 1991. Benthic Foraminiferal $\delta^{18}O$ in the Ocean's Temperature-Salinity-

Density Field: Constraints on Ice Age Thermohaline Circulation. Paleoceanography, 6(1): 1-20.

Zhao, M., Beveridge, N.A.S., Shackleton, N.J., Sarnthein, M. and Eglinton, G., 1995. Molecular stratigraphy of cores off northwest Africa: Sea surface temperature history over the last 80 ka. Paleoceanography, 10(3): 661-675.

ANEXOS

ANEXO 1. MICROPLANKTON RESPONSE TO ENVIRONMENTAL CONDITIONS IN THE ALBORAN SEA (WESTERN MEDITERRANEAN): ONE YEAR SEDIMENT TRAP RECORD

Marine Micropaleontology 78 (2011) 14–24

Contents lists available at ScienceDirect

Marine Micropaleontology

journal homepage: www.elsevier.com/locate/marmicro

Research paper

Microplankton response to environmental conditions in the Alboran Sea (Western Mediterranean): One year sediment trap record

I. Hernández-Almeida [a,*], M.A. Bárcena [a], J.A. Flores [a], F.J. Sierro [a], A. Sanchez-Vidal [b], A. Calafat [b]

[a] Departament of Geology, University of Salamanca, 37008 Salamanca, Spain
[b] GRC Marine Geociences, Departament of Stratigraphy Paleontology and Marine Geosciences, University of Barcelona, 08028 Barcelona, Spain

ARTICLE INFO

Article history:
Received 28 May 2010
Received in revised form 14 September 2010
Accepted 21 September 2010

Keywords:
Coccolithophores
Planktonic foraminifera
Diatom
Sediment trap
1997–98 ENSO event
SST
Alboran Sea

ABSTRACT

The present work analyses the seasonal evolution of planktonic assemblages and particle fluxes through the water column in the Eastern Alboran Sea (Western Mediterranean) at 35ª55.47'N/01ª30.77'W. A Sediment trap was deployed below the influence of the Almeria-Oran Front (AOF), a semi-permanent geostrophic front, during July 1997 to June 1998. Overall, the temporal variability of coccolithophore, planktonic foraminifer, diatom, benthic and wind-carried biogenic particle fluxes is linked to the seasonal evolution of sea surface hydrological structures. Maximum planktonic fluxes were found during high-productivity periods and wind-induced upwelling, following a trimodal pattern, with maximum fluxes in July 1997, November–December 1997, and April–May 1998. These periods were characterized by vertical mixing and the full development of anticyclonic gyres in the Alboran Sea. The annual flux of coccolithophores was dominated by the "small *Gephyrocapsa* Group" and *Emiliania huxleyi*, whereas *Turborotalita quinqueloba* and *Globigerina bulloides* dominated the foraminiferal fluxes, and *Chaetoceros* Resting Spores (RS) were predominant in the diatom assemblage. Benthic specimens were also collected with the sediment trap, suggesting a variable influence of bottom water activity. Wind-driven particles (phytoliths and fresh-water diatoms) were collected along the year, but their fluxes followed the local wind regime.
The high Sea Surface Temperature (SST) during fall due to weaker than usual westerly winds, and the pressure anomaly prevailing in the Alboran Sea during early winter, were reflected in the planktonic assemblages by the proliferation of warm, lower photic layer inhabitants and/or oligotrophic taxa of coccolithophores (*Florisphaera profunda*), planktonic foraminifers (*Globigerinoides ruber* and *Globorotalia inflata*) and diatoms (*Leptocylindrus danicus*). These unusual climatic conditions in the eastern Alboran Sea must have been caused by the 1997–1998 ENSO event.

1. Introduction

Planktonic communities are important tracers of oceanographic changes, as they appear to be sensitive indicators of surface water conditions. Every group/species have specific spatial and temporal distributions in surface waters depending of factors such as upwelling, temperature, salinity, nutrients and light (Margalef, 1978). For this reason planktonic studies based on water samples and sediment trap records have emerged as an important tool in order to infer past global change and to determine climatic indicators in longer time-series (Okada and Honjo, 1973; Okada and McIntyre, 1979; Giraudeau and Rogers, 1994; Knappertsbusch, 1993; Abrantes and Moita, 1999). During the last decades, several studies based on downward particle fluxes have been focused in the Mediterranean Sea (Pujol and Vergnaud-Grazzini, 1995; Rutten et al., 2000; Ziveri et al., 2000; Schiebel et al., 2004) and more specifically in the Alboran Sea (Peinert and Miquel, 1994; Fabres et al., 2002; Bárcena et al., 2004; Sanchez-Vidal et al., 2004; 2005). Results obtained in these works highlighted the control of physical-chemical characteristics of the water column on the development of certain planktonic communities; providing a useful information in order to interpret the Mediterranean fossil record (Flores et al., 2000; Bárcena et al., 2001; Colmenero-Hidalgo et al., 2004).

The Alboran Sea is a relevant area to study flux of organisms since it has a relative high productivity that contrast with the generalized oligotrophy of the Mediterranean Sea. Primary productivity in Alboran Sea is mainly related to the local circulation pattern, which is controlled by the entrance of Atlantic surface waters into the Mediterranean basin and the development of anticyclonic gyres, stimulating phytoplankton productivity in the area (Packard et al., 1988).

As part of the MTP II-MATER project (Mediterranean Targeted Project II-MAss Transfer and Ecosystem Response), sediment traps were deployed in the Almeria-Oran Front (AOF) from July 1997 to May 1998 to record the annual evolution of biogenic flux in the area. In this paper we

* Corresponding author. Faculty of Sciences, Plaza de los Caídos s/n. 37008, Salamanca, Spain. Tel.: +34 923 29 44 97; fax: +34 923 29 45 14.
E-mail address: ihalmeida@usal.es (I. Hernández-Almeida).

0377-8398/$ – see front matter © 2010 Elsevier B.V. All rights reserved.
doi:10.1016/j.marmicro.2010.09.005

describe the seasonal evolution of coccolithophores, planktonic foraminifers, diatoms and phytoliths, and compare them with other biological (chlorophyll-*a* concentration) and environmental records (sea surface temperature –SST–, bottom current and wind data) from previous studies in the Alboran Sea for the same time period (Garcia-Gorriz and Carr, 2001; Vargas-Yañez et al., 2002; Sanchez-Vidal et al., 2005). The objective of this study is to describe the phytoplankton abundance and composition in the AOF and its relationship to short-term hydrographical changes in the Mediterranean region and with other ocean-wide processes.

2. Study area: hydrographic and meteorological considerations

The Alboran Sea is a transitional region between two oceanic domains: the Atlantic Ocean and the Mediterranean Sea. Surface circulation is very active and is characterized by the presence of two semi-permanent gyres, which are formed after the entrance of North Atlantic Surface Waters (NASW) through the Strait of Gibraltar. Once the NASW has entered the Alboran Basin, as a result of mixing with the dwelling Mediterranean waters these water mass changes its characteristics and is known as Modified Atlantic Waters (MAW). Both anticyclonic gyres are highly variable in terms of structure and permanence and, moreover, their development is controlled by several factors such as atmospheric pressure, temperature, salinity, etc. (Heburn and La Violette, 1990; Viúdez et al., 1998; Vargas-Yañez et al., 2002) (Fig. 1).

Unlike the general oligotrophy of the Mediterranean Sea, the Alboran Sea has two systems of high productivity associated with the gyres and with periods of intense westerlies activity: one located in the northern area of the Western Alboran Gyre (WAG) (Minas et al., 1991; Sarhan et al., 2000), and the Almeria-Oran Front (AOF) (Viúdez et al., 1998), related to the Eastern Alboran Gyre (EAG) (Fig. 1). The AOF is a semi-permanent geostrophic front that results from the interaction between Atlantic waters and denser Mediterranean waters (Tintore et al., 1988). Moreover, the incoming NASW introduce and transport to the east high amounts of nutrients and biogenic material produced in the western sector of the basin (La Violette, 1984; Minas et al., 1991; Garcia-Gorriz and Carr, 2001).

According to Garcia-Gorriz and Carr (2001), the temporal evolution of the Alboran basin productivity is characterized by the succession of four regimes during the year: bloom regime from November to March, the non-bloom, from May to September and two transitional periods, in April–May, when thermal stratification starts, and in October–November, coinciding with maximum wind variability and de-stratification within the basin. Former authors also defined a temperature range that separates the bloom regime (for SST ≤ 17.4 °C) from the non-bloom (SST ≥ 19.5 °C) (Fig. 2a). Fluvial run-off is negligible in the Alboran Sea since no significant rivers flow into the AOF region (Sanchez-Vidal et al., 2005) (Fig. 1).

2.1. Special conditions during the 1997–1998 period

According to McPhaden (1999), the 1997–1998 El Niño-Southern Oscillation (ENSO) event was the strongest for the last century. The former author suggested that unusual climatic conditions around the world were related to this event. In the Alboran Sea, this special conditions consist in the high SST (>19.5 °C) and thermal stratification during late summer and early fall 1997, that increased until mid-fall, with unusually warm SST (reaching up to 22.5 °C) and weak winds during October 1997 (Garcia-Gorriz and Carr, 2001; Bárcena et al., 2004; Sanchez-Vidal et al., 2005). Therefore, the unusual fall conditions prevented the normal development

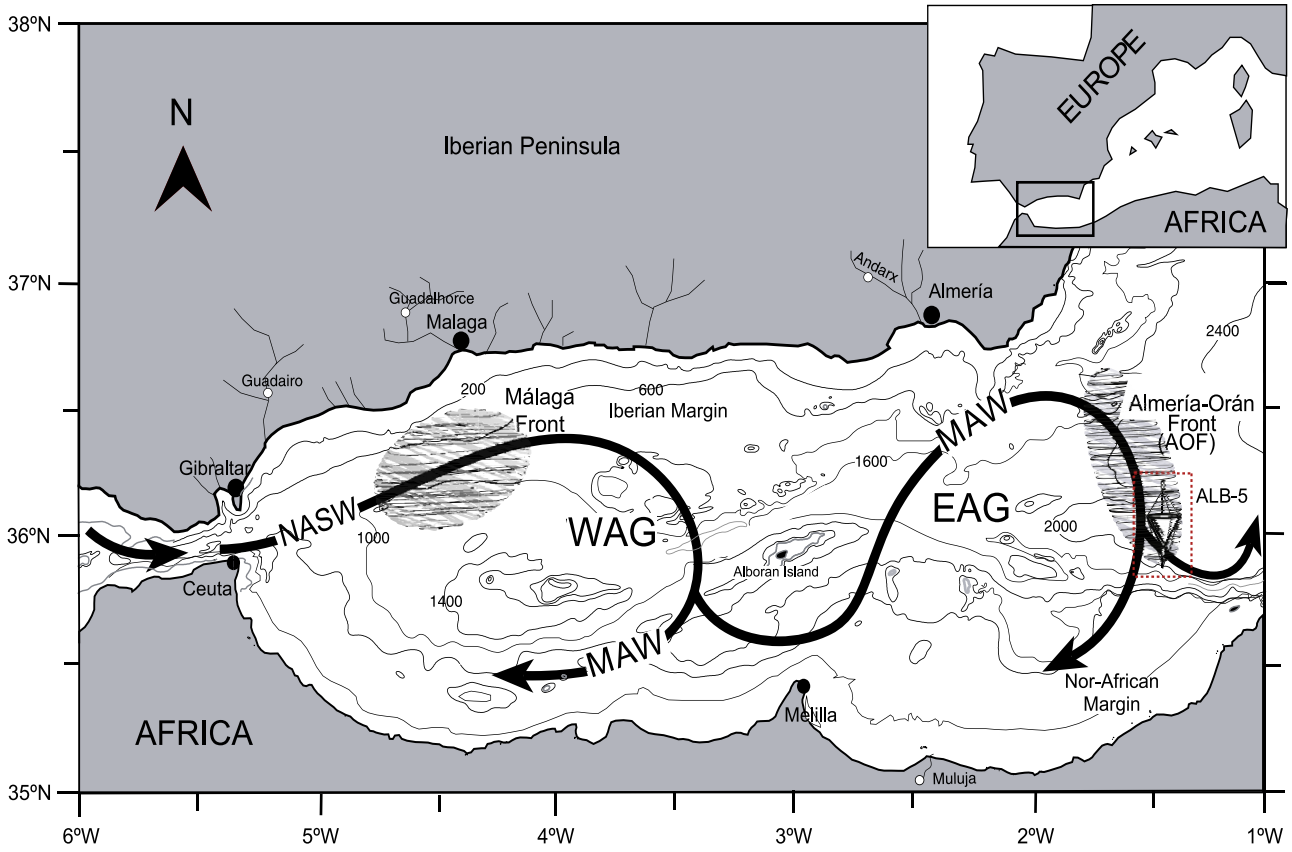

Fig. 1. Geographic and oceanographic location of the study area. Scheme of surface circulation in the Alboran Sea and position of sediment trap ALB-5. Arrows indicate the theoretical trajectories of water masses and dashed areas indicate high productivity zones. Dashed areas represent the northern border of the Western Alboran Gyre (WAG) and Almeria-Oran Front (AOF). Arrows represent the theoretical surface circulation in the Alboran Sea, North Atlantic Surface Waters (NASW), Modified Atlantic Waters (MAW), Western Alboran Gyre (WAG), Eastern Alboran Gyre (EAG) and AOF.

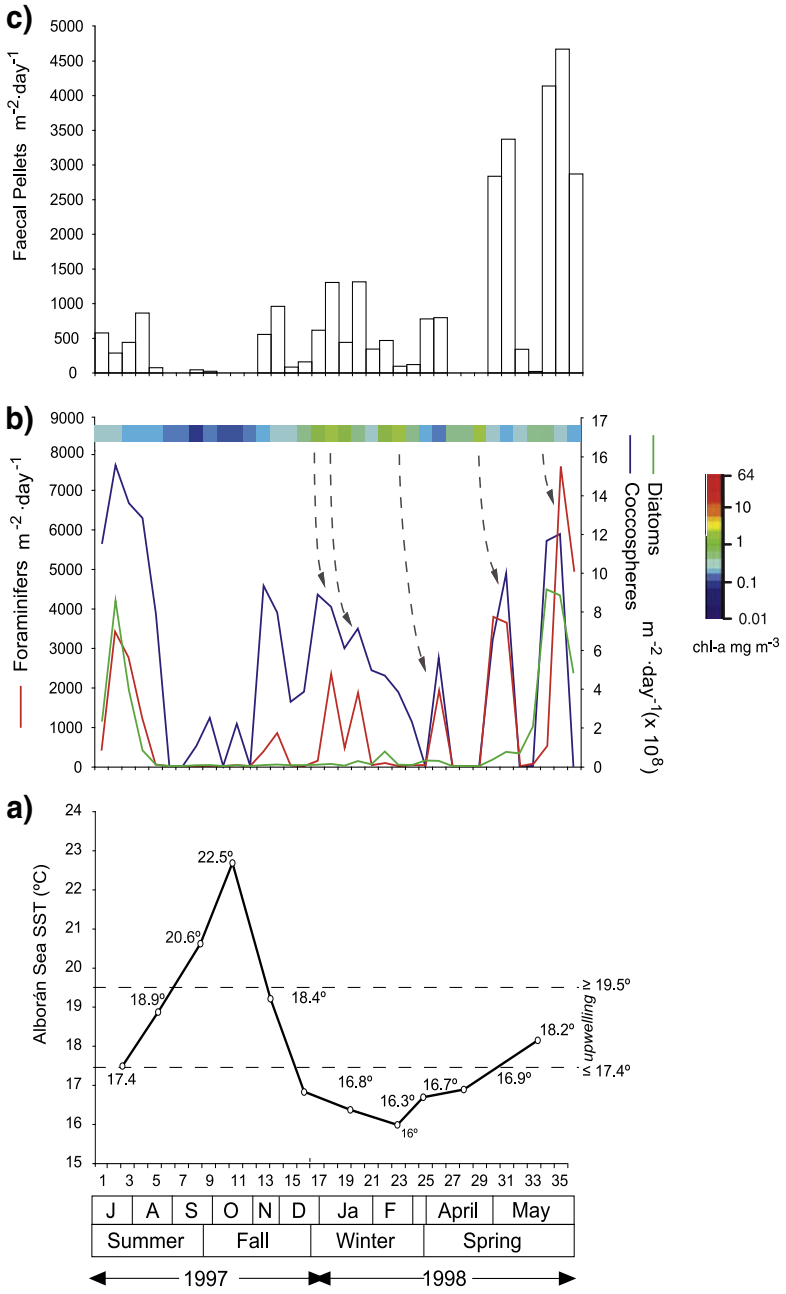

Fig. 2. Temporal evolution of a) surface temperature in the western gyre region (data obtained from Garcia-Gorriz and Carr, 2001), b) fluxes of main planktonic groups and chlorophyll-*a* concentration in surface waters and c) fluxes of faecal pellets recorded by the sediment trap ALB-5F, located in the Alboran Sea, between July 1997 and May 1998. Upper coloured bar at b) is an estimation of the chlorophyll-*a* concentration derived from SeaWifs images (Melin, 2000). Grey dashed arrows indicate the lag between associated pigment maxima at sea surface and the planktonic flux maxima in the sediment trap.

of the winter upwelling. Later, a southward drift of warmer than usual NASW getting into the Alboran Sea forced the collapse of the gyre from February to March 1998 (Vargas-Yañez et al. 2002).

This special regime characterized by high temperatures likely yielded changes in the planktonic assemblage along the Mediterranean region during the 1997–1998 period. Rigual-Hernández et al. (2010) observed lower silica organisms fluxes during the winter 1997–1998 in a 12 years sediment trap record from the Gulf of Lion (Western Mediterranean). Mercado et al. (2005, 2007) observed extraordinary warm conditions during the 1997 fall that produced a shift in the phytoplanktonic community of the Alboran Sea. Bárcena et al. (2004) reported low productive conditions during the 1997–1998 year. We therefore suggest that 1997–1998 ENSO event had promoted unusual meteorological and hydrographic conditions through remote teleconnections that affected the Mediterranean region, and in our particular case, to the planktonic assemblages of the Alboran Sea.

3. Materials and methods

3.1. Mooring configuration

Sediment trap ALB-5F was deployed on the north-Africa continental margin located at 35º55.47'N/01º30.77'W below a water column of 2070 m and 30 m above the sea floor (Fig. 1). The mooring line was equipped with a Technicap PPS3 sediment trap and Aanderaa current meters at several levels of the water column. A complete

Table 1
Daily flux (expressed as organisms m^{-2} day^{-1}) of coccolithophore taxa taxa, *Emiliania huxleyi*, *Gephyrocapsa oceanica*, small *Gephyrocapsa* group, Warm coccolithophore group, *Helicosphaera carteri*, *Syracosphaera* spp., *Gephyrocapsa muellerae*, *Florisphaera profunda*, *Calcidiscus leptoporus*, most abundant planktonic foraminifers, *Turborotalita quinqueloba*, *Globigerina bulloides*, *Globigerinoides ruber*, *Globorotalia inflata*, the main diatom groups, *Chaetoceros* RS, Marine Planktonic Group, *Leptocylindrus danicus*, Benthic and Neritic group, Fresh-water diatoms and Phytoliths, at the mooring site in the Almeria-Oran Front from July 1997 through May 1998.

Period	Sample	Total coccosph. ($\times10^8$)	SGG ($\times10^7$)	*E. huxleyi* ($\times10^7$)	*F. profunda* ($\times10^6$)	WCCG ($\times10^6$)	*C. leptop.* ($\times10^5$)	*H. carteri* ($\times10^6$)	Syracos. spp. ($\times10^6$)	Total forams ($\times10^3$)	*T.quinquel.* ($\times10^3$)	*G. bulloides* ($\times10^3$)	*G. inflata* ($\times10^2$)	*G. ruber* ($\times10$)	Total diatoms ($\times10^7$)	Chaet. RS ($\times10^7$)	MPG ($\times10^6$)	NBG ($\times10^6$)	*L. danicus* ($\times10^5$)	Phytoliths ($\times10^5$)	Fresh-water ($\times10^5$)
I	1	1.13	6.67	2.86	3.29	0.82	2.52	1.96	5.42	0.40	0.16	0.16	0.19	3.20	2.29	2.00	2.35	0.55	2.35	0.00	0.29
	2	1.52	9.91	3.02	1.74	1.83	19.9	2.57	3.55	3.33	1.14	1.59	2.88	5.76	8.38	7.24	9.96	1.20	14.4	6.00	3.60
	3	1.33	8.68	3.22	2.53	0.0	11.5	2.37	0.00	2.72	1.29	1.18	1.57	3.49	3.83	3.27	4.68	0.56	9.95	1.49	3.48
	4	1.25	8.45	2.54	1.95	7.04	13.6	3.23	1.90	0.98	0.54	0.34	0.19	2.56	0.79	0.63	1.06	0.36	3.81	1.76	2.49
	5	0.76	3.73	1.70	2.37	15.3	1.42	1.47	0.93	0.03	0.00	0.00	0.19	6.40	0.06	0.02	0.11	0.12	0.17	0.59	1.47
	6	0.00	0.00	0.00	0.00	0.00	0.00	0.00	0.00	0.00	0.00	0.00	0.00	0.00	0.00	0.00	0.00	0.00	0.00	0.00	0.00
	7	0.00	0.00	0.00	0.00	0.00	0.00	0.00	0.00	0.00	0.00	0.00	0.00	0.00	0.00	0.00	0.00	0.00	0.00	0.00	0.00
	8	0.10	0.31	0.60	0.37	0.11	0.23	0.00	0.07	0.00	0.00	0.00	0.00	0.00	0.03	0.01	0.06	0.07	0.04	0.58	0.34
	9	0.24	1.67	0.42	1.22	0.92	1.42	0.00	0.28	0.00	0.00	0.00	0.00	0.00	0.04	0.02	0.09	0.01	0.00	1.06	0.76
	10	0.00	0.00	0.00	0.00	0.00	0.00	0.00	0.00	0.00	0.00	0.00	0.00	0.00	0.00	0.00	0.00	0.00	0.00	0.00	0.00
	11	0.21	0.96	0.84	1.71	0.50	2.58	0.06	0.24	0.02	0.00	0.00	0.00	1.92	0.04	0.02	0.12	0.04	0.00	0.53	0.88
II	12	0.00	0.00	0.00	0.00	0.00	0.00	0.00	0.00	0.00	0.00	0.00	0.00	0.00	0.00	0.00	0.00	0.00	0.00	0.00	0.00
	13	0.91	6.92	0.63	0.55	3.27	3.78	2.44	2.37	0.37	0.03	0.16	0.32	9.60	0.05	0.01	0.19	0.09	0.10	0.49	0.78
	14	0.77	5.70	0.47	3.13	3.77	11.4	1.83	1.02	0.83	0.20	0.29	1.28	3.84	0.08	0.04	0.18	0.08	0.00	0.29	0.94
	15	0.32	2.48	0.42	1.62	0.23	0.71	0.00	0.29	0.01	0.00	0.00	0.12	0.00	0.03	0.00	0.11	0.08	0.00	0.29	1.17
	16	0.37	2.78	0.39	2.28	0.00	4.06	0.00	0.19	0.00	0.00	0.00	0.00	0.00	0.05	0.01	0.19	0.10	0.00	0.53	0.94
	17	0.86	7.19	0.44	2.04	0.56	6.88	1.56	0.61	0.12	0.00	0.06	0.40	0.00	0.06	0.01	0.25	0.22	0.09	1.07	1.07
	18	0.80	6.81	0.40	2.42	1.14	17.5	1.13	1.56	2.32	1.32	0.64	1.66	6.40	010	0.03	0.32	0.32	0.06	0.88	1.47
	19	0.59	4.91	0.27	1.34	0.91	6.81	0.73	0.40	0.45	0.31	0.12	0.00	0.00	0.02	0.01	0.07.	0.01	0.06	0.23	0.29
	20	0.69	5.80	0.31	1.50	1.40	7.37	1.71	1.41	1.84	0.97	0.61	0.75	2.33	0.25	0.15	0.62	0.26	0.64	0.58	1.17
	21	0.48	3.55	0.40	1.22	0.50	15.5	0.80	2.03	0.01	0.00	0.01	0.00	0.00	0.08	0.05	0.15	0.15	0.17	0.35	0.58
	22	0.45	3.89	0.12	0.96	0.46	13.2	0.61	0.67	0.07	0.00	0.06	0.00	0.00	0.73	0.43	2.35	0.51	0.88	1.03	2.64
	23	0.37	3.01	0.10	0.74	0.12	3.15	1.43	1.69	0.00	0.00	0.00	0.00	0.00	0.06	0.03	0.16	0.09	0.12	0.36	0.73
III	24	0.22	1.59	0.19	0.04	0.06	0.40	0.00	0.02	0.02	0.00	0.00	0.12	0.00	0.04	0.02	0.17	0.09	0.00	0.29	0.23
	25	0.00	0.00	0.00	0.00	0.00	0.00	0.00	0.00	0.00	0.00	0.00	0.00	0.00	0.27	0.19	0.53	0.20	0.15	1.23	1.00
	26	0.54	3.48	1.08	0.98	1.83	8.41	1.63	1.00	1.90	1.36	0.12	0.99	1.42	0.25	0.17	0.54	0.30	0.13	2.41	0.39
	27	0.00	0.00	0.00	0.00	0.00	0.00	0.00	0.00	0.00	0.00	0.00	0.00	0.00	0.00	0.00	0.00	0.00	0.00	0.00	0.00
	28	0.00	0.00	0.00	0.00	0.00	0.00	0.00	0.00	0.00	0.00	0.00	0.00	0.00	0.00	0.00	0.00	0.00	0.00	0.00	0.00
	29	0.00	0.00	0.00	0.00	0.00	0.00	0.00	0.00	0.00	0.00	0.00	0.00	0.00	0.00	0.00	0.00	0.00	0.00	0.00	0.00
	30	0.63	3.86	1.18	0.77	0.94	0.14	3.51	0.91	3.73	2.41	0.87	1.49	0.00	0.32	0.24	0.36	0.38	0.00	1.37	0.68
	31	0.97	6.82	1.73	1.47	1.53	0.17	2.20	1.24	3.54	2.58	0.32	1.49	4.27	0.71	0.59	0.74	0.39	0.20	4.89	0.19
	32	0.00	0.00	0.00	0.01	0.00	0.00	0.00	0.00	0.00	0.00	0.00	0.00	0.00	0.63	0.48	0.92	0.42	0.49	1.47	1.30
	33	0.00	0.00	0.00	0.00	0.00	0.00	0.00	0.01	0.02	0.00	0.00	0.00	2.13	2.00	1.77	1.71	0.55	1.47	0.98	0.00
	34	1.14	7.64	2.14	2.51	1.91	0.23	2.44	3.67	0.02	0.00	0.02	0.00	0.00	8.93	8.13	6.36	1.51	1.99	3.98	0.00
	35	1.17	8.45	2.04	2.89	0.36	4.73	2.75	0.70	7.40	2.77	3.9	3.63	0.00	8.64	8.07	4.15	1.44	13.1	2.19	0.00
	36	0.00	0.00	0.00	0.00	0.00	0.00	0.00	0.00	4.85	2.70	1.7	0.74	0.00	4.74	4.24	3.99	0.90	2.64	4.28	1.65
Annual Flux		17.9	125	27.6	46.7	45.5	21.2	36.4	32.2	35.1	17.8	12.2	18.1	47.6	43.6	38.0	42.6	11.1	53.1	41.2	30.6
Average		0.49	3.48	0.76	1.30	1.26	0.58	1.01	0.89	0.97	0.49	0.33	0.50	1.32	1.21	1.05	1.18	22.2	1.48	1.14	0.84

description of the sediment trap as well as of the technical procedures of maintenance and configuration of the mooring line was described in Heussner et al. (1990) and Sanchez-Vidal et al. (2005). Current meters recorded water speed and direction every hour throughout the experiment (291 days); average speed was 3.93 (±3.14) cm s^{-1} (Sanchez-Vidal et al., 2005).

3.2. Sampling period

The ALB-5F sediment trap was deployed from July 1997 to May 1998 during three different periods: (I) from 1st of July to 3rd October 1997, (II) from 15th November 1997 to 10th of March 1998, and (III) from 1st April to 22nd May 1998. The samples were taken every ten days throughout the study period, except between April and May (third period), when the sampling interval was three days (Table 1). A total of 29 samples were studied; unfortunately, owing to technical reasons seven samples from September to October 1997 were invalid for performing micropaleontological analyses, since they had not collected a sufficient amount of material. Sediment trap efficiency was 80.5% for the first two periods and 100% for the third.

3.3. Sample treatment and calculations

A high-precision peristaltic pump was used to split each sample into eight identical and homogeneous sub-samples, following Heussner et al. (1990). For geochemical treatments, we followed the methodology described in Fabres et al. (2002).

For micropaleontological analyses, the original dry mass was known, and 1/8 aliquots were used. The original samples were wet-sieved onto a 63 μm mesh in order to separate foraminifer from smaller diatoms and coccolithophores. The reduced amount of collected sediment made it necessary to carry out the micropaleontological investigations on the same sample aliquot, thus avoiding loss of information from the total sample. The methodological laboratory treatment can be found in Bárcena et al. (2004). Qualitative and quantitative analyses were done with a Nikon Eclipse 80-I petrographic microscope with a phase contrast device. For diatom studies, we used a 1000 magnification, while ×1250 was used for coccolithophore analyses.

In order to convert coccoliths into coccospheres, we used the Knappertbusch formula (1993) using the specific relationship between coccoliths/coccospheres for each species. Due to the different planktonic foraminifer species represented in the coarse and fined fraction (>150 μm and 63–150 μm) in our samples, we have grouped both fractions to avoid any loss of information (Carstens et al., 1997; Smart, 2002).

4. Results

4.1. Transport mechanism of planktonic shells

Faecal pellets, derived of high zooplanktonic activity (Quétel et al., 1993; Rutten et al., 2000), provided an effective mechanism of vertical transport for biogenic particles recorded in our sediment trap, as seen in the short time elapsed (2–3 weeks) between the periods of high chlorophyll-*a* concentration, increase of faecal pellets and interception of planktonic shells in the sediment trap ALB-5F (2070 m depth) (Fig. 2b and c). These aggregates sink faster than single particles such as coccolithophores or clay minerals, which can remain suspended in the water column for long time, increasing vertical transport to the sea floor over several months (Ziveri et al., 1995). Furthermore, the temporal agreement between biogenic and lithogenic fluxes (Sanchez-Vidal et al., 2005) may indicate the incorporation of mineral particles into faecal pellets, producing a ballast effect (Armstrong et al., 2002) on settling particles, as reported by Sanchez-Vidal et al. (2005). An additional source of material would be the particles (mainly benthic and neritic diatoms) supplied by bottom currents and wind-carried opaline particles from the continent (phytoliths and fresh-water diatoms), which have a minor contribution and their significance will be discussed further.

4.2. Calcium carbonate fraction

Coccolithophores and foraminifers were the main components of this fraction, although other calcareous organisms, such as pteropods and bivalves also contributed to it, but in very low quantities.

4.2.1. Coccolithophores

The total coccolithophore flux also followed a tri-modal pattern, exhibiting the same trend as calcium carbonate (Sanchez-Vidal et al., 2005), decreasing trends at the end of summer and beginning of fall, while during spring and early summer an increase of calcareous flora productivity was observed (Fig. 3a). The daily flux of coccospheres ranged between 15.2×10^7 and 1.0×10^7 (average: 4.9×10^7 coccospheres $m^{-2}\,day^{-1}$) (Fig. 3a).

The main component of the assemblage was the "small *Gephyrocapsa* Group" (sGG) (<3 μm), representing 49% of the total assemblage (Fig. 3b). The highest relative values were recorded between mid-fall and early winter, but high relative contributions were also recorded during middle spring and early summer. In terms of flux, the most significant contribution occurred in early summer, with values of 10×10^7 coccospheres $m^{-2}\,day^{-1}$). The sGG also displayed secondary peaks during spring and mid-fall to early winter (Fig. 3b).

Emiliania huxleyi (average: 11%), in terms of both flux and relative contribution, shows a variable pattern. The highest contribution was recorded during fall, reaching up to 60% of the total assemblage, while highest fluxes recorded during summer (3.2×10^7 coccospheres $m^{-2}\,day^{-1}$) (Fig. 3c).

Florisphaera profunda (average: 2.5%) showed highest contribution (8%) and daily flux (0.55×10^7 coccospheres $m^{-2}\cdot day^{-1}$) during fall (Fig. 3d). Several taxa (contributions between 2.8 and 1.4%; see Table 1), such as *Syracosphaera* spp., *Calcidiscus leptoporus, Helicosphaera carteri*, *Gephyrocapsa muellerae* and *Gephyrocapsa oceanica*, followed a similar temporal pattern along the sampling period, with their highest daily flux recorded at the beginning of summer and during spring. *Umbilicosphaera* spp., *Rhabdosphaera clavigera*, *Umbelosphaera* spp. and *Discospahera tubifera* represent the "Warm Coccolithophore Group" (WCCG) (Okada and McIntyre, 1979). The warm group accounted for 1.7% of the total assemblage. Mid-summer is the most productive period for this group, with a relative contribution up to 20% and a daily flux of 1.6×10^7 coccospheres $m^{-2}\,day^{-1}$) (Fig. 3e).

4.2.2. Planktonic foraminifers

Planktonic foraminifers were present throughout the year. Maximum fluxes occurred in three peaks at the beginning of summer, winter and during spring, with values of 3400, 2300 and 7500 foraminifers $m^{-2}\,day^{-1}$ respectively (Fig. 4a) (average: 1000 foraminifers $m^{-2}\,day^{-1}$).

Around 85% of the total planktonic foraminifera assemblage was composed by two species, *Turborotalita quinqueloba* (average 20%) (Fig. 4b) and *Globigerina bulloides* (average 18%) (Fig. 4c). The first one, *T. quinqueloba,* displayed the highest average relative contribution for the studied period. The highest fluxes of the species were recorded during summer, winter and spring; while the maximum contribution (both, relative and absolute) was observed during spring, with values of 72% and 2700 foraminifers $m^{-2}\,day^{-1}$ respectively (Fig. 4b). *T. quinqueloba* contributed to the foraminiferal assemblage with an average flux of 490 foraminifers $m^{-2}\,day^{-1}$.

Globigerina bulloides showed a clear seasonal component; during fall, the contribution of *G. bulloides* was negligible, but during summer, winter and spring it showed the highest daily fluxes, especially during May 1998, with 3900 foraminifers $m^{-2}\,day^{-1}$. Moreover, the

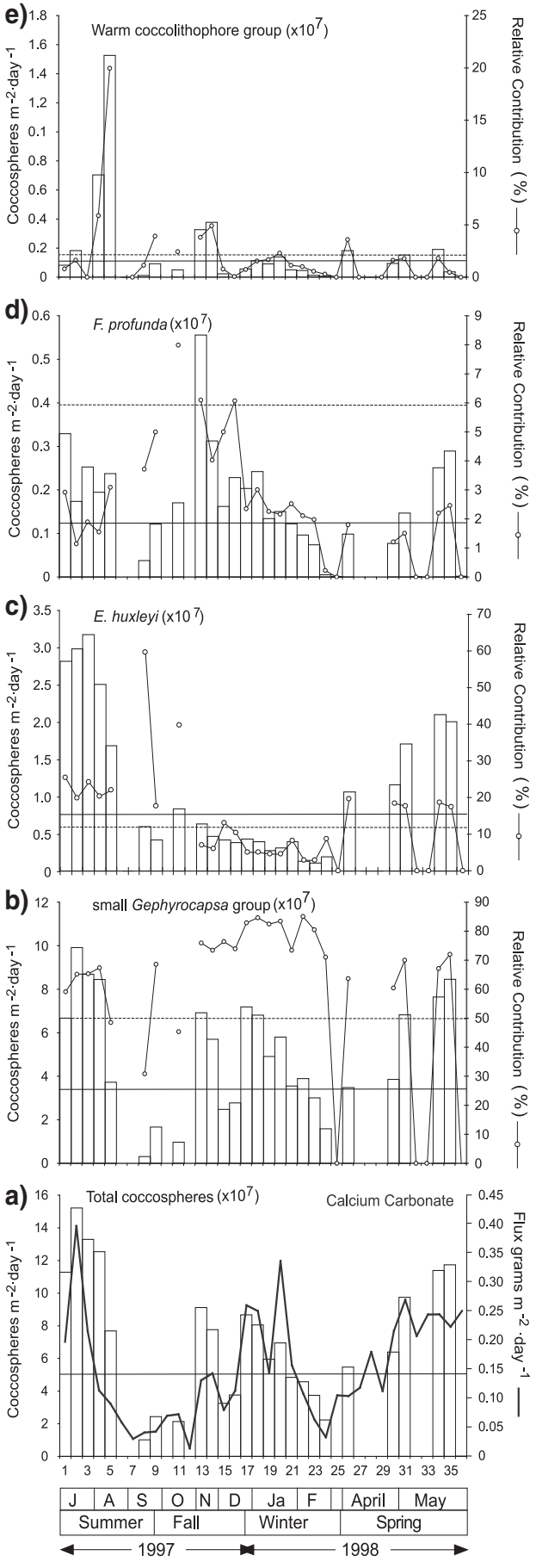

Fig. 3. Seasonal evolution of coccolithophore flux (bars) and relative contribution (lines) of the most significative species, a) total coccosphere and calcium carbonate (solid grey line), b) sGG, c) *Emiliania huxleyi*, d) *Florisphaera profunda*, e) Warm Coccolithophore Group (WCCG), in the sediment trap ALB-5F, located in the Alboran Sea, between July 1997 and May 1998. Horizontal solid lines indicate the average flux, and horizontal dashed lines indicate the average relative contribution.

maximum relative contribution (83%) was recorded during winter (January–February). The average flux and relative contribution was 339 foraminifers m^{-2} day^{-1} and 17% respectively (Fig. 4c).

Globorotalia inflata (average: 8.8%) was especially important during fall and late winter. The most significant daily flux was recorded during May 1998, with 360 foraminifers m^{-2} day^{-1} (Fig. 4d). The main flux contribution of *Globigerinoides ruber* (both varieties: white and pink) was observed in November 1997 (up to 100 foraminifers m^{-2} day^{-1}), although the species was scarcely represented in the rest of the studied period. The relative contribution of this species reached up to 75% of the assemblage during fall (Fig. 4e).

4.3. Biogenic opal faction

Diatoms, radiolarians, silicoflagellates, sponge spicules, siliceous dinoflagellates and phytoliths were the major components of the biosiliceous particles that settled in the Alboran Sea during the studied period. In our analyses, diatoms were numerically the main contributors to the opal fraction; their daily flux was several orders of magnitude higher than that of the rest of the siliceous microorganisms. Silicoflagellates (mainly *Dictyocha fibula*), dinoflagellates (*Actiniscus pentasterias*) sponge spicules and radiolarians displayed maxima fluxes at the beginning of summer 1997 and mid-spring 1998.

4.3.1. Diatoms

The flux of diatoms is expressed as the number of valves m^{-2} day^{-1}. Daily diatom flux displayed a bi-modal pattern, with two peaks at the beginning of summer 1997 and during late spring 1998, reaching values of around 8×10^7 valves m^{-2} day^{-1}. During the rest of the year, diatom flux was three orders of magnitude lower. The diatom flux followed the same pattern as opal (Fig. 5a). A slight increase in both diatom and opal levels, was observed during mid-winter. The mean daily flux was 1.2×10^8 valves m^{-2} day^{-1} (Fig. 5a).

A total of 66 diatom taxa were recognised in the samples. Diatoms were grouped as a function of their ecological significance into planktonic, neritic and benthic, and fresh-water, following Bárcena et al. (2004) considerations. Likewise, other species were treated individually due to their higher abundances or important ecological significance, such as *Chaetoceros* resting spores (RS) and *Leptocylindrus danicus*, respectively.

Chaetoceros RS was the main contributor to the diatom assemblage with daily fluxes of 1×10^7 valves m^{-2} day^{-1} (average). Its relative contribution represented more than 56% of the total, ranging from 27% to 98%. In terms of fluxes, *Chaetoceros* RS shoed two maxima, early summer, and the highest daily flux during spring, with 8.1×10^7 valves m^{-2} day^{-1} (Fig. 5b).

The Marine Planktonic Group (MPG), followed the opposite trend to that of *Chaetoceros* RS. The highest relative contribution was observed during the second half of fall and the first half of winter (up to 60%), while the lowest was recorded during spring and summer (Fig. 5c). The mean relative contribution was 20%. The flux followed a bi-modal pattern, with maxima during July 1997 and May 1998. The group contributed with daily fluxes of 1.2×10^6 valves m^{-2} day^{-1} (average).

Neritic and benthic diatoms (Neritic and Benthic group –NBG–) showed their highest relative contributions at the end of summer 1997 and early winter 1997–98 (average up to 10%). The highest flux was recorded during spring 1998 with daily fluxes of 1.5×10^6 valves m^{-2} day^{-1} (Fig. 5d). The most significant fluxes of *L. danicus* were recorded during early summer 1997 (14×10^5 valves m^{-2} day^{-1}) and

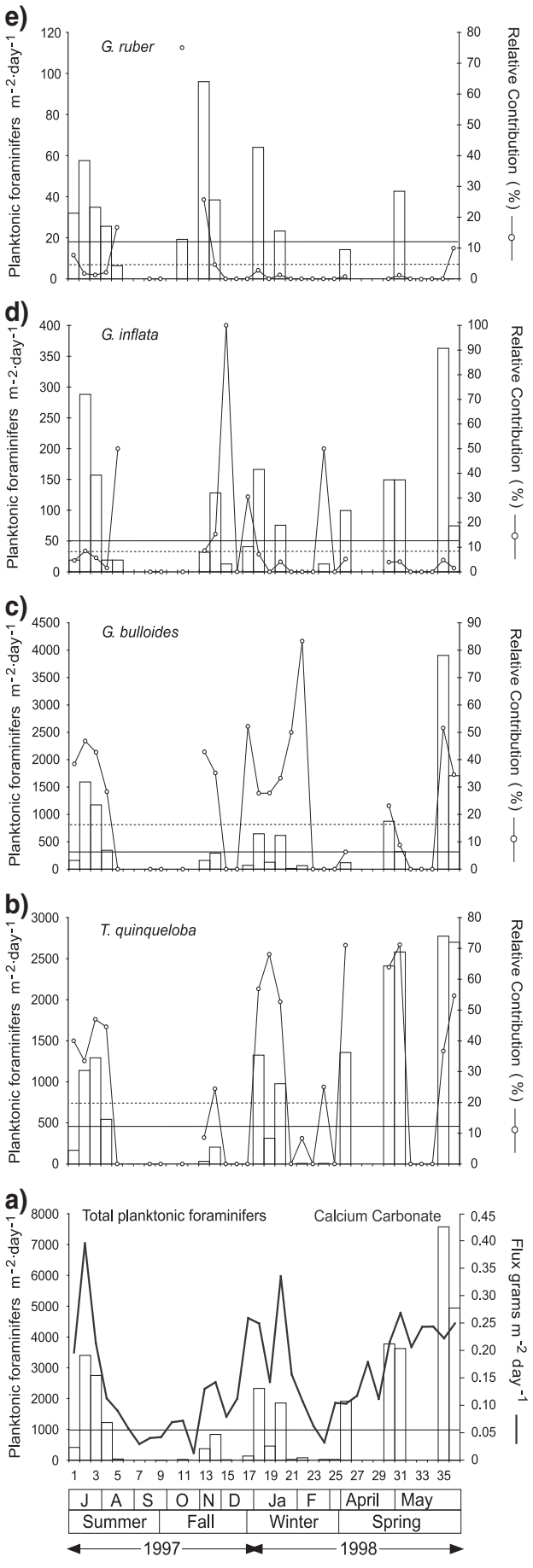

during mid-spring (Fig. 5e). For the rest of the year the contribution of this species was negligible, with the exception of a relative high during August 1997 (5%). The annual average contribution was around 1% (Fig. 5e).

Fresh-water diatoms (mainly *Aulacoseira granulata*) and phytoliths represent continental input to the sediment trap (origin and transport mechanism discussed in section 5.3). Fresh-water diatoms are mainly represented during early summer 1997 (up to 3.6×10^5 valves $m^{-2}\,day^{-1}$), while phytoliths show two peaks, early summer 1997 and spring 1998 (more than 5×10^5 phytoliths $m^{-2}\,day^{-1}$) (Fig. 6).

5. Discussion

5.1. Microplanktonic communities as response to environmental conditions

Oceanographic and atmospheric variability in the Alboran Sea during the 1997–1998 period provided different scenarios featured by the ecological succession of different planktonic species and phytoplankton groups. The occurrence of these scenarios are dependent of development of upwelling, a favourable wind-regime (westerly winds), nutrient availability, sea surface temperature and surface circulation of the Alboran Sea (Garcia-Gorriz and Carr, 2001; Sanchez-Vidal et al., 2004).

Highest biogenic particle fluxes recorded by sediment trap ALB-5F (Sanchez-Vidal et al., 2005) are related with high-chlorophyll-*a* concentrations events observed in previous weeks in the Alboran basin (WAG and/or EAG) by satellite images (Garcia-Gorriz and Carr, 2001) during the 1997–1998 period. These high productivity events correspond in our study with specific planktonic assemblages. Several opportunistic taxa show a rapid response to nutrients availability, such as sGG and *E. huxleyi* (Knappertsbusch, 1993; Brand, 1994), or the genus *Chaetoceros* (Abrantes, 1988; Abrantes and Moita, 1999), which appears at ALB-5F as resting spore stage in response to environmental stress (water column turbulence) during the upwelling events (Hargraves and French, 1983; Sautter and Sancetta, 1992). This enhanced productivity of coccolithophores and diatom cells serves as food-resource for zooplankton (Hemleben et al., 1989), such as the planktonic foraminifer *G. bulloides*, a taxon with multiple trophic strategies (Schiebel et al., 2001; Sautter and Sancetta, 1992) and *T. quinqueloba*, a characteristic species of spring blooms and upwelling stages (Weaver and Pujol, 1988; Sautter and Sancetta, 1992; Schiebel et al., 2004).

Planktonic organism density and species found in the AOF are comparable to those recorded in the WAG by Bárcena et al. (2004). The differences in fluxes between both records may be related to less intense upwelling events at AOF, as inferred from the lower chlorophyll-*a* concentrations at ALB 5-F.

5.1.1. Early-summer period

The increase in the fluxes of *T. quinqueloba* and *G. bulloides*, sGG and *E. huxleyi*, *Chaetoceros* RS and the diatoms MPG (Figs. 3–5) indicates the advection of cold upwelled waters south-eastwards resulting in a period of high nutrient availability with a favourable water-mixing at the WAG, then transported to the AOF, due to a westerly wind regime during June 1997. Other minor components of the coccolithophore assemblage, *Syracosphaera* spp., *Helicosphaera carteri* and *Calcidiscus leptoporus*, showed a very similar trend (Table 1), indicating a clear preference for productive periods, in

Fig. 4. Seasonal evolution of planktonic foraminifers flux (bars) and relative contribution (lines) of the most important species, a) total foraminifers and calcium carbonate (solid grey line), b) *Turborotalita quinqueloba*, c) *Globigerina bulloides*, d) *Globorotalia inflata*, e) *Globligerinoides ruber*, in the sediment trap ALB-5F, located in the Alboran Sea, between July 1997 and May 1998. Horizontal solid lines indicate the average flux, and horizontal dashed lines indicate the average relative contribution.

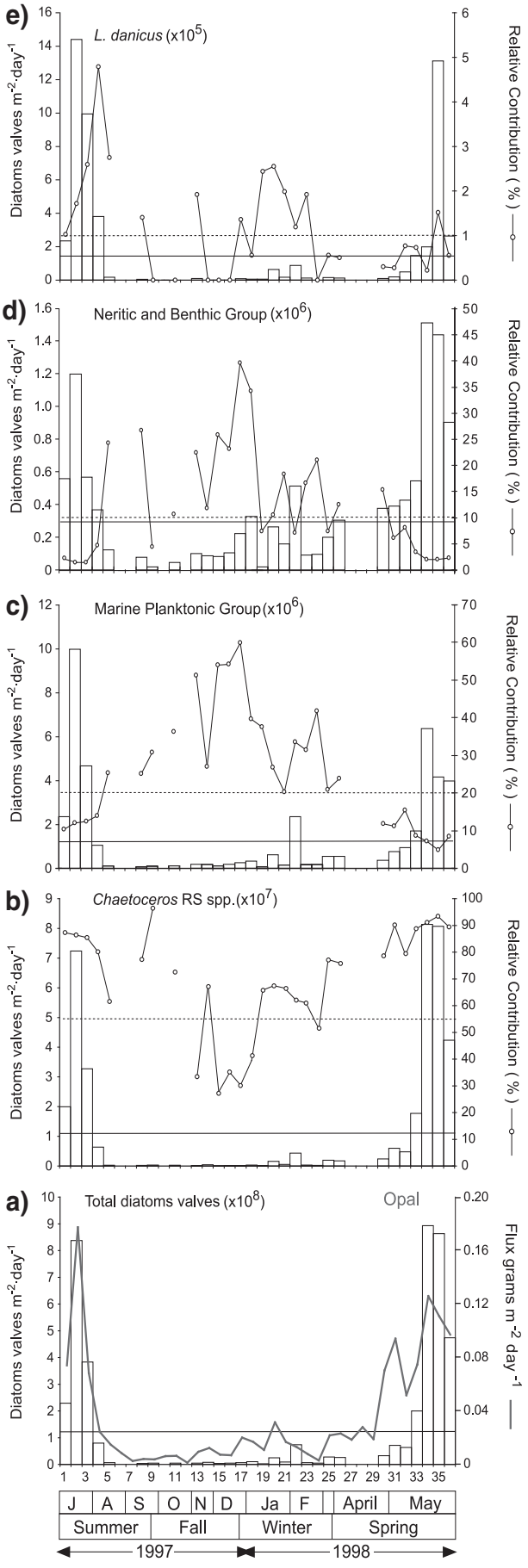

clear agreement with Ziveri et al. (1995, 2000) findings, who observed a significant increase in the coccosphere flux of these three coccolithophore species during upwelling episodes. In the same sense, *Gephyrocapsa muellerae* and *G. oceanica* fluxes seem to be directly controlled by nutrient availability. These species has been related to cold and fertile waters associated with upwelling conditions (Giraudeau, 1992; Ziveri et al., 1995; Broerse et al., 2000). This behaviour is supported by oceanographic-satellite observations since Garcia-Gorriz and Carr (2001) reported this period as one of the most intense productivity events with an increase of nutrients from spring to summer, related with a wind-induced upwelling.

5.1.2. Late summer and fall period

The anomalous sea-surface warmer conditions during this period (up to 22.5 °C) (Garcia-Gorriz and Carr, 2001) promoted a water-column stratification and caused deepening of the thermocline. These conditions contributed to the proliferation of several taxa, such as WCCG (*Umbilicosphaera* spp., *R. clavigera*, *Umbelosphaera* spp. and *D. tubifera*) (Okada and McIntyre, 1979), which are typical dwellers of warm and oligotrophic waters during mid-summer in the Mediterranean Sea (Ziveri et al., 2000). In the same sense, increase in *L. danicus* percentages (Fig. 5e) agrees with the upwelling relaxation and the beginning of a thermal stratification in the upper water column (Varela et al., 2003, Bárcena et al, 2004). This scenario with poor nutrient content in surface waters induces oligotrophic conditions, favouring development of predatory and gracing species, such as *Globigerinoides ruber* and *Globorotalia inflata* (Hemleben et al., 1989; Pujol and Vergnaud-Grazzini, 1995) (Fig. 4). Moreover, opportunitic and multy-diet character of *G. bulloides* (Sautter and Sancetta, 1992; Pujol and Vergnaud-Grazzini, 1995; Schiebel et al., 2001) allowed it to reach more than 40% in this period. Summarizing, 1997–1998 ENSO event likely led to warm SST and weak winds in the Alboran region during this period (Garcia-Gorriz and Carr, 2001; Sanchez-Vidal et al., 2005) favoured the proliferation of taxa typical of warm and oligotrophic environments better adapted to stratified waters.

The typical deep-dwelling species, *F. profunda* (Okada and Honjo, 1973), exhibits higher percentages during November and December 1997 (Fig. 3d). Bárcena et al. (2004) reported two peaks of this taxon in the WAG during the same period, and related them to times of maximum rainfall and river discharge. In the AOF, high wind speed recorded during these months (Sanchez-Vidal et al., 2005) likely created an environment with high turbulence in the upper photic zone and low light intensity, conditions favourable for *F. profunda* development (Ahagon et al., 1993; Schiebel et al., 2004).

This low-productive scenario lasted until November 1997, when the development of WAG and EAG favoured the water column de-stratification and advection nutrient-rich waters into the Eastern Alboran Sea (Garcia-Gorriz and Carr, 2001; Sanchez-Vidal et al., 2004). This upwelling event triggered a planktonic bloom in the WAG as reported by Bárcena et al. (2004), and recorded at our sediment trap, ALB-5F, with high relative and absolute fluxes values of eutrophic to mesotrophic species.

5.1.3. Winter period

This period was characterized by a massive destratification of the water column during late December 1997–January 1998; strong winds affected large parts of the Alboran Basin and caused an extensive bloom (Garcia-Gorriz and Carr, 2001; Sanchez-Vidal et al., 2004) (Fig. 2b), but with pigment concentrations lower than those

Fig. 5. Seasonal evolution of planktonic diatoms flux (bars) and relative contribution (lines) of the most significative species, a) total diatoms valves and opal (solid grey line), b) *Chaetoceros* RS, c) Marine planktonic Group, d) Neritic and Benthic Group, e) *Leptocylindrus danicus*, in the sediment trap ALB-5F, located in the Alboran Sea, between July 1997 and May 1998. Horizontal solid lines indicate the average flux, and horizontal dashed lines indicate the average relative contribution.

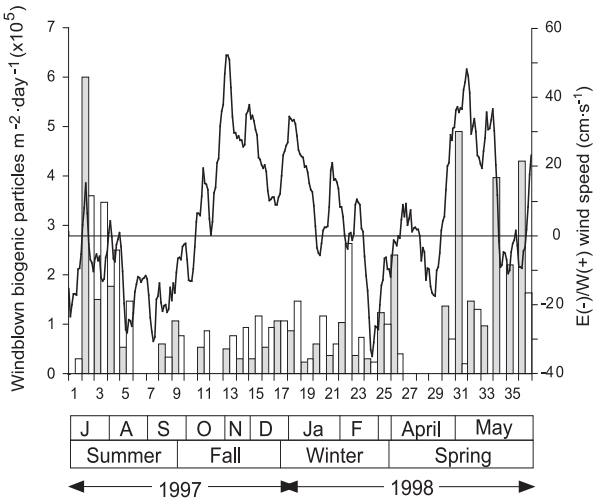

Fig. 6. Seasonal evolution of flux of the windblown biogenic particles, fresh-water diatoms (grey) and phytoliths (black), in the sediment trap ALB-5F, located in the Alboran Sea, between July 1997 and May 1998. Wind data from the Almeria meteorological Station (36º 50'N, 021º 23'W) showing the maximum daily wind speed moving average (period 10 days).

recorded in summer 1997 and spring 1998 (Garcia-Gorriz and Carr, 1999). Planktonic communities in the AOF did not respond equally, while coccospheres and planktonic foraminifers increased their fluxes; diatoms did not flourish with the same intensity (Figs. 3–5). An equivalent situation was also detected for the same period in the Alboran Sea by Sanchez-Vidal et al. (2004) and Mercado et al. (2005, 2007). These authors explained this shift from opal to calcareous phytoplankton domain as a response to the weak upwelling conditions and low-nutrient concentration in the surface waters, that favoured coccolithophores development, better adapted to this conditions than diatoms (Eppley et al., 1969; Bethoux et al., 2002; Schiebel et al., 2004). In this sense, LeBlanc et al. (2004) and Sanchez-Vidal et al. (2005) found lower opal values in the Alboran Sea during 1997 winter than those recorded during summer and spring, indicative of a decline of the siliceous phytoplankton.

Opposite distribution of *Chaetoceros* RS and MPG along the studied period responds to the different nutrient requirements of both groups. *Chaetoceros* RS prefers persistent upwelling conditions, while *Thalassionema nitzschioides*, the main component of the MPG, is a species with prevalence by weaker upwelling episodes (Blasco et al., 1981; Abrantes, 1988; Abrantes and Moita, 1999), like the winter period of our study. The high percentage values of *L. danicus* during 1997 winter are equivalent to the increase of this species in the WAG, as observed by Bárcena et al. (2004). The former author related the increase of *L. danicus* to the unfavourable surface water conditions occurring in the Alboran, with water stratification caused by a warmer than usual NASW getting into the basin (Vargas-Yañez et al., 2002).

The record of both neritic and benthic diatoms in the ALB-5F sediment trap (Fig. 5d) reveals an intense bottom current activity. Highest peaks of this group could be related to the intense westward–eastward current reversal at ALB5 mooring recorded by Sanchez-Vidal et al. (2005) during winter that would have resuspended bottom sediments from the nearby margin.

5.1.4. Spring period

The spring is characterized by planktonic bloom, with an increase in fluxes in all the main groups (diatoms, coccolithophores and foraminifers) but a reduced diversity, because only a few taxa, typical of this productive conditions were dominant (Figs. 3–5). At the beginning of March 1998 gyres are practically collapsed (Garcia-Gorriz and Carr, 2001) and caused a decrease in all constituents observed in ALB-5. This scenario is reversed during the following months, when favourable conditions – developed western gyre – transported nutrient from western Alboran (Garcia-Gorriz and Carr, 2001) and allowed a gradual increase of foraminifer, coccolithophores and diatoms. Typical upwelling taxons (*T. quinqueloba* and *G. bulloides*, sGG, *E. huxleyi*, RS *Chaetoceros* and the diatom MPG) dominated this event. Increase in solar radiation during spring may have contributed to the phytoplanktonic flourishing (Margalef, 1978), and hence, higher prey availability favoured zooplankton development (Hemleben et al., 1989).

5.2. Additional inputs

5.2.1. Aeolian biogenic component

Phytoliths are robust bodies of opaline silica in epidermal cells of plants (Blackman, 1971) and they are injected into the atmosphere during dry-season brush fires (Pokras and Mix, 1985). Fresh-water diatoms are dispersed by deflation of Holocene basins and dry lake deposits (Pokras and Mix, 1985). Hence, the presence of a mixture of microfossils with distinct ecological requirements (terrestrial and lacustrine environments) (Fig. 6) allows us to interpret this fact as a wind-transported material rather than as a run-off origin. Moreover, there are no important river systems in the Alboran Basin (Fig. 1). Increase in windblown fresh-water diatoms and phytoliths in our sediment trap may reflect periods of enhanced deflation and wind transport (aridity) and changes in continental grass cover (Pokras and Mix, 1985).

In this sense, Saharan dust storms are considered the main process of dust particles input to the Mediterranean area (Loyë-Pilot and Martin, 1996). Guerzoni et al. (1997) and Moreno et al. (2002) have suggested that the Central Sahara and South Algeria could be the main source areas of dust particles entering the western Mediterranean Sea. These dust storms show a clear seasonal cycle, with maximums during dry and warmest seasons, spring and summer (Moulin et al., 1998; Barnaba and Gobbi, 2004), in clear correspondence with our windblown biogenic particles record (Fig. 6).

The occurrence of phytoliths and fresh-water diatoms in our sediment trap confirms the results obtained in paleostudies of the Mediterranean sediments and supports the general assumption of an eolic transport agent of this biogenic material to the Mediterranean basin (Abrantes, 1991; Flores et al., 2000; Bárcena et al., 2001).

6. Summary and conclusions

Biogenic particles flux recorded in sediment trap ALB-5F, composed by coccolithofores, planktonic foraminifers, diatoms and phytoliths, mirrors the variability of meteorological and hydrographic conditions occurred in the Alboran Sea during the period from July 1997 to May 1998.

The main fluxes in surface productivity during the studied period took place during mid-spring to early summer, and a minor bloom occurred during mid-fall to early winter. These episodes are related to local pulses of productivity forced by the development of anti-cyclonic gyres in the Alboran Basin as well as a predominance of westerly winds over the area. The good correspondence between seasonal microorganism fluxes and high pigment concentrations in surface waters suggests a control of particle export by the seasonal productivity cycle in the surface and subsurface waters transported towards the bottom by faecal pellets or/and marine snow.

Succession in coccolithophores, planktonic foraminifers and diatoms communities were related to changes of water column conditions. Species adapted to well-mixed and nutrient-rich waters, such as *Chaetoceros* RS, sGG, *G. bulloides*, *T. quinqueloba*, dominated during the upwelling conditions of early summer 1997 and mid-spring 1998. Increases in temperature, upwelling relaxation and surface water stratification during late summer to fall 1997 allowed the blooming of warm and oligotrophic planktonic taxa, like *G. inflata*,

G. ruber, *F. profunda*, WCCG and *L. danicus*. Weaker upwelling and low-nutrient conditions during 1997–1998 winter may have favoured the shift from opal to calcareous phytoplankton domain. Unusual surface warmer conditions during late summer and fall in the Alboran Sea could be related to the 1997–1998 ENSO event.

Increase in fresh-water diatoms and phytoliths in the Alboran Sea indicates a significant continental input from Sahara desert as a consequence of an intensification of westerly winds during spring and early summer. Furthermore, continuous changes in current directions (E–W) detected by the current meters deployed in the ALB-5 mooring during fall and winter suggest that an important particle input to the sediment trap came from the seafloor and neighbouring continental margin sediment by resuspension.

Acknowledgements

This work was funded by Ministerio de Educación y Ciencia Project GRACCIE (CONSOLIDER-INGENIO CSD 2007-00067) and CGL2008-05560/BTE as well as Junta de Castilla y Leon Grupo GR34, and by a MEC FPI Grant to Iván Hernández-Almeida (BES-2006-12787). We are grateful to the anonymous reviewers for helping improve this work with their suggestions.

Appendix A. Supplementary data

Supplementary data to this article can be found online at doi:10.1016/j.marmicro.2010.09.005.

References

Abrantes, F., 1988. Diatom productivity peak and increased circulation during latest. Quaternary: Alboran Basin (western Mediterranean). Mar. Micro. 13, 79–96.
Abrantes, F., 1991. Variability of upwelling off NW Africa during the latest Quaternary: diatom evidence. Paleoceanogr. 6 (4), 431–460.
Abrantes, F., Moita, T., 1999. Water column and recent sediment data on diatoms and coccolithophorids, off Portugal, confirm sediment record of upwelling events. Oceanol. Acta 22 (3), 319–336.
Ahagon, N., Tanaka, Y., Ujiie, H., 1993. Florisphaera profunda, a possible nannoplankton indicator of late Quaternary changes in sea-water turbidity at the northwestern margin of the Pacific. Mar. Micro. 22, 255–273.
Armstrong, R.A., Lee, C., Hedges, J.I., Honjo, S., Wakeham, S.G., 2002. A new, mechanistic model for organic carbon fluxes in the ocean: Based on the quantitative association of POC with ballast minerals. Deep Sea Res. II 49, 219–236.
Bárcena, M.A., Cacho, I., Abrantes, F., Sierro, F.J., Grimalt, J.O., Flores, J.A., 2001. Paleoproductivity variations related to climatic conditions in the Alboran Sea (western Mediterranean) during the last glacial–interglacial transition: the diatom record. Palaeogeogr. Palaeoclimatol. Palaeoecol. 167 (3–4), 337–357.
Bárcena, M.A., Flores, J.A., Sierro, F.J., Perez-Folgado, M., Fabres, J., Calafat, A., Canals, M., 2004. Planktonic response to main oceanographic changes in the Alboran Sea (Western Mediterranean) as documented in sediment traps and surface sediments. Mar. Micro. 53, 423–445.
Barnaba, F., Gobbi, G.P., 2004. Aerosol seasonal variability over the Mediterranean region and relative impact of maritime, continental and Saharan dust particles over the basin from MODIS data in the year 2001. Atmos. Chem. Phys. 4, 2367–2391.
Bethoux, J.P., Morin, P., Ruíz-Pino, D.P., 2002. Temporal trends in nutrients ratios: chemical evidence of Mediterranean ecosystem changes driven by human activity. Deep-Sea Res. 49, 2007–2016.
Blackman, E., 1971. Opaline silica bodies in the range grasses of southern Alberta. Can. J. Bot. 49, 769–781.
Blasco, D., Estrada, M., Jones, B., 1981. Short time variability of phytoplankton populations in upwelling regions – The example of Northwest Africa. In: Richards, F.E. (Ed.), Coastal Upwelling and Estuarine Sciences 1. American Geophysical Union, Washington D.C, pp. 339–347.
Brand, L.E., 1994. Physiological ecology of marine coccolithophores. In: Winter, A., Siesser, W.G. (Eds.), coccolithophores. Cambridge University Press, Cambridge, pp. 39–49.
Broerse, A.T.C., Brummer, G.-J.A., Van Hinte, J.E., 2000. Coccolithophore export production in response to monsoonal upwelling off Somalia (northwestern Indian Ocean). Deep Sea Res. II 2179–2205.
Carstens, J., Hebbeln, D., Wefer, G., 1997. Distribution of planktic foraminifera at the ice margin in the Arctic (Fram Strait). Mar. Micro. 29, 257–269.
Colmenero-Hidalgo, E., Flores, J.A., Sierro, F.J., Bárcena, M.A., Löwemark, L., Schönfeld, J., Grimalt, J.O., 2004. Ocean surface water response to short-term climate changes revealed by coccolithophores from the Gulf of Cadiz (NE Atlantic) and Alboran Sea (W Mediterranean). Palaeogeogr. Palaeoclimatol. Palaeoecol. 205 (3–4), 317–336.
Eppley, R.W., Rogers, J.N., Harrison, W.G., 1969. Half-saturation constants for uptake of nitrate and ammonium by marine phytoplankton. Limnol. Oceanogr. 14, 912–920.
Fabres, J., Calafat, A., Sanchez-Vidal, A., Canals, M., Heussner, S., 2002. Composition and spatio-temporal variability of particle fluxes in the Western Alboran Gyre, Mediterranean Sea (SW Mediterranean). J. Mar. Sys. 33–34, 431–456.
Flores, J.A., Bárcena, M.A., Sierro, F.J., 2000. Ocean-surface and wind dynamics in the Atlantic Ocean off Northwest Africa during the last 140000 years. Palaeogeogr. Palaeoclimatol. Palaeoecol. 161 (3–4), 459–478.
Garcia-Gorriz, E., Carr, M.E., 1999. The Climatological Annual Cycle of Satellite-Derived Phytoplankton Pigments in the Alboran Sea. Geophys. Res. Lett. 26 (19), 2985–2988.
Garcia-Gorriz, E., Carr, M.E., 2001. Physical control of phytoplankton distributions in the Alboran Sea: a numerical and satellite approach. J. Geophys. Res. 106, 16795–16805.
Giraudeau, J., 1992. Distribution of Recent nannofossils beneath the Benguela system: southwest African continental margin. Mar. Geol. 108, 219–237.
Giraudeau, J., Rogers, J., 1994. Phytoplankton biomass and sea-surface temperature estimates from sea-bed distribution of nanofossils and planktonic foraminifera in the Buenguela upwelling system. Micropal. 40 (3), 275–285.
Guerzoni, S., Molinaroli, E., Chester, R., 1997. Saharan dust inputs to the western Mediterranean Sea: depositional patterns, geochemistry and sedimentological implications. Deep-Sea Res. II 44, 631–645.
Hargraves, P.E., French, F.W., 1983. Diatom resting spores: significance and strategies. In: Fryxell, G. (Ed.), Survival strategies of the algae. Cambridge University Press, New York, pp. 49–68.
Heburn, G.W., La Violette, P.E., 1990. Variations in the structure of the anticyclonic gyres found in the Alboran Sea. J. Geophys. Res. 95, 1599–1613.
Hemleben, Ch., Spindler, M., Anderson, O.R., 1989. Modern Planktonic Foraminifera. Springer Verlag, Berlin, p. 363.
Heussner, S., Ratti, C., Carbonne, J., 1990. The PPS 3 time-series sediment trap and the trap sample techniques used during the ECOMARGE experiment. Cont. Shelf Res. 10, 943–958.
Knappertsbusch, M., 1993. Geographic distribution off living and Holocene coccolitophores in the Mediterranean Sea. Mar. Micro. 21, 219–247.
La Violette, P.E., 1984. The advection of submesoscale thermal features in the Alboran Sea gyre. J. Phys. Oceanogr. 14, 550–565.
Leblanc, K., Quéguiner, B., Prieur, L., Claustre, H., Oubelkheir, K., Bruyant, F., 2004. Siliceous phytoplankton production and export related to trans-frontal dynamics of the Almería-Oran frontal system (western Mediterranean Sea) during winter. J. Geophys. Res. 109 (C07010).
Loyë-Pilot, J.M., Martin, 1996. M.D. Loyë-Pilot and J.M. Martin, Saharan dust input to the western Mediterranean: an eleven years record. In: Guerzoni, S., Chester, R. (Eds.), The impact of desert dust across the Mediterranean. Kluwer Academic Publishers, Dordrecht, pp. 191–200.
Margalef, R., 1978. Life-forms of phytoplankton as survival alternatives in an unstable environment. Oceanol. Acta 1 (4), 493–509.
McPhaden, J., 1999. Genesis and Evolution of the 1997-1998. Science 283, 950–954.
Melin, F., 2000. SeaWiFS Images Archive, SeaWiFS dataset for the Eastern Atlantic. September 1997–May 1998. Space Applications Institute (SAI), Marine Environment Unit (ME), Joint Research Centre (JRC).
Mercado, J., Ramírez, T., Cortés, D., Sebastián, M., Vargas, M., 2005. Temporal changes of the phytoplankton communities in an upwelling area of the Alboran Sea. Scientia Marina 69 (4), 451–465.
Mercado, J., Cortés, D., Garcia, A., Ramírez, T., 2007. Seasonal and inter-annual changes in the planktonic communities of the northwest Alboran Sea (Mediterranean Sea). Prog. Oceanogr. 74 (2–3), 273–293.
Minas, H., Coste, B., Le Corre, P., Minas, M., Raimbault, P., 1991. Biological and geochemical signatures associated with the water circulation through the Strait of Gibraltar and in the western Alboran Sea. J. Geophys. Res. 96 (C5), 8755–8771.
Moulin, C., Lambert, C.E., Dayan, U., Masson, M.V., Ramonet, M., Bousquet, P., Legrand, M., Balkanski, Y.J., Guelle, W., Marticorena, B., Bergametti, G., Dulac, F., 1998. Satellite climatology of African dust transport in the Mediterranean atmosphere. J. Geophys. Res. 103 (D11), 13137–13144.
Moreno, A., Cacho, I., Canals, M., Prins, M.A., Sanchez-Goñi, M.F., Grimalt, J.O., Weltje, G.J., 2002. Saharan dust transport and high-latitude glacial climatic variability: the Alboran Sea record. Quaternary Res. 58, 318–328.
Okada, H., Honjo, S., 1973. The distribution of oceanic coccolithophorids in the Pacific. Deep-Sea Res. 20, 355–374.
Okada, H., McIntyre, A., 1979. Seasonal distribution of modern coccolithophores in the Western North Atlantic Ocean. Mar. Biol. 54, 319–328.
Packard, T.T., Minas, H.J., Coste, B., Martínez, R., Bonin, M.C., Gostan, J., Garfield, P., Christensen, J., Dortch, Q., Minas, M., Copin-Montegut, G., Copin-Montegut, C., 1988. Formation of the Alboran oxygen minimum zone. Deep-Sea Res. 35 (7), 1111–1118.
Peinert, R., Miquel, J.C., 1994. The significance of frontal processes for vertical particle fluxes: a case study in the Alboran Sea (SW Mediterranean Sea). J. Mar. Sys. 5, 377–389.
Pokras, E.M., Mix, A.C., 1985. Eolian evidence for spatial variability of late Quaternary climates in tropical Africa. Quat. Res. 24 (2), 137–149.
Pujol, C., Vergnaud-Grazzini, C., 1995. Distribution patterns of live planktic foraminifers as related to regional hydrography and productive systems of the Mediterranean Sea. Mar. Micro. 25, 187–217.
Quétel, C.R., Remoudaki, E., Davies, J.E., Miquel, J.-C., Fowler, S.W., Lambert, C.E., Bergametti, G., Buat-Ménard, P., 1993. Impact of atmospheric deposition on particulate morphs in warm shallow seawater. J. Sediment. Petrol. 39, 1579–1587.
Rigual-Hernández, A.S., Bárcena, M.A., Sierro, F.J., Flores, J.A., Hernández-Almeida, I., Sanchez-Vidal, A., Palanques, A., Heussner, S., 2010. Seasonal to interannual variability and geographic distribution of the silicoflagellate fluxes in the Western Mediterranean. Mar. Micro. 77 (1–2), 46–57.
Rutten, A., de Lange, G.J., Ziveri, P., Thomson, J., van Santvoort, P., Colley, S., Corselli, C., 2000. Recent terrestrial and carbonate fluxes in the pelagic eastern Mediterranean;

a comparison between sediment trap and surface sediments. Palaeogeogr. Palaeoclimatol. Palaeoecol. 158 (3–4), 197–213.
Sanchez-Vidal, A., Calafat, A., Canals, M., Fabres, J., 2004. Paricle Flux in the Almería-Oran Front: control by coastal upwelling and sea surface circulation. J. Mar. Sys. 52, 89–106.
Sanchez-Vidal, A., Calafat, A., Canals, M., Frigola, J., Fabres, J., 2005. Particle fluxes and organic carbon balance across the Eastern Alboran Sea (SW Mediterranean Sea). Cont. Shelf Res. 25, 609–628.
Sarhan, T., Garcia-La fuente, J., Vargas, J.M., Plaza, F., 2000. Upwelling mechanisms in the northwestern Alboran Sea. J. Mar. Sys. 23, 317–331.
Sautter, L.R., Sancetta, C., 1992. Seasonal associations of phytoplankton and planktic foraminifera in an upwelling region and their contribution to the seafloor. Mar. Micro. 18, 263–268.
Schiebel, R., Waniek, J., Bork, M., Hemleben, Ch., 2001. Planktic foraminiferal production stimulated by chlorophyll redistribution and entrainment of nutrients. Deep-Sea Res. I 48, 721–740.
Schiebel, R., Zeltner, A., Treppke, U.F., Waniek, J.J., Bollmann, J., Rixen, T., Hemleben, C., 2004. Distribution of diatoms, coccolithophores and planktic foraminifers along atrophic gradient during SW monsoon in the Arabian Sea. Mar. Micro. 51 (3–4), 345–371.
Smart, C.W., 2002. A comparison between smaller (>63 m) and larger (>150 m) planktonic foraminiferal faunas from the Pleistocene of ODP Site 1073 (Leg 174A), New Jersey margin, NW Atlantic Ocean. J. Micropaleontol. 21 (2), 137–147.
Tintore, J., La Violette, P.E., Blade, I., Cruzado, A., 1988. A study o fan intense density front in the Eastern Alboran Sea: the Almeria-Oran Front. J. Phys. Oceanogr. 18, 1384–1397.
Varela, M., Bode, A., Lorenzo, J., 2003. Differences in species composition between spring and summer phytoplankton blooms induce bay upwelling in the norhwestern Iberian margin. Thalassas 19 (2a), 222.
Vargas-Yañez, M., Plaza, F., Garcia-Lafuente, J., Sarhan, T., Vargas, J.M., Vélez-Belchi, P., 2002. About the seasonal variability of the Alboran Sea circulation. J. Mar. Sys. 35, 229–248.
Viúdez, A., Pinot, J.M., Haney, R.L., 1998. On the upper layer circulation in the Alboran Sea. J. Geophys. Res. 103 (C10), 21653–21666.
Weaver, P.P.E., Pujol, C., 1988. History of the laste deglaciation in the Alboran Sea (Western Mediterranean) and adjacent North Atlantic as revealed by coccolith floras. Palaeogeogr. Palaeoclimatol. Palaeoecol. 64, 35–42.
Ziveri, P., Thunell, R.C., Rio, D., 1995. Export production of coccolithophores in an upwelling region: Results from San Pedro Basin, Southern California Borderlands. Mar. Micro. 24, 335–358.
Ziveri, P., Rutten, A., de Lange, G., Thomson, J., Corselli, C., 2000. Present-day coccolith fluxes recorded in central eastern Mediterranean sediment traps and surface sediments. Palaeogeogr. Palaeoclimatol. Palaeoecol. 158 (3–4), 175–195.

ANEXO 2. LISTADO DE FIGURAS Y TABLAS

Capítulo 1 1

Figure 3.2. Construction of the age model was performed by correlating the benthic isotope stack LR04 with Site U1314 benthic $\delta^{18}O$. Tie points of both records are joined by dashed lines. From top to bottom: A) LR04 benthic stack; B) sedimentation rate of site 1314 after tuning; C) chronology as a function of depth in Site U1314; benthic $\delta^{18}O$ from Site U1314 as function of depth.

Figure 3.3. Comparison of benthic $\delta^{18}O$ records from the North Atlantic. From bottom to top: A) U1313 (Ferretti *et al.*, 2010), B) U1308 (Hodell *et al.*, 2008), C) 983 (Kleiven *et al.*, 2003), D) 980 (Flower *et al.*, 2000), E) U1314, F) benthic $\delta^{18}O$ LR04 stack (Lisiecki and Raymo, 2005), G) B08 sea-level reconstruction (Bintanja and van de Wal 2008) and H) summer insolation at 65º N (Laskar *et al.*, 2004). Vertical dashed grey lines join equivalent millennial-climate events in the North Atlantic sites. Marine Isotope Stages (MIS) are shown at the top (glacials in blue and interglacials in black).

Figure 3.4. Site U1314 records from 779 to 1069 ka. From bottom to top: A) IRD/g, B) faunal-based SST, using ANN technique, C) planktonic $\delta^{18}O$, D) benthic $\delta^{18}O$ (dark blue), benthic $\delta^{18}O$ LR04 stack (Lisiecki and Raymo, 2005) (light blue) and B08 sea-level reconstruction (Bintanja and van de Wal 2008) (orange dashed line) E) benthic $\delta^{13}C$, with 5 points running average (black). Pink lines correspond with samples were *C. wuellerstorfi* individuals were picked for the stable isotope analyses, and grey lines correspond to *M. pompilloides*, values represented with corrector factor applied (see 3. Material and Methods) G) Summer insolation at 65º N (Laskar *et al.*, 2004). Vertical grey bars indicate IRD discharge events, either linked to deglaciations or to millennial-scale oscillations. Marine Isotope Stages (MIS) are shown at the top (glacials in blue and interglacials in black).

Figure 3.5. Site U1314 records between 1069 and 950 ka. From bottom to top: A) IRD/g, B) planktonic $\delta^{18}O$, C) faunal-based SST, using ANN technique, D) benthic $\delta^{18}O$ (dark blue), benthic $\delta^{18}O$ LR04 stack (Lisiecki and Raymo, 2005) (light blue) and B08 sea-level reconstruction (Bintanja and van de Wal 2008) (orange dashed line), and E) insolation at the Equator in Spring (orange solid line) and Autumn (blue dashed line) (Laskar *et al.* 2004). Vertical grey bars indicate IRD discharge events, either linked to deglaciations or to millennial-scale oscillations. Marine Isotope Stages (MIS) are shown at the top (glacials in blue and interglacials in black).

Figure 3.6. Power Spectrum of IRD/g, SST and planktonic $\delta^{18}O$ calculated by the Blackman-Tukey method for the time period before MIS 25 (~ 950 ky). The data used in the time series analysis were interpolated at 1000-year intervals. These calculations were made using *Analyseries* (Paillard *et al.*, 1996).

Figure 3.7. Site U1314 records between 1069 and 950 ka. From bottom to top: A) IRD/g, B) planktonic $\delta^{18}O$, C) faunal-based SST, using ANN technique, D) benthic $\delta^{18}O$ (dark blue), benthic $\delta^{18}O$ LR04 stack (Lisiecki and Raymo, 2005) (light blue) and B08 sea-level reconstruction (Bintanja and van de Wal 2008) (orange dashed line), and E) obliquity parameter (Laskar *et al.* 2004). Vertical grey bars indicate IRD discharge events, either linked to deglaciations or to millennial-scale oscillations. Marine Isotope Stages (MIS) are shown at the top (glacials in blue and interglacials in black).

Figure 3.8. From bottom to top: A) benthic $\delta^{18}O$ from Site U1314, B) benthic $\delta^{13}C$ from Site U1314

(pink, only *C. wuellerstorfi* values shown) and U13108 (Hodell *et al.*, 2008) (red). Vertical grey dashed lines depict when the thermohaline circulation become disturbed. Marine Isotope Stages (MIS) are shown at the top (glacials in blue and interglacials in black).

Capítulo 4 63

with blue vertical bars. Interglacial sub-stages 21.7, 21.5, 21.3 and 21.1 are shown with orange vertical bars.

Capítulo 5 91

Table 5.1. Tie points used in the correlation between benthic $\delta^{18}O$ from Site U1314 and benthic isotope stack LR04.

Table 5.2. Correlation matrix between Axis 1 from DCA and Site U1314 proxies. The bold values correspond to significant correlations at $p < 0.01$ level.

Figure 5.1. Location of IODP Site U1314 (black star: 56º21'N, 27ºW; 2820 m water depth), modern surface (pink), and deep circulation (blue) in the North Atlantic (Krauss, 1986; Schmitz and McCartney, 1993). Map generated with *Ocean Data View v.3.4.3.* software (Schlitzer, 2008). East Greenland Current (EGC), Norwegian Current (NC), Labrador Current (LC), North Atlantic Current (NAC), Denmark Strait Overflow Water (DSOW), Iceland Scotland Overflow Water (ISOW), Labrador Sea Water (LSW), North Atlantic Deep Water (NADW), and Southern Source Water (SSW).

Figure 5.2. Construction of the age model was performed by correlating the benthic isotope stack of Lisiecki and Raymo (2005) (LR04) with Site U1314 benthic $\delta^{18}O$. Tie points of both records are joined by dashed lines.

Figure 5.3. Site U1314 records from 1069 t o779 ka. From bottom to top: A) benthic $\delta^{18}O$, with green filled up to 3.5 ‰, the glacial threshold (McManus *et al.* 1999); B) benthic $\delta^{13}C$; C) RAR (red filled), opal AR (dashed red line) and phaeodarian main percentage peaks (blue dots); D) Diatom Index; E) IRD AR; F) percentage of *C. davisiana* and G) Shannon-Weaver diversity index. Marine Isotope Stages (MIS) are shown at the top (glacials in blue and interglacials in black).

Figure 5.4. Radiolarian species representing more than 1%. Water mass affinity according to DCA represented in vertical left-side line and text. Marine Isotope Stages (MIS) are shown at the top (glacials in blue and interglacials in black).

Figure 5.5. Radiolarian species representing more than 1%. Water mass affinity according to DCA represented in vertical left-side line and text. Marine Isotope Stages (MIS) are shown at the top (glacials in blue and interglacials in black).

Figure 5.6. DCA diagram of the radiolarian species (red triangles) and samples (black dots) from Site U1314. Only samples occupying extreme positions along Axis 1 have been labelled with the age (ka). Arrows indicate inferred (environmental) variables.

Figure 5.7. Correlation between RAR and opal AR. * Correlation is significant at $p < 0.01$ level.

Figure 5.8. A) Mantel correlogram of the multispecies time series for the interval 1069-779 ka using inner product measure (sample spacing is 1089 year) and B) time spectra using the discrete Fourier transform of the Mantel correlogram. See Hammer (2007) for procedure description. Spectral analysis (Lomb periodogram) of the different paleoceanographic records from Site

U1314: C) RAR and D) opal AR for the same interval. Numbers above peaks denote respective periodicities. The 0.01 and 0.05 significance levels ('white noise lines') are shown as red dashed lines.

Capítulo 6 135

Capítulo 7 147

Figura 7.4. Desde abajo hacia arriba: A) registro del contenido en Mn (µg/g) obtenido de los análisis de composición elemental, y B) relación del Mn/Ca (línea discontinua) obtenida de los datos elementales de limpieza reductiva en foraminíferos planctónicos, en el testigo U1314 entre 1060 y 779 ka. Las barras verticales azules indican los estadios marinos isotópicos glaciares.

Figura 7.5. Desde abajo hacia arriba: A) registro de la tasa de acumulación de IRD (partículas/ cm^2*ka), B) relación Ti/Al, valores <0,1 corresponden con sedimentos continentales, valores entre 0,1-0,2 corresponden con basaltos procedentes de Islandia y valores > 0,2 a basaltos de las Islas Feroe (Hyun y Kim, 1999), C) P detrítico (µg/g) obtenido de la extracción secuencial de P y D) susceptibilidad magnética en el testigo U1314 entre 1060 y 779 ka. Las barras verticales azules indican los estadios marinos isotópicos glaciares.

Figura 7.6. Desde abajo hacia arriba: A) Porcentaje de filosilicatos (área gris), B) registro de Mg (µg/g) y C) Zn (µg/g) para el periodo 830-779 ka. La barra vertical azul indica el estadio marino isotópicos glaciares 20.

Figura 7.7. Desde abajo hacia arriba: A) IRD/g, B) reconstrucción de temperaturas a partir de la relación Mg/Ca (en rojo, media de cinco puntos), C) $\delta^{18}O$ planctónico, D) $CaCO_3$ (%), y E) reconstrucción de temperaturas a partir de la funciones de transferencia.

ANEXO 3. LISTADO DE ABREVIATURAS Y ACRÓNIMOS

A continuación, se enumeran alfabéticamente las abreviaturas y acrónimos usados en esta Tesis Doctoral, con el fin de facilitar su lectura. La mayoría son acrónimos que proceden del inglés, por ello se ha incluido su significado en inglés, y la versión castellana que más se le aproxime. Los términos procedentes el latín también aparecen en cursiva.

AABW: *Antarctic Bottom Water* (Agua antártica de fondo)

AF: *Arctic Front* (Frente Ártico)

AMOC: *Atlantic Meridional Overturning Circulation* (Corriente de retorno atlántica)

ANN: *Artificial Neural Networks* (Redes neuronales artificiales)

AR: *Accumulation Rate* (Tasa de acumulación)

B08: Bintanja et al. (2008), reconstrucción global del nivel del mar

B/(P+B): *Benthic foraminifera/(Planktonic foraminifera + Benthic foraminifera)* (Bentónicos/(Planctónicos + Bentónicos)

CLIMAP: *Climate: Long range Investigation, Mapping and Prediction* (Proyecto de investigación climática para realizar mapas del pasado y predicciones)

DCA: *Detrended Correspondance Analyses* (Análisis de correspondencia sin tendencia)

DI: *Diatom Index* (Índice de abundancia de diatomeas)

DSOW: *Denmark Strait Overflow Water* (Agua que atraviesa el estrecho de Dinamarca)

e.g.: *exempli gratia* (por ejemplo)

EGC: *East Greenland Current* (Corriente del este de Groenlandia)

et al.: *et alii* (y colaboradores)

FI: *Fragmentation Index* (Índice de fragmentación)

G-IG: *Glacial-Interglacial* (Glaciar-interglacial)

GNAIW: *Glacial North Atlantic Intermediate Water* (Agua Noratlánticas intermedia glacial)

GRIP: *Greenland Ice-Core Project* (Proyecto de testigo de hielo del casquete de Groenlandia)

GIN: *Greenland-Iceland-Norwegian* (Groenlandia-Islandia-Noruega)

***H*:** *Shannon-Weaver diversity index* (Índice de diversidad de Shannon-Weaver)

i.e.: *id est* (en otras palabras)

IC: *Irminger Current* (Corriente de Irminger)

ICP: *Inductive Coupled Plasma* (Plasma de acoplamiento inductivo)

IODP: *Integrated Ocean Drilling Program* (Programa integrado de perforación oceánica)

IRD: *Ice-rafted debris* (Detritos transportados por hielo)

ISOW: *Iceland-Scotland Overflow Water* (Agua que atraviesa el promontorio entre Islandia y Escocia)

ka (en redacción en castellano): kilo-años

ka: *thousand years ago* (hace miles de años)

kyr: *thousand years* (miles de años)

LC: *Labrador Current* (Corriente del Labrador)

LDW: *Lower Deep Water* (Agua inferior profunda)

LGM: *Last Glacial Maximum* (Último máximo glacial)

LNADW: *Lower North Atlantic Deep Water* (Agua Noratlántica profunda inferior)

LR04: Lisiecki and Raymo (2005), compilación de registros de $\delta^{18}O$ bentónico

LSW: *Labrador Sea Water* (Agua del Labrador)

Ma: *Million years ago (*hace millones de años)

MARGO: *Multiproxy Approach for the Reconstruction of the Glacial Ocean Surface* (Reconstrucción de la superficie oceánica durante los periodos glaciales a partir de varios indicadores)

MAT: *Modern Analog Technique* (Método de análogos modernos)

mcd: *Meters of Composite Depth* (Metros de profundidad compuesta)

MIS: *Marine Isotope Stage* (Estadio isotópico marino)

MPT: *Mid-Pleistocene Transition* (Transición del Pleistoceno Medio)

NAC: *North Atlantic Current* (Corriente Noratlántica)

NADW: *North Atlantic Deep Water* (Agua Noratlántica profunda)

NAO: *North Atlantic Oscillation* (Oscilación del Atlántico Norte)

NC: *Norwegian Current* (Corriente de Noruega)

NHG: *Northern Hemisphere Glaciation* (Glaciación del Hemisferio Norte)

ODP: *Ocean Drilling program* (Programa de perforación oceánica)

PF: *Polar Front* (Frente Polar)

RAR: *Radiolarian Accumulation Rate* (Tasa de acumulación de radiolarios)

SST: *Sea Surface Temperature* (Temperatura superficial del mar)

sw: *sea-water* (agua del mar)

TC: *total carbon* (carbono total)

TOC: *total organic carbon* (carbono orgánico total)

VPDB: *Vienna Pee Dee Belemnite*

ANEXO 4. LISTADO TAXONÓMICO

FORAMINIFEROS PLANCTÓNICOS

Globigerina bulloides d'Orbigny, 1826
Globigerinella siphonifera d'Orbigny, 1839
Globigerinita glutinata Egger, 1893
Globigerinoides ruber d'Orbigny, 1839
Globigerinoides sacculifer Brady, 1877
Globorotalia crassaformis Galloway and Wissler, 1927
Globorotalia inflata d'Orbigny, 1839
Globorotalia hirsuta d'Orbigny, 1839
Globorotalia scitula Brady, 1882
Globorotalia truncatulinoides d'Orbigny, 1839
Neogloboquadrina pachyderma Ehrenberg, 1861
Orbulina universa d'Orbigny, 1839
Turborotalita humilis Brady, 1884
Turborotalita quinqueloba Natland, 1938

RADIOLARIOS

Spumellaria

Actinomma boreale Cleve, 1899
Actinomma delicatulum (Dogiel and Reschetnjak, 1952)
Actinomma haysi Bjørklund, 1976
Actinomma leptodermum leptodermum (Jørgensen, 1900)
Actinomma medianum Nigrini, 1967
Actinomma popofskii (Petrushevskaya, 1967)
Actinomma sol Cleve, 1901
Actinomma trinacrium Haeckel, 1862
Amphirhopalum ypsilon Haeckel, 1887
Anomalocantha dentata (Mast, 1910)
Cenosphaera reticulata Haeckel, 1860
Cladococcus viminalis Haeckel, 1862
Didymocyrtis tetrathalamus (Haeckel, 1887)
Druppatractus irregularis Popofsky, 1912
Druppatractus variabilis Dumitrica, 1973
Dictyocoryne profunda Ehrenberg, 1860

Heliodiscus asteriscus Haeckel, 1887
Hexacontium pachydermum Jørgensen, 1900
Larcopyle buetschlii Dreyer, 1889
Larcopyle polyacantha titan Lazarus et al., 2005
Larcopyle weddellium Lazarus et al, 2005
Larcospira minor (Jørgensen, 1900)
Phorticium clevei (Jørgensen, 1900)
Porodiscus sp. 1
Spongocore puella Haeckel, 1887
Spongodiscus sp. Takahashi and Honjo, 1981
Spongopyle osculosa Dreyer, 1889
Spongotrochus glacialis Popofsky, 1908
Stylatractus sp. 1
Stylochlamydium venustum (Bailey, 1856)
Stylodictya validispina Jørgensen, 1905
Styptosphaera spumacea Haeckel, 1887
Tetrapyle octacantha Müller, 1858

Nassellaria
Androcyclas gamphonycha (Jørgensen, 1900)
Arachnocorys sp.1
Artostrobus annulatus (Bailey, 1856)
Artostrobus joergenseni Petrushevskaya, 1967
Botryocampe inflata (Bailey, 1856)
Botryostrobus auritus/australis (Ehrenberg) group Nigrini, 1977
Botryostrobus tumidulus (Bailey, 1856)
Carpocanistrum sp. 1 (Nigrini, 1970)
Ceratocyrtis galeus (Cleve, 1899)
Ceratocyrtis histricosus (Jørgensen, 1905)
Cornutella profunda Ehrenberg, 1854
Corocalyptra craspedota (Jørgensen, 1900)
Cycladophora cornutoides (Petrushevskaya, 1967)
Cycladophora davisiana (Ehrenberg, 1862)
Dictyophimus hirundo (Haeckel, 1887)
Eucyrtidium acuminatum (Ehrenberg, 1844)
Eucyrtidium calvertense Martin, 1904
Eucyrtidium hexagonatum Haeckel, 1887
Eucyrtidium sp. 1 (cf. *E. calvertense* ?) Dolven, 2004
Eucyrtidium teuscheri Haeckel, 1887

Lamprocyclas maritalis Haeckel, 1887
Lipmanella xiphephorum (Jørgensen, 1900)
Lithocampe platycephala (Ehrenberg, 1873)
Lithomelissa setosa Jørgensen, 1900
Lithomelissa thoracites Haeckel, 1862
Lithomitra lineata/arachnea group (Ehrenberg, 1838)
Lithostrobus cuspidatus (Bailey, 1856)
Lophophaena sp. 1
Peridium longispinum Jørgensen, 1900
Peripyramis circumtexta Haeckel, 1887
Phormospyris sp. det. Benson, 2003
Plagonidae fam.
Pseudodictyophimus gracilipes (Bailey, 1856)
Pseudodictyophimus gracilipes multispina (Bailey, 1856)
Pterocanium auritum Nigrini and Caulet, 1992
Pterocanium praetextum praetextum (Ehrenberg, 1872)
Pterocanium trilobum (Haeckel, 1861)
Pterocorys zancleus (Müller, 1858)
Sethoconus dogieli Petrushevskaya, 1967
Stichocorys seriata Jørgensen, 1905
Stichopilium bicorne Haeckel, 1887
Theocorythium trachelium (Ehrenberg, 1872)
Trissocyclis sp. 1

Phaeodaria
Euphysetta nathorstii Cleve, 1899
Lirella melo (Cleve, 1899)

ANEXO 5. PROTOCOLO DE LIMPIEZA PARA ELEMENTOS TRAZA

(Modificado del protocolo del GRC-GM de la Universidad de Barcelona, publicado por Pena *et al.*, 2005)

1. CONSIDERACIONES PREVIAS

- Asegurarse de que hay suficiente:
  - mezcla de ácido cítrico + NH_4
  - NaOH 0,1M
  - HNO_3 0,001M
  - HNO_3 ultrapuro al 1% (sólo para la disolución)
- Tubos limpios (sólo para la disolución)
- Encender al menos 1,5 horas antes el baño caliente del reductivo. El baño oxidativo hay que encenderlo al final del reductivo.
- Poner un vial vacío como prueba en blanco para detectar posibles contaminaciones.
- Colocar dentro de la campana de flujo laminar las pipetas, los botes para el agua y el HNO_3, el vaso de precipitados para residuos y los viales cerrados.
- Limpiar las puntas de las pipetas: 2 veces con HNO_3 y 3 con agua desionizada y purificada (Milli-Q). Igualmente hay que limpiar la punta de pipeta entre muestra y muestra en las extracciones para no contaminar.
- No coger nunca los reactivos de la botella, verter una pequeña cantidad en un vaso de precipitado para evitar contaminar todo el reactivo de la botella con las pipetas. Los reactivos para la limpieza se preparan con agua Milli-Q.

2. LIMPIEZA DE ARCILLAS

- Limpiar la punta de la pipeta pequeña y añadir 30-40 µl de agua Milli-Q en cada vial y colocarlos 30” en baño de ultrasonidos. No hace falta cerrar los viales al ultrasonicar, siempre que permanezcan en el interior de la campana de flujo laminar.
- Añadir agua Milli-Q hasta completar cada vial, esperar a que decanten los foraminíferos, dando pequeños golpecitos, y retirar el sobrante de agua con la pipeta de 1000 (ponerla a ~750 µl). Hacerlo de 3 en 3 para que no decanten también las arcillas. Repetir 3 veces en total.
- Añadir metanol hasta 0,4 µl de la marca del vial y colocar en baño de ultrasonidos 30”. Después retirar el metanol. Repetir otra vez y después llenar los viales de agua Milli-Q (para limpiar el metanol), dejar que decanten los foraminíferos y retirar el sobrenadante.
- Si se cree que las muestras pudieran tener alta contaminación arcillosa, repetir los pasos 1 y 2.

3. LIMPIEZA REDUCTIVA

- Cambiar la punta de pipeta de 1000 µl y limpiarla. Pasar los viales a la campana específica para compuestos de amoniaco, y añadir agua y HNO_3 nuevo en los botes de limpieza.
- Mezclar el ácido cítrico+NH4 (2000 µl) con la hidracina (500 µl) y agitar un poco la mezcla.
- Añadir 100 µl de la mezcla en cada vial y poner el cierre de seguridad.
- Colocar los viales en un baño caliente 16 minutos, ultrasonicando 5" cada 2 minutos (poner el cronómetro a 2 minutos 7 veces e ir apuntando en una tabla para asegurarse de que se hace 7 veces). Calentar un poco de agua Milli-Q en un vaso de precipitados.
- Apagar el baño del reductivo, encender el baño del oxidativo y sacar los viales. Abrirlos con cuidado porque a veces están presurizados y puede saltar, rellenar rápidamente con agua Milli-Q vial y tapa para parar la reacción, después extraer el agua sobrante con la pipeta. Se limpian 2 veces más con agua Milli-Q.
- Añadir 400 µl de agua Milli-Q caliente, dejarla 5 minutos y luego retirarla. Realizar este paso dos veces.
- Añadir agua Milli-Q fría en vial y tapa y retirarla.

4. LIMPIEZA OXIDATIVA

- Cambiar la punta de pipeta de 1000 µl y limpiarla. Pasar los viales a la campana de flujo laminar, tirar el líquido del vaso de residuos, para no inhalar NH_3 y poner agua y HNO_3 nuevos en los botes.
- Mezclar 10 ml de NaOH con 100 µl de H_2O_2 y agitar un poco.
- Poner 250 µl de la mezcla en cada vial, cerrarlos con el cierre de seguridad y poner en el baño caliente 5 min. A la mitad del tiempo sacar los viales y dar unos golpes contra la encimera para evitar que se formen burbujas (sujetar los viales con las palmas de las manos o con la tablita de plástico). Al final colocar los viales 15" en baños de ultrasonidos. Repetir y apagar el baño.
- Sacar los viales, abrirlos y rellenar con agua Milli-Q vial y taparlos. Dar golpecitos para que decanten los foraminíferos (porque suelen formarse burbujas) y extraer el agua sobrenadante con la pipeta. Repetir dos veces más.

5. LIXIVIADO CON ÁCIDO DÉBIL (*weak acid leaching*)

- Añadir 250 µl de HNO_3 0,001 M en cada vial y colocar los viales 30" en ultrasonidos.
- Añadir agua Milli-Q hasta rellenar los viales y después de esperar a que decanten los foraminíferos retirar el sobrenadante. Repetir 3-4 veces más.
- Eliminar el máximo de agua con la pipeta pequeña, para que solamente queden foraminíferos en el vial. Cerrarlos y guardar los viales hasta que se haga la disolución.

6. DISOLUCIÓN

- **Sólo se hace el día anterior al análisis en el ICP-MS.**
- Hacer una lista con las muestras y el código asignado a cada una.
- Echar 400 µl de HNO_3 1% (ultrapuro)+ Rh en cada vial. Hacerlo en grupos de 8.
- Poner las muestras en el baño de ultrasonidos 15" para facilitar la disolución o más si fuera necesario, dando golpecitos para evitar que los fragmentos de foraminíferos se queden en burbujas.
- Agitar los viales y después ponerlos en grupos de 8 en la microcentrífuga 5 minutos a 6000 rpm.
- Transferir 370 µl de muestra en un tubo limpio de 14 ml usando una pipeta y añadir 2630 µl de HNO_3+Rh. Agitar con el vortex para homogeneizar.

7. PREPARACIÓN DE REACTIVOS

- **Reactivos del reductivo:** Ácido cítrico + NH_4. Se prepara dentro de la campana específica para amoniaco. Se pesan 5,25 g de ácido cítrico en un vaso de precipitados. Se añaden 100 ml de NH_4 (30%). Se calienta el vaso de precipitados con el ácido cítrico y un mezclador magnético a 40-50 ºC., y finalmente se transfiere la mezcla a un bote de plástico limpio y se meter al frigorífico.

- **Reactivos del oxidativo:** H_2O_2 al 30 % (mantener en la nevera). Pesar 4 g de NaOH 0,1M (Aristar grade) y mezclarlo con un litro de agua Milli-Q.

- **Lixiviado con ácido débil (*weak acid leaching*):** HNO_3 0,001M. Se prepara mezclando 69,4 µl de HNO_3 (65 %) con agua Milli-Q hasta completar un litro (o 37,4 µl HNO_3 (65 %) con agua Milli-Q hasta completar medio litro).

- **Disolución:** HNO_3 1 % ultrapuro. Se prepara diluyendo el HNO_3 5 % ultrapuro (Aristar grade) a 1/5 con agua Milli-Q.

ANEXO 6. PROTOCOLO DE DIGESTIÓN TOTAL DE SEDIMENTO

(Modificado del protocolo del laboratorio de biogequímica de la IUPUI)

1. SEGURIDAD

- No utilizar la campana para digestiones con microondas utilizando HF cuando la velocidad de flujo es menor de 27 metros/minuto.
- Utilizar siempre protección adecuada cuando se este manipulando ácidos, especialmente cuando se utiliza HF. En caso de que la piel entre en contacto con HF, aplicar gel de glutamato de calcio en la zona afectada.

2. PREPARACIÓN DE MUESTRAS

- Colocar los recipientes en el carrusel, colocando primero el anillo enroscado marrón, con la rosca hacia arriba, en cada hueco.
- Pesar la 0.1 g de muestra en los recipientes.
- Añadir 10 ml de agua purificada y desionizada (Milli-Q) a cada recipiente. A partir de aquí, hay que usar guantes de látex y gafas de protección.
- Añadir los ácidos calibrados de metales traza. Los siguientes pasos han de realizarse bajo la campana de extracción de gases. Verter los ácidos en tubos centrífuga de 50 ml, y pipetear en los recipientes. La punta de pipeta ha de ser previamente lavada con un ácido débil.
  - 5 ml de HNO_3 (ácido nítrico).
  - 4 ml de HF (ácido fluorhidrico)
  - 1 ml de HCl (ácido clorhídrico)
- Una vez finalizado, verter el ácido sobrante de los tubos centrífuga en el desagüe de la campana y aclarar con agua, taparlos y tirarlos.
- Colocar las membranas de ruptura en los accesorios de ventilación. Enroscar los accesorios de ventilación a la cubierta de la funda blanca (a excepción de la cubierta de control de presión).
- Colocar la cubierta de control de presión en el recipiente que contendrá la muestra que se presuponga será más reactiva (normalmente es la que tiene más sedimento y/o más materia orgánica).
- Tapar cada recipiente. La cubierta de control de presión tiene un tapón especial. Es importante asegurarse de apretar los tapones con fuerza.
- Colocar el carrusel de recipientes en el microondas y unir los tubos de ventilación de cada recipiente.

3. USO DEL MICROONDAS

- Encender el microondas en el interruptor localizado en la parte inferior derecha del panel trasero.
- Abril la válvula lateral del microondas y colocar la línea de detección de presión en un vaso de precipitado dentro del microondas. Inyectar 10 cc de agua con una jeringuilla en el vaso de precipitado.
- Colocar la válvula en posición neutral.
- Colocar el carrusel de recipientes en el microondas.
- Unir las líneas de detección de presión a las cubiertas de control de presión de cada recipiente.
- Ajustar la línea de detección de presión en la anilla del la pared superior del interior del microondas.
- Presionar F4 en el panel de control para hacer rotar el carrusel con la puerta abierta para asegurarse de que los tubos de control de presión no se enredan.
- Cerrar la puerta.
- Presionar F3 para seleccionar método.
- Presionar F1 para seleccionar un protocolo ya configurado, y presionar *enter*.
- Presionar F1 para cargar programa
- Presionar F4 para inicio.
- Presionar F1 para confirmar.

4. DILUCCIÓN DE LAS MUESTRAS

- Cuando el proceso de digestión en el microondas ha finalizado y la presión en los recipientes ha descendido a menos de 10 psi, abrir despacio el accesorio de ventilación del recipiente de control de presión. Luego, retirar la línea de detección de presión. A partir de aquí es indispensable el uso de guantes y gafas de protección.
- Retirar el carrusel del microondas y colocarlo en la campana de extracción de gases.
- Abril la válvula lateral del microondas e inyectar otros 10 cc de agua en el vaso de precipitado. Colocar el interruptor de la válvula en posición neutral.
- Apagar el microondas
- Liberar la presión de cada recipiente levantando despacio cada accesorio de ventilación.
- Retirar los tubos de las fundas de kevlar.
- Dejar enfriar unos minutos, y añadir 0.1 g de ácido bórico a cada recipiente.
- Transferir la muestra a tubos centrífuga etiquetados de 50 ml. Aclarar los tapones y recipientes con agua Milli-Q.
- Diluir la muestra hasta los 50 ml.

5. LIMPIEZA

- Aclarar con agua abundante los tapones marrones y anillos con rosca, y dejar secar.
- Aclarar con agua los recipientes y los accesorios de ventilación.
- Retirar las membranas de ruptura.
- Sumergir los recipientes, accesorios de ventilación en una jarra con 4 l de ácido clorhídrico débil para limpiarlos.
- Colocar la jarra en una placa caliente a temperatura media-baja.
- Limpiar la campana con agua y secar.

ANEXO 7. PROTOCOLO DE DETERMINACIÓN DE FOSFATOS

(Modificado del protocolo del laboratorio de biogequímica de la IUPUI)

Se ha utilizado la técnica de determinación de fosfatos por colorimetría (método azul de molibdeno). En este procedimiento, una pequeña cantidad de reactive es añadido a la muestra. El reactivo tiene un ligando el cual, cuando entra en contacto con el ion fosfato, se vuelve de color azul. Cuanto más fosfato, más intenso es el azul del complejo de molibdeno. La determinación de la intensidad del color se realiza mediante instrumentación espectrofotométrica, siendo la *absorción* máxima una longitud de onda cerca del infrarrojo, unos 880 nanómetros.

El día que se analiza el fosfato, se mezcla parte del ácido ascórbico con la mezcla de reactivos, preparada con antelación, para así obtener el reactivo para desarrollar color. Después se agrega 1ml de reactivo para desarrollar color por cada 10 ml de muestra, y tras dejar 30 minutos para que se desarrolle el color, se analiza la solución con un espectrofotómetro. Los estándares se preparan a partir del estándar de fosfato con concentración 100 μM.

La única advertencia es que las soluciones ácidos deben ser diluidas antes del análisis (de otro modo, el color no se desarrolla), el reactivo para desarrollar color y las muestras (después de añadir el reactivo) solo pueden ser usadas el día de la preparación, y no se pueden analizar muestras con valores de fosfato mayores que 12μM porque la curva de los estándares se convierte en no-lineal (por lo tanto las muestras más concentradas tienen que ser diluidas). Todos los reactivos son almacenados en la cabina debajo del espectrofotómetros.

1. ENCENDIDO DEL ESPECTROFOTÓMETRO

- Encender el espectrofotómetro y esperar una hora a que aumente de temperatura.
- Inmediatamente después de encender el espectrofotómetro, hincar el programa para determinación del color Shimadzu-UPVC.

2. PROCEDIMIENTO

- Añadir 1ml de reactivo para desarrollar color a 10 ml de muestra (no es imprescindible que el volumen sea el exacto siempre que lo mantengamos para todas las muestras, blancos y estándares).
- Agitar las muestras y permitir que desarrolle el color colocándola en alguna zona oscura durante 30 minutos.
- Mientras las muestras desarrollan el color, preparar los blancos y estándares, añadir el reactivo para desarrollar color.

3. ANÁLISIS

- Colocar los estándares para calibrar el espectrofotrómetro.
- Configurar en el menú del programa los tiempos de "sorber y purgar". Ajustar el tiempo de sorber en 6 segundos y el de purga en 0.
- Realizar varios sorbos para limpiar el espectrofotómetros, después hacer click en *OK*:
- Hacer click en *auto-zero* antes de analizar blancos y estándares.
- Primero, sorber un blanco dos veces.
- Una vez hemos analizado los estándares, hacer click en *unknown* y comenzar a analizar las muestras.
- Sorber la primera muestra y permitir a la máquina registrar una lectura.
- Hacer click en esta lectura, y volver a sorber la primera muestra.
- Una vez la lectura ha sido realizada, hacer click en el comando *reading* dos veces, para obtener una media del la concentración e fosfato para cada muestra.
- Continuar con el mismo procedimiento con el resto de las muestras, sin olvidar salvar los datos, indicando fecha e iniciales de la persona que realiza el análisis.
- Finalmente, apagar el espectrofotómetro

4. LIMPIEZA

- Lavar los viales utilizados con HCl diluido durante una hora.
- Aclarar con agua desionizada y purificada (Milli-Q) y secar en el horno a 60 ºC.

5. PREPARACIÓN DE REACTIVOS

- **Mezcla de reactivos:** dissolver 6 g de amonio molibdato en 250 ml de agua Milli-Q. Disolver 0,1454 g de tartrato de antimonio y potasio en 500 ml de ácido sulfúrico (73 ml de ácido sulfúrico concentrado en 427 ml de agua Milli-q. Preparar con precaución, porque la reacción desprende mucho calor). Cuando los reactivos están disueltos, mezclar las dos soluciones en una botella de cristal ámbar y almacenar debajo de la campana de gases.
- **Reactivo para desarrollar color:** añadir 0,37 g de ácido ascórbico a 70 ml de mezcla de reactivos y agitar. El volumen resultante permite realizar entre 60 y 70 análisis de fosfato, y debe de ser preparado en el mismo día del análisis.

AGRADECIMIENTOS

"Se buscan hombres para un viaje peligroso. Salario bajo. Frío intenso. Largos meses en la más completa oscuridad. Peligro constante. Es dudoso que puedan regresar a salvo. En caso de éxito, recibirán honores y reconocimiento"

Así rezaba el anuncio publicado por Ernest Shackleton para reclutar tripulantes que quisieran participar en una expedición a la Antártida. Cuando lo leí por primera vez (he de confesar que no hace tanto tiempo), me pareció que era una forma divertida de describir el viaje que comencé hace algo más de cuatro años como becario de investigación. Como en esa expedición, yo también he tenido la suerte de contar con una extensa tripulación que me ha acompañado en mi particular viaje y ha hecho posible que llegue a buen puerto. Empiezo agradeciendo a mis directores de Tesis, Francisco Sierro y José Abel Flores, la calidad personal y científica que me han demostrado, y que me hayan motivado para superarme. Y por supuesto gracias a Mª Ángeles Bárcena, por confiar en mí y abrirme una primera puerta en el mundo de la investigación.

Este barco ha hecho escalas en diferentes puertos, en el que he conocido a gente excepcional en todos los sentidos. Gracias a Isabel Cacho por acogerme en su grupo en la Universidad de Barcelona, y a Jaume, Gemma, Leo, etc., que a pesar de recordarme a menudo que tenía que devolverles ciertos papeles y una paletilla, me acogieron como uno más entre ellos. Y por supuesto a toda la familia barcelonesa Isma, Jose, María…

Many thanks to Gabe Filippelli and IUPUI biogeochemistry lab group at Indianapolis, for teaching all the secrets of the geochemistry and be patients with my primitive English, and especially to Ange for helping me in and out of the lab, thanks all for make me feel less strange in such distant lands.

I am grateful to Kjell Bjørklund, who kindly hosted me in the Natural History Museum at Oslo, and taught me everything about radiolarians. You have shown me that these jewel-like snowflakes have many things to tell in paleoceanography. I also thank Øyvind Hammer for his critical discussions and suggestions of statistical approaches during my stay at Oslo. Karl-Heinz Baumann and Kentaro Hatakaeda are thanked for their help solving my queries and selflessly providing data and resources used in this Thesis.

Gracias a mis compañeros del Grupo de Geociencias Oceánicas, los que hicieron de cicerones cuando llegué al grupo (Elena, Bea, Rubén, Marta, Isa y Carmen), como a los que han compartido conmigo, penurias, alegrías, y sobre todo merendolas en el departamento: Alejandra, Margarita (¡que sería de nosotros si no te preocuparas por alimentarnos!), José Ignacio (por compartir tu sabiduría reposada), Miguel Ángel (por tu disponibilidad para mostrarme los entresijos de la estadística), Débora, Eloy (¡gracias por dejarme ganar siempre al padel!), Andrés y Mieke (siempre disponibles y colaboradores), Marta, Montse (a la que agradezco

que me enseñara a utilizar MAT y ANN) y Aleix (por ser tan forofo del Barça o más que yo), y demás colegas, becarios (algunos ya doctores) y profesores del departamento de Geología. Llegados a este punto no puedo por menos hace un inciso y agradecer especialmente la amistad y el apoyo mostrado por Mariem y Diego; nunca sabré que hubiera hecho sin ellos, lo que sí se es lo que he conseguido teniéndolos cerca, ¡esto también es en parte vuestro!

Muchas gracias a toda la gente que conocí mi primer año de carrera y sigo manteniendo como amigos (Cañas, Marien, Diego, Patri, Rebeca, Jesús, Javi, Emma, Sonia, Cristina, Bea, Vanesa, y un largo etcétera), por enseñarme que la vida universitaria ofrece muchas más cosas que las puramente académicas.

También quiero recordar a ese grupo de personas que conocí casi por accidente, la hermandad sagrada de la chuletilla riojana, Ana, Xabi, JuanCar, Oier, Maite, Mariem, Salva, Murelaga, y por supuesto nuestro apreciado monitor, Txema. Gracias por seguir acudiendo a la llamada de Cenicero cada verano para hacer terapia anti-stress a base de bromas y barbacoas, ¡y ya son 10 años!

Gracias a mis inseparables amigos, Javi, Sergio, Futre y Nacho, sois importantes para mí, sin vosotros, todo esto sería menos llevadero.

A mi familia, mis padres, Chuchi y Dioni, y a Carlos Javier y Tere, por ser un salvavidas en los momentos de tormenta, y a Irene, esa pequeña borrasca que arrasa todo a su paso, pero que tanto quiero (a ver cuando empiezas a hablar y a llamarme “tito”).

Y por último, pero no menos importante, gracias a ti, Oli, por acompañarme en este viaje y haberme ayudado a mantener firme el timón hasta llegar a buen puerto.

La realización de esta Tesis Doctoral ha sido posible gracias a la concesión de la beca predoctoral BES-2006-12787 del subprograma de Formación de Personal Investigador (FPI) del Ministerio de Educación otorgada al autor, y al proyecto del Ministerio de Ciencia e Innovación GRACCIE (CONSOLIDER-INGENIO CSD 2007-00067), así como a la financiación de los proyectos CGL2008-05560/BTE, CGL2006-10593, y a los fondos de la Junta de Castilla y León (Grupo de excelencia GR34). Adicionalmente, se ha obtenido financiación de la Universidad de Salamanca a través del Programa de Difusión de Resultados de la Agencia de Investigación. La presente Tesis Doctoral ha sido usado muestras suministradas por el *Integrated Ocean Drilling Program* (IODP).